Tetra-Stranded Metallo-Supramolecular Cylinders.

Design, Synthesis and DNA Binding Studies.

by

Natalia Calle Alonso

A thesis submitted to the University of Birmingham for the degree of

Doctor of Philosophy

School of Chemistry

University of Birmingham

December 2012

Abstract

The work described in this thesis concerns the design, synthesis, DNA binding and biological activity of palladium(II) supramolecular cylinders that might be capable of recognizing a DNA four-way junction.

An introduction to DNA structure will be presented, as well as the different binding modes of natural and synthetic agents that can recognise and bind to DNA. Since this work is focused on the design of large metallo-structures, the general principles of supramolecular chemistry will be summarised with particular emphasis on metallo-supramolecular structures.

Palladium(II) supramolecular cylinders have already been reported and these show promising cytotoxicity against different cancer cell lines. However, these complexes present poor solubility in aqueous solutions. It is therefore the aim of this thesis to improve the water solubility of palladium(II) supramolecular cylinders without significantly changing their structure or quenching their cytotoxic activity.

The DNA binding properties of the newly synthesised palladium(II) complexes will be presented. Several spectroscopic techniques, such as circular and linear dichroism and ethidium bromide displacement assays, as well as electrophoresis experiments were carried out and these will be discussed.

Initial DNA four-way junction experiments and cytotoxicity studies will also be discussed.

To Pablo

Acknowledgments

First of all I would like to thank Professor Mike Hannon for the chance he gave me to come to Birmingham for one year in the first place and letting me stay here to continue this challenging project. Thank you for all the chemical and personal advice during all these years.

I am grateful to the EU Marie Curie Training Site and the University of Birmingham for funding. To the School of Chemistry Analytical Facility, especially to Graham Burns, Peter Ashton, Dr. Neil Spencer, Dr. Louise Male and Dr. Chi Tsang for their hard work. I would also like to thank Dr. Nik Hodges and Prof. Steve Busby for allowing me to use their facilities in the School of Biosciences at the University of Birmingham. Thanks also to Ian Bodfish and Stuart Arkless for always doing such a great job, which made mine much easier.

Thanks to Ana Mª González-Vadillo for her friendship and support all the way through this journey.

A big thanks goes to all the members of the Hannon group that I had a chance to work with during this time. Special thanks to Carlos, Lucia, Alessio, Wei, Susana, Siriporn, Victoria, Lexi, Giulia, Nick, Laura, Hannah, Zahra, Ana, Lindsey and Jeni for their friendship and for helping me at some point during my project. The biggest thanks goes to my dearest friend Jenna, simply for being Jenna. For her unconditional friendship and for sharing almost every day for four years, all the good and the bad, but always smiling and making me smile.

I would like to express my deepest gratitude to all my family, especially to my parents, for all their love and support during all my life.

Thanks to all my friends from Carrascosa de la Sierra for all the fun and laughs we had and the ones to come. To Maria for always being so caring. To Antonio for showing me all my potential. To Andrea, Luca, Mino and Antonio for all the good moments lived at 255 Reservoir Road. To Alex for his sweet love. To Silvia for becoming such a great friend in such a short time. And to Chris for all the great food, dancing and hilarious games.

And last but not least, thanks to Damian for his passionate, immense and endless love and for becoming such an important part of my live.

Table of Contents

Abbreviations

General

Δ-TRISPHAT	Δ-tris(tetrachloro-1,2-benzenediolato)phosphate(V)
ε	molar absorption coefficient ($mol^{-1}dm^3cm^{-1}$)
Φ	unwinding angle
λ	wavelength
λ_{exc}	excitation wavelength
λ_{max}	wavelength maximum
3WJ	three-way junction
4WJ	four-way junction
A	adenine
ADD	1,1'-(azodicarbonyl)dipiperidine
AFM	atomic force microscopy
ATP	adenosine-5'-triphosphate
bpy	bipyridine
C	cytosine
ct-DNA	calf thymus DNA

CCDC	Cambridge crystallographic data centre
CD	circular dichroism
COSY	^{1}H-^{1}H correlation spectroscopy
Cys	cysteine
CuAAC	copper(I)-catalyzed azide-alkyne cycloaddition
DAPI	4’,6-diamidino-2-phenylindole
dba	dibenzylidenacetone
DEAD	diethyl azodicarboxylate
DNA	deoxyribonucleic acid
DOSY	diffusion-ordered NMR spectroscopy
dppf	1,1’-bis(diphenylphosphino)ferrocene
dppz	dipyrido[3,2-a:2’,3’-c]phenazine
EB	ethidium bromide
EDTA	ethylenediaminetetraacetic acid
en	ethylenediamine
FW	formula weight
G	guanine

His	histidine
HIV	human immunodeficiency virus
HMG	high mobility group
HPLC	high-performance liquid chromatography
HSQC	heteronuclear single-quantum correlation spectroscopy
IC_{50}	half maximal inhibitory concentration
ICD	induced circular dichroism
ILD	induced linear dichroism
LD	linear dichroism
MALDI-TOF	matrix-assisted laser desorption/ionization time of flight
MTT	3-(4,5-dimethylthiazol-2-yl)-2,5-diphenyltetrazolium bromide
NOE	nuclear Overhauser effect
NOESY	nuclear Overhauser effect spectroscopy
oc	open circular plasmid DNA
PAGE	polyacrylamide gel electrophoresis
PAH	polycyclic aromatic hydrocarbon
PCR	polymerase chain reaction

PCy_3	tricyclohexylphosphine
PDB	protein data bank
PNA	peptide nucleic acid
RNA	ribonucleic acid
sc	supercoiled plasmid DNA
T	thymine
TAE	Tris-Acetate EDTA
Taq	DNA polymerase
TATA	eukaryotic DNA sequence TATAAATA
THAP	2,4,6-trihydroxyacetophenone
THF	tetrahydrofuran
UV-Vis	ultraviolet-visible spectroscopy

Used in NMR listings

δ	chemical shift
br	broad
C_q	quaternary carbon
d	doublet
dd	doublet of doublets

ddd	doublet of doublets of doublets
J	coupling constant
m	multiplet
NMR	nuclear magnetic resonance
s	singlet
t	triplet

Used in MS listings

EI	electron impact ionization
ES	eletrospray ionization
MS	mass spectrometry

Used in infrared listings

ν	wavenumber
br	broad
FTIR	Fourier transform infrared
m	medium
s	strong
w	weak

Chapter 1. Introduction

This thesis focuses on the design and synthesis of novel metallo-supramolecular structures that might potentially bind DNA structures. To set out the scene, a short introduction on DNA is presented in this chapter, as well as the different known binding modes that natural and synthetic agents use to recognize DNA structures. A brief insight into metallo-supramolecular chemistry is also given and reviewed.

1.1. Introduction to DNA

DNA is the acronym for deoxyribonucleic acid. It is the key component of chromosomes and provides information about how to build proteins. In chromosomes, DNA is tightly packed and complexed with a histone (8 protein units) forming a DNA-protein complex called a nucleosome.[(1)] DNA is a polymer formed by deoxyribonucleotides that are connected through phosphodiester bonds. These deoxyribonucleotides are made up of three components: a five carbon sugar (2'-deoxy-D-ribose), a nitrogenous base that can be a pyrimidine (cytosine or thymine) or a purine (adenine or guanine) and a phosphate group (Figure 1.1).

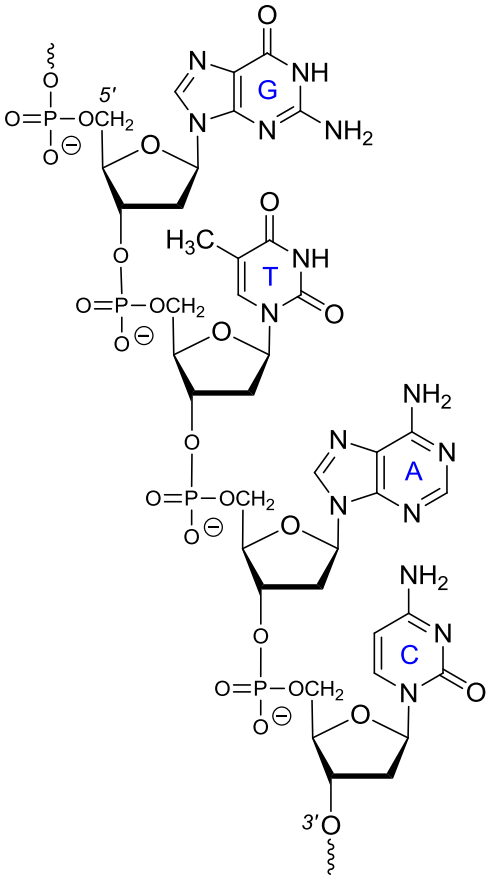

Figure 1.1: Polynucleotide chain of DNA.

In cells, DNA forms a double helix when two polynucleotide strands coil around a common axis.[2] The strands are antiparallel with opposite polarity; one goes from 5' to 3' whereas the complementary strand goes from 3' to 5' (Figure 1.2).[3] In standard DNA, the bases are not randomly arranged. Adenine (A) is always paired with a thymine (T) on the complementary strand and vice versa, and guanine (G) is always paired with cytosine (C) and vice versa. The paring occurs via hydrogen bonds, two for A-T and three for G-C, holding the two strands of the duplex together.[4]

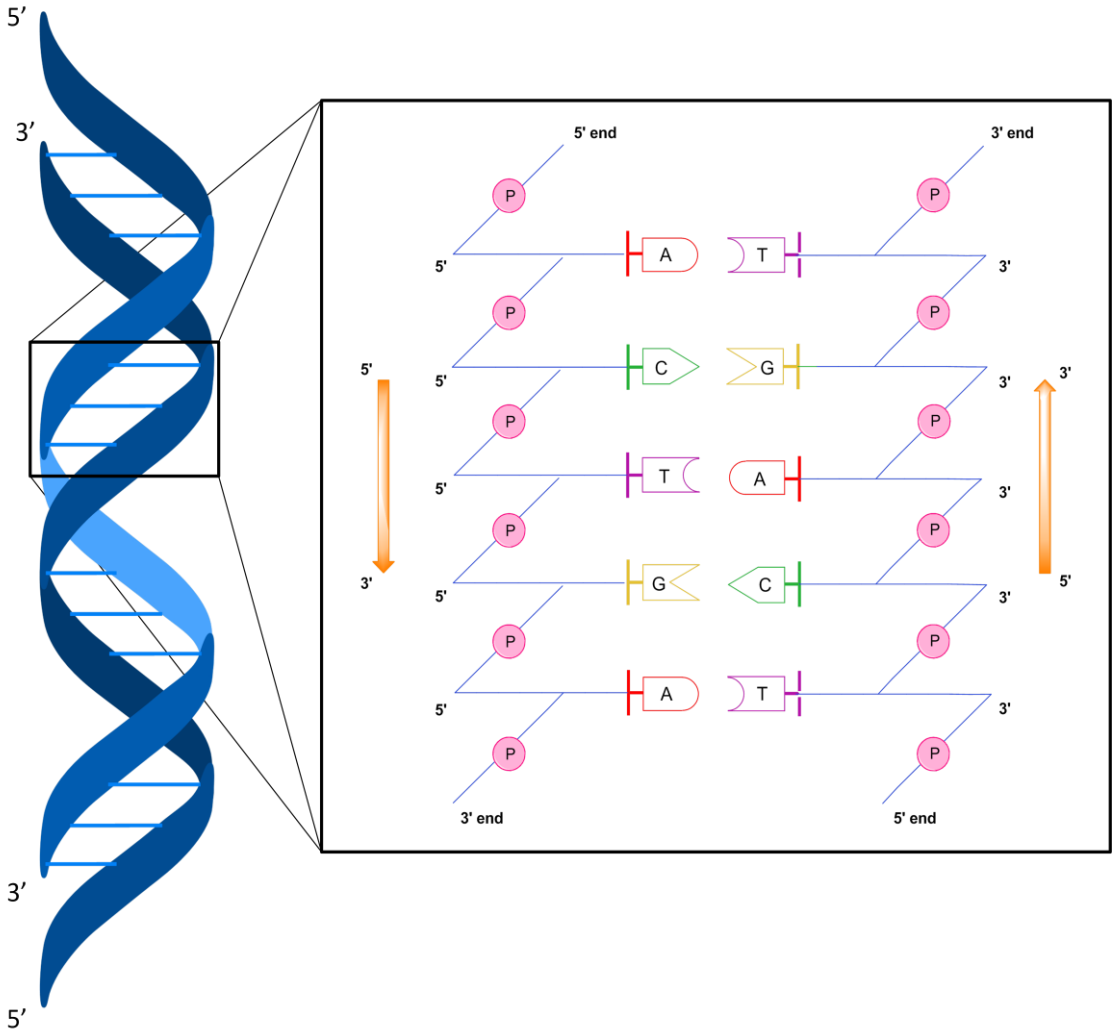

Figure 1.2: The antiparallel nature of the DNA double helix.

The primary structure of nucleic acids is the sequence of nucleoside monophosphates. As a result of the base pairing, the nucleic acid assumes a form which is called the secondary structure, such as A-DNA, Z-DNA and B-DNA (Figure 1.3). The latter is the form that predominates in the aqueous environment of the cell. The tertiary structure is the three-dimensional shape of how the entire linear polymer is folded.

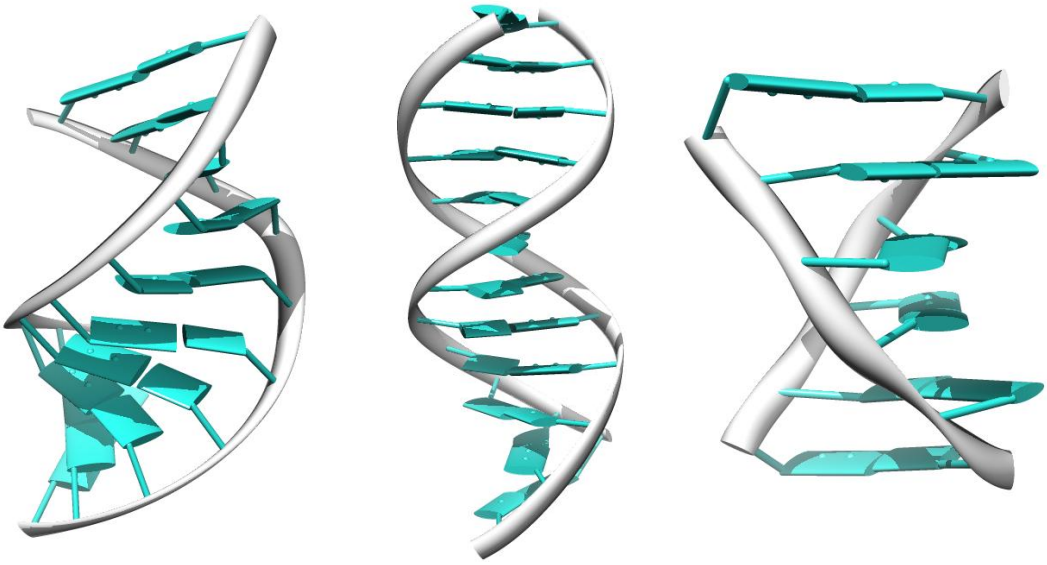

Figure 1.3: Comparison of the A-DNA (PDB 440D)[5] (left), B-DNA (PDB 1BNA)[6] (centre) and Z-DNA (PDB 2DCG)[7] (right) forms of the DNA double helix.

B-DNA is a right handed duplex and is present in more than 90% of known DNA sequences. Under ideal conditions, the diameter of the B-DNA helix is 2 nm. The distance required to complete one helical turn (360º) or pitch is 3.54 nm. As there are 10.4 base pairs in each turn of the helix, the distance between each base pair is 0.34 nm. The pairing of the non-symmetric bases and their stacking, at a 36º torsion angle, gives a small, narrow and shallow (minor) groove and a large, wide and deep (major) groove.[8]

A-DNA is a right handed helix with major and minor grooves equal in width due to the particular orientation of its base pairs. To this date, there is no evidence of the presence of this DNA form in any living organism, however it can be found in double-stranded RNA and DNA-RNA hybrids.[1]

Z-DNA is a left handed helix where pyrimidine bases alternate with purine bases in *anti* and *syn* conformations, respectively. As a result of this, the sugar-phosphate backbone of Z-DNA forms a zigzag pattern, where the major groove is barely apparent and the minor groove is deep and narrow.[1]

1.2. DNA recognition modes

In the 1960's five different modes of molecular recognition of DNA were established: major groove recognition, minor groove recognition, intercalation between the base pairs, backbone binding and binding to the bases.[9] The first four binding modes are non-covalent and the interaction is mainly electrostatic or via hydrogen bonding, while the last one forms covalent bonds to the DNA bases. Recently new ways have been reported for recognition of other DNA structures (*vide infra*).

1.2.1. Major groove recognition

The DNA major groove is targeted by many proteins and large synthetic or semi-synthetic agents. However, since most synthetic drugs are relatively small for the major groove, little research has been focused in the recognition of the DNA major groove.[10]

1.2.1.1. Major groove recognition by proteins

Proteins can recognize both DNA grooves, but tend to bind in the DNA major groove due to the dimensional difference between the grooves.[11]

Proteins interact with DNA by electrostatic attraction, hydrogen bonding, bridging water molecules and Van der Waals contacts. The protein surfaces that interact with the DNA are enriched with positive charges from lysine and arginine aminoacids. This positive charge acts as the main force for the protein–DNA interaction, approaching the negatively charged DNA phosphate backbone. Even if dominant, this attraction is not sequence-specific as the negative charge from the DNA backbone is all over the DNA. Sequence-specificity is dictated by hydrogen bond interactions. In 90% of the cases, proteins act as the hydrogen bond donor group and DNA as the acceptor group.[12]

Van der Waals contacts also contribute in some degree to sequence-specificity as the right geometry and shape are required for a perfect contact. Only the α-helix domain of the protein interacts with the DNA major groove. The α-helix must be tilted to sit in the major groove as α-helices normally have 3 turns or more (Figure 1.4b). If it stays parallel to the groove it will not fit (Figure 1.4a).[13]

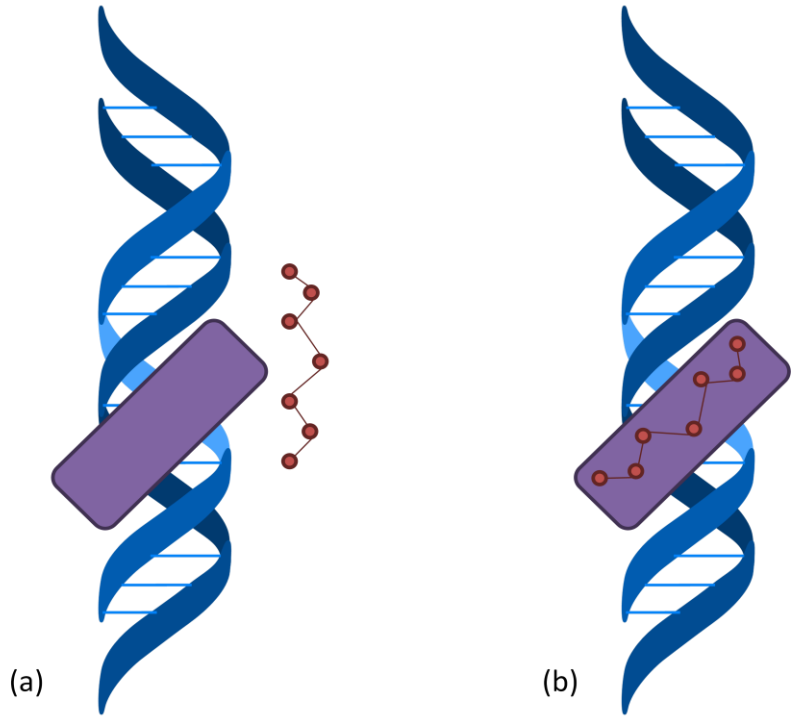

Figure 1.4: Docking of α-helix domain of proteins in the DNA major groove. Purple area highlights the available region for protein interaction.

Proteins that are found to recognize the DNA major groove are helix-turn-helix proteins, zinc finger proteins, leucine zipper proteins[9] and enzymes from prokaryotic and eukaryotic organisms.[14]

Zinc finger proteins (typically Cys_2His_2) usually contain several units or fingers that make simultaneous contacts along the DNA. Each finger possesses a ββα domain with a zinc metal ion tetrahedrally coordinating two cysteins of the antiparallel β-sheet and two histidines of the α-helix (Figure 1.5).[14,15]

Figure 1.5: Crystal structure of the zinc finger domain of KLF4 bound in the DNA major groove (PDB 2WBU).[15]

1.2.1.2. Major groove recognition by oligonucleotides

Oligonucleotides (synthetic or natural) can recognize the major groove of DNA via hydrogen bonding to the purine bases, forming a triple stranded DNA or Hoogsteen motif (H-DNA) (Figure 1.6).[16]

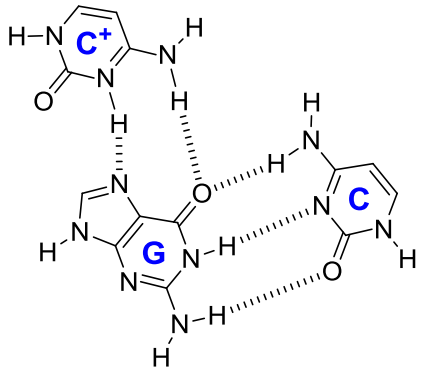

Figure 1.6: Example of a Hoogsteen G:C·C^+ base contact.

This can be used to artificially control the gene expression via the antigene approach. The third strand can be designed to bind in a specific sequence of the duplex DNA of a given gene and inhibit it.[17] However there are some limitations; for example not all diseases have DNA targeting sequences to form a triple helix, or nucleases can digest the oligonucleotide before it arrives in the cell.[18] Also, oligonucleotides do not selectively bind DNA, they can also bind RNA.[9]

1.2.1.3. Major groove recognition by peptide nucleic acids (PNAs)

In 1991 Nielsen *et al.*[19] reported the formation of a neutral oligonucleotide by replacing the sugar phosphate backbone with a polyamide (peptide-like backbone) and called them PNAs (Figure 1.7).

They usually invade the DNA double helix and displace one DNA strand to form $(DNA)(PNA)_2$ triplexes (Figure 1.7).[20]

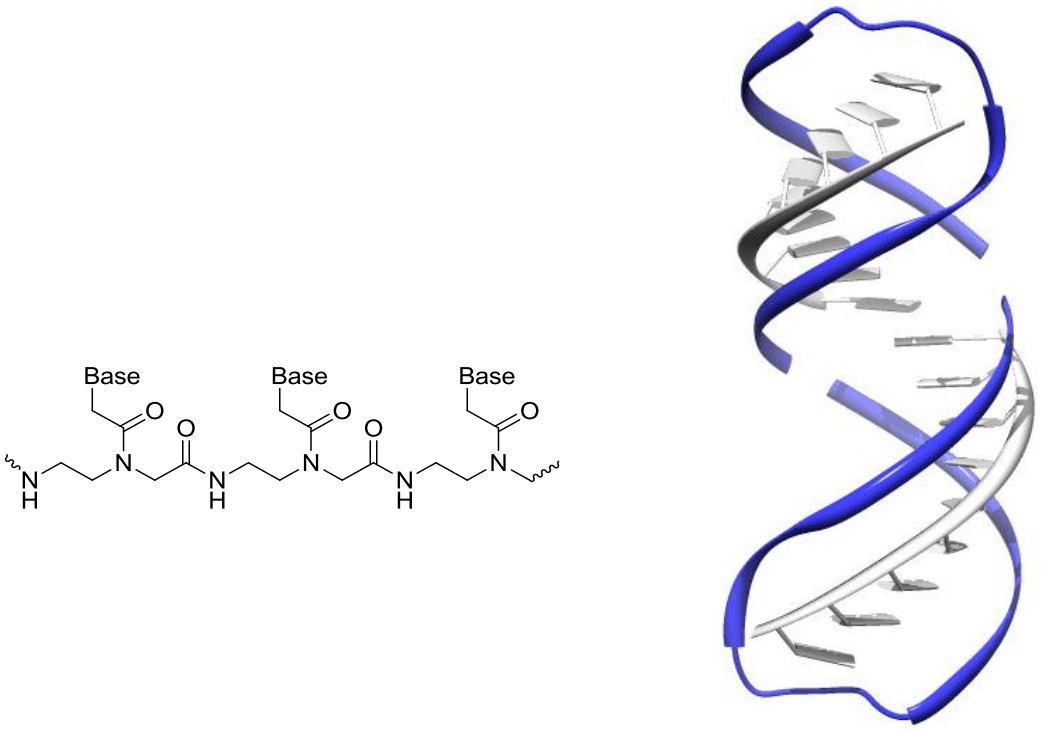

Figure 1.7: General structure of a PNA (left) and PNA complexed with DNA forming a $(DNA)(PNA)_2$ triplex (PDB 1PNN)[20] (right).

1.2.1.4. Major groove recognition by calix[n]arenes

A calix[n]arene is a macrocyclic oligomer formed by hydroxyalkylation of a phenol and an aldehyde. They have a hydrophobic cavity that can hold small molecules or ions. Metallacalix[n]arenes are calix[n]arenes in which the methylene has been replaced by a metal ion and the phenol ring by a bent nitrogen heterocycle.[21] Calix[n]arenes and metallacalix[n]arenes are known to give a variety of host-guest interactions.[22,23]

Recently it has been proposed that metallacalix[4]arenes (Figure 1.8) can bind in the major groove of DNA via non-covalent interactions, as seen by different spectroscopic techniques and AFM studies.[24]

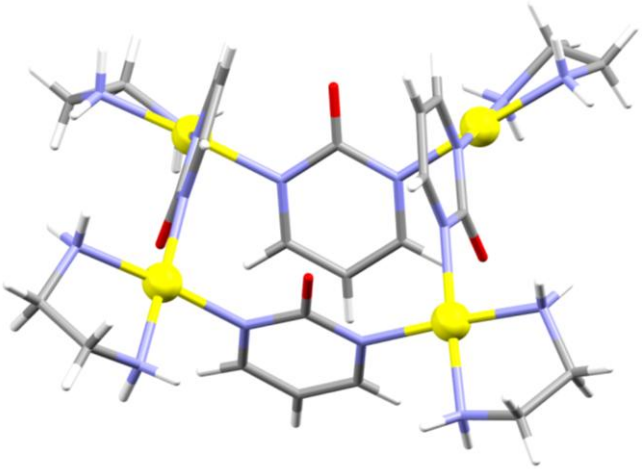

Figure 1.8: Crystal structure of a platinum-calix[4]arene (CCDC 146631).[25]

Positively charged dimeric calix[4]arenes (Figure 1.9) have also been shown to interact with the DNA major groove, via hydrogen bond interactions between the top cationic moieties of the calix[4]arene and the DNA bases and the negatively charged phosphate backbone. Minor groove insertion and intercalation are precluded due to the large dimensions of the dimeric calix[4]arene (3 nm x 1 nm).[26,27]

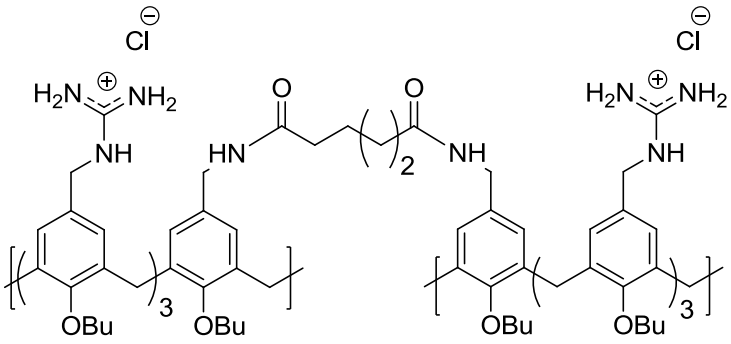

Figure 1.9: Dimeric calix[4]arene shown to recognize the DNA major groove.

1.2.2. Minor groove recognition

The driving forces for the interaction between the DNA minor groove and natural and synthetic agents are electrostatic interactions with the phosphate backbone at the walls of the groove, van der Waals contacts, hydrophobic interactions and hydrogen bonding.[28] A crescent shape of the minor groove binder is a requirement for effective van der Waals contacts. Some sequence specificity is observed in hydrogen bond interactions between the base pairs and the minor groove agent. Some selectivity is also evident towards AT rich regions as they have an overall negative charge and produce a narrower and deeper groove than GC rich regions.[11,29]

The most common examples of minor groove binders are distamycin A, and netropsyn (natural molecules), diarylamidines (DAPI, berenil, and pentamidine) and bis-benzimidazoles (Hoechst 33258) (Figure 1.10).[29]

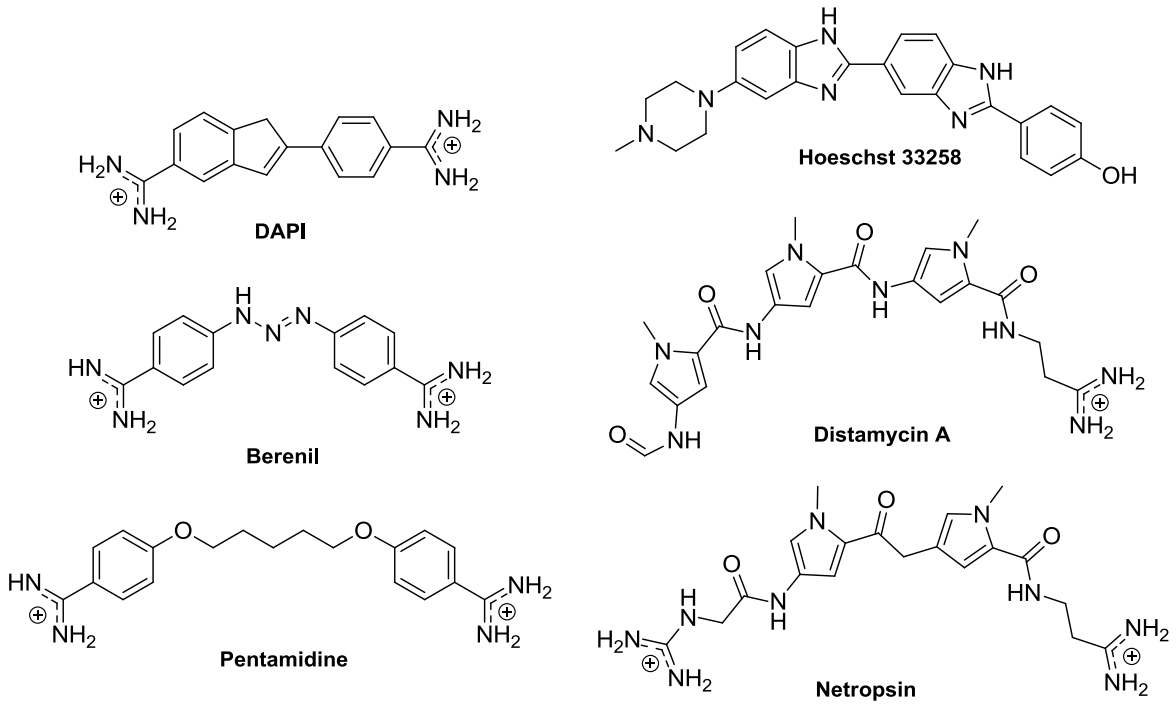

Figure 1.10: Structures of some minor groove binders.

1.2.2.1. Minor groove recognition by natural agents

Distamycin A is a natural cationic minor groove binder. It is an antibiotic with an oligopeptide structure with three pyrrole rings. It shows high affinity for AT rich regions in the DNA minor groove. It can be found as a 1:1 complex [30] as well as an antiparallel 2:1 complex[31,32] (Figure 1.11).

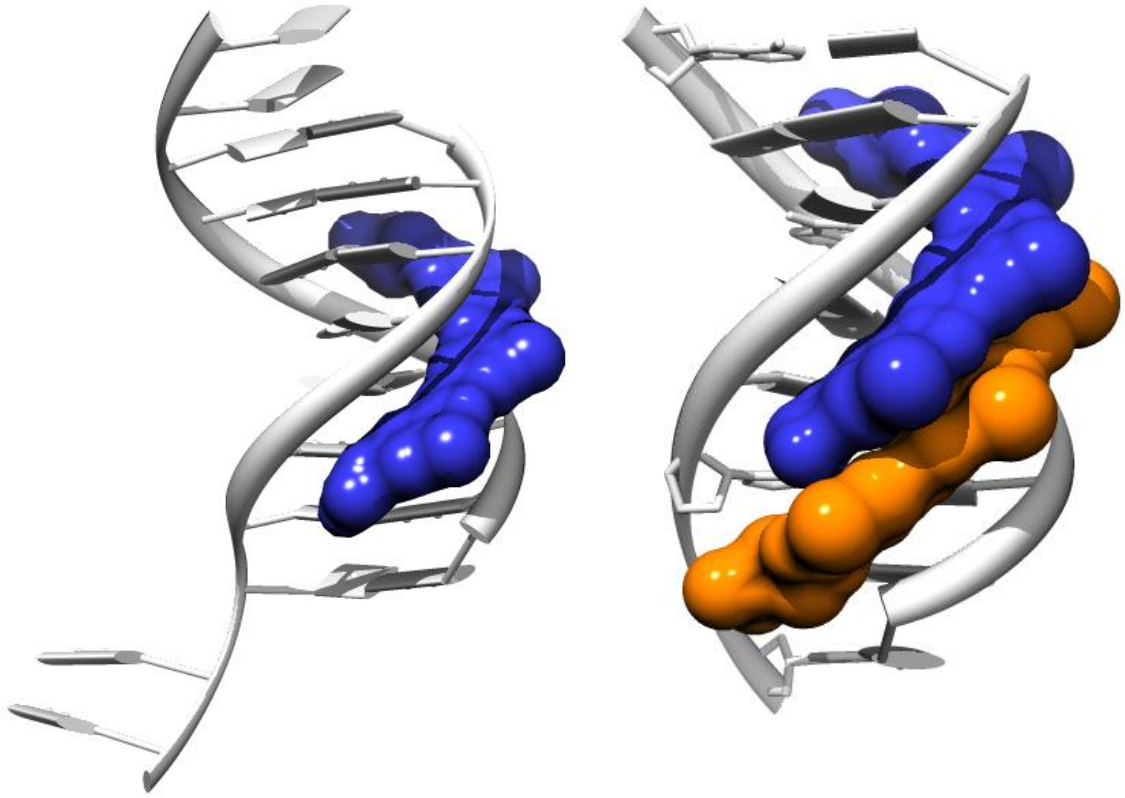

Figure 1.11: Distamycin A complexed with DNA in a 1:1 ratio (PDB 1JTL)[30] (left) and in a 2:1 ratio (PDB 1JUX)[32] (right).

When acting as a stacked dimer, distamycin A is able to bend five or six AT base pairs. This results in a change in the directionality of the curvature. As a monomer, distamycin A bends the DNA towards the minor groove, while when acting as a dimer it bends the DNA towards the major groove. This could be used for the modulation of DNA transcription, as by altering the major groove shape some of these transcription factors might have a reduced affinity to DNA.[33]

1.2.2.2. Minor groove recognition by synthetic agents

During many years research has been focused on the design of synthetic minor groove binders which consequently had clinical application as anti-cancer, anti-viral and anti-bacterial agents.

Pentamidine is an antimicrobial drug used for the treatment of severe pneumonia in HIV-positive patients and sleeping sickness.[9] A temporary caged aza-pentamidine (Figure 1.12) has been shown to be activated by light via cleavage of its protecting groups. This results in a control of its DNA binding properties and its antifungal activity triggered by light.[34]

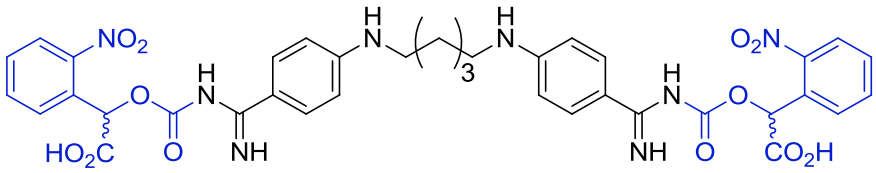

Figure 1.12: Caged aza-pentamidine (protecting groups shown in blue).

As well as electrostatic interactions with the phosphate backbone at the walls of the groove, van der Waals contacts, hydrophobic interactions and hydrogen bonding, water mediated binding interactions have also been detected in minor groove binders. The phenylamidine group of a DAPI derivative interacts via hydrogen bonding with the N3 of an adenine through a water molecule in the minor groove.[35,36]

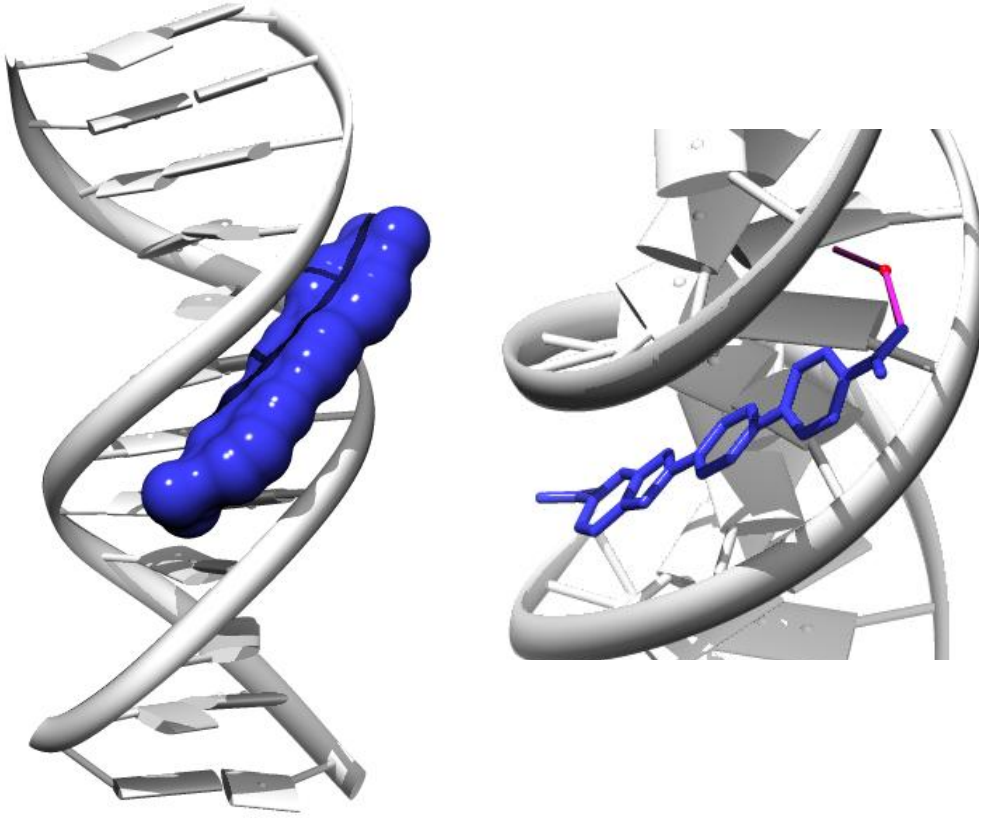

Figure 1.13: DAPI analogue binding in the DNA minor groove (left) and water mediated hydrogen bond contact (in pink) of DAPI analogue (right) (PDB 2B0K).[35]

Dervan and co-workers have created polyamides analogous to the natural distamycin A minor groove binder. These polyamides, which have an imidazole in place of a pyrrole, follow the same binding principle of the distamycin A dimer discussed above. The heterocyclic rings of one strand interact via π-stacking with the amide groups on the other strand. Also, the new imidazole nitrogen introduced into the ring can form hydrogen bonds with the NH_2 of guanine bases.[37,38]

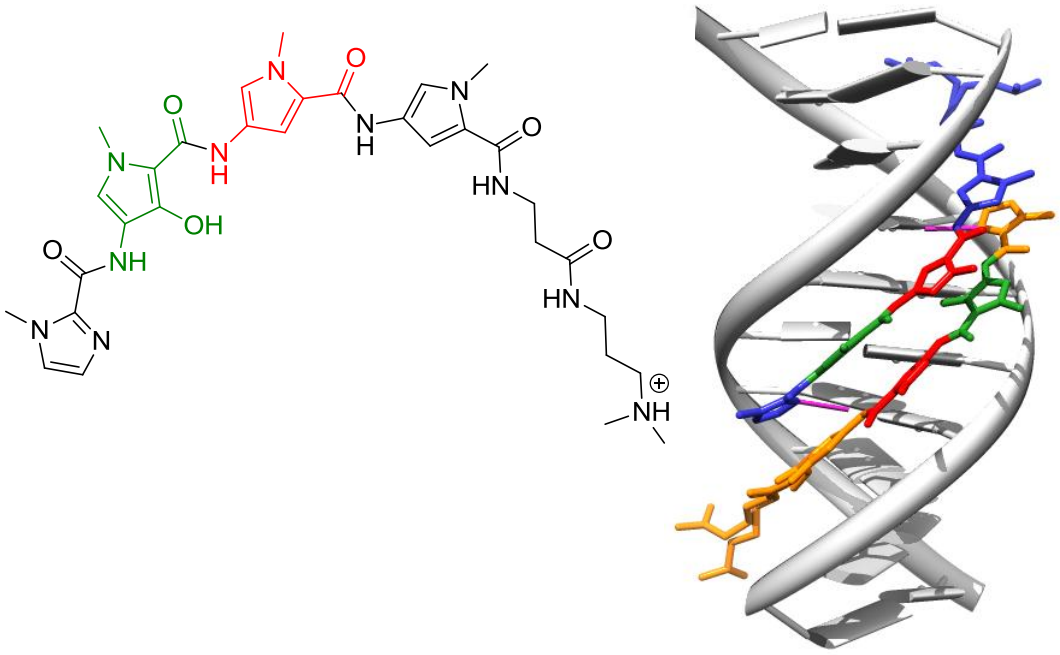

Figure 1.14: Structure of polyamide (left) and two polyamide strands in the DNA minor groove (PDB 407D)[38] (right).

Analogous polyamide linked dimers have been shown to span eleven to sixteen base pairs in the minor groove[39] (traditional minor groove binders recognize only three or four base pairs).

1.2.2.3. Minor groove recognition by proteins

Proteins usually bind in the major groove due to their relatively large size; however they can also bind in the minor groove. TATA binding proteins are an example.[40] In the recognition process, the minor groove opens up and the DNA double helix is unwound by 120º and bent by 80º, compressing the major groove. The interaction occurs between the β-sheet domains of the protein and the hydrophobic regions of the groove (Figure 1.15).[41]

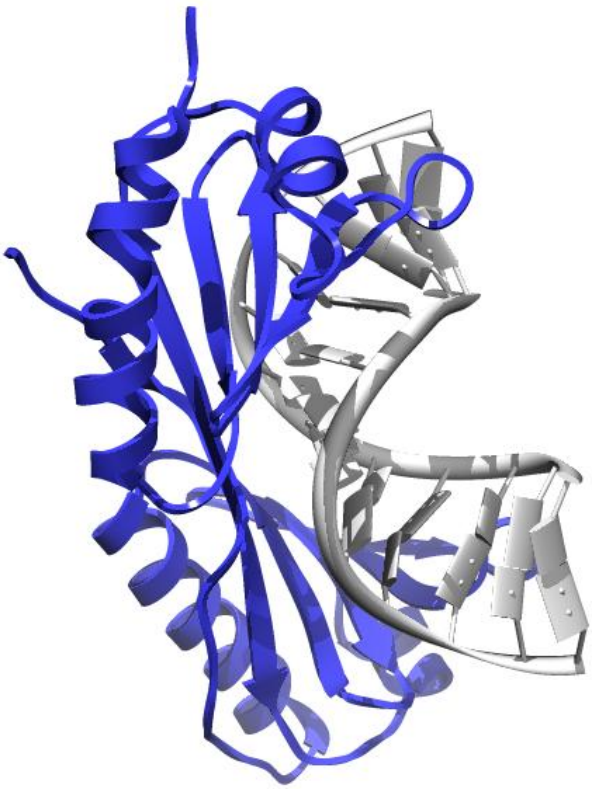

Figure 1.15: TATA-binding protein recognizing the DNA minor groove (PDB 1TGH).[41]

1.2.3. Intercalation

In 1961 Lerman suggested that small planar polycyclic, electron-deficient, aromatic molecules can recognize DNA through intercalation, using the hydrophobic cavity between two base pairs. Face-face π-π interactions are formed between the aromatic rings of the intercalator and the heterocyclic rings of the bases above and below it. The van der Waals contacts formed between the intercalator and the bases sandwiching the intercalator are more favourable than similar contacts between the bases themselves.[42] This interaction can be reinforced by ionic forces between a positive charge in the intercalator and the negatively charged sugar phosphate backbone of the DNA. Transcription,

replication and DNA repair processes can be inhibited due to the structural modifications caused by the intercalator binding, such as unwinding of the DNA double helix.[43] Usually the size of these drugs is around two to three six-membered rings.

Examples include; proflavine, ellipticine, ethidium bromide, doxorubicin, daunomycin and daunorubicin (Figure 1.16).

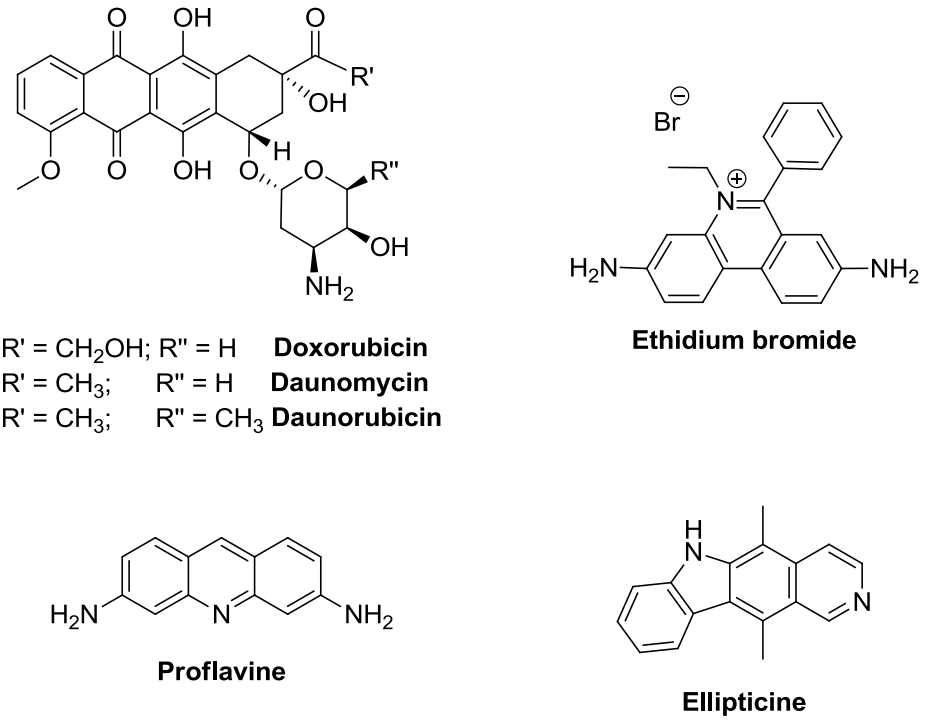

Figure 1.16: Structures of some intercalator agents.

A positive charge can be introduced in an intercalating drug by incorporating a transition metal.[44-46] The first example of these intercalators is based on a square planar platinum(II) terpyridine unit synthesized by Lippard (Figure 1.17).[47]

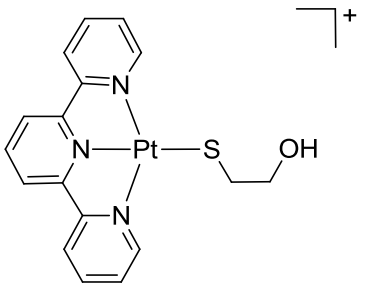

Figure 1.17: Platinum terpyridine intercalator drug.

Metals are attractive not only for the fact that they can impart a positive charge to the drug, but also other characteristics such as luminescence (e.g. ruthenium(II) polypyridine complexes) and DNA cleavage properties (e.g. rhodium(III) centres acting through photoinduced oxidation) are important.

Recently, a ruthenium complex (Δ-$[Ru(bpy)_2(dppz)]^{2+}$) synthesised by Barton and co-workers has been crystallised with a DNA helix that bears two adenine:adenine (A:A) mismatches.[48] The crystal structure reveals that the ruthenium complex is able to intercalate through the minor groove between the mismatched bases via metalloinsertion and between the non-mismatched bases via metallointercalation (Figure 1.18). Binding at the mismatched site results in the mismatched adenine bases being pushed out of the helical core (in dark grey in Figure 1.18) and an enhanced luminiscence.[49]

The related Λ-$[Ru(phen)_2(dppz)]^{2+}$ complex has shown perpendicular and canted intercalation in a non-mismatched DNA duplex.[50]

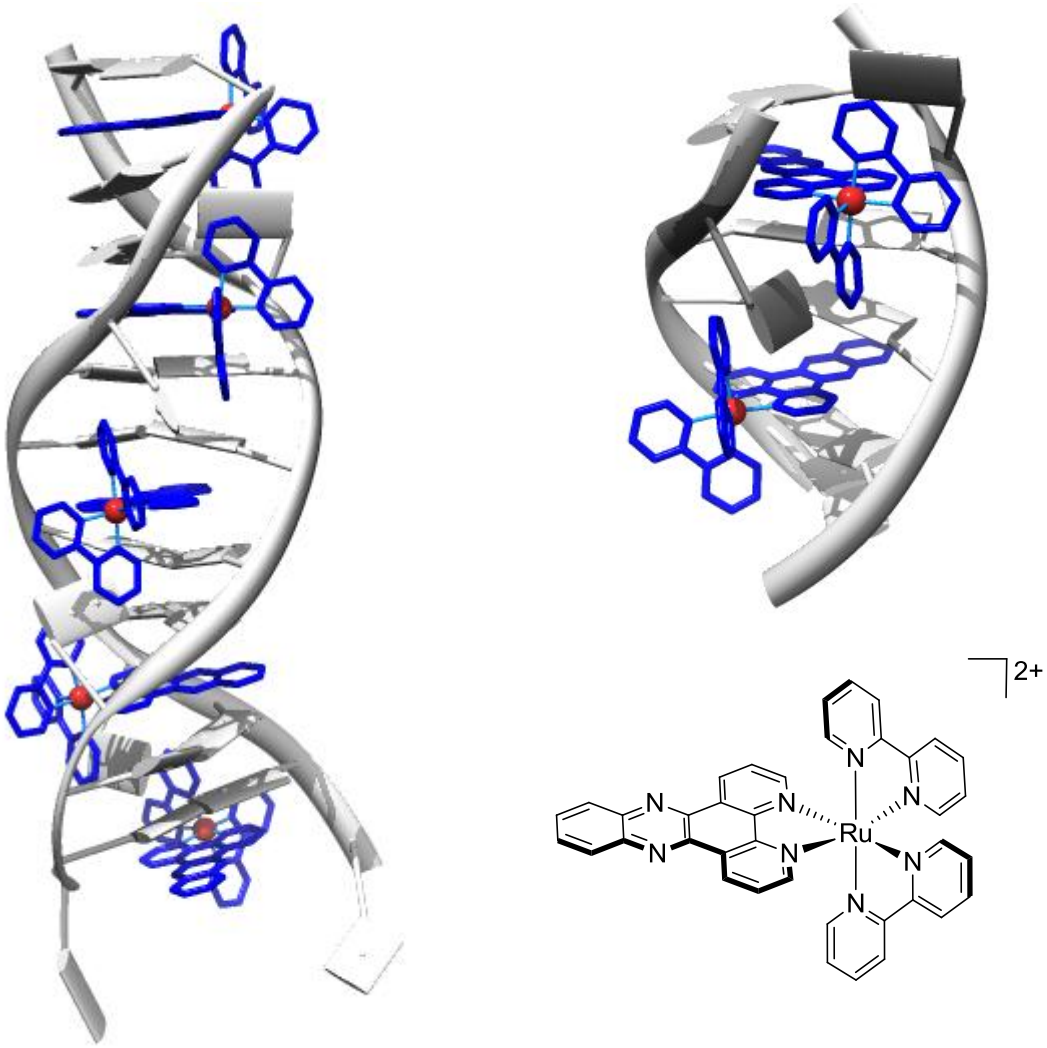

Figure 1.18: Δ-[Ru(bpy)$_2$(dppz)]$^{2+}$ complex (bottom right) inserted in a mismatched A:A DNA double helix (left) and metalloinsertion and metallointercalation of ruthenium drug (top right) (PDB 4E1U).[49]

Another approach used in the design of intercalating drugs is the combination of two intercalators, forming bis-intercalators. These are linked by a flexible chain that is suficiently long enough to allow the two intercalators to insert into two sites on the same DNA duplex.[9]

The bis-intercalator in Figure 1.19 shows a rapid formation of the mono-intercalated adduct that is then slowly converted into the thermodynamically more stable bis-intercalated adduct.[51]

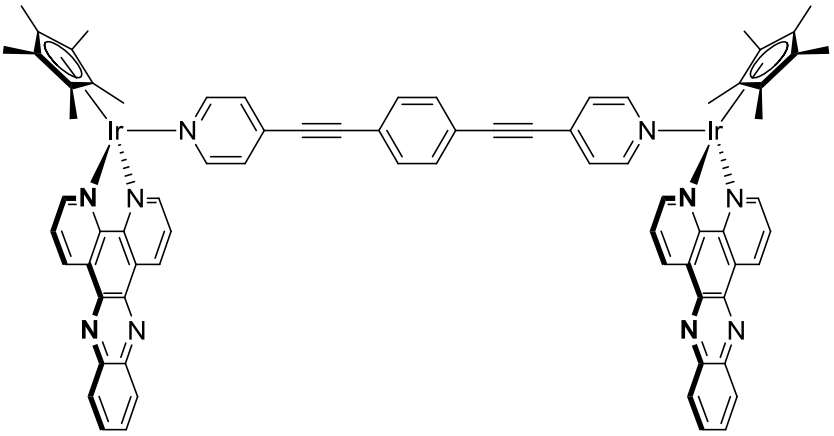

Figure 1.19: Structure of iridium bis-intercalator.

1.2.4. Backbone binding

The sugar-phosphate DNA backbone has a hard oxygen-rich polyanion surface that can interact with metal cations from groups I and II. Also, proteins with cationic residues like arginine can interact by hydrogen bonding.

Farrell has developed an octacationic trinuclear platinum backbone binder that can bind along the phosphate backbone or stretch across the minor groove making hydrogen bond contacts (shown in pink in Figure 1.20) with the phosphate backbones on either side.[52-54]

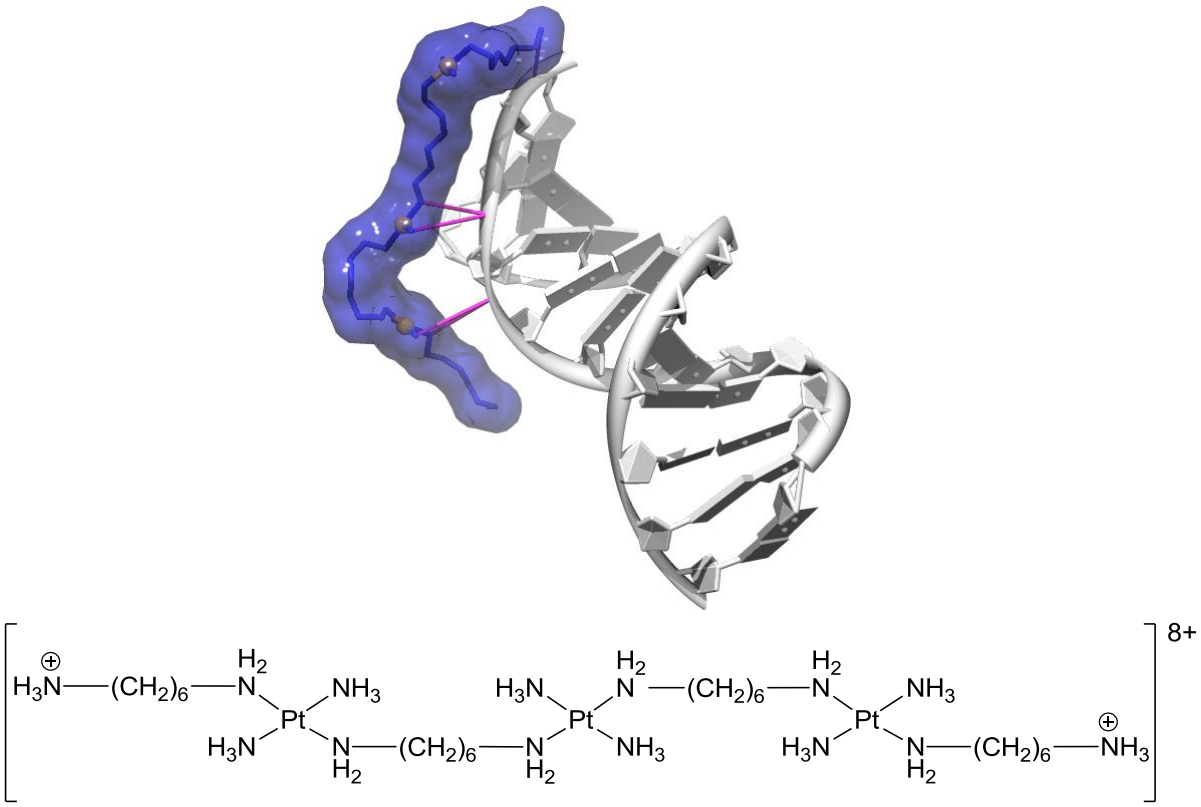

Figure 1.20: Farrell's octacationic backbone binder (PDB 2DYW).[52]

1.2.5. Binding to the DNA bases

This is the most common form of DNA recognition used by clinical drugs. It involves a covalent link between the drug and DNA. It shows certain sequence preference to N7 of guanine bases in the major groove and to a lesser extent to adenine bases.

The most renowned compound that recognizes DNA by binding to its bases is cis-diamminedichloroplatinum(II), known as cisplatin. Cisplatin is the most successful anticancer agent in the clinic. It is very effective against testicular cancer and plays an important role in the treatment of ovarian, head, neck,

cervical and bladder cancers, as well as melanomas and lymphomas.[55] Cisplatin forms bifunctional DNA cross-links, with the 1,2-intrastrand GG crosslink between adjacent guanines being the most significant one.[56] The binding of cisplatin to guanine bases causes the DNA to bend or kink at around 45º, affording a wider and flatter minor groove opposite the platination site (Figure 1.21).[57,58] This specific structural motif is believed to be the cause of cell death. One hypothesis suggests that HMG-domain proteins (nuclear high-mobility group proteins) recognize this motif and therefore the DNA repair processes cannot occur. The other hypothesis, which is not exclusive, is based on the fact that HMG-domain proteins are kept away from their natural binding site and this causes cell stress which ends up in cell death.[55]

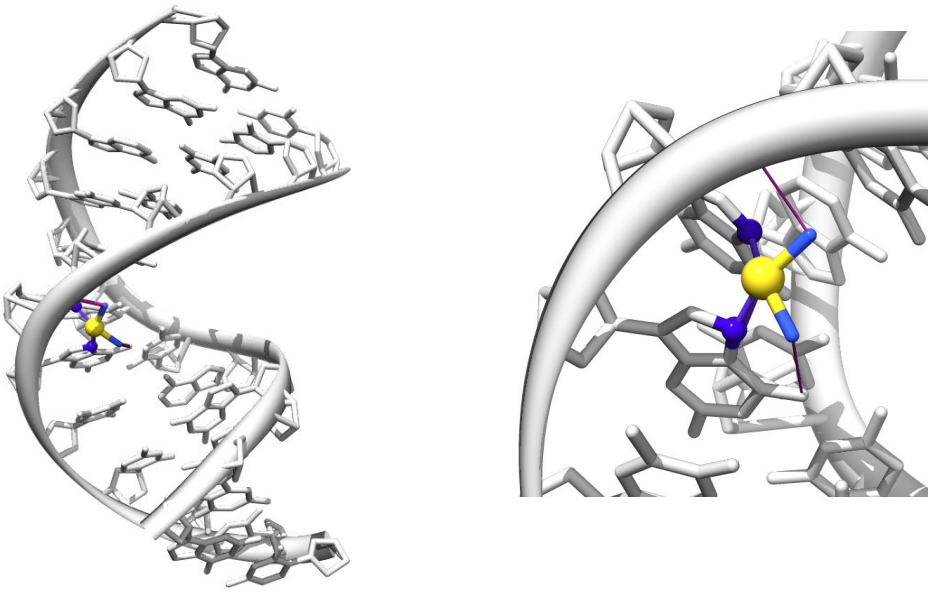

Figure 1.21: Kinking of DNA double helix upon cisplatin binding (left) and coordination of cisplatin to N7 (dark blue) of two adjacent guanines (hydrogen bonding to phosphate backbone in pink) (right) (PDB 1AIO).[57]

Following the success of cisplatin, five other platinum based derivatives entered into the clinic; oxaliplatin and carboplatin (worldwide) and nedaplatin, lobaplatin and heptaplatin (regionally) (Figure 1.22).[59,60] They work in a similar fashion to cisplatin, however their reactions are much slower. These DNA binding kinetics cause less toxic effects which is important since one of the main drawbacks of cisplatin are its side effects and toxicity.[61]

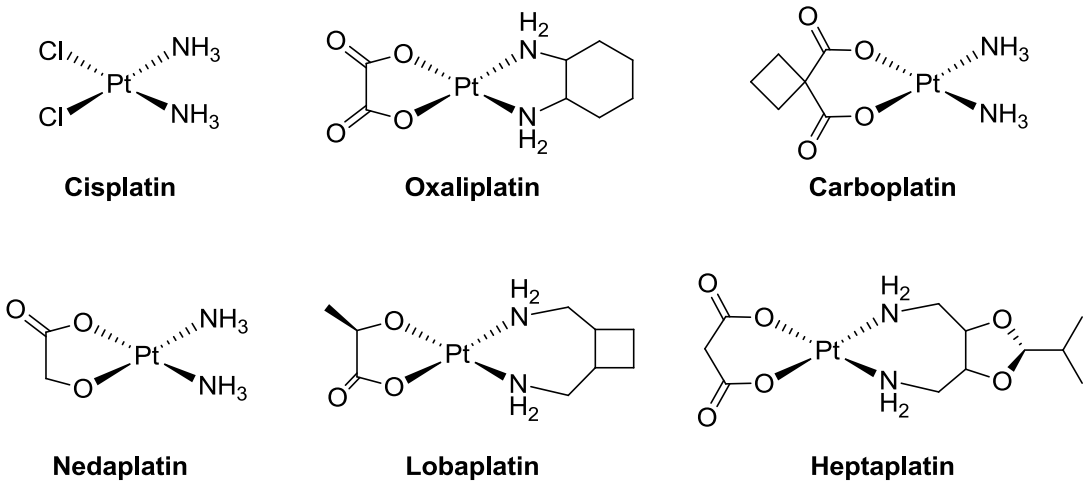

Figure 1.22: Platinum-based drugs.

1.2.6. Recognition of other DNA structures

Synthetic molecules not only recognize the double helix of DNA. Higher order structures, such as nucleosomal DNA, triplex and tetraplex DNA and DNA junctions, can also be targeted.

1.2.6.1. Nucleosomal DNA

Dervan's polyamides that bind in the minor groove can also bind higher order structures such as nucleosomes.[62] Nucleosomes are found in chromosomes, where DNA is wrapped around small basic proteins called histones.[63] This wrapping yields two sections of double helical DNA that are adjacent to each other. Therefore, two linked polyamides are able to bind to two adjacent minor grooves in the nucleosome (Figure 1.23).[62]

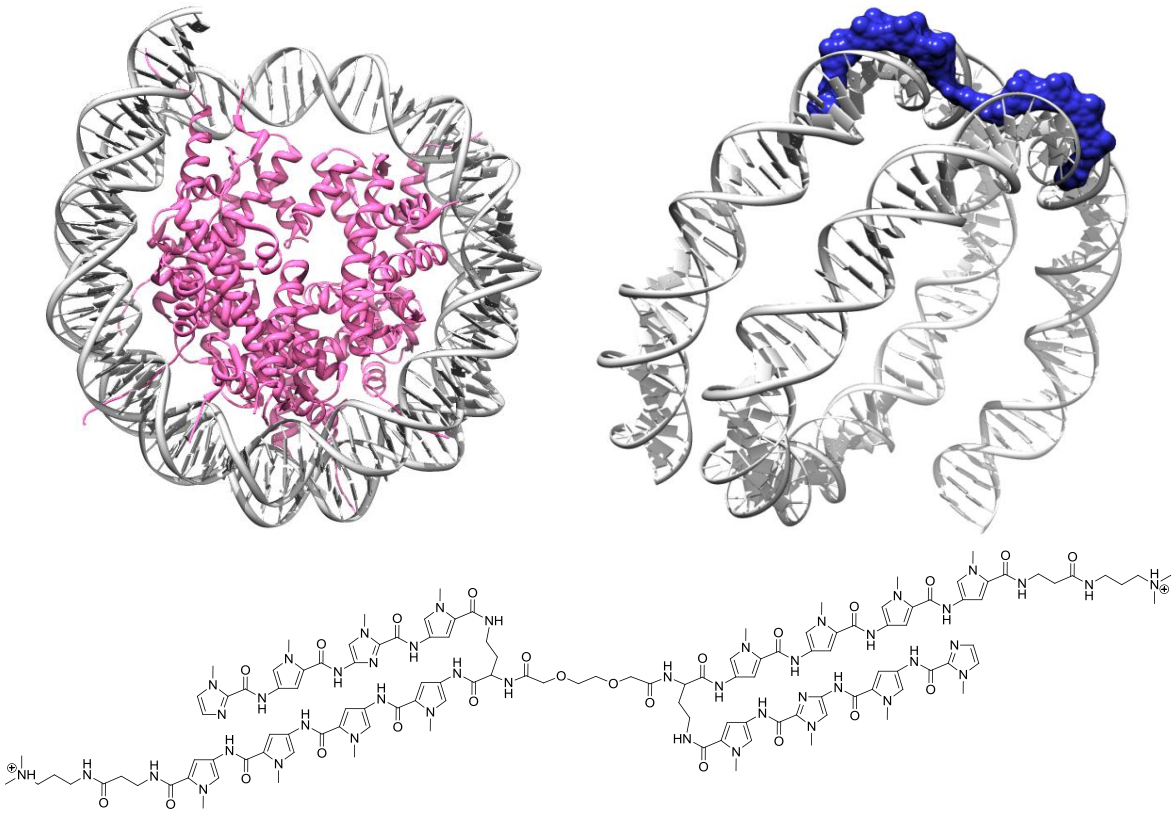

Figure 1.23: DNA wrapped around histone proteins (pink) in the nucleosome (left), linked polyamide recognizing nucleosomal DNA (protein structure removed for clarity) (right) (PDB 1S32)[62] and structure of linked polyamide (bottom).

1.2.6.2. Triplex DNA

Triplex DNA is not as stable as duplex DNA, even when there is specificity on sequence recognition of the third oligonucleotide strand. This is due to the electrostatic repulsion of the three phosphate backbones.[64] Therefore, triplex-binding ligands have been used to increase the oligonucleotides binding strength on triplex formation. These ligands are able to bind to triple helices and not to double helices, or they show a strong preference for triplex over duplex DNA. Several triplex binders have now been described, such as benzopyridoindoles, coralyne chloride, disubstituted amidoanthraquinones and naphthylquinolines[65] (Figure 1.24). These binders are able to intercalate between bases that form Hoogsteen motifs.

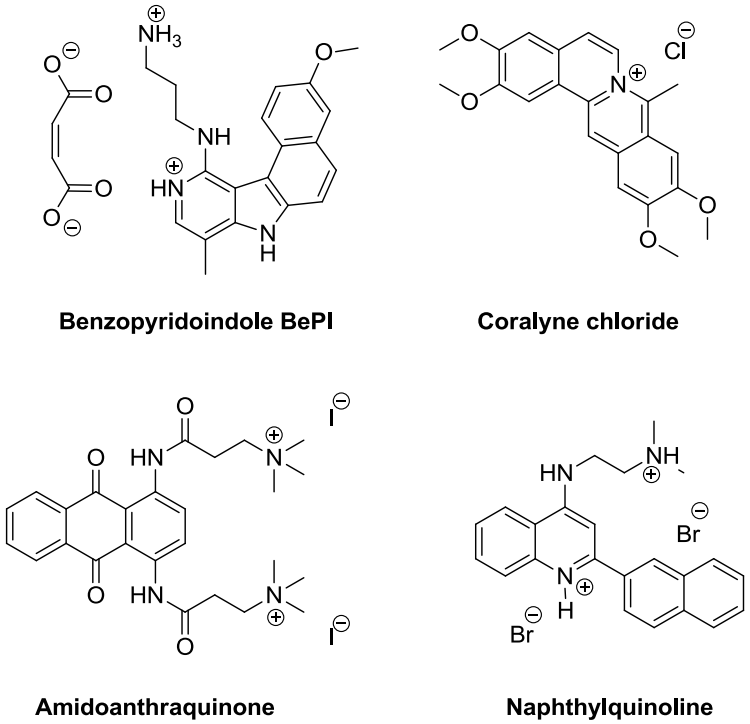

Figure 1.24: DNA triplex-binding ligands.

Triplex DNA structures are of great interest as they might help to understand cellular processes such as DNA transcription and gene expression. The formation of a triplex with a synthetic modified oligonucleotide strand, the so called antigene approach (*see section 1.2.1.2*), and the stabilization of triplex with triplex binders are two different approaches to attempt to interfere with the transcription of genes.[66,67]

1.2.6.3. Tetraplex (or quadruplex) DNA

In 2009, Elisabeth H. Blackburn, Carol W. Greider and Jack W. Szostak were awarded the Nobel Prize in Physiology or Medicine "for the discovery of how chromosomes are protected by telomeres and the enzyme telomerase".[68-70]

Telomeres are formed of short repetitive nucleotide regions (quadruplex) at the end of the chromosomes. In normal cells, telomeres shorten after each replication cycle as DNA polymerase cannot fully replicate the end sequence. This eventually leads to cell death. However, in cancerous cells the telomeric ends are stabilized by the action of the over-expressed enzyme telomerase. Telomerase is able to catalyze the synthesis of telomeric DNA. This means that there is not DNA loss during replication in cancerous cells. It is believed that the inhibition of telomerase in tumour cells would cause cell death. For this reason, quadruplex DNA has emerged as a new target for anti-cancer drugs.[11,71]

The quadruplex or tetraplex is made up of four strands and its DNA structure is rich in guanine bases (G-quadruplex). The G-quadruplex structure is

based on a planar tetrad with an electron-rich π-surface, where the strands are held together by Hoogsteen hydrogen bonds. The orientation of the strands can vary (parallel or folded and antiparallel) giving different structures according to the directionality of the strands and the connectivities of loop regions at their ends (Figure 1.25). The stability of these structures lies in base-stacking interactions.[72]

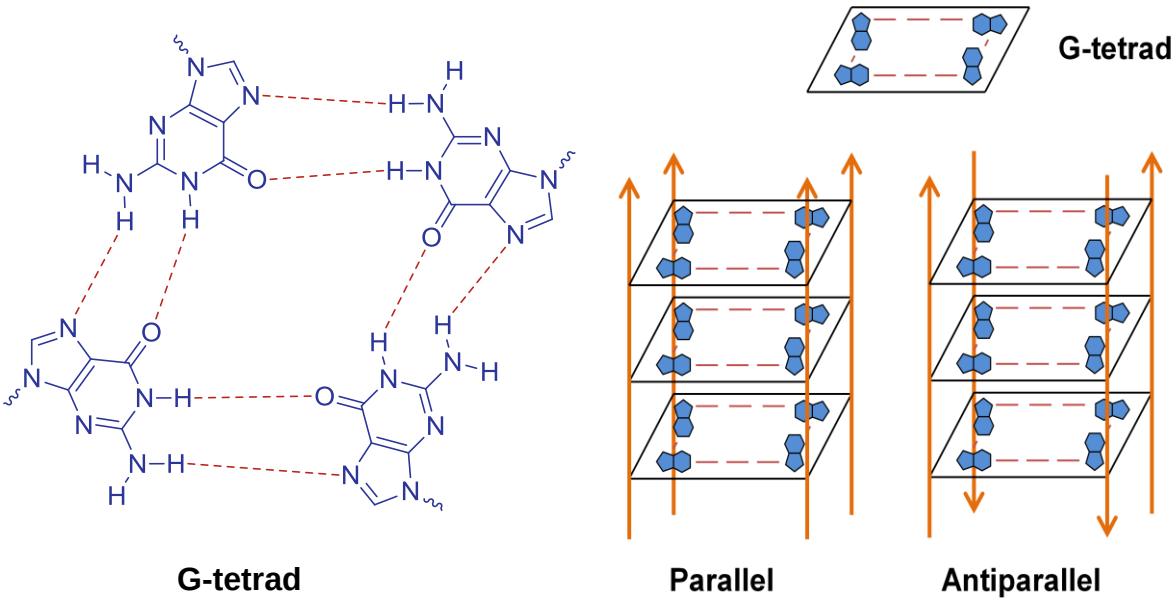

Figure 1.25: G-tetrad structure.

In 1991 Zahler demonstrated that K^+-stabilized G-quadruplex structures (Figure 1.26) could inhibit telomerase,[73] therefore great interest emerged in the design of small organic molecules that are able to bind to G-quadruplex and thus inhibit telomerase and disrupt telomeres.

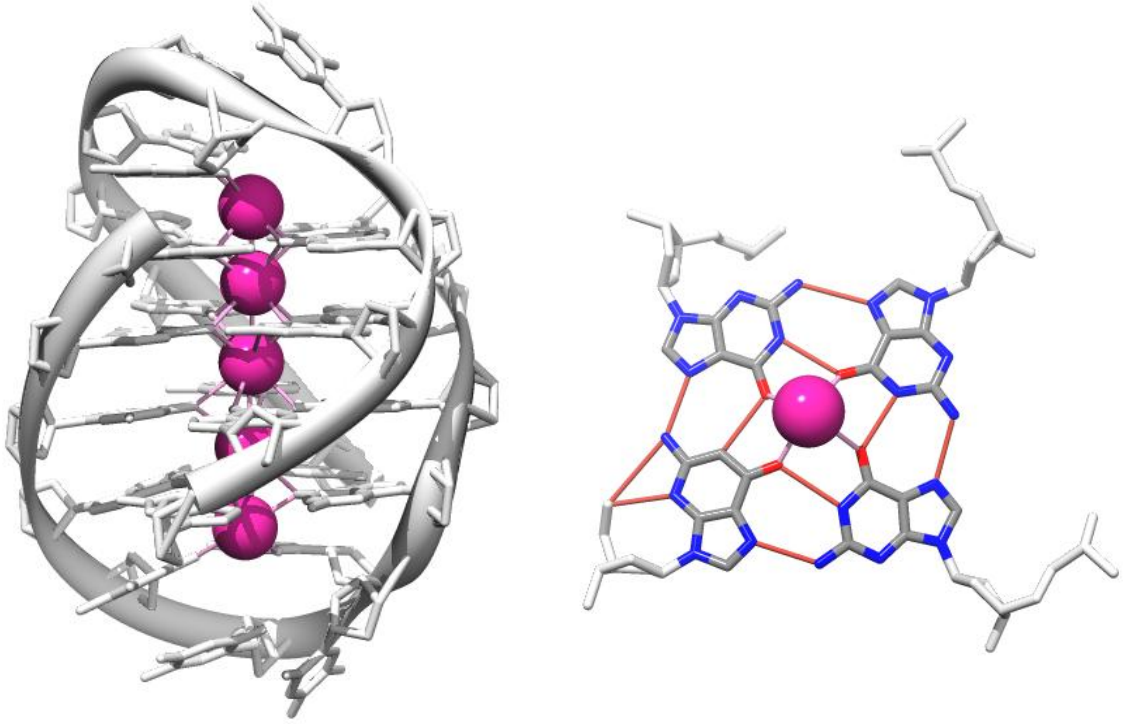

Figure 1.26: K^+-stabilized G-quadruplex DNA (left) and K^+ contacts with guanines (in pink) and Hoogsteen hydrogen bonds between guanines (in red) (right) (PDB 2GWE).[74]

Recently, a tetra-substituted naphthalene diimide compound functionalized with positively charged N-methyl-piperazine side chains has been shown to bind and thermally stabilize the 3'-ends of human telomeric G-tetrads of quadruplexes. The four side chains interact with the grooves of the quadruplex while the naphthalene core interacts via π-π stacking to the DNA bases (Figure 1.27). It has also been found to be a potent inhibitor of cell growth.[75]

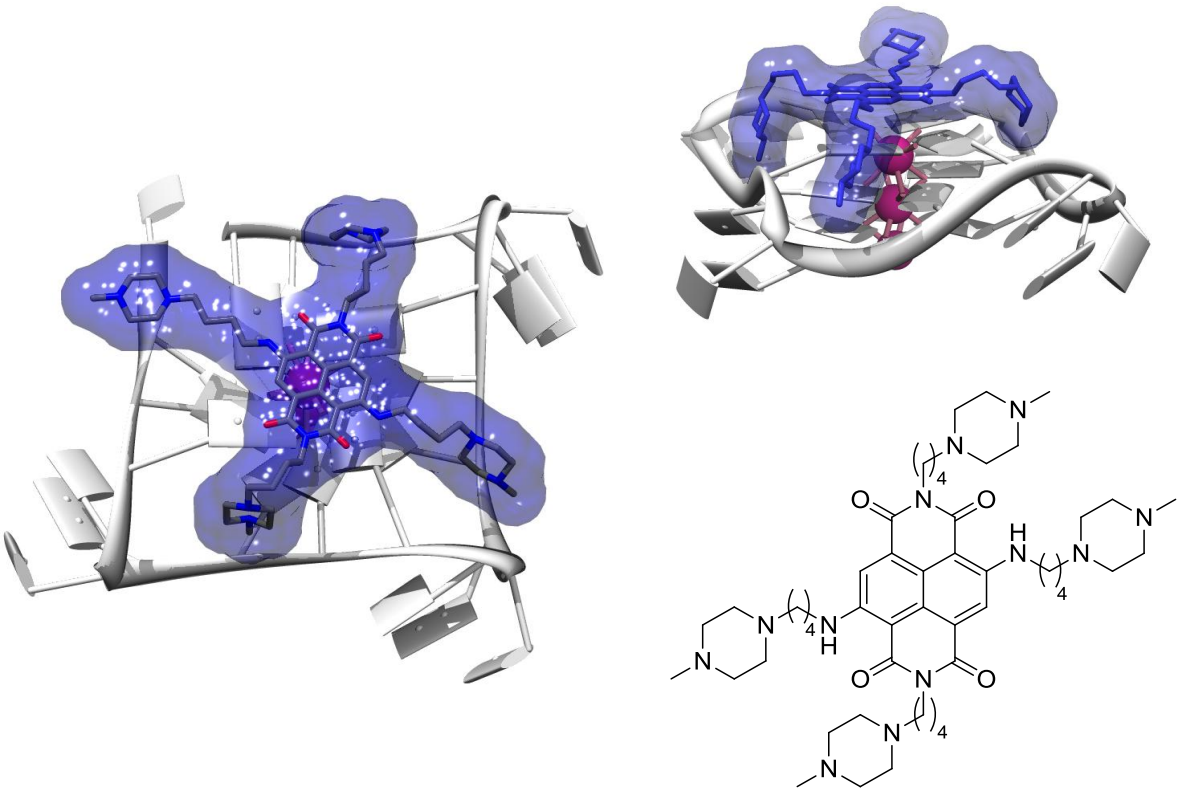

Figure 1.27: Tetra-substituted naphthalene diimide quadruplex binder (bottom right) bound to a human telomeric G-tetrad; side view (left) and top view (top right) (PDB 3T5E).[75]

Metal-containing ligands are also able to bind G-quadruplexes.[76,77] Sleiman has shown that Fujita's platinum molecular square[78] (Figure 1.28) is an excellent stabilizer of the G-quadruplex motif, and it significantly binds selectively to the tetraplex over duplex DNA.[79]

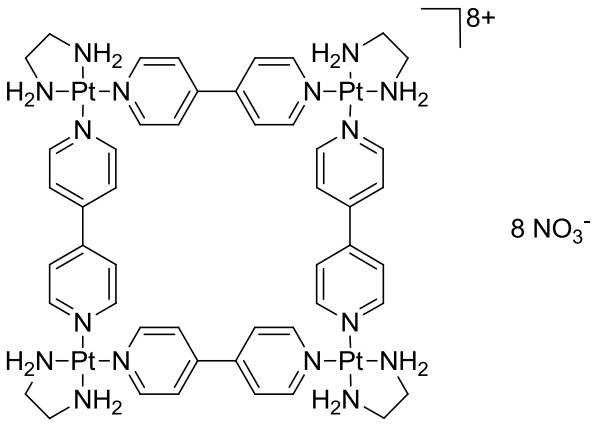

Figure 1.28: Structure of Fujita's platinum molecular square.

1.2.6.4. DNA junctions

A DNA junction is a branched structure consisting of several double strands converging at one point.

DNA three way junctions are structures transiently formed during DNA replication (in the replication fork). They are intermediates during triplet repeat expansions (myotonic dystrophy I, Huntington's disease) and during phage genetic recombination. They are also present in inverted terminal repeats of certain viral genomes.[80,81]

Sasaki has reported a bidentate minor groove binder that can recognize a DNA three-way junction structure. Two Hoechst 33258 are connected by a polyether linker at their convex side. Strong binding occurs when each Hoechst 33258 molecule interacts with the A_3T_3 minor groove regions of the arms of the junction (Figure 1.29).[82]

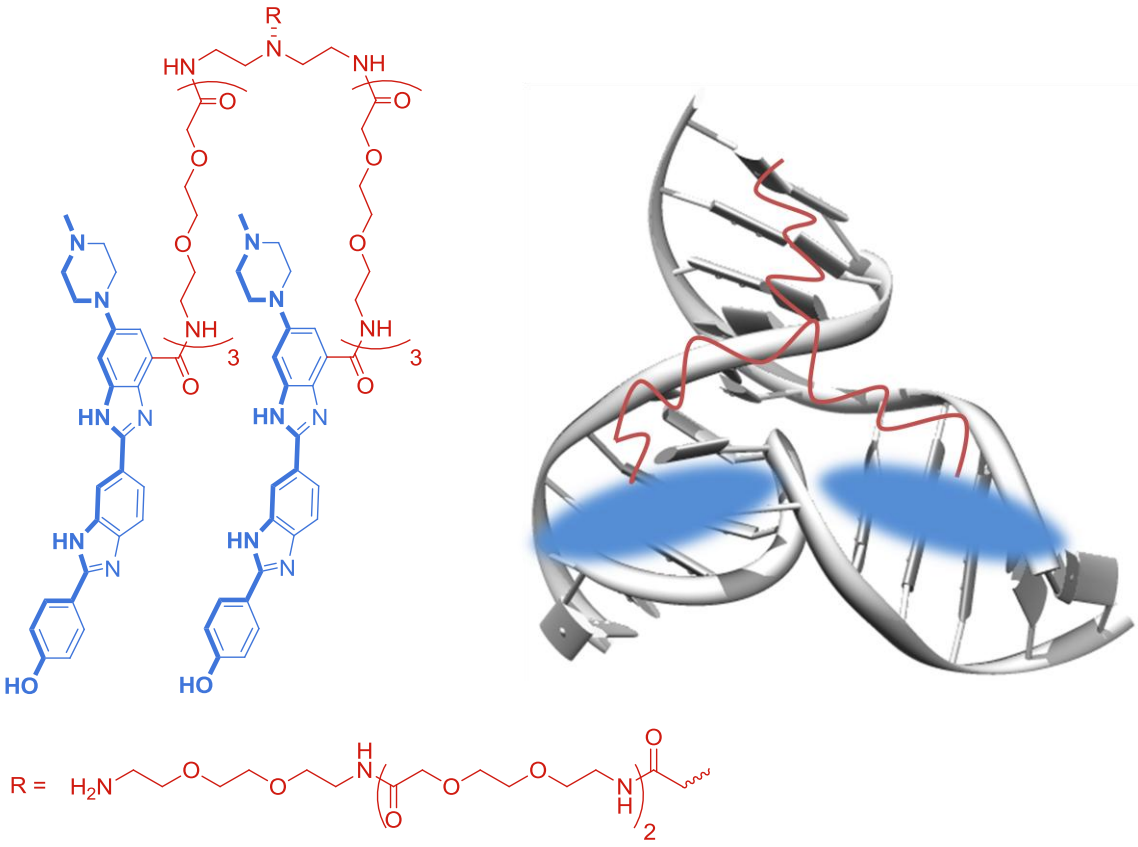

Figure 1.29: Structure of Sasaki's bidentate minor groove binder (left) and schematic representation of a DNA-3WJ (PDB 1EKW)[83] and Sasaki's binder (right).

In 2006, Hannon *et al.* reported the first synthetic molecule able to bind to the central hydrophobic cavity of a DNA three-way junction. This dinuclear iron(II) complex is cylindrical in shape and is of the perfect size to sit in the central cavity of the junction without perturbing the DNA structure. Two types of interactions are observed; π-π stacking to the DNA bases and electrostatic attraction between the cationic cylindrical molecule and the negatively charged phosphate DNA backbone (Figure 1.30).[81]

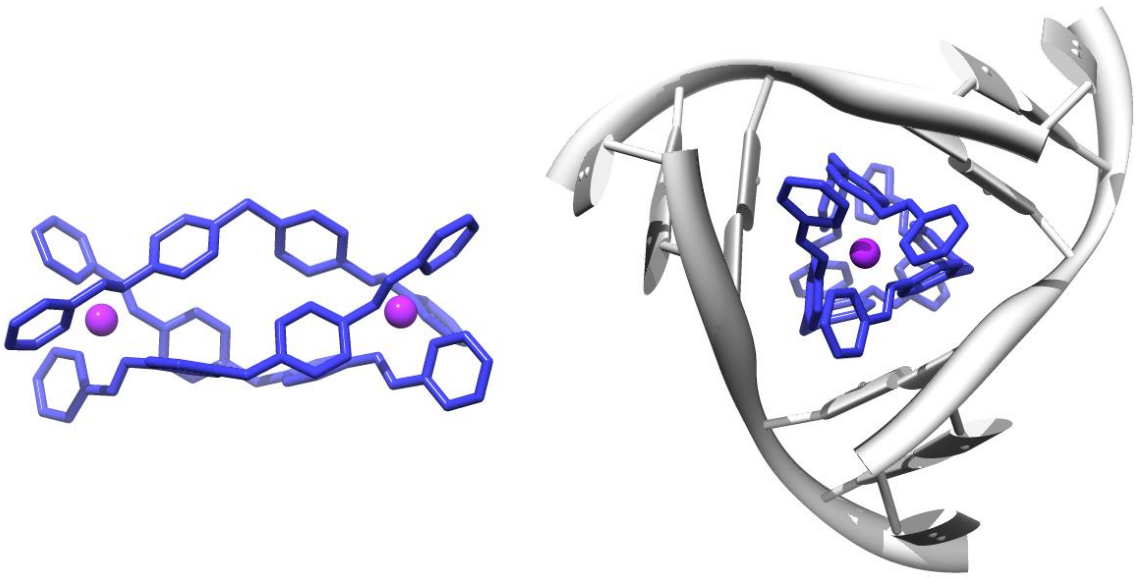

Figure 1.30: Crystal structure of dinuclear iron(II) complex (CCDC 622770)[84] (left) and complex bound at the heart of a DNA three-way junction (PDB 2ET0).[81]

One of the most studied junctions is the four-way junction or Holliday junction. It is accepted to be the central intermediate during homologous genetic recombination. This process is important in DNA repair mechanisms and the restart of failed replication forks.[85] It also provides genetic diversity which is essential for the evolution of the species.[86] Holliday junctions are also involved in replication processes of bacteriophage T4 as they allow viral integration.[87] Double strand breaks can occur in two homologous double helices due to different factors such as radiation and the DNA repair process starts. The nicked strands are able to invade the homologous strands and these are then covalently linked to the original strands at the nicked site, forming a Holliday junction. This Holliday junction migrates away from the original nicked site across the strands in a process called branch migration. As a result of this, DNA strands are swapped producing heteroduplex regions, which results in an exchange of genetic material.

At some point, migration of the Holliday junction ends and resolves the entangled DNA strands into two separate ones. The junction bends and forms the X-stacked Holliday junction. If one of the DNA helices rotates by 180º, a process called isomerisation, the result is the open form of the Holliday junction. Endonucleases can cut at different points producing non-crossover products, where only two strands have exchanged genetic material, or crossover products, where all the strands have new genetic material (Figure 1.31).[87,88]

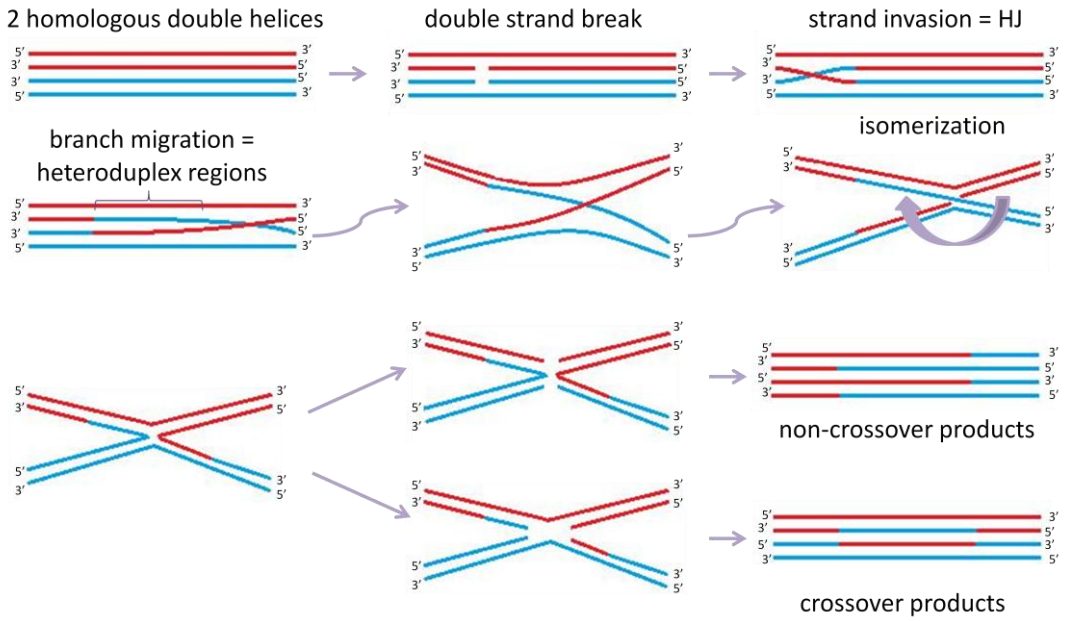

Figure 1.31: Homologous recombination process.

The structure of a DNA four-way junction was found to be dependent on the type and concentration of cations in solution (Figure 1.32). At low salt concentration, the four-way junction adopts the open form where the arms of the junction are fully extended. An H-shaped structure gives the minimal electrostatic repulsion between the negatively charged phosphate backbones. In the presence

of metal ions, a more compact structure is formed where the four arms are paired and stacked with each other. Group II metals, such as calcium and magnesium are able to fold the four-way junction structure at concentrations greater than 100 μM. Group I metals, such as sodium and potassium, require very high concentrations to partially fold the junction structure. Metal complexes ($[Co(NH_3)_6]^{3+}$) and polyamines (spermine) are more efficient, as they are able to promote folding of the Holliday junction structure at concentrations ranging from 2 to 25 μM.[87,89]

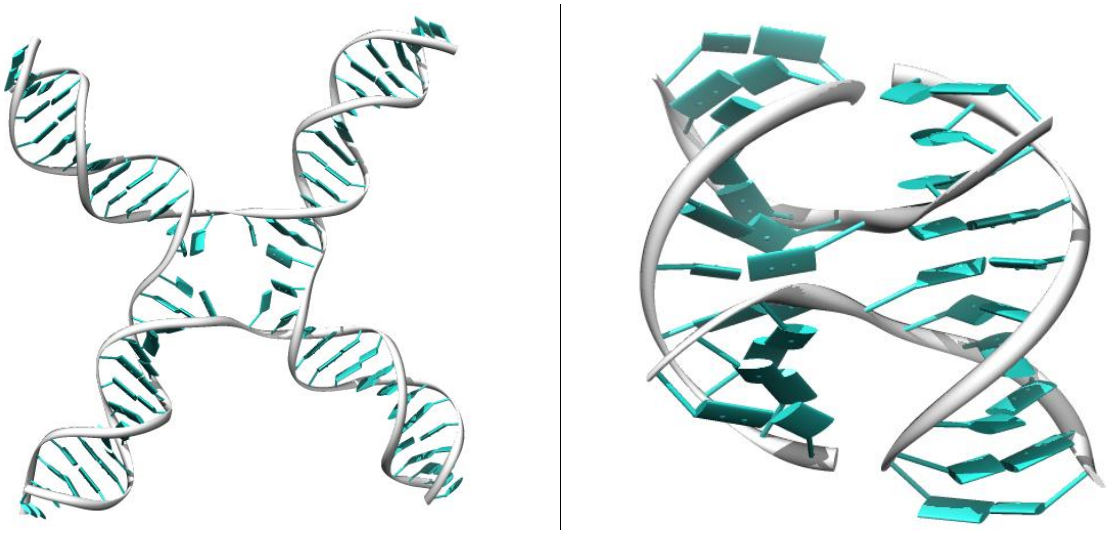

Figure 1.32: Holliday junction structures: open form (PDB 1Z1G)[90] (left) and X-stacked form (PDB 3T8P)[91] (right).

Holliday junctions can be recognized by a number of proteins in cells which direct branch migration and resolution during the homologous recombination process. The binding is structurally selective, however proteins can also distort the junction structure upon binding.[92,93]

Cardin has developed a family of compounds based on alkyl-chain-linked dimers of acridine with varying spacer length. These compounds are able to bind across the centre of the junction ejecting two adenines at either side of the junction crossover (Figure 1.33).[94]

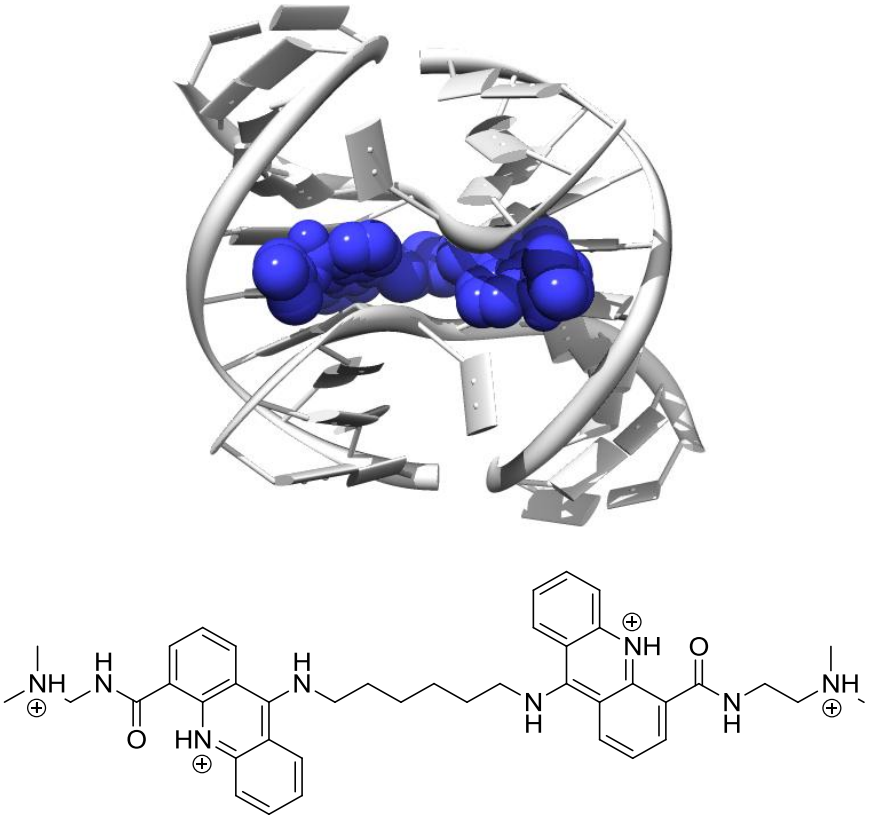

Figure 1.33: Bis-acridine intercalator bound to a DNA-4WJ (PDB 2GWA).[94]

In section 1.2., the different binding modes that natural and synthetic agents employ to recognize DNA has been discussed. It is noted that correct structural design of synthetic DNA binders is required for molecules to succeed in the DNA recognition process. In this way, intercalators need to have aromatic rings at the correct site to be able to sandwich between the DNA base pairs. If higher order DNA structures or the DNA major groove are the target, large molecules need to

be synthesised. Metallo-supramolecular chemistry is able to generate these large molecules. The main principles of this chemistry and some metallo-supramolecular structures are reviewed in the next section.

1.3. Metallo-supramolecular chemistry

Traditionally molecular chemistry is based on molecules formed by atoms linked by strong bonds, such as covalent bonds. In supramolecular chemistry molecules are used to build bigger aggregates by intermolecular interactions using weak bonds such as hydrogen bonds, Van der Waals interactions, electrostatic interactions, hydrophobic interactions or π-π stacking interactions of aromatic units.[95,96] Supramolecular chemistry is inspired by the formation and interactions observed in proteins and oligonucleotides, reviewed above.[97] This new chemistry concept was first defined by Jean-Marie Lehn in 1978 who received the Nobel Prize in Chemistry in 1987.[95] Since then, supramolecular chemistry has been extensively studied and the different nanosized motifs synthesised have led to several applications, such as sensing,[98,99] electronics,[100,101] molecular motors,[102] environmental control,[103] diagnostic and chemotheraupetic agents[104] and catalysis.[105]

It was in 1994 when Constable introduced the term metallo-supramolecular chemistry to describe those assemblies that are built by employing metals (M) and their interaction with donor groups of organic molecules (ligands, L). The nature of M and L determines the strength of the interaction M-L.[106]

One of the most important properties of this type of chemistry is the self-assembly process[107] used in the synthesis of these arrays (metal-directed self-assembly); only the ligand and the metal are needed to yield the aggregate, due to a molecular recognition process giving only one product, the most stable one. The product can be designed by studying the steric and electronic characteristics of the building blocks and finding a balance between rigidity and flexibility. The starting materials contain the molecular information for the selective binding.[108]

Different architectures can be formed by studying the characteristics of the ligands and the metals. The metal has to be selected according to its coordination number and geometry, and the ligand for the relative position and number of its donor atoms.[109,110] In this way, a vast number of structures can be formed; linear and zigzag coordination polymers, molecular squares, rectangles, hexagons, triangles, windows, lattices, ladders, square tiles and cubes, adamantanoid and dodecahedral cages, double-stranded, triple-stranded, quadruple-stranded and circular helicates and rotaxanes and catenates.[111-113] Some of these structures will be discussed below based on the number of metals and geometry adopted.

1.3.1. $[M_2L_2]$ architectures

Self-assembly directed by metal-coordination has led to the preparation of molecular squares that are able to host different guests in their internal cavities.

This is the case of the platinum metallacycle formed from 2,7-diazapyrenium (Scheme 1.1).[114]

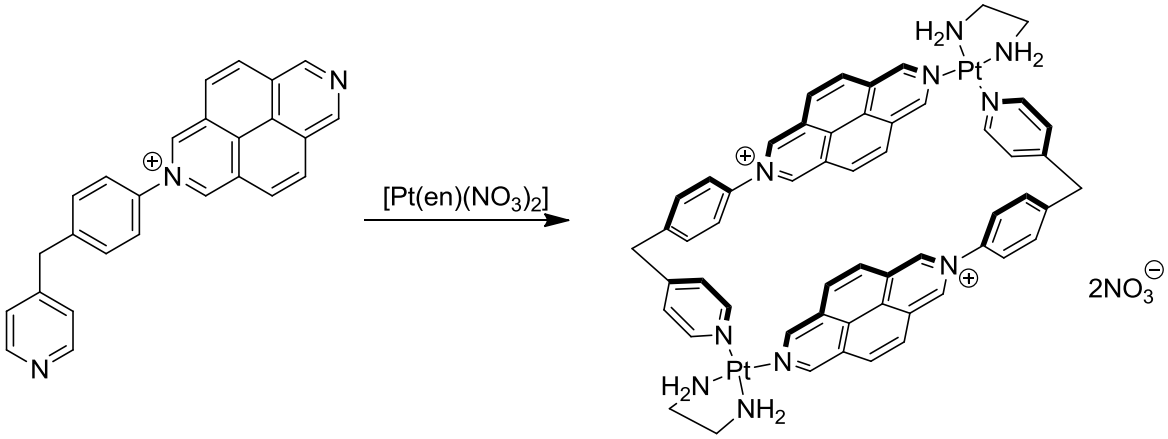

Scheme 1.1: Synthesis of Pt(II) rectangular metallacycle of 2,7-diazapyrenium based ligand.

This metallacycle can host different environmental pollutants which are polycyclic aromatic hydrocarbons (PAH) of two or more fused rings (Figure 1.34). The molecular recognition process is based on π-π interactions between the pyrenes of the metallacycle and the guests (pyrene and triphenylene), as well as hydrophobic forces.[114]

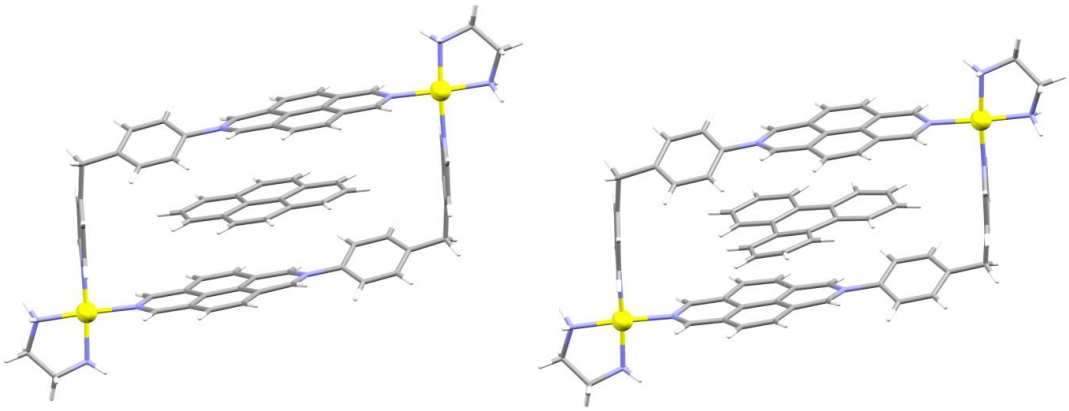

Figure 1.34: Pt(II) metallacycle hosting a pyrene (CCDC 783766)[114] (left) and a triphenylene (CCDC 783768)[114] (right).

It has been shown recently that this platinum metallacycle can coil the DNA and is able to block the amplification of DNA in a PCR assay. It also shows high cytotoxicity against five different cancer cell lines. These results show a potential use of this compound as an anticancer agent.[115]

Double helices can also be formed in an $[M_2L_2]$ architecture. Helices in general attract the attention of supramolecular chemists for their analogy to DNA, and as a simple model to understand the self-assembly and molecular recognition processes. Helices can also be used to easily introduce chirality into molecules that can be used for several applications, such as catalysis or opto-electronics.[116]

Helices can be formed as a result of the wrapping of two or more multitopic ligands around a central core of metal centres. Alternatively, helices can be formed as a result of the aggregation of smaller supramolecular units. These two types of helices are observed in Ward's silver helicate.[117] A double helicate is formed by the self-assembly of bidentate pyrazolyl-pyridine ligands coordinating

silver metal centres. These molecular complexes associate into larger polymeric arrays by silver-silver contacts (Figure 1.35).

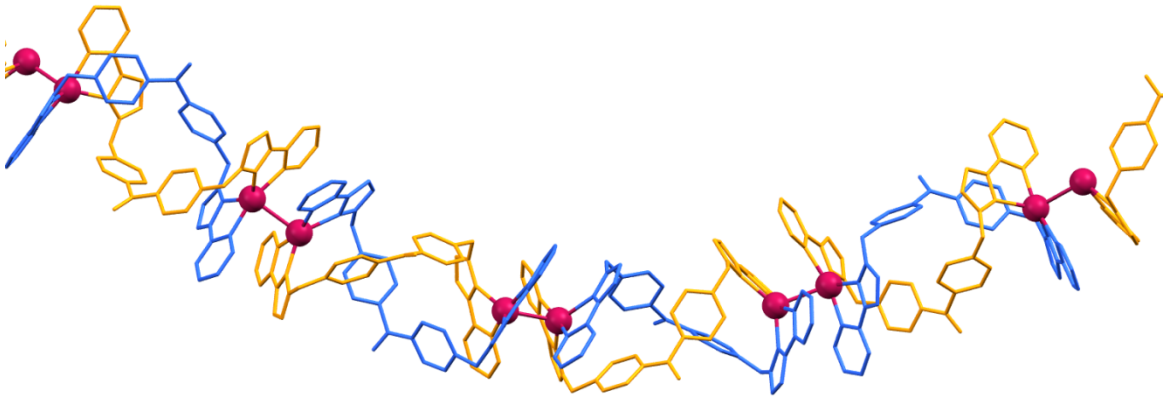

Figure 1.35: Polymeric double stranded helicate with Ag-Ag contacts (in magenta) (CCDC 862638).[117]

Three of these double helices can associate to form a larger triple helicate with a quasi-cylindrical shape. The centre of the triple helix is occupied by perchlorate counter-ions (yellow) (Figure 1.36).[117]

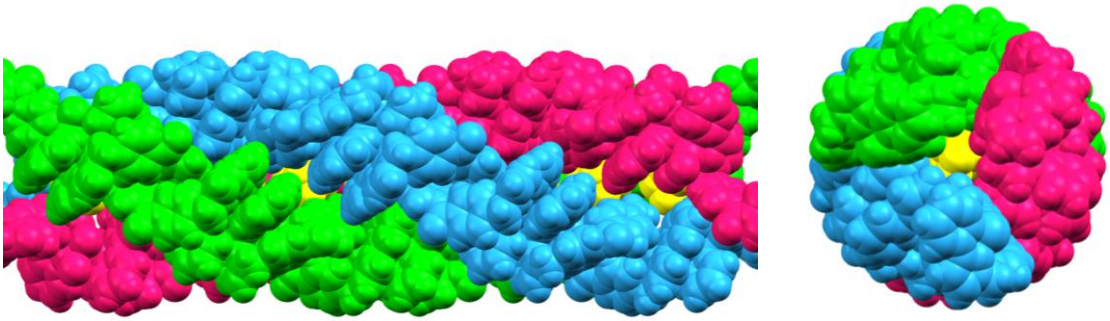

Figure 1.36: Triple helix of double helicates; long-side view (left) and end-on view (right) (CCDC 862638).[117]

1.3.2. $[M_2L_3]$ architectures

A triple helix can also be formed when three ligands wrap around to metal centres. Hannon and co-workers have synthesised an imine based ligand that is able to coordinate octahedral metals to form triple helices. This bidentate ligand is formed by the conjugation of two pyridyl-imine units to an aryl ring. Consequently the imine bond is stable to hydrolysis. When coordinated to iron centres a racemate of triple helices is formed.[118] The two enantiomers can be resolved by cellulose column chromatography with a 20 mM NaCl solution as eluent.[119] This helicate is stabilized by inter-strand face-edge π-stacking interactions between the phenylene rings of the spacer units (Scheme 1.2).[118]

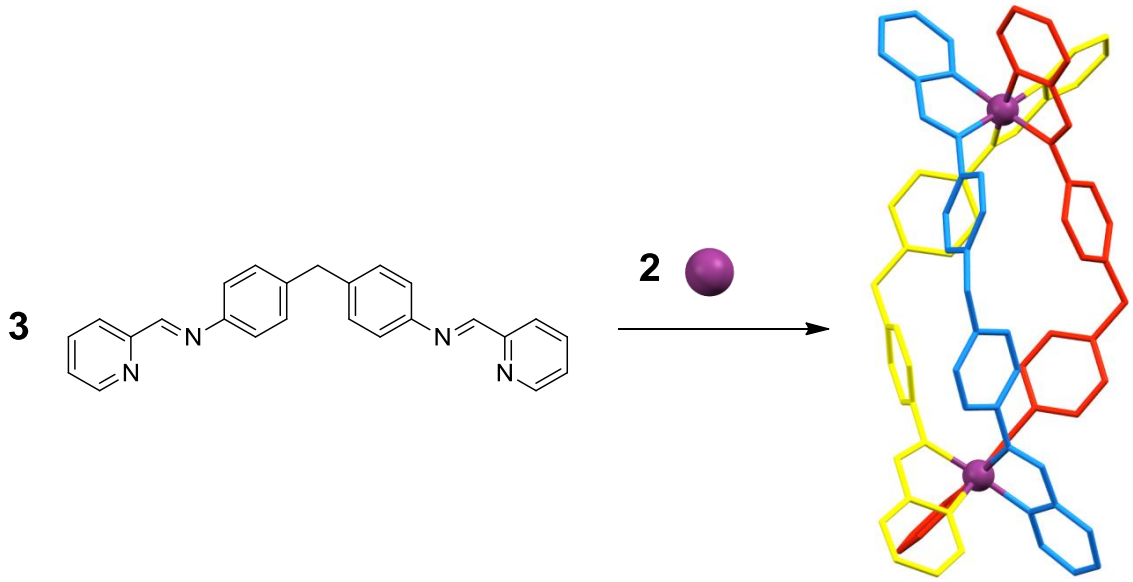

Scheme 1.2: Synthesis of iron(II) triple helicate. Crystal structure shows M enantiomer. (CCDC 622770).[84]

This helicate is able to coil and bend DNA by binding around the major groove.[120] It can also recognize the central cavity of DNA and RNA three-way

junctions (*vide supra*).[81,121] It is proposed that the helicate can interact with the loops and grooves of telomeric G-quadruplex DNA.[122] Recently, it has been demonstrated that this triple helicate can act as an amyloid-β inhibitor which could be used to treat Alzheimer's disease, as the accumulation of amyloid-β peptides is a sign of this illness.[123] The helicate is also a potent inhibitor of cellular proliferation in several cancerous cell lines. It induces cytostasis and apoptosis in myeloid leukemia cells and it is not genotoxic.[124] It is also able to displace Taq DNA polymerase from DNA which indicates that it might be able to interfere with DNA transaction processes (e.g. DNA replication). Its ruthenium analogue is also able to inhibit the polymerase chain reaction (PCR). However, due to the instability of the iron cylinder at the high temperatures which are required to performed a PCR experiment, this inhibition was not observed in the case of the iron cylinder.[125]

1.3.3. $[M_2L_4]$ architectures

The first saturated tetra-stranded helicate was reported by Steel in 1998. The use of square planar metal centres and monodentate ligands was crucial. The tetra-stranded complex was initially obtained via isolation of a dimeric complex, which reorganized and crystallised in the presence of hexafluorophosphate salts to yield the tetra-stranded helicate. Within the central cavity a hexafluorophosphate counter-ion is encapsulated (Scheme 1.3). This anion makes weak contacts with

the palladium(II) metal centres acting as a bridging ligand. This was also the first example of encapsulation of a polyatomic anion by a helicate.[126]

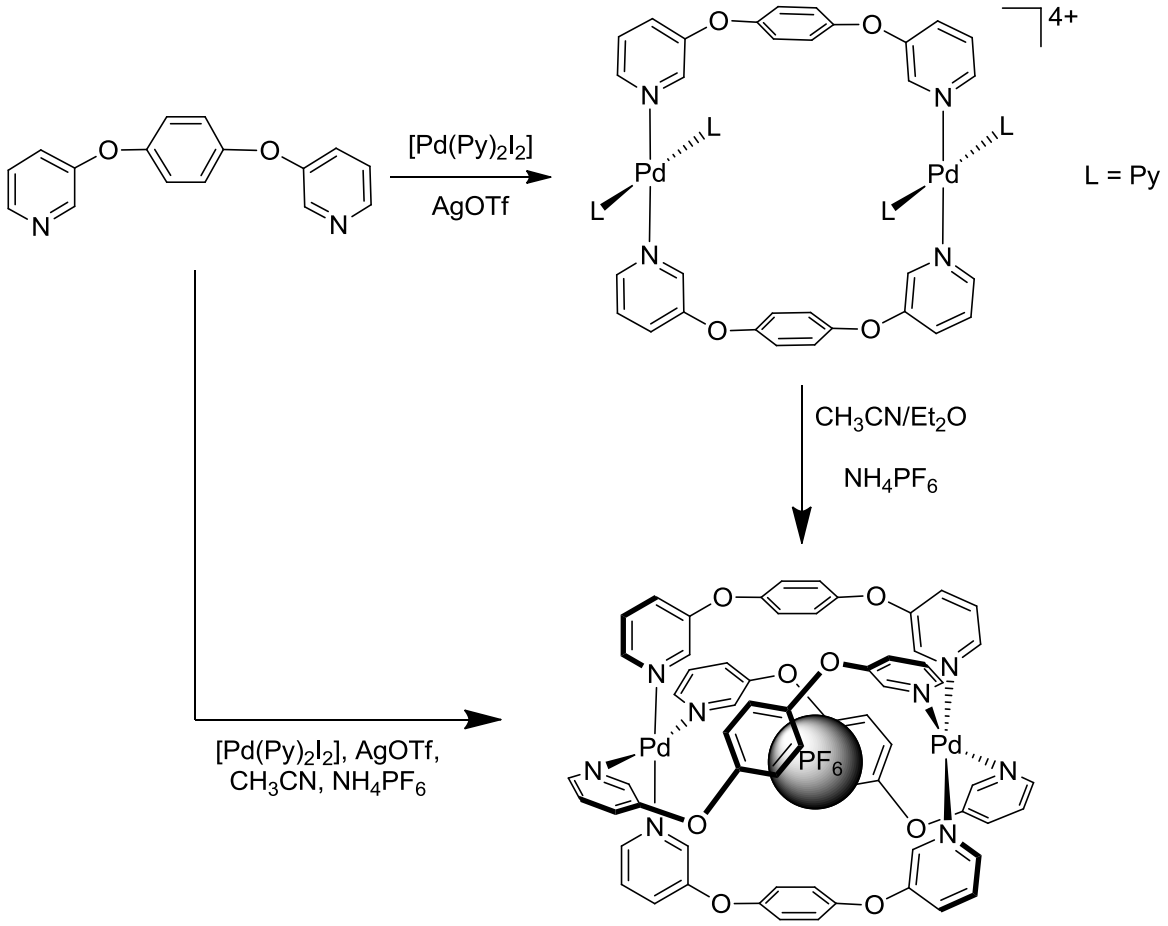

Scheme 1.3: Synthesis of the first tetra-stranded helicate.

Another interesting tetra-stranded palladium(II) complex has been designed by Clever. This tetra-stranded cage forms an interlocked dimer upon prolonged heating, and can host three tetrafluoroborate counter-ions (Scheme 1.4). The dimeric species has a strong chloride-anion binding ability and two of the tetrafluoroborate counter-ions can be displaced by chlorides, leaving the central tetrafluoroborate counter-ion strongly bound.[127]

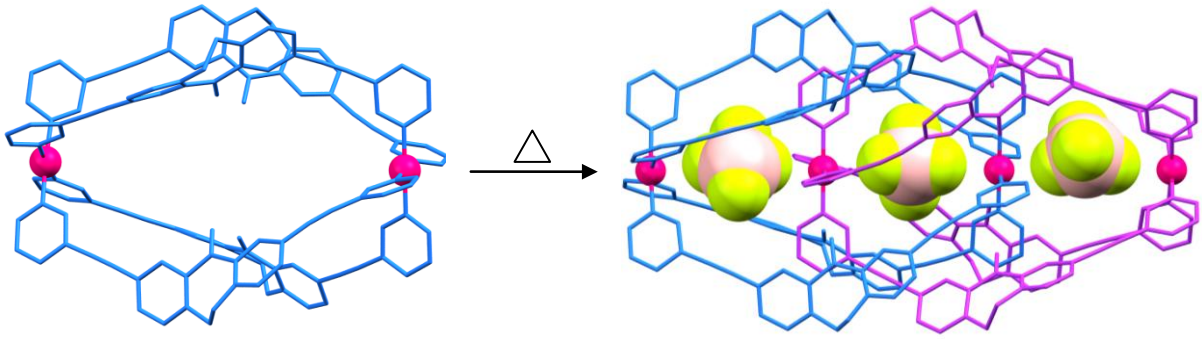

Scheme 1.4: Formation of an interlocked dimer from a tetra-stranded cage (CCDC 844925).[127]

These dimerization and encapsulation behaviours have also been seen in similar tetra-stranded cages.[128]

1.3.4. $[M_3L_3]$ architectures

One of the crucial requirements to yield a specific supramolecular assembly is the length, symmetry and flexibility of the ligands.[129] In this way, shorter bidentate ligands would form $[M_2L_2]$ species while longer bidentate ligands would form $[M_3L_3]$ supramolecules. This is observed in Würthwein nickel supramolecular square and triangle formation (Figure 1.37).[130]

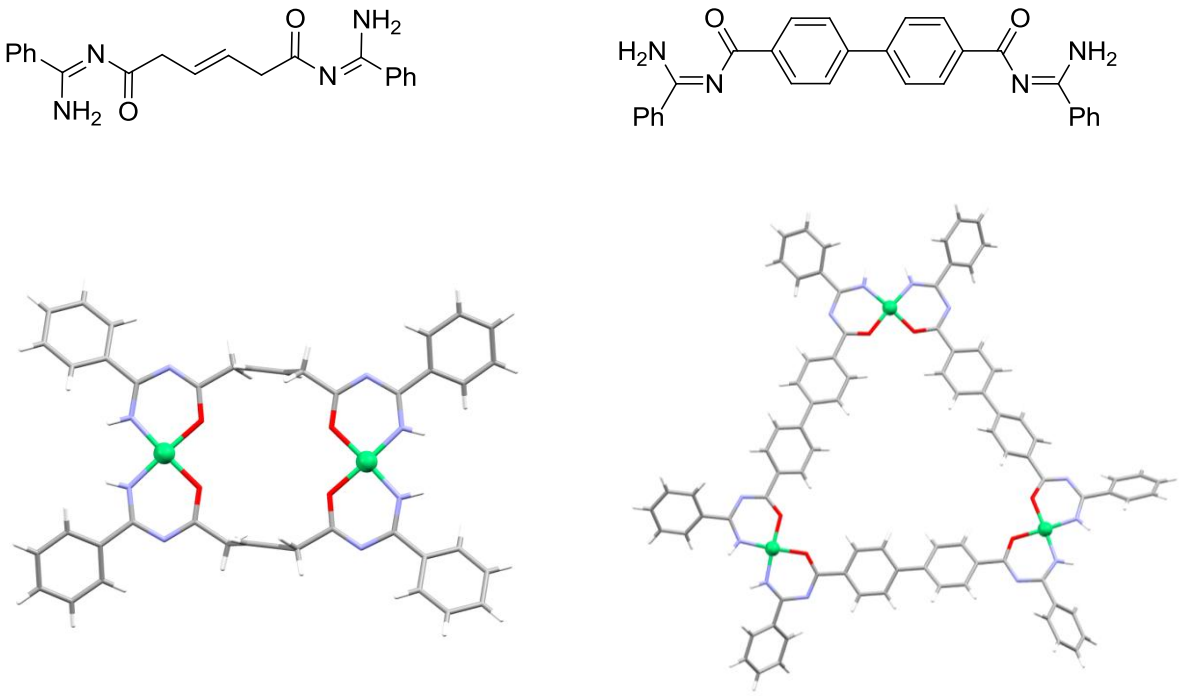

Figure 1.37: Ligand structures (top) and crystal structures of $[Ni_2L_2]$ (CCDC 854333)[130] (bottom left) and $[Ni_3L_3]$ (CCDC 854334)[130] (bottom right).

1.3.5. $[M_4L_4]$ architectures

As mentioned above, in 1995 Fujita synthesised a platinum molecular square $[Pt_4L_4]$ which was later shown to bind G-quadruplex DNA. One year after, Fujita presented his results on its palladium analogue (Figure 1.38). If the ligand length was increased by addition of different spacer units between the pyridine rings, a supramolecular double-walled triangle $[Pd_3L_6]$ was formed as a minor product.[131]

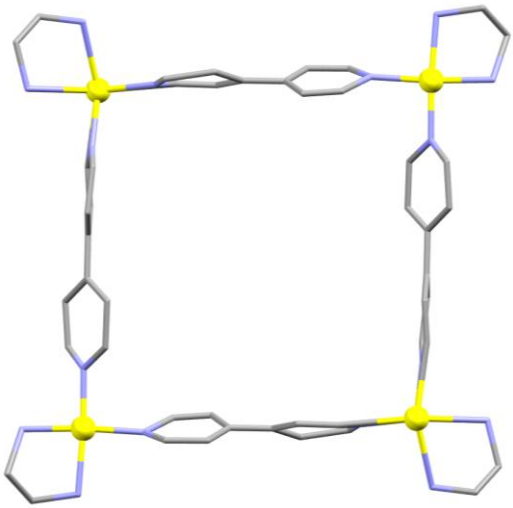

Figure 1.38: Crystal structure of Fujita's Pd(II) molecular square (CCDC 753499).[131]

1.3.6. $[M_4L_8]$ architectures

Fujita explored then the introduction of a biphenyl unit between the coordinating pyridines in his ligand design. This ligand was reacted with naked palladium(II) ions ($[Pd(NO_3)_2]$) resulting in a dynamic equilibrium between a double-walled triangle $[Pd_3L_6]$ and a tetrahedron $[Pd_4L_8]$. This equilibrium could be driven to one or the other structure depending on the counter-ion used. In the presence of nitrate anions the ratio between the double-walled triangle and the tetrahedron was 1:1. When using triflates, the double-walled triangle was formed as the major product. The formation of the pure tetrahedron was achieved when employing an aromatic anion, such as *p*-tosylate. This is due to the π-stacking of the π-surface of the anion to the phenyl rings on the spacer (Figure 1.39).[132]

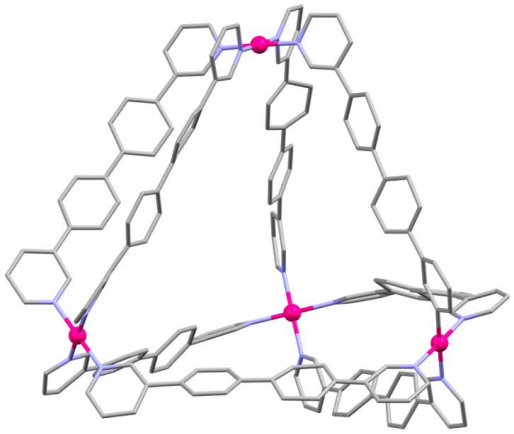

Figure 1.39: Crystal structure of Fujita's palladium(II) tetrahedron (CCDC 297117).[132]

1.4. Closing remarks

In summary, an overview of supramolecular chemistry has been given and some metallo-supramolecular structures have been used as examples. The emphasis was focused into structures that will be involved in the next chapter. The main characteristics of DNA and how it can be recognized by natural and synthetic agents has also been discussed. Recognition of duplex DNA via its major groove and minor groove, and by intercalation, phosphate binding and covalent binding to the DNA bases has been presented. Recognition of higher order DNA structures has also been summarized. The thesis aims are to create a large, water soluble supramolecular agent that might recognize the Holliday junction. The design features and approach to achieve this are described in chapter 2. Therefore, an understanding of the different modes in which a drug can interact with DNA is important in the evaluation of how the synthesised compounds interact with DNA and this will be discussed in chapter 3.

Chapter 2. Towards Solubilization of Palladium(II) Tetra-Stranded Cylinders

2.1. Introduction

As stated in Chapter 1, Hannon *et al*. have developed a triple-stranded helicate that is able to bind in the DNA major groove. Still more exciting, this cylindrical drug is of the perfect size and shape to fit in the central cavity of a Y-shaped DNA three-way junction (Figure 2.1).[81]

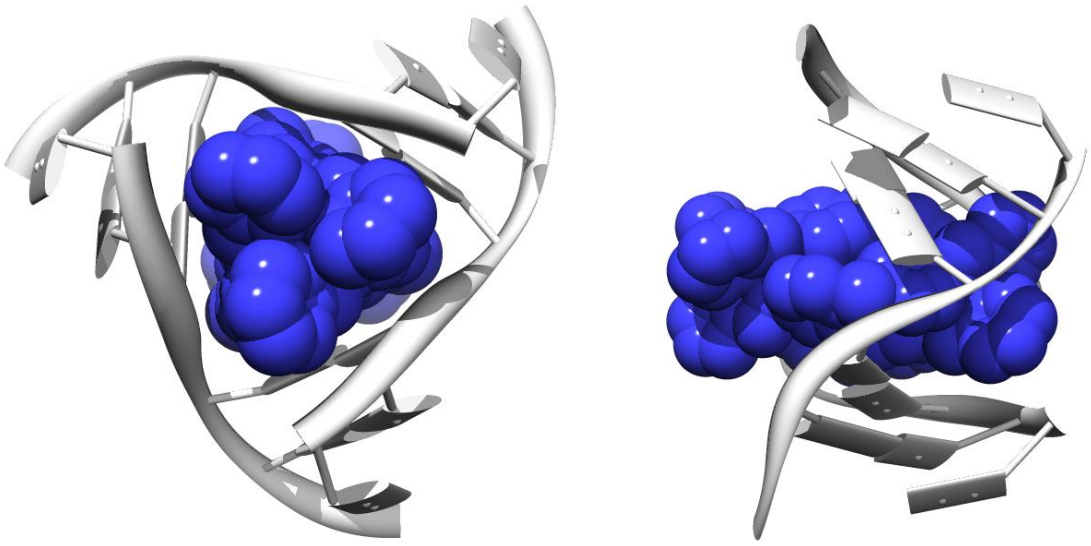

Figure 2.1: Crystal structure of Hannon's iron(II) cylinder bound in the central cavity of a DNA 3WJ; front view (left) and side view (right) (PDB 2ET0).[81]

Inspired by this breakthrough, Hannon and co-workers aimed to develop a tetra-stranded cylinder that might be capable of recognizing and binding within the central cavity of a DNA four-way junction (Figure 2.2). A DNA four-way junction, or Holliday junction, is an intermediate during homologous recombination and is important in DNA repair and the restart of failed replication forks (*see section 1.2.6.4.*).[85] A potentially four-way junction binding drug might be able to stop DNA repair processes. One of the applications could be that when a cancer patient receives radiotheraphy, or is administered an alkylating anticancer drug like cisplatin, DNA strand breaks are produced and the Holliday junction-binding drug might stop normal DNA repair processes, causing the death of the tumour.

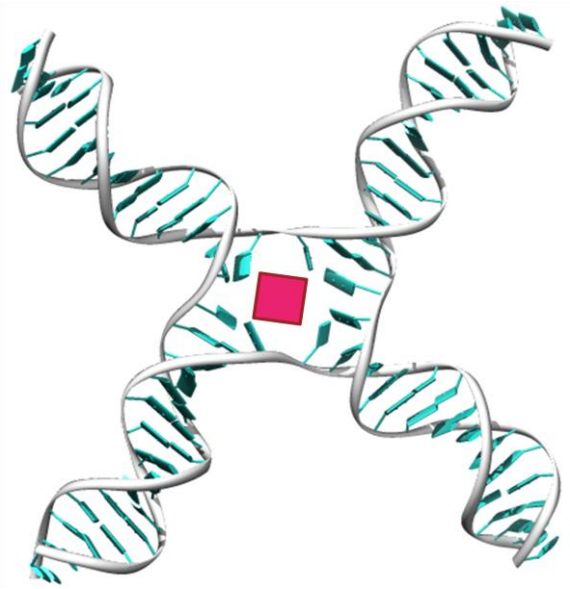

Figure 2.2: Graphical representation of a potentially four-way junction binding drug in the central cavity of a DNA 4WJ (PDB 1Z1G).[90]

The molecular design was inspired by that of the triple-stranded cylinder to ensure a similar interaction upon binding. It has been shown that each of the three

strands of the iron(II) cylinder interact with the bases of each of the three DNA strands at the centre of the trigonal cavity of the junction.[81] Therefore, it was hoped that a tetra-stranded cylinder will bind to the square central cavity of a DNA four-way junction in a similar fashion. For the triple stranded cylinder, an octahedral metal centre such as iron(II) was the metal of choice. In the case of the tetra-stranded molecule, a square planar metal was selected as this will give the square disposition of ligands that might be required to bind the square cavity of the DNA four-way junction. Palladium(II) was the first choice due to its reactivity, however other metals were also explored (*vide infra*). In terms of ligand design (Figure 2.3), the triple stranded iron(II) cylinder has three bidentate ligands with pyridine-imine units to satisfy the octahedral requirements of the iron(II) centres. In order to obtain a tetra-stranded complex in a square planar configuration, monodentate ligands are required. A pyridine unit was selected as there is a great number of examples of polypyridyl complexes.[110] The diphenyl spacer unit was maintained as it was shown to play an important role in DNA three-way junction recognition, with π-π stacking to the DNA bases.[81] It will also allow a dinuclear species since coordination of the two pyridines from the same ligand to the same metal centre cannot occur.

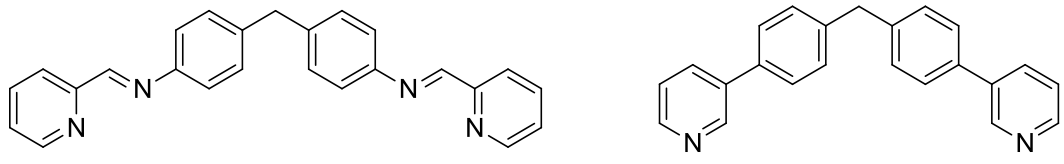

$\mathbf{L^{im}}$ $\mathbf{L}$

Figure 2.3: Structure of the bidentate ligand ($\mathbf{L^{im}}$) used for the triple-stranded iron(II) cylinder (left) and structure of a monodentate ligand (**L**) used for tetra-stranded palladium(II) cylinders (right).

It is worth mentioning that a DNA four-way junction is a more challenging target than a DNA three-way junction as the four-way junction can exist as two isomeric forms depending on the ion concentration. These forms are the X-stacked form, where the two arms interact with each other by stacking; and the open form, where the four DNA strands are spread out due to the electrostatic repulsion of the phosphate backbones (*see section 1.2.6.4.*).[87]

Following these principles for molecular design, Hannon, Ryabova and Kaur synthesised several of these tetra-stranded complexes.[133,134] The crystal structure of the simplest one, $\mathbf{[Pd_2L_4][(BF_4)_4]}$, is shown in Figure 2.4, which confirms the formation of the tetra-stranded palladium(II) complex. This cylinder crystallises with a plane of symmetry through the centre of the four ligands and is therefore achiral. This is a consequence of the rigidity of the ligand, which results in an increase in the diameter of the cylinder compared to the chiral triple-stranded iron(II) cylinder.[133]

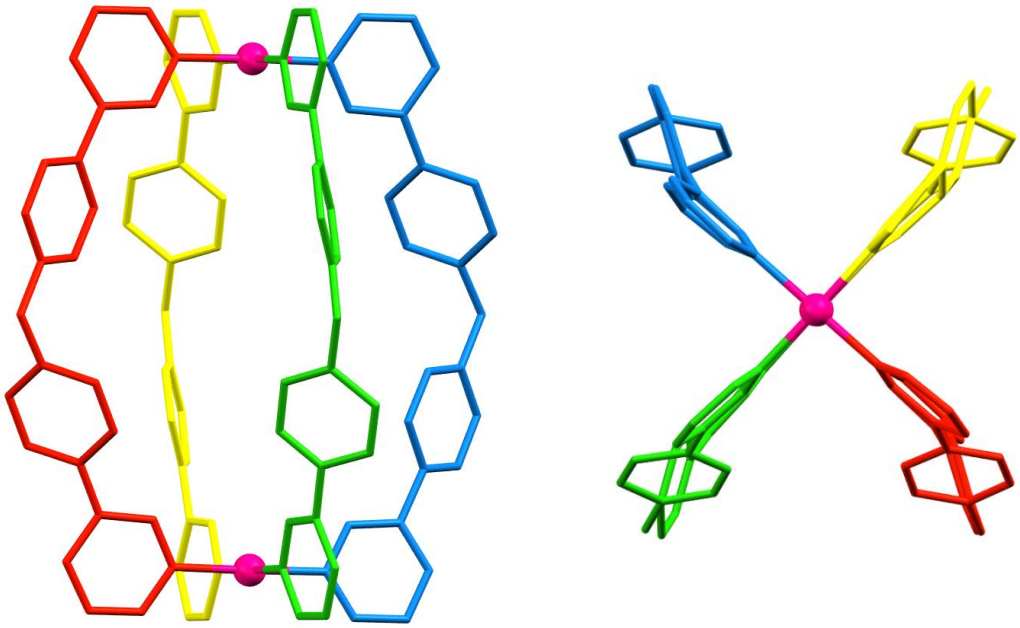

Figure 2.4: Crystal structure of the palladium(II) cylinder **[Pd_2L_4][$(BF_4)_4$]**.[133]

The platinum(II) cylinder of the same ligand was also synthesised. The crystal structure revealed that these palladium and platinum cylinders are structurally identical. However, the synthesis of the platinum(II) complex was not straightforward and several purification cycles via HPLC were needed.[133,134]

When using silver(I) as metal centre a tetra-stranded cylinder was not formed. Instead, two metallo-supramolecular polymers that display a zigzag architecture were obtained. The first silver(I) polymer presented an almost linear two-coordinate environment with a 1:1 metal to ligand stoichiometry. The second silver(I) polymer showed a three-coordinate environment for silver centres and a distorted trigonal planar geometry.[133] This is due to the varied coordination numbers (from two to six) and various geometries (linear, trigonal, tetrahedral and octahedral) that silver can adopt, and consequently a wide variety of

metallo-supramolecular arrays can be obtained. The final structure that will be formed is affected by the ligand composition, the counter ion and solvent, and the metal to ligand ratio used.(135)

In order to investigate the effects of increasing the ligand size **L^{Triple}** was also synthesised by Hannon and Kaur (Figure 2.5). In **L^{Triple}**, ethynyl bonds have been incorporated between the central phenyl rings and the pyridine binding units. The cylindrical structure is analogous to that of **[Pd$_2$L$_4$][(BF$_4$)$_4$]**, except that it is significantly larger. It remains an achiral molecule as the triple bond retains the rigidity of the ligand system.(133,134)

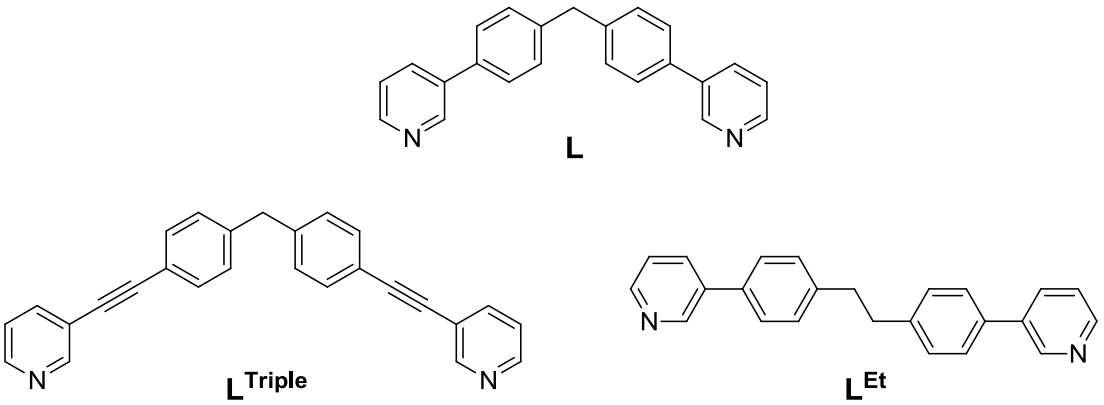

Figure 2.5: Structure of ligands used in the first generation of compounds.

The last ligand system explored by Hannon and Kaur was **L^{Et}** (Figure 2.5). The central methylene unit was replaced by an ethylene, hoping to confer ligand flexibility. This minor change in the ligand design led to two products upon complexation with palladium(II), a double-walled triangle **[Pd$_3$L$^{Et}_6$][(BF$_4$)$_6$]** and a tetrahedron **[Pd$_4$L$^{Et}_8$][(BF$_4$)$_8$].** Similar palladium(II) architectures have been described by Fujita and co-workers and reviewed in Chapter 1.(131,132) The

double-walled triangle was the major product and was crystallised from the crude mixture (Figure 2.6).[133]

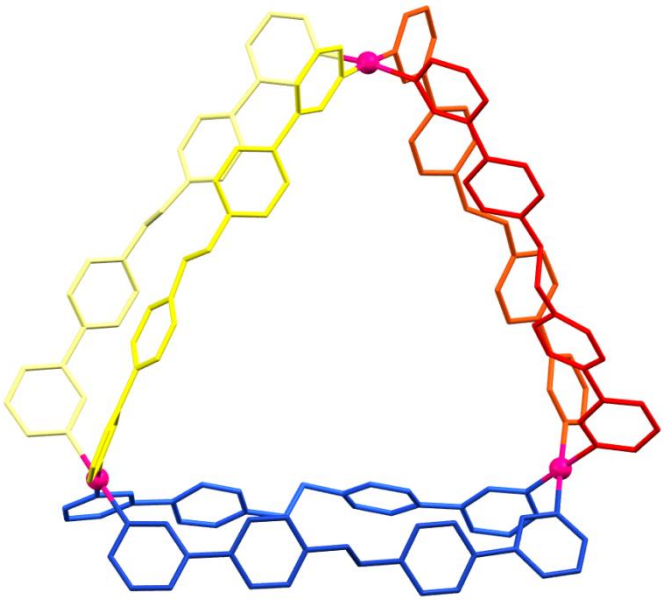

Figure 2.6: Crystal structure of the palladium(II) double-walled triangle **$[Pd_3L^{Et}_6][(BF_4)_6]$**.[133]

These complexes were tested against different human cancer cell lines in order to assess their cytotoxicity. The first complex **$[Pd_2L_4][(BF_4)_4]$** showed considerable cytotoxicity against ovarian A2780 and A2780cis (resistant to cisplatin) and breast T47D cancerous cells (Table 2.1). The IC_{50} values obtained via an MTT assay for three days were comparable or better to those obtained for cisplatin.[133,134]

Table 2.1: IC_{50} values (μM) for palladium(II) cylinder **$[Pd_2L_4][(BF_4)_4]$** and cisplatin.[133]

	A2780	**A2780cis**	**T47D**
$[Pd_2L_4][(BF_4)_4]$	8.1 ± 1.3	10.3 ± 1.2	5.6 ± 0.5
Cisplatin	4.5 ± 0.8	16.0 ± 1.8	28.3 ± 1.7

Preliminary toxicological studies showed that this cylinder was also non-mutagenic and non-genotoxic.[133] These exciting results place this palladium(II) cylinder as a promising anticancer agent. The drawback of this compound is its low water solubility that prevented more detailed DNA binding studies.[133]

2.2. Research aims

Encouraged by the promising cytotoxicity, the challenge now is to improve the solubility of these compounds without significantly modifying their structure or quenching their activity against cancerous cells, and this is the focus of this chapter. It has been shown in the first generation of compounds that modifications on the length of the spacer unit affect the self-assembly process, therefore a single atom spacer will be kept between the phenyl rings. Additional bonds, such as the triple bond of **L^{Triple}**, will not be considered either, as that palladium(II) complex was not toxic against cancerous cells.

2.3. Results and discussion

In this chapter four different strategies are explored towards the solubilization of the first generation of tetra-stranded palladium(II) cylinders (Figure 2.7).

i) Modification of the spacer atom of the diphenyl unit (X).

ii) Exchange of the counter-ion of the complex (Y).

iii) Addition of potentially solubilizing groups at the edges of the pyridine rings (R).

iv) Increase of the complex charge (+).

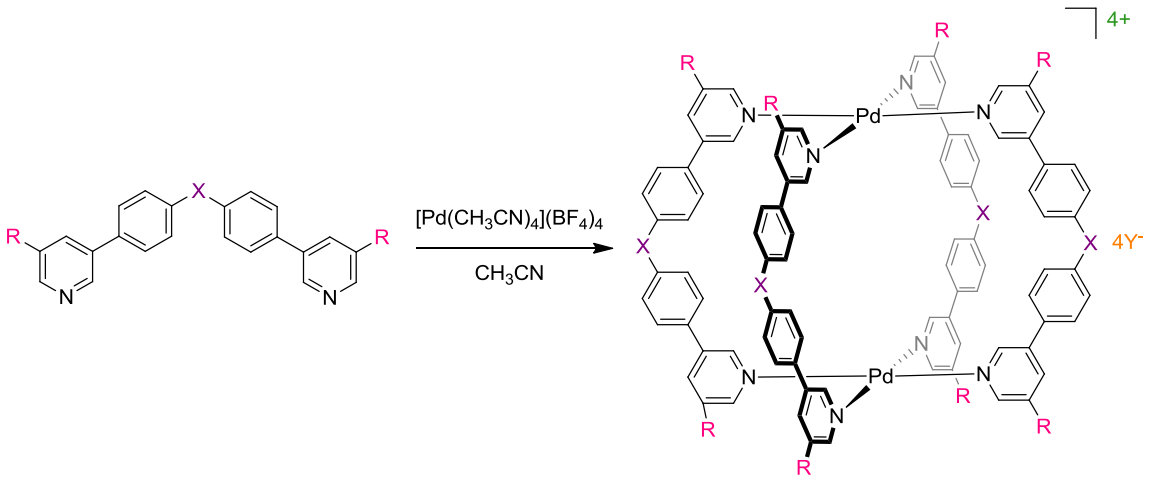

Figure 2.7: Molecular design for second generation of palladium(II) cylinders.

These four different approaches are discussed below and exemplified with new synthesised cylinders. A fifth strategy where the general design is affected is also explored.

2.3.1. Modification of the spacer unit

In general, Hannon *et al*. have used a diphenylmethane spacer unit in their helicating ligands.[118] This carbon spacer unit could be modified to improve the solubility properties of the complexes and to potentially increase their DNA binding affinity. For this study, oxygen, nitrogen and sulfur were the chosen atoms for the central unit of the spacer group, as these are electron-rich atoms that can interact with solvent molecules or with the DNA bases. Oxygen had already been used as spacer group in the first generation of compounds and the solubility of this complex was slightly increased in organic solvent/water mixtures.

In addition, it was thought that introduction of some functionality at the edges of the pyridine rings would be appropriate at this early stage too. Therefore, methyl ether groups were added at position 3[†] of the pyridine ring. This functional group was selected as 3-bromo-5-methoxypyridine is commercially available and will allow a straightforward synthetic route due to the low reactivity of the methyl ether group. This group also has the potential to be modified at a later stage.

Position 3 of the pyridine ring was selected so as to add a substituent without substantially affecting the general structure of the ligand. Positions 2 and 6 were ruled out due to their proximity to the metal binding site. Position 4 was also undesirable as a substituent in this position might interfere with the DNA binding.

[†] Position 3 refers to the new numbering that the ligand will receive once the methyl ether group is introduced. It is formally position 5 in the parent ligand.

2.3.1.1. Molecular design of ligand L^{OMe}

Prior to the modification of the spacer unit with oxygen, nitrogen and sulfur, ligand **L^{OMe}** with a carbon spacer unit was synthesised so that the consequences of the addition of the methyl ether group could be assessed. In order to access ligand **L^{OMe}** the following retrosynthetic analysis was considered (Scheme 2.1).

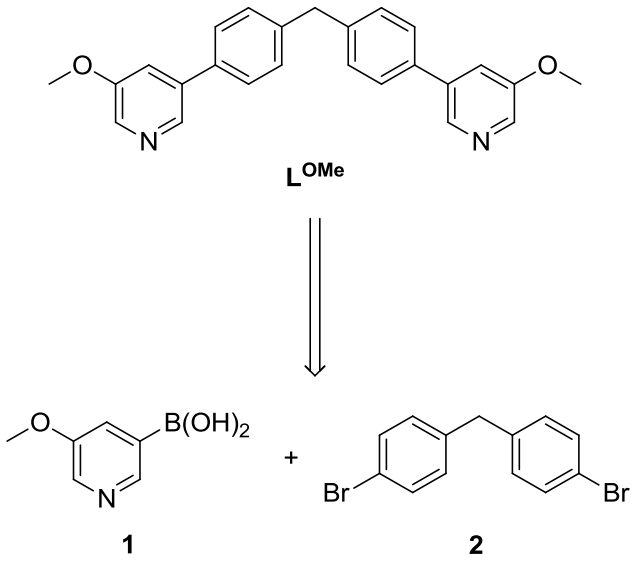

Scheme 2.1: Retrosynthetic analysis for ligand **L^{OMe}**.

5-(Methoxypyridin-3-yl)boronic acid **1** and bis(4-bromophenyl)methane **2** are not commercially available and need to be synthesized as building blocks for ligand **L^{OMe}**. **1** and **2** can then react via Suzuki cross-coupling reaction to form **L^{OMe}**. The Suzuki coupling reaction was chosen over other C-C bond formation reactions, such as Negishi coupling, due to the low toxicity of the boronic acid precursor required and the easy elimination of the boron-containing side products.

2.3.1.2. Synthesis of 5-(methoxypyridin-3-yl)boronic acid (1)

5-(Methoxypyridin-3-yl)boronic acid **1** was formed via metalation of 3-bromo-5-methoxypyridine with *n*-butyllithium under an argon atmosphere at low temperature, achieved with a dry ice-acetone cooling bath. It is reported in the literature that the relative acidity of bromopyridines in THF can result in deprotonation of bromopyridines when the lithium-halogen exchange occurs.[136] To avoid this side reaction, extremely low temperatures (-100 ºC) are needed otherwise low yields are obtained. To prevent the deprotonation, an inverse-addition mode was performed. *n*-Butyllithium was added to toluene in a dry purged flask and then 3-bromo-5-methoxypyridine was added forming a brown precipitate. It is known that lithium-halogen exchange requires a coordinating solvent such as THF to disassociate the *n*-butyllithium aggregate. However, when using non-coordinating toluene the lithiation reaction occurs, therefore it is thought that the nitrogen of the pyridine is able to activate this exchange.[136] THF was added to the brown precipitate slowly, in order to keep the temperature below -70 ºC. When the organolithium intermediate was formed it was quenched by addition of triisopropyl borate and finally a 2 M HCl solution. Once neutralized, sodium chloride was added to the aqueous phase in order to enhance the partition of the boronic acid into the organic phase and therefore the yield (76%) (Scheme 2.2).

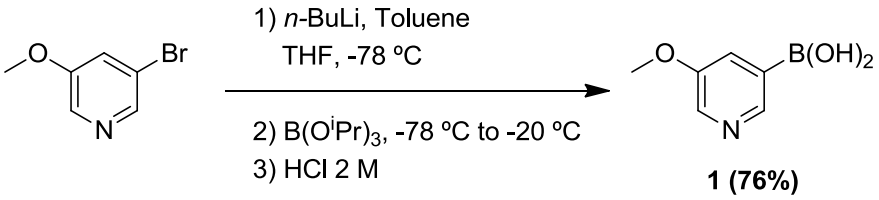

Scheme 2.2: Synthesis of 5-(methoxypyridin-3-yl)boronic acid **1**.

Characterization of boronic acids is often complicated due to the formation of cyclic and linear anhydrides and semi-anhydrides when dehydrated. For example, *p*-toluene boronic acid can form its pure anhydride when warming it in anhydrous solvents such as carbon tetrachloride or chloroform.[137] Infrared spectroscopy (IR) can easily distinguish both species (boronic acid and anhydride) or a mixture of both (semi-anhydride) (Figure 2.8). In the case of **1**, the IR spectra showed no OH band at around 3300 cm^{-1}, indicating the absence of the boronic acid. However, it presented a strong and sharp band around 720 cm^{-1} which corresponds to the presence of the anhydride species. A band around 1412 cm^{-1} was also detected which confirmed the B-O linkage.

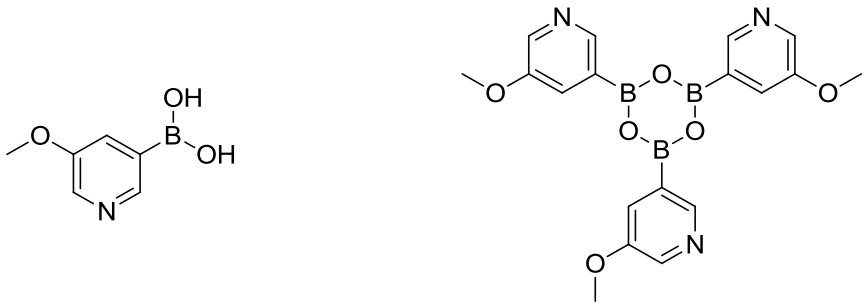

Figure 2.8: Structures of boronic acid and its anhydride.

The electron impact (EI+) mass spectrum did not show the presence of the molecular ion, however a peak at *m/z* 167 Da was observed and assigned to the compound where one of the hydroxyl groups has been substituted by a methoxy group. This is also observed when boronic acids are heated in the presence of methanol to yield the corresponding methyl boronate and free boronic acid.[138] During the mass spectrometry experiment the sample was dissolved in methanol and due to the high temperature of the instrument source the substitution occurred. The boron's isotopic pattern consisting of ^{10}B (20% distribution) and ^{11}B (80% distribution) is also observed.

A similar effect is also observed when performing a ^{1}H NMR experiment in deuterated methanol. Boronic acid **1** degrades or interconverts with time and this becomes more evident after 20 hours in the NMR tube (Figure 2.9).

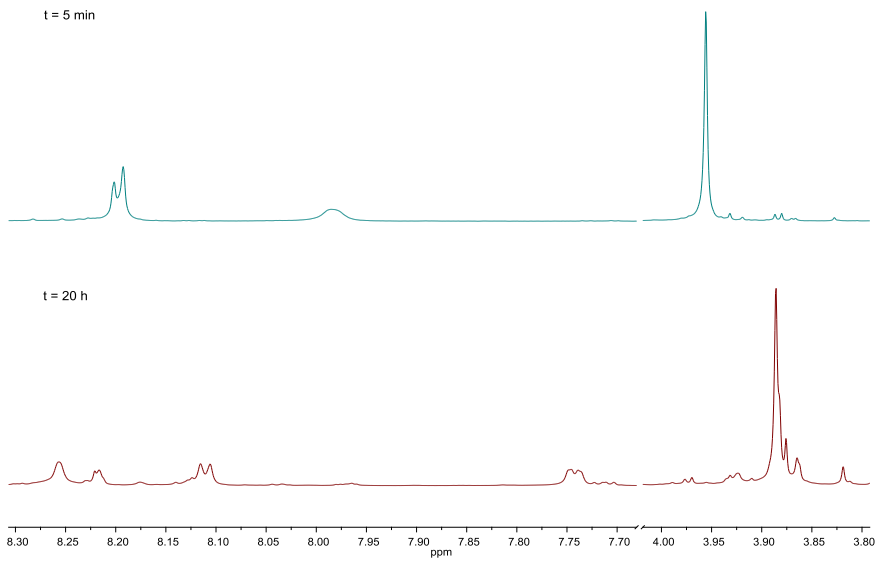

Figure 2.9: ^{1}H NMR spectra of **1** at t = 5 min and at t = 20 h (300 MHz, MeOD).

Boronic acid **1** was not further characterized and was used directly in the Suzuki coupling reaction. This is a common practice when using unstable boronic acids.

An alternative method was also investigated so that the boronic acid **1** could be isolated and not its anhydride. This was based on a modified literature protocol[(139)] where the borylation occurs *in situ*. The initial bromopyridine and triisopropylborate are placed together in a dry purged flask and *n*-butyllithium is added dropwise. This is based on the assumption that the lithium-halogen exchange is much faster than the reaction of *n*-butyllithium and triisopropylborate. Hence, the formed lithiopyridine reacts rapidly with the borate source so that it cannot undergo side reactions.[(139)]

By following this procedure the boronic acid **1** was isolated in 48% yield as the water soluble HCl salt, as confirmed by EI+-MS with a peak at *m/z* 189 Da. The infrared spectrum presents a broad band at 3194 cm^{-1} which indicates the presence of the boronic acid. However, a sharp band at 693 cm^{-1} is also present. This band is assigned to the presence of the anhydride. Therefore, the isolated product might be a mixture of boronic acid and anhydride, the so-called semi-anhydride.

Both boronic acids synthesised by the two different methods discussed above (inverse addition mode and *in situ* reaction) were reacted with **2** under the same reaction conditions in a Suzuki coupling. Conversion and yields were comparable. Therefore, since **1** was synthesised in a higher yield following the first

method, the inverse addition mode, this was the chosen protocol to synthesise successive batches of **1**.

2.3.1.3. Synthesis of the spacer building block 2

The second building block necessary to synthesise ligand $\mathbf{L^{OMe}}$ was prepared in two steps following a slightly modified literature protocol (Scheme 2.3).[140]

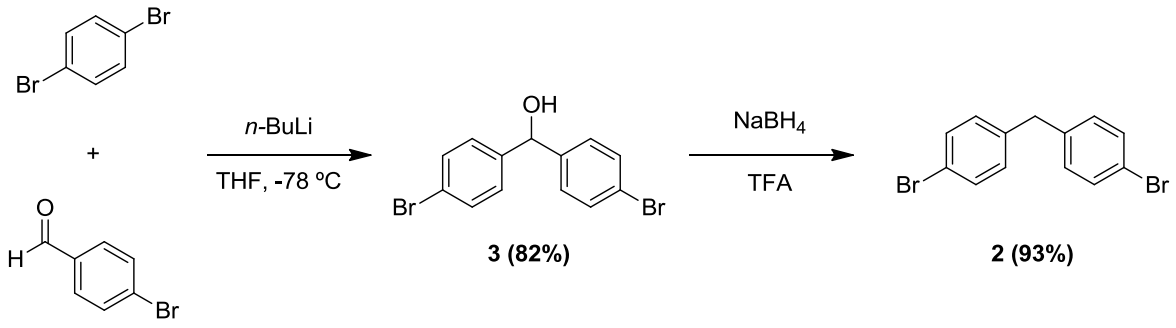

Scheme 2.3: Two step synthesis of the carbon spacer building block.

The mono-substituted lithium salt of 1,4-dibromobenzene was formed by addition of *n*-butyllithium under argon atmosphere and low temperature. This mixture was then added to 4-bromobenzaldehyde to form the intermediate alcohol **3**. Alcohol **3** was then reduced with sodium borohydride in trifluoroacetic acid, followed by quenching of the carbocation with water to yield **2**. Alcohols that can form relatively stable carbocations in trifluoroacetic acid media can be reduced to the corresponding hydrocarbons due to the propensity of trifluoroacetic acid to stabilize carbocations. This particular secondary carbocation is also stabilized by the adjacent electron-rich phenyl rings. Both compounds **2** and **3** were fully

characterized, with the ^{1}H and ^{13}C NMR, EI+-MS and IR data in agreement with that reported in the literature.(140)

2.3.1.4. Synthesis of ligand L^{OMe}

Once the building blocks were formed, the synthetic route towards the formation of ligand **L^{OMe}** continued. Synthesis of ligand **L^{OMe}** was first attempted following the previous reported protocol for the first generation of compounds.(133) 5-(Methoxypyridin-3-yl)boronic acid **1** and bis(4-bromophenyl)methane **2** were reacted in a Suzuki cross-coupling reaction using $Pd(PPh_3)_4$ as catalyst and Na_2CO_3 as base in a 1:1 mixture of water and THF (Scheme 2.4).

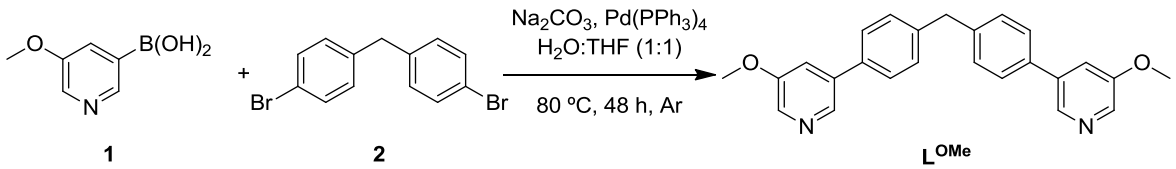

Scheme 2.4: Synthesis of ligand **L^{OMe}** using $Pd(PPh_3)_4$ as catalyst.

This protocol led to the formation of triphenylphosphine oxide. This side product made the purification of ligand **L^{OMe}** more complex as both (ligand and triphenylphosphine oxide) were co-eluting on silica column chromatography and further purification (a second work up) was required to isolate the pure ligand **L^{OMe}**. The yield was acceptable (60%), however this protocol was time consuming and therefore ineffective.

A new strategy was then applied based on a modified literature procedure.[141] The $Pd(PPh_3)_4$ catalyst was substituted by $Pd_2(dba)_3$, avoiding the formation of triphenylphosphine by-products (Scheme 2.5).

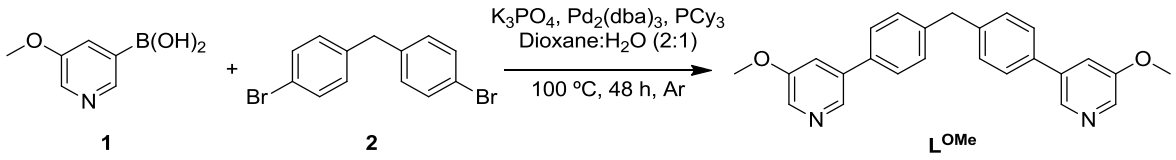

1 **2** $\mathbf{L^{OMe}}$

Scheme 2.5: Synthesis of ligand $\mathbf{L^{OMe}}$ using $Pd_2(dba)_3$ as catalyst.

As confirmed by thin layer chromatography, ligand $\mathbf{L^{OMe}}$ was formed as the predominant product; however starting materials and some side products were present too. Ligand $\mathbf{L^{OMe}}$ was purified by silica flash column chromatography in 66% yield.

ESI+ mass spectrometry and ^1H NMR spectroscopy confirmed the formation of ligand $\mathbf{L^{OMe}}$. The ^1H NMR spectrum in deuterated chloroform reveals a single set of resonances characteristic of a symmetric ligand (Figure 2.10).

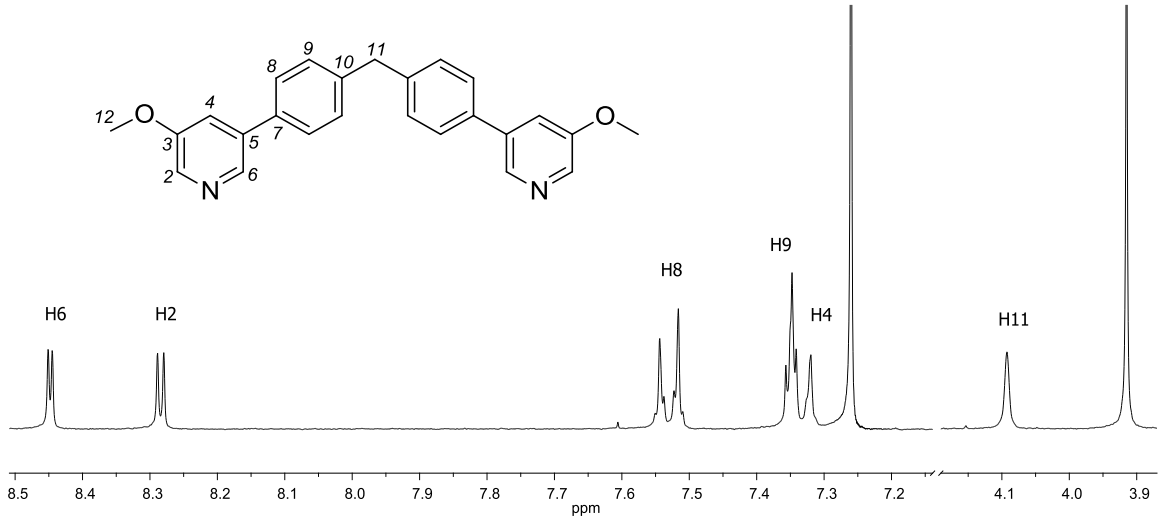

Figure 2.10: ^{1}H NMR spectrum of ligand **L^{OMe}** (300 MHz, $CDCl_3$).

Formation of the desired ligand **L^{OMe}** was also confirmed by X-ray crystallography as shown in Figure 2.11. Crystals of **L^{OMe}** were grown by slow evaporation of a solution of ligand **L^{OMe}** in deuterated chloroform. The coordinating pyridine rings are nearly on the same plane with a small angle of 5º with respect to one another. This forces the phenyl rings to twist by 58º with respect to each other and by 37º with respect to the pyridine rings. The methyl ether groups at the sides of the pyridine rings are both pointing towards the outer edge of the ligand. This will be different upon formation of the complex (*vide infra*).

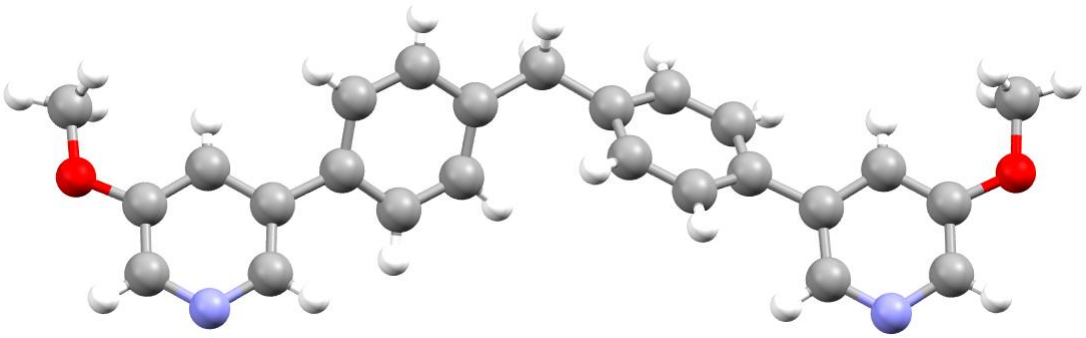

Figure 2.11: Crystal structure of ligand **L^{OMe}**.

2.3.1.5. Synthesis of the palladium(II) complex [Pd$_2$L$^{OMe}_4$][(BF$_4$)$_4$]

The first generation of palladium(II) complexes were synthesised overnight at room temperature using tetrakis(acetonitrile)palladium(II) tetrafluoroborate as the palladium source.[133] When employing this procedure a mixture of two compounds was isolated on a 10:1 ratio based on their relative ^{1}H NMR signal intensities, with the desired tetra-stranded complex being the major product (Figure 2.12).

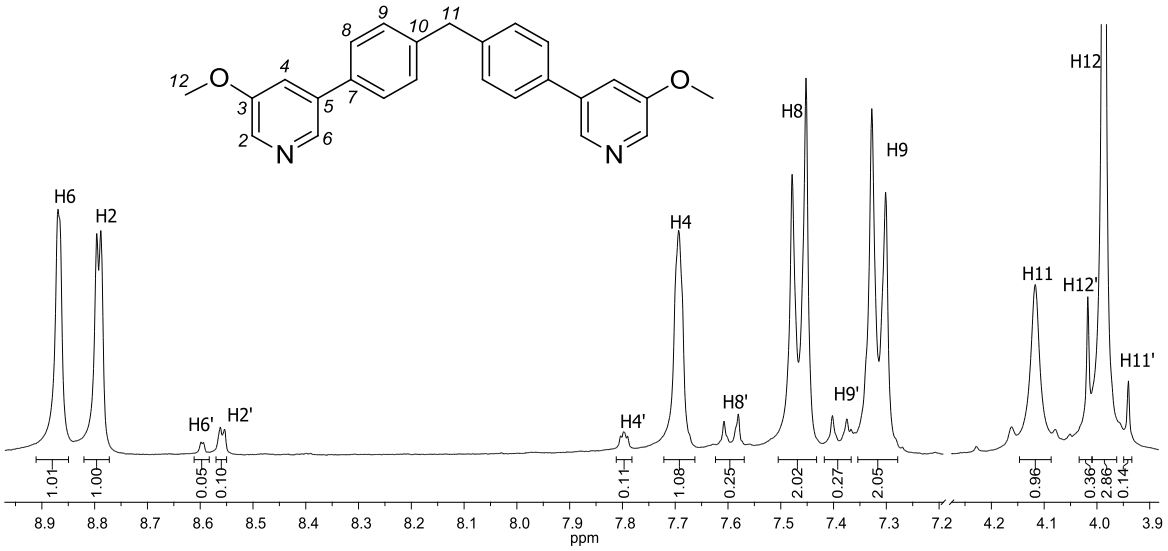

Figure 2.12: ^{1}H NMR spectrum of isolated crude mixture of **[Pd$_2$L$^{OMe}_4$][(BF$_4$)$_4$]** (300 MHz, CD_3CN).

This mixture could not be purified by washing with different solvents as performed on the first generation. This same reaction was monitored via ^{1}H NMR spectroscopy in deuterated acetonitrile. It was observed that the formation of the tetra-stranded cylinder occurred within minutes and that the amount of the second product decreased with time (Figure 2.13).

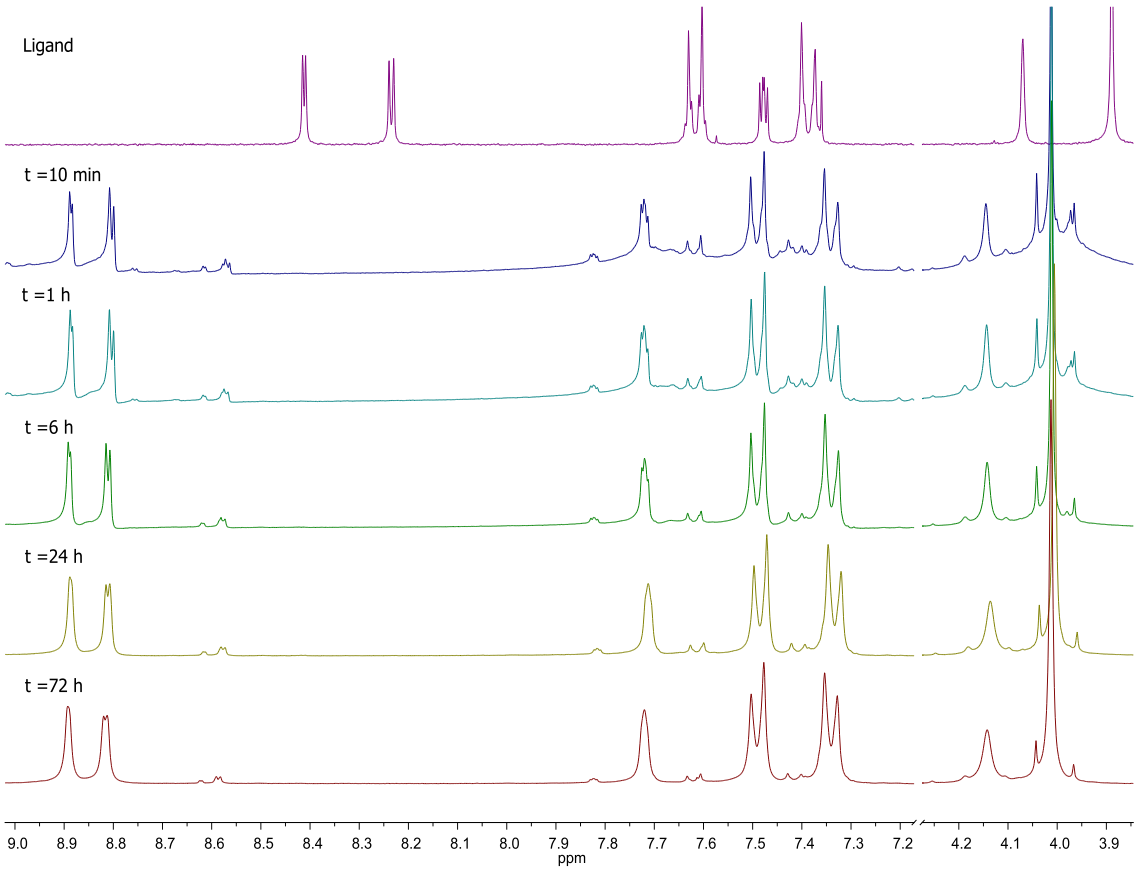

Figure 2.13: ^{1}H NMR spectra of the reaction between **L^{OMe}** and **[Pd(CH$_3$CN)$_4$][(BF$_4$)$_4$]** in CD$_3$CN (300 MHz, CD$_3$CN).

It was also noticed that if the ^{1}H NMR of the isolated **[Pd$_2$L$^{OMe}_4$][(BF$_4$)$_4$]** crude mixture was carried out in deuterated dimethyl sulfoxide, the ratio 10:1 progressively balanced to 1:1 after four days (Figure 2.14).

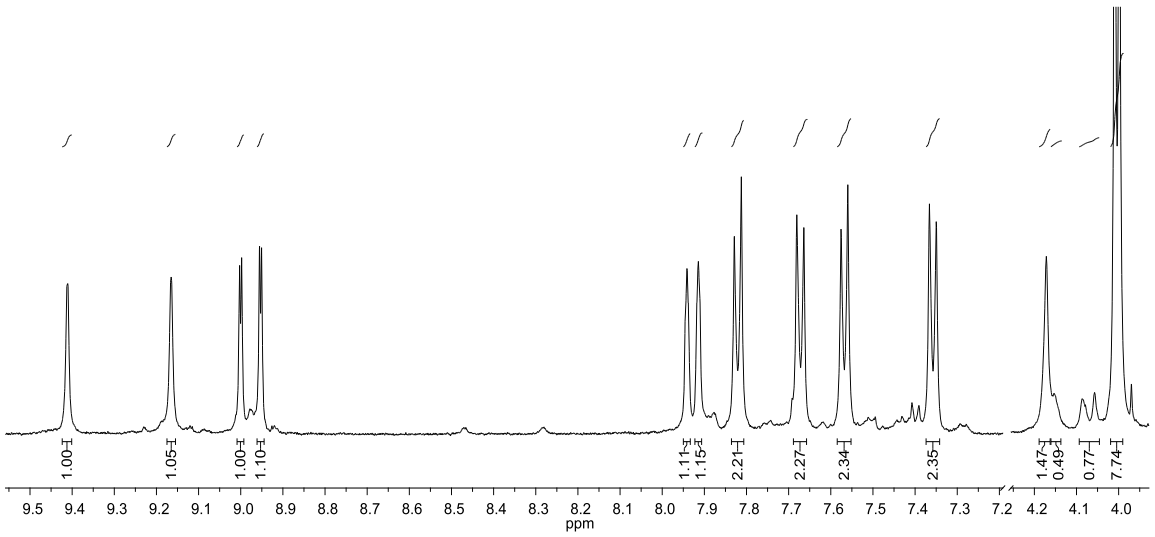

Figure 2.14: ^{1}H NMR of **$[Pd_2L^{OMe}_4][(BF_4)_4]$** crude mixture when the ratio of the two components becomes 1:1 (500 MHz, DMSO-d_6).

This change occurred without any observed precipitate and without a change in the amount of material as the overall integrals were constant (relative to the solvent), showing that there was an interconversion and not a degradation of the first major compound. It was then decided to monitor the reaction in deuterated dimethylsulfoxide by ^{1}H NMR spectroscopy (Figure 2.15). The formation of the two compounds occurred within minutes and the ratios were constant with time.

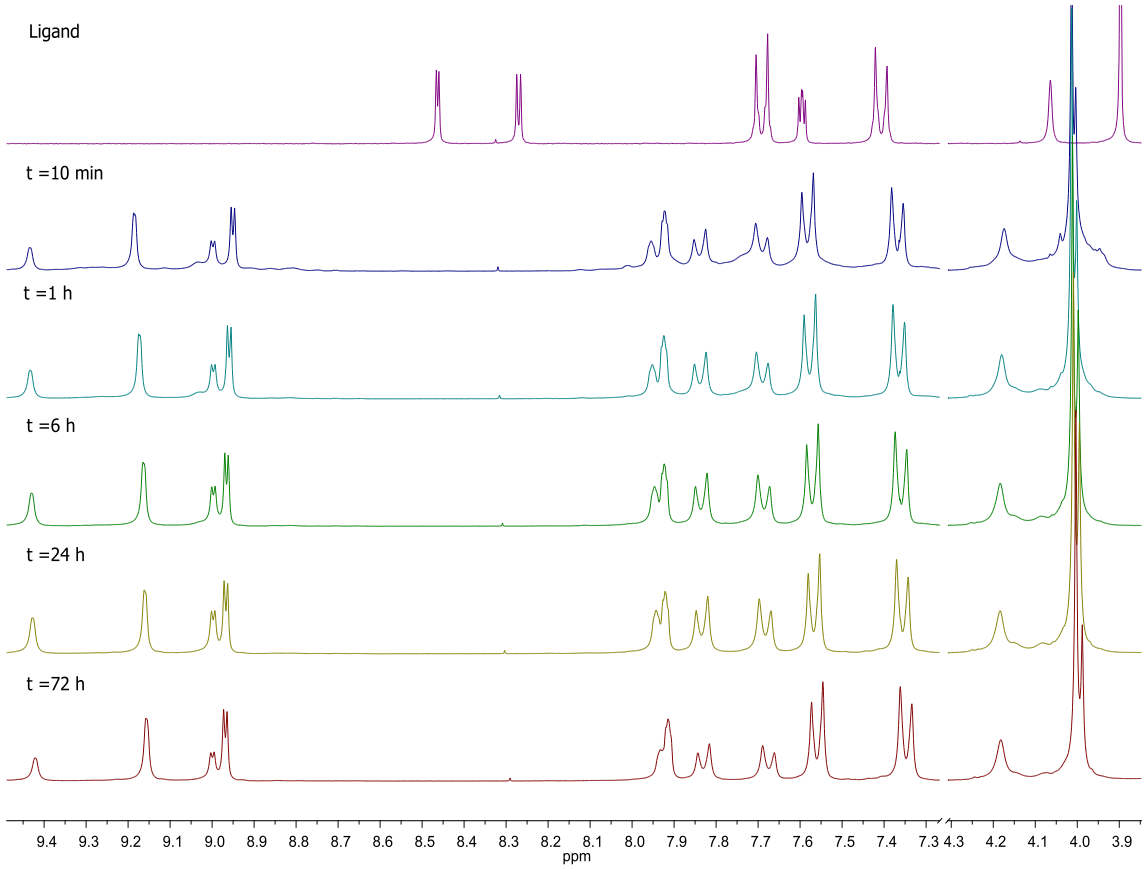

Figure 2.15: ^{1}H NMR spectra of the reaction of $\mathbf{L^{OMe}}$ and $\mathbf{[Pd(CH_3CN)_4][(BF_4)_4]}$ in DMSO-d_6 (300 MHz, DMSO-d_6).

Unfortunately, this second species was not detected by ESI-MS despite numerous attempts. Only the desired tetra-stranded complex was observed. This could imply that the two species are isomers or that the second species did not fly in the mass spectrometer.

In order to better understand the nature of this second species an NMR diffusion experiment was performed. The DOSY NMR (diffusion-ordered spectroscopy) in deuterated dimethyl sulfoxide showed two species with different translation diffusion coefficients (Figure 2.16).

This implies that there are two different molecules of different size and shape that therefore diffuse with different coefficients. These two clearly different species may be assigned to a tetra-stranded box-like **$[Pd_2L^{OMe}{}_4][(BF_4)_4]$** and a double-walled triangular **$[Pd_3L^{OMe}{}_6][(BF_4)_6]$** species.

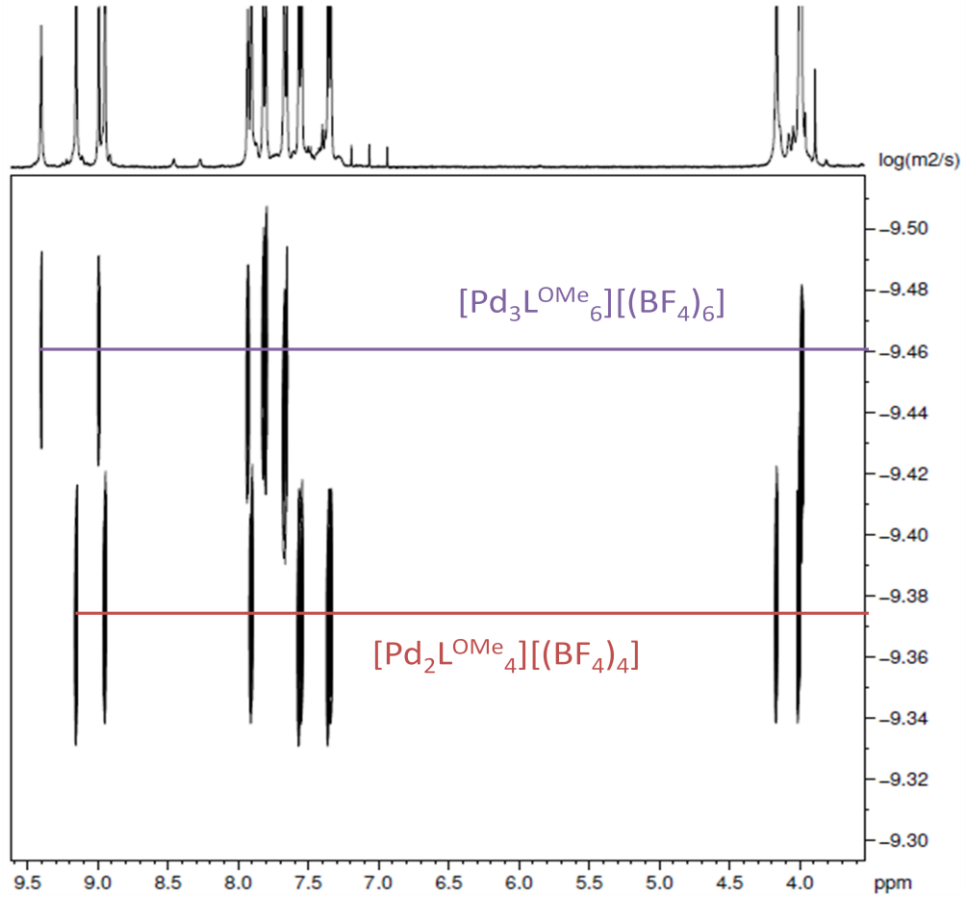

Figure 2.16: DOSY NMR for **$[Pd_2L^{OMe}{}_4][(BF_4)_4]$** crude (400 MHz, DMSO-$d_6$).

Similar findings were previously reported by Hannon *et al*. in copper helicates.[142] These copper helicates were formed via reaction of ligand **$L^{im\text{-}Me}$** (Figure 2.17) and **$[Cu(CH_3CN)_4][PF_6]$** in methanol yielding two different compounds as shown by ^{1}H NMR and ESI$^+$-MS.

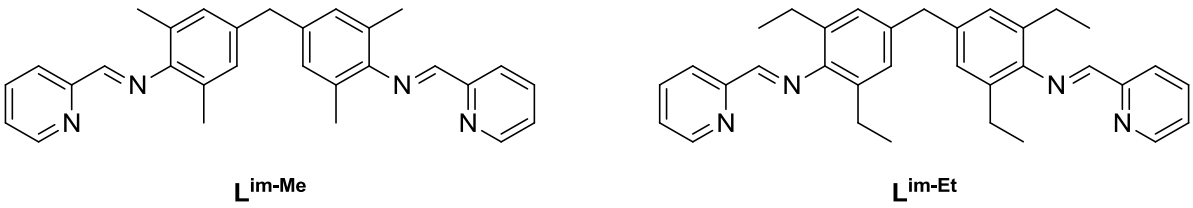

$L^{im\text{-}Me}$ $L^{im\text{-}Et}$

Figure 2.17: Structures of ligands $L^{im\text{-}Me}$ and $L^{im\text{-}Et}$.

These compounds were identified as a dimeric helix $[Cu_2L^{im\text{-}Me}{}_2][(PF_6)_2]$ which corresponded to the major species and a triangular helical trimer $[Cu_3L^{im\text{-}Me}{}_3][(PF_6)_3]$ as the minor species (Figure 2.18). The trimer was entropically disfavoured when reacting $L^{im\text{-}Et}$ (Figure 2.17) with $[Cu(CH_3CN)_4][PF_6]$.(143)

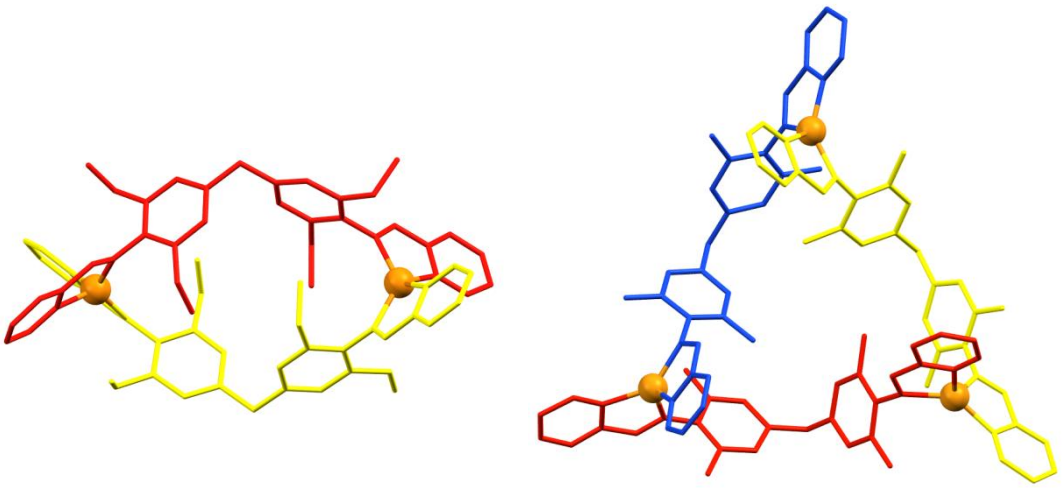

Figure 2.18: Crystal structures of $[Cu_2L^{im\text{-}Et}{}_2][(PF_6)_2]$ dimer (CCDC 231266)(143) (left) and $[Cu_3L^{im\text{-}Me}{}_3][(PF_6)_3]$ trimer (CCDC 187879)(142) (right).

The diffusion coefficients for the $[Cu_2L^{im\text{-}Me}{}_2][(PF_6)_2]$ dimer and $[Cu_3L^{im\text{-}Me}{}_3][(PF_6)_3]$ trimer in deuterated dichloromethane were found to be $1.1 \cdot 10^{-9}$ m^2s^{-1} and $9.6 \cdot 10^{-10}$ m^2s^{-1} respectively.(142) These can be related to those obtained in deuterated dimethyl sulfoxide for the palladium $[Pd_2L^{OMe}{}_4][(BF_4)_4]$

dimer ($4.2 \cdot 10^{-10}$ m^2s^{-1}) and the palladium **$[Pd_3L^{OMe}_6][(BF_4)_6]$** trimer ($3.5 \cdot 10^{-10}$ m^2s^{-1}). The larger species in solution will move more slowly giving a smaller diffusion coefficient. A larger structure, such as **$[Pd_4L^{OMe}_8][(BF_4)_8]$**, can be discarded as this species will present two different environments for each four ligands. This type of supramolecular motif has been reported by Fujita (*see section 1.3.6.*)[132] and has also been observed as a minor product in the first generation of compounds when using ligand **L^{Et}**.[133]

NOE NMR experiments were also performed on this two-component mixture. When exciting at both H9 protons, two different NOE contacts for the CH_2 spacer unit (H11) were evident (Figure 2.19). A singlet was observed for the dimer and two doublets were observed for the trimer.

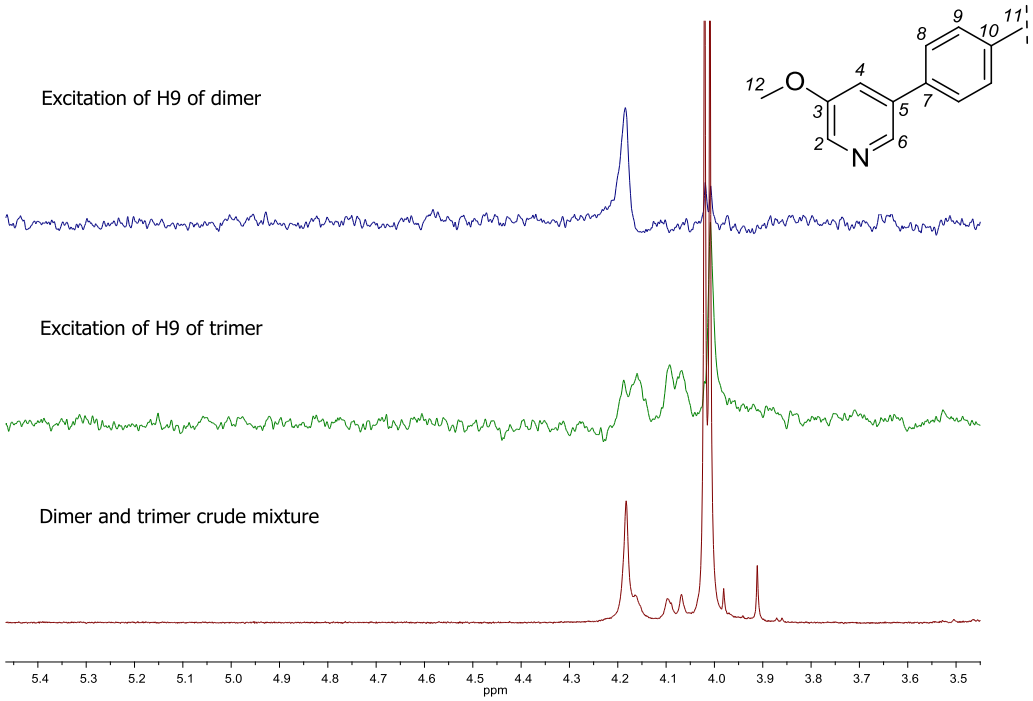

Figure 2.19: NOE ^{1}H NMR spectra of **$[Pd_2L^{OMe}_4][(BF_4)_4]$** crude with selective excitation on H9 of both species present in solution (500 MHz, DMSO-d_6).

These two different resonances have been observed and assigned to the presence of a chiral and an achiral CH_2 spacer unit in previous work in the Hannon group.[143] In that case this splitting was observed in a double-stranded copper cylinder due to the flexibility of the ligand $\mathbf{L^{im}}$ and the lability of the copper metal ions. These kind of complexes can adopt two conformations in solution that are in equilibrium leading to two isomeric structures: a helicate (*rac*-isomer) or a metallo-cyclophane or box architecture (*meso*-isomer). The box isomer appears when the ligand is too flexible to impose the same stereochemistry at both copper centres. The difference between both is the manner in which the ligands wrap around the axis defined by the metal ions (shown in orange); over and over in the box and over and under in the helix (Figure 2.20).

Figure 2.20: Schematic representation of copper box and helix cylinders.

In the helicate, both protons in the CH_2 spacer unit are equivalent and therefore resonate as a singlet in the ^{1}H NMR, whereas in the box they are different. One proton points into the cavity of the box while the other one points towards the exterior of the box (Figure 2.21). This is shown in the ^{1}H NMR as a pair of doublets.

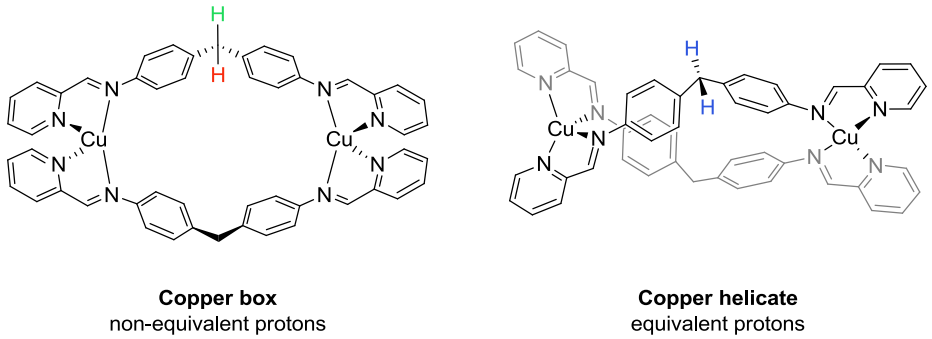

Figure 2.21: Copper box (left) and helicate (right) showing the positions of the CH_2 protons.

The same effect will apply to the palladium trimer structure. One of the protons of the methylene spacer unit will be pointing towards one of the other ligands on the same edge of the triangle, and the other could be pointing out of the triangle (Figure 2.22). A coupling constant of 13 Hz was observed for the pair of doublets which is in complete agreement to that observed for the copper-cyclophane.

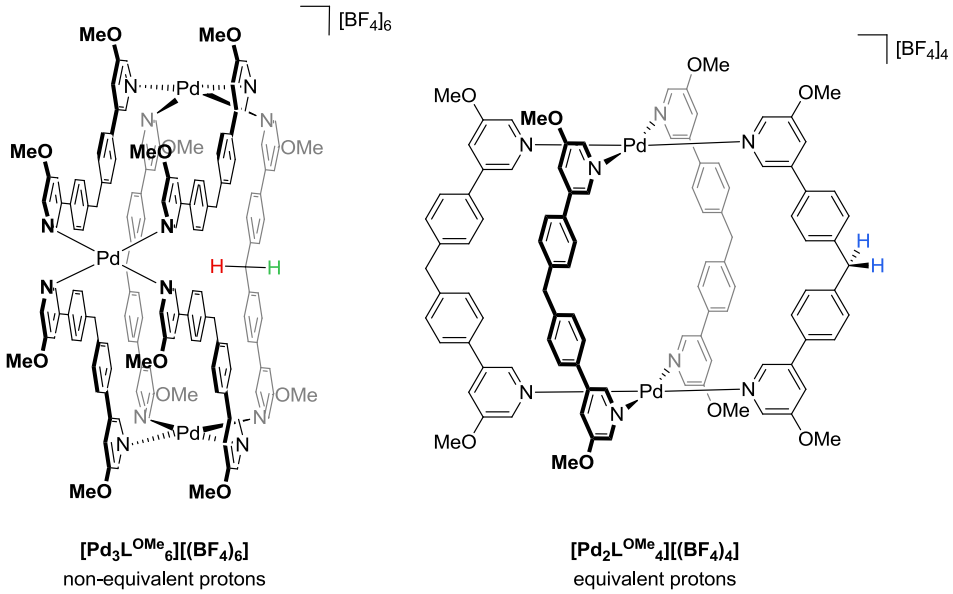

Figure 2.22: Trimer (left) and dimer (right) showing the position of the CH_2 protons.

Double-walled triangular species have also been identified in the first generation of palladium(II) complexes with **L^{Et}** (*see section 2.1.*) and when exchanging the tetrafluoroborate counter-ions of the parent palladium(II) cylinder with trifluoroacetic anions. It was crystallized from a crude mixture however, once again, the molecular ion for this species was not able to be observed via ESI-MS.[133]

Variable temperature ^{1}H NMR experiments were performed on the 1:1 mixture of compounds in deuterated dimethyl sulfoxide (Figure 2.23).

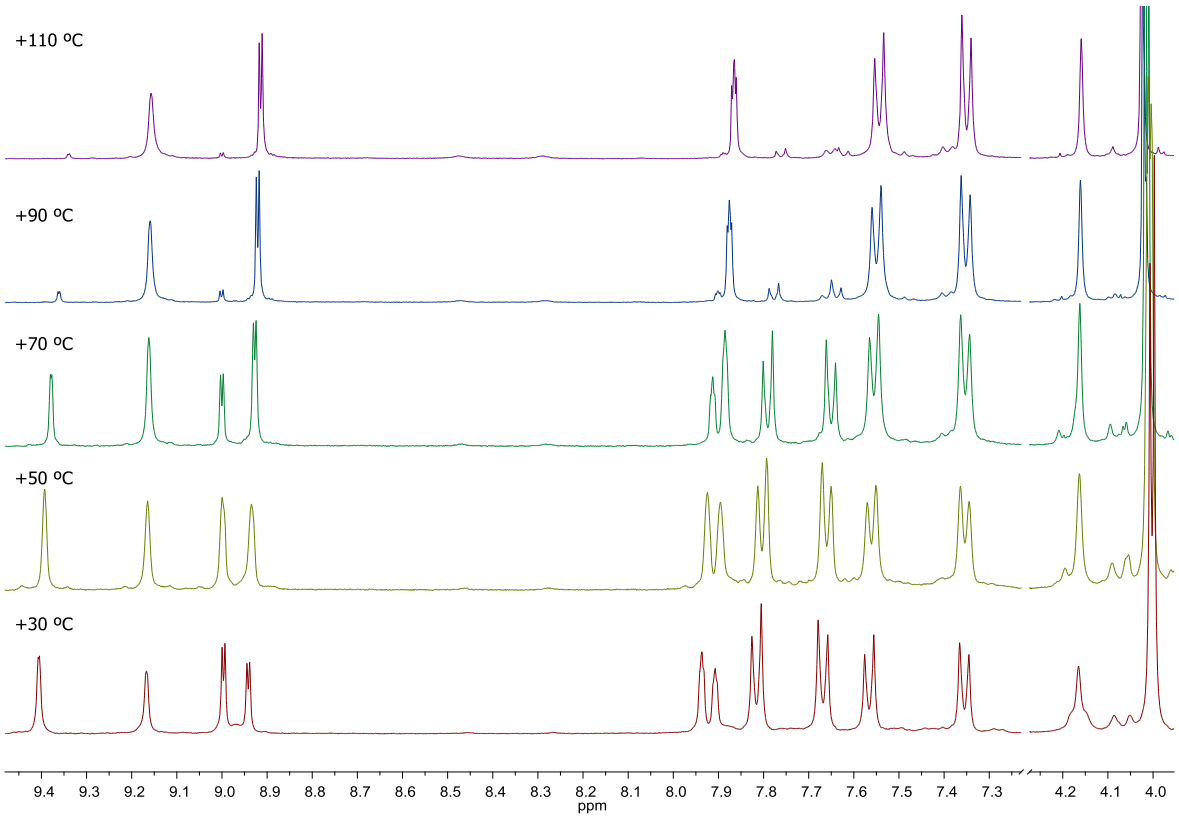

Figure 2.23: Variable temperature ^{1}H NMR of **[Pd$_2$L$^{OMe}_4$][BF$_4$)$_4$]** crude mixture (400 MHz, DMSO-d$_6$).

It was observed that the trimeric species nearly disappeared when increasing the temperature. This means that the species with lower nuclearity is favoured at high temperature. When the sample was cooled down, the trimeric species started to appear again however it needed 4 days to equilibrate to the 1:1 ratio. It is then clear that there is an equilibrium between these two species. The tetra-stranded complex is favoured at higher temperatures and the triangle formation occurs with time in dimethyl sulfoxide. This might be due to the lability of the Pd-N bond.

Different HPLC purification methods on reverse-phase columns were explored in order to isolate both compounds separately and properly characterize both species. An acetonitrile-water gradient from 100% water to 100% acetonitrile over 40 minutes gave an analytical HPLC chromatogram with trimer, dimer and free ligand eluting together at around 30 minutes; hence it was impossible to separate them. Increasing the polarity of the solvent system was explored in order to separate these two species. It was known from the first generation of complexes that when using trifluoroacetic acid to increase the polarity of the solvent system, the tetrafluoroborate counter-ion was exchanged during the course of the HPLC run. This led to the formation of trimeric species,[133] therefore trifluoroacetic acid was discounted. A good separation was achieved instead by incorporating a 0.05% solution of tetrabutylammonium tetrafluoroborate salt in both acetonitrile and water solvents. A ramp over 40 minutes from water to acetonitrile yielded two main peaks. These two peaks were collected separately and analyzed via ^{1}H NMR. The first peak corresponded to the ligand and the second to the

tetra-stranded complex. This tetra-stranded complex contained a significant amount of tetrabutylammonium salt. The sample was passed through a desalting column resulting in a decrease of the salt concentration but complete removal could not be achieved. This might be due to the “large” size of the tetrabutylammonium salt for this kind of size exclusion column. However, a “smaller” salt (tetramethylammonium tetrafluoroborate) was also employed without success.

The trimer could not be identified from any of the smaller peaks from the HPLC chromatogram via ESI-MS (a sufficient amount for a ^{1}H NMR experiment could not be collected). Free ligand was not observed in any of the previous NMR studies, however it was present in the HPLC analysis. This could indicate that the trimer is decomposing during the HPLC purification process to yield the free ligand.

Since HPLC could not be used to fully purify the tetra-stranded palladium(II) cylinder, a new strategy needed to be applied. Variable temperature ^{1}H NMR showed that the desired tetra-stranded complex was the more stable species at high temperatures. It was therefore decided to perform the reaction with heat instead of at room temperature. Ligand $\mathbf{L^{OMe}}$ was coordinated to palladium(II) by adding tetrakis(acetonitrile)palladium(II) tetrafluoroborate to a hot solution of ligand $\mathbf{L^{OMe}}$ in acetonitrile. The mixture was heated at 80 ºC for 6 hours. Diethyl ether was added to the solution to precipitate a white solid in 78% yield. The ^{1}H NMR shows peaks corresponding to only one species, which corresponds to the peaks of the dimeric species seen previously in the crude mixture. If compared to the free

ligand, there is a downfield shift of the protons close to the nitrogen upon coordination of the palladium metal centre due to a deshielding effect, caused by a reduced electron density of these protons, especially for protons α to the nitrogen (H2 and H6) (Figure 2.24). The proton assignment was performed with the aid of a 2D-COSY and a 2D-NOESY. The NOESY experiment proved to be particularly useful as contacts between H6 and H8 as well as contacts between H2 and H12 were observed.

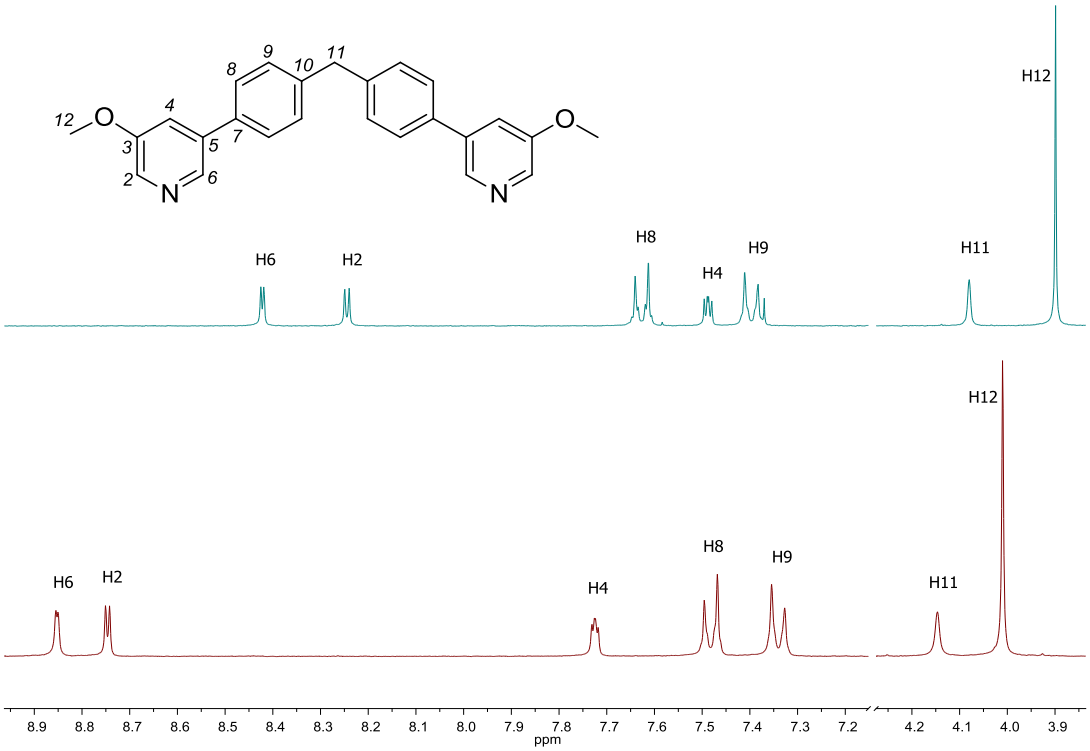

Figure 2.24: Comparison of ^{1}H NMR spectra in CD_3CN of $\mathbf{L^{OMe}}$ (top) and $\mathbf{[Pd_2L^{OMe}{}_4][(BF_4)_4]}$ (bottom)‡.

‡ Please note that assignment of the protons of $\mathbf{L^{OMe}}$ was performed with the aid of a NOESY experiment in $CDCl_3$. Ligand $\mathbf{L^{OMe}}$ was not soluble enough to perform the NOESY experiment in CD_3CN. It has been assumed that the positions of the protons have not significantly changed even if the chemical shifts are slightly different. This will be the case for all $\mathbf{L^{X\text{-}OMe}}$ ligands in this section.

It was also observed that the ^{1}H NMR spectrum suffered variations in the chemical shifts of H6 and H2 protons depending on the concentration selected to perform the experiment (Figure 2.25). These are the protons closest to the coordinating nitrogen donors and thus this could indicate some lability of the Pd-N bond.

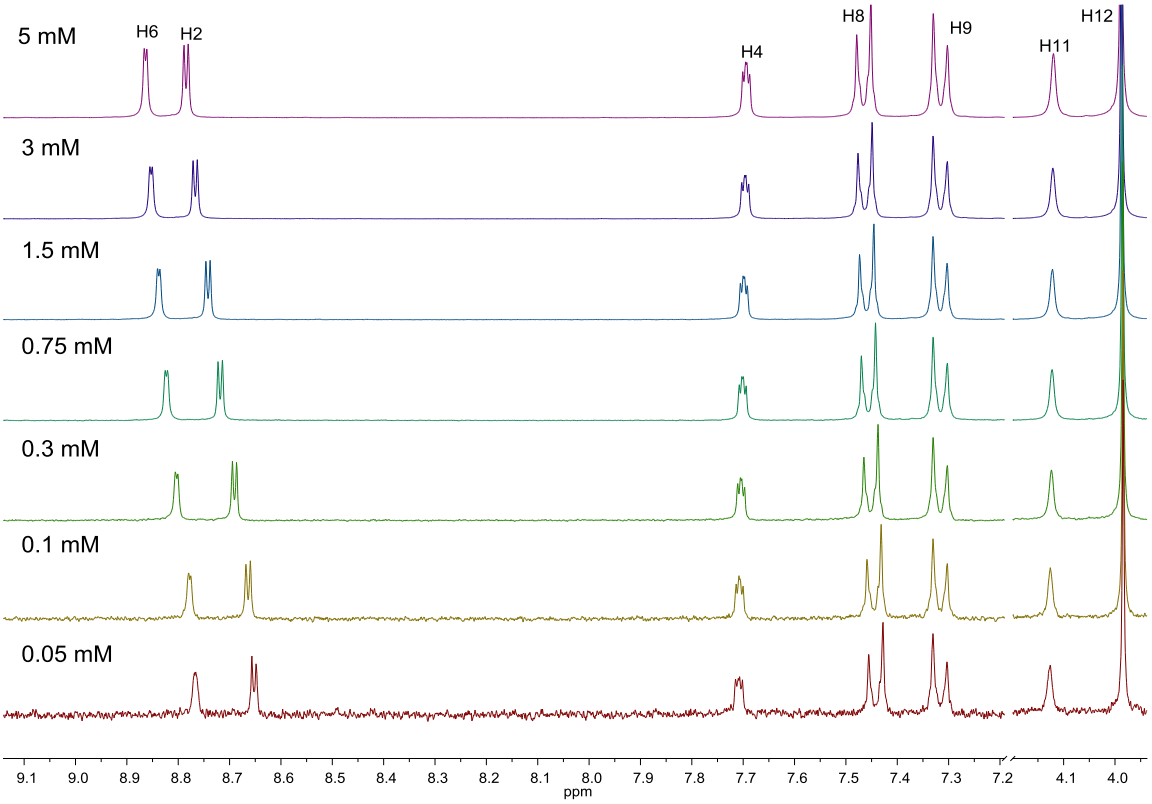

Figure 2.25: Stacked ^{1}H NMR spectra of **[Pd$_2$L$^{OMe}_4$][(BF$_4$)$_4$]** at different concentrations (300 MHz, CD_3CN).

MALDI-TOF was employed to attempt to characterize the tetra-stranded complex. It showed a peak for the molecular ion $[(Pd_2L^{OMe}_4)+3BF_4]^+$ at *m/z* 2003 Da and another peak at *m/z* 778 Da that could be assigned to $[(Pd_2L^{OMe}_4)+BF_4+NaBF_4]^{3+}$. The other peaks could not be assigned to any other

species related to the tetra-stranded complex. This might be due to the interaction of the complex with the matrix, 2,4,6-Trihydroxyacetophenone (THAP), so that the spectra cannot be interpreted. Other matrixes were employed (gentisic acid and 6-aza-2-thiothymine) with no success. It has also been observed previously that the detection of high charge species of this kind is very rare via MALDI-TOF, with the molecular ion being the only possible species found.

ESI+-MS gave a more useful result, as $[Pd_2L^{OMe}_4]^{4+}$, $[Pd_2L^{OMe}_4(BF_4)]^{3+}$, $[Pd_2L^{OMe}_4(BF_4)_2]^{2+}$ and $[Pd_2L^{OMe}_4(BF_4)_3]^{+}$ species could be detected. Some free ligand was also observed due to the breakage of the complex during ionization. Low cone voltages (10-15 eV) are normally used to minimize this kind of side product, however sometimes they are inevitable. In contrast to the iron(II) triple stranded cylinders, the cationic species were always present together with their counter-ions. This might indicate a strong attraction of the tetrafluoroborate counter-ions to the palladium(II) metal centres.

The infrared spectrum showed a characteristic band at 1032 cm^{-1} for the non-coordinated BF_4^- anions.

^{19}F NMR spectroscopy was also used to determine whether the four tetrafluoroborate counter-ions are equivalent or not. The ^{19}F NMR showed two peaks (Figure 2.26). These two peaks are very close to each other and therefore cannot be due to different environments of the anions within the molecule. This splitting is due to the boron isotopes (^{10}B and ^{11}B). The abundance of these isotopes is 20% and 80% respectively and that is the ratio observed between the

relative intensity of their NMR signals. These observations have been previously reported by Levinger *et al*.[144] The chemical shifts are also in good agreement with that of free tetrafluoroborate anions in acetonitrile solutions.[127]

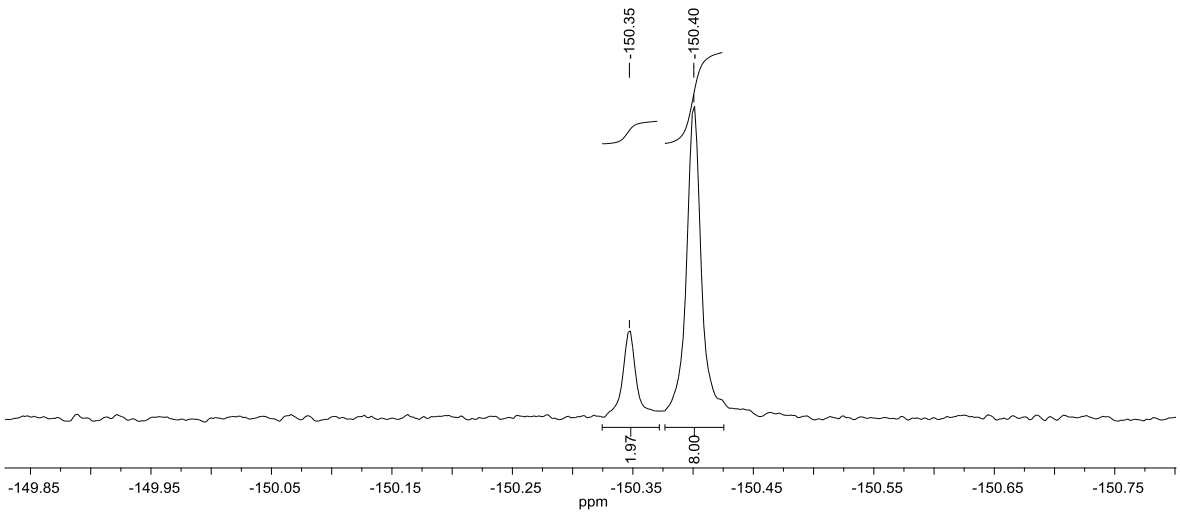

Figure 2.26: ^{19}F NMR of **[$Pd_2L^{OMe}_4$][$(BF_4)_4$]** (300 MHz, CD_3CN).

Colourless crystals of this pure tetra-stranded complex suitable for X-ray diffraction were obtained by the slow diffusion of diethyl ether into a solution of the complex in acetonitrile. The X-ray crystal structure confirms the formation of the tetra-stranded, dinuclear palladium(II) complex (Figure 2.27). Each metal centre occupies a four-coordinate, square planar environment with Pd-N bond distances of 2.023(8) - 2.039(8) Å and N-Pd-N angles of 88.3(3) - 92.1(3)º. The two palladium centres are related by an inversion centre at the centre of the cavity such that only half of the molecule is crystallographically unique, with a symmetry relation of -x,-y,-z+2. There is also an approximate plane of symmetry through the four ligands which yields an achiral structure, as was also seen in the first generation of palladium(II) cylinders.

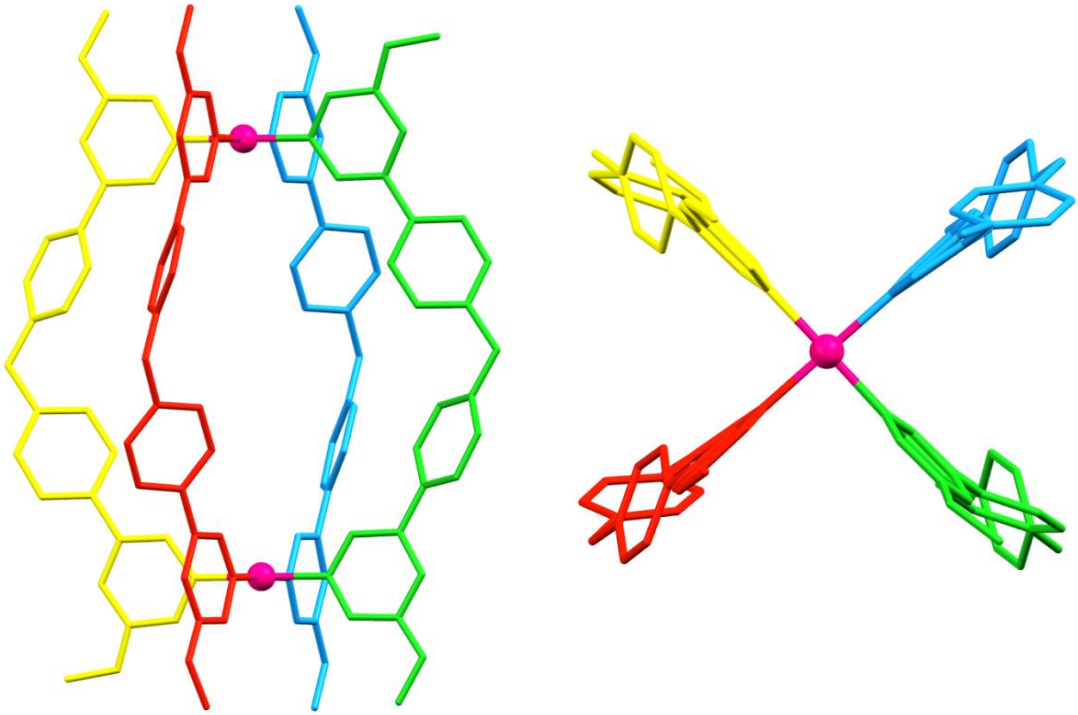

Figure 2.27: Crystal structure of **$[Pd_2L^{OMe}{}_4][(BF_4)_4]$**, side view (left) and top view (right). Hydrogen atoms, solvent molecules and counter-ions have been omitted for clarity.

The four ligands bridge the two palladium(II) centres resulting in a Pd···Pd separation of 12.4 Å. Within the ligands, the phenyl rings are twisted with respect to one another by 59º and 65º and with respect to the pyridine rings by 33º and 37º. The twisting of the phenyl rings in the complex is greater than that observed for the ligand (59º and 65º *versus* 58º). This results in a wider angle between the coordinating pyridines (9º and 13º in the complex and 5º in the ligand). The disposition of the four ligands around the two palladium(II) metal centres yields a central cavity (Figure 2.28).

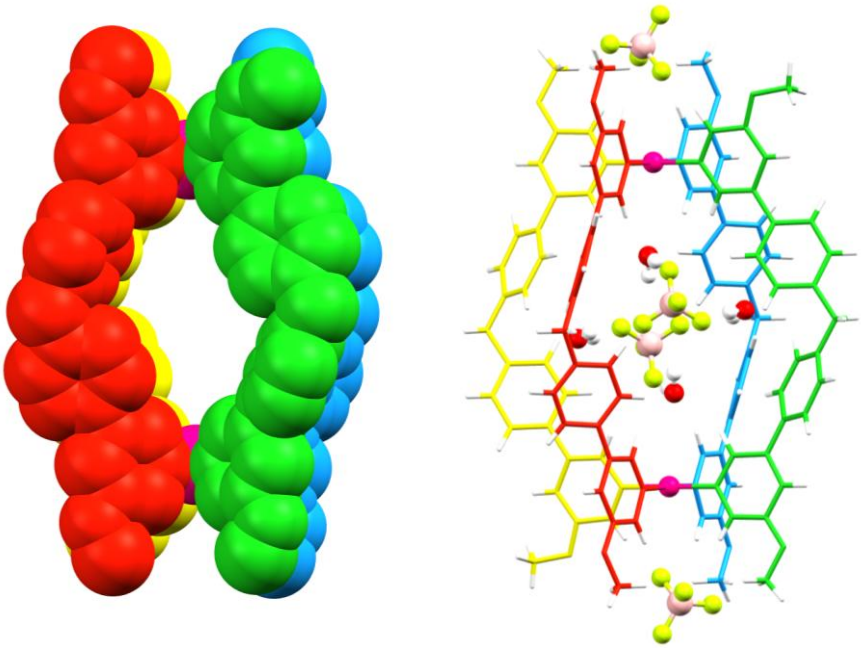

Figure 2.28: Spacefill representation of **$[Pd_2L^{OMe}_4][(BF_4)_4]$** (left). Hydrogen atoms, solvent molecules and counter-ions have been omitted for clarity. Capped sticks representation of **$[Pd_2L^{OMe}_4][(BF_4)_4]$** (right).

This cavity is home to two tetrafluoroborate counter-ions and four water molecules (Figure 2.28), that interact with each other via hydrogen bonds with donor-acceptor distances of 2.782(12) - 3.233(11) Å (Figure 2.29).

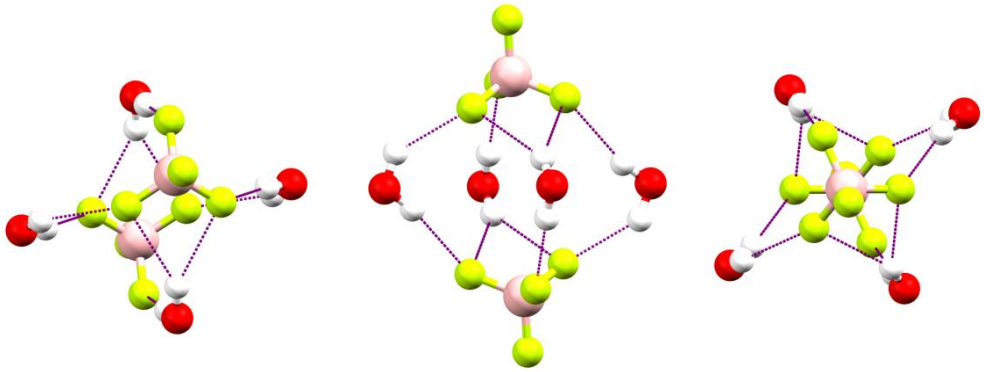

Figure 2.29: Views of the interaction between encapsulated tetrafluoroborate counter-ions and water molecules.

The other two tetrafluoroborate counter-ions are outside the cavity along the axis of the palladium centres. Each of these anions interacts with another tetrafluoroborate anion of the next molecule in the crystal packing via weak hydrogen bonds with acetonitrile molecules (Figure 2.30).

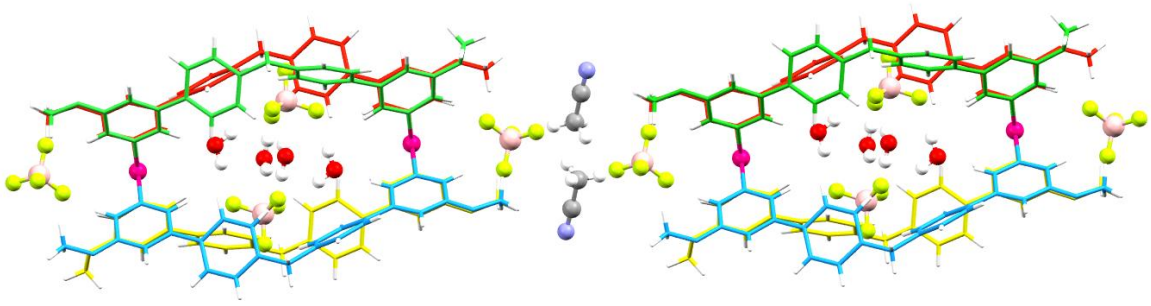

Figure 2.30: Crystal packing of two **$[Pd_2L^{OMe}_4][(BF_4)_4]$** molecules.

The overall length of this cylinder is greater than that observed for the first generation palladium(II) complex due to the introduction of the methyl ether group (C···C 19.7 Å and 15.0 Å : H··H 21.2 Å and 16.6 Å, respectively). The new palladium(II) complex is also bigger than its predecessor in terms of its diameter (C···C 14.4 Å : H··H 15.6 Å compared to C···C 13.7 Å : H··H 14.9 Å, measured from the central methylene spacer unit of one ligand to the opposite ligand). This difference in diameter arises from the different twisting observed on the spacer phenyl rings. In the parent palladium(II) cylinder the phenyl rings twist with respect to one another by 71º and 74º, while in the newly synthesised complex the twist is 59º and 65º.

This novel palladium(II) cylinder is soluble in dimethyl sulfoxide as is the parent analogue. However, it shows better solubility in acetonitrile and acetone, as well as organic solvent/water mixtures.

2.3.1.6. Synthesis of ligands $L^{O\text{-}OMe}$, $L^{NH\text{-}OMe}$ and $L^{S\text{-}OMe}$

In order to improve the solubility of the newly synthesised palladium(II) complex **$[Pd_2L^{OMe}{}_4][(BF_4)_4]$**, the CH_2 spacer unit was substituted by O, NH and S to form ligands **$L^{O\text{-}OMe}$**, **$L^{NH\text{-}OMe}$** and **$L^{S\text{-}OMe}$** respectively. Analogous retrosynthetic analysis was performed for the formation of the new ligands (Scheme 2.6).

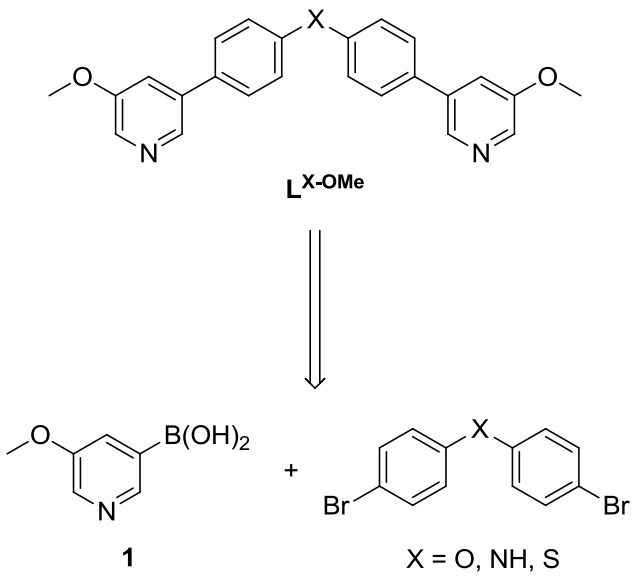

Scheme 2.6: Retrosynthetic analysis of ligands **$L^{X\text{-}OMe}$** (X = O, NH, S).

Bis(4-bromophenyl) ether and bis(4-bromophenyl)amine are commercially available, while bis(4-bromophenyl)sulfide was synthesised in 80% yield via bromination of diphenyl sulfide in dichloromethane (Scheme 2.7). Flash column

chromatography on silica gel with hexane as eluent was used to separate the monobrominated product from the desired bis(4-bromophenyl)sulfide **4**.

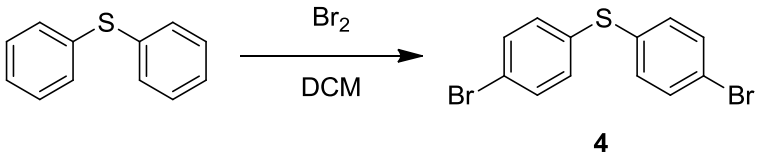

4

Scheme 2.7: Synthesis of bis(4-bromophenyl)sulfide **4**.

Synthesis of $\mathbf{L^{O\text{-}OMe}}$, $\mathbf{L^{NH\text{-}OMe}}$ and $\mathbf{L^{S\text{-}OMe}}$ ligands was also achieved via Suzuki coupling reaction following the $Pd_2(dba)_3$ protocol used for the synthesis of ligand $\mathbf{L^{OMe}}$ (Scheme 2.8).

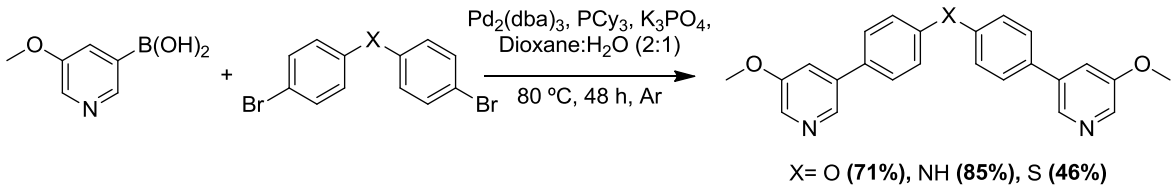

X= O **(71%),** NH **(85%),** S **(46%)**

Scheme 2.8: Synthesis of ligands $\mathbf{L^{O\text{-}OMe}}$, $\mathbf{L^{NH\text{-}OMe}}$ and $\mathbf{L^{S\text{-}OMe}}$.

High resolution ESI^+-MS confirms the formation of $\mathbf{L^{O\text{-}OMe}}$, $\mathbf{L^{NH\text{-}OMe}}$ and $\mathbf{L^{S\text{-}OMe}}$ ligands with the presence of the corresponding protonated molecular ions.

As expected the ^1H NMR spectra (Figure 2.24) are very similar to each other with nearly a complete overlay of the pyridine protons (H2, H6 and H4). The main differences are in the phenyl protons (H8 and H9) due to the effect of the different spacer units (CH_2, O, NH and S). The peak corresponding to the CH_2 protons at 4.09 ppm is obviously missing in the three spacer modified ligands, and

in the case of ligand $\mathbf{L^{NH\text{-}OMe}}$, the proton assigned to the NH from the spacer appears at 6.12 ppm.

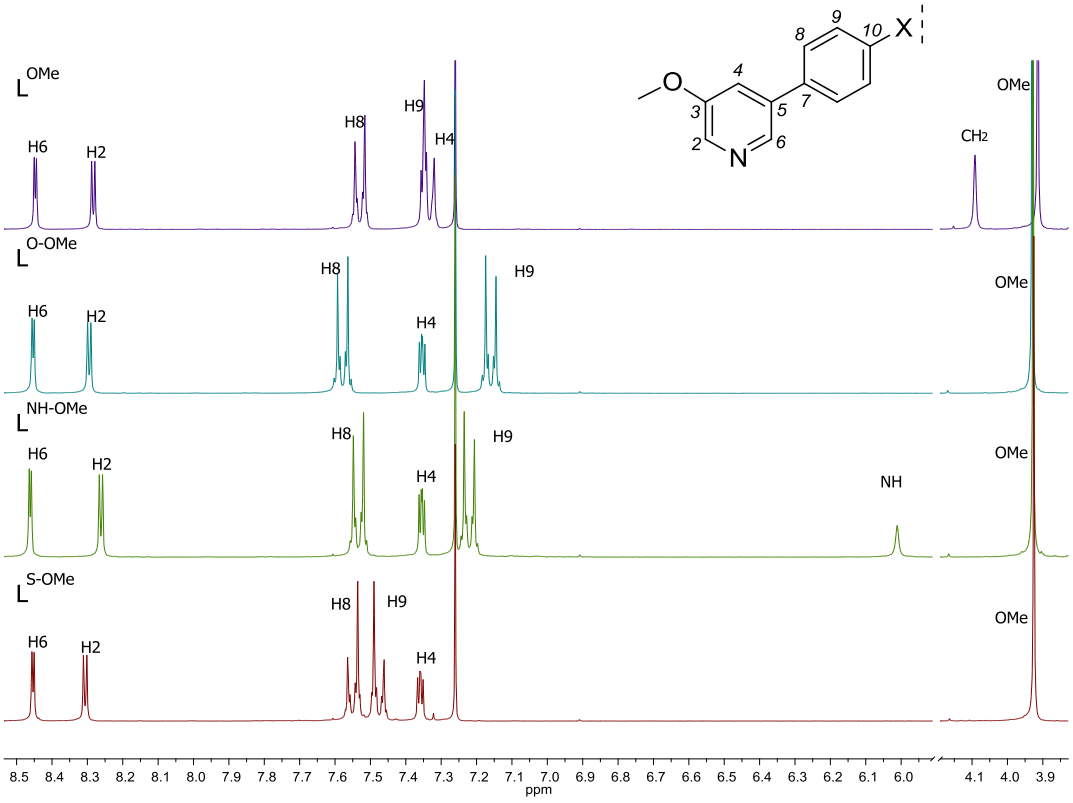

Figure 2.31: ^{1}H NMR spectra of the four methyl ether ligands: $\mathbf{L^{OMe}}$, $\mathbf{L^{O\text{-}OMe}}$, $\mathbf{L^{NH\text{-}OMe}}$ and $\mathbf{L^{S\text{-}OMe}}$ (300 MHz, $CDCl_3$).

Colourless crystals of $\mathbf{L^{O\text{-}OMe}}$ suitable for X-ray diffraction were obtained via slow evaporation of a deuterated chloroform solution of $\mathbf{L^{O\text{-}OMe}}$ (Figure 2.32). This structure is very similar to that seen for its analogue $\mathbf{L^{OMe}}$. The two pyridine rings are nearly coplanar with a small angle of 4º. Also the phenyl rings are twisted with respect to one another by 61º and with respect to the pyridine rings by 38º.

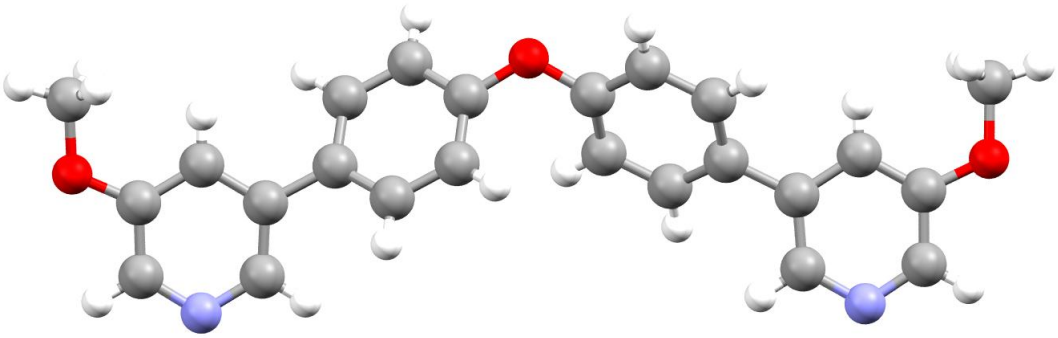

Figure 2.32: Crystal structure of ligand $\mathbf{L^{O\text{-}OMe}}$.

2.3.1.7. Synthesis of the palladium(II) complexes $[Pd_2L^{O\text{-}OMe}{}_4][(BF_4)_4]$, $[Pd_2L^{NH\text{-}OMe}{}_4][(BF_4)_4]$ and $[Pd_2L^{S\text{-}OMe}{}_4][(BF_4)_4]$.

As for the palladium complex of ligand $\mathbf{L^{OMe}}$, complexation of ligands $\mathbf{L^{O\text{-}OMe}}$, $\mathbf{L^{NH\text{-}OMe}}$ and $\mathbf{L^{S\text{-}OMe}}$ was achieved by heating the corresponding ligand and tetrakis(acetonitrile)palladium(II) tetrafluoroborate for 6 hours at 80 ºC.

Formation of the complexes was confirmed by NMR, ESI^+-MS and IR as was also verified for $\mathbf{[Pd_2L^{OMe}{}_4][(BF_4)_4]}$. In the case of the ^{1}H NMR, the complexes show bigger differences between each other compared to their ligands on their own (Figure 2.33). This indicates the different donor character of the different ligands upon coordination.

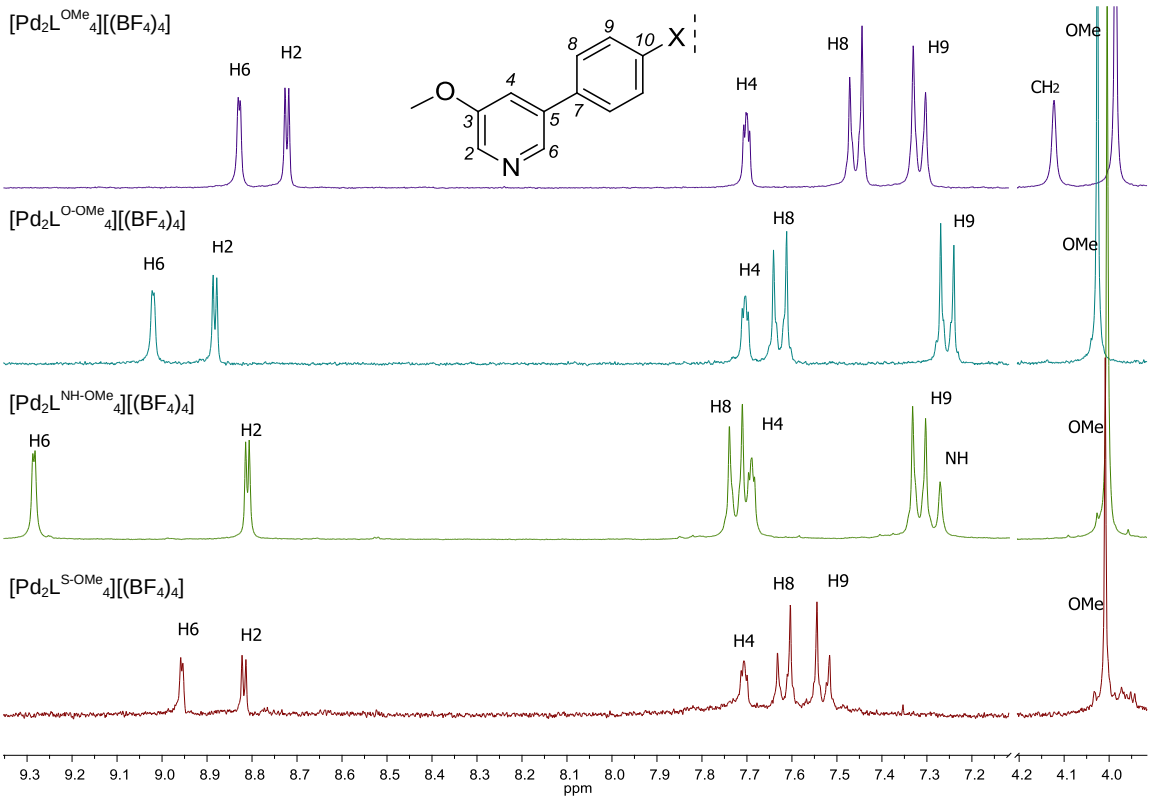

Figure 2.33: ^{1}H NMR spectra of the four methyl ether palladium(II) complexes: **$[Pd_2L^{OMe}{}_4][(BF_4)_4]$**, **$[Pd_2L^{O\text{-}OMe}{}_4][(BF_4)_4]$**, **$[Pd_2L^{NH\text{-}OMe}{}_4][(BF_4)_4]$** and **$[Pd_2L^{S\text{-}OMe}{}_4][(BF_4)_4]$** (300 MHz, CD_3CN).

Doubly and triply charged species are observed in the electrospray mass spectra for **$[Pd_2L^{O\text{-}OMe}{}_4][(BF_4)_4]$** and **$[Pd_2L^{NH\text{-}OMe}{}_4][(BF_4)_4]$**. A mass spectrum for **$[Pd_2L^{S\text{-}OMe}{}_4][(BF_4)_4]$** could not be obtained. This could be due to poor solubility or a lack of ionization of the species in the spectrometer.

A band around 1030 cm^{-1} was observed for all three complexes in their infrared spectra corresponding to the non-coordinated tetrafluoroborate anions.

^{13}C NMR spectra were recorded in deuterated acetonitrile for all methyl ether complexes, except for **$[Pd_2L^{S\text{-}OMe}{}_4][(BF_4)_4]$** due to its low solubility in acetonitrile. It was decided not to use deuterated dimethyl sulfoxide as it would be

very difficult to recover the solid from this solvent. Table 2.2 shows a comparison of the different chemical shifts observed in the ^{13}C NMR spectra. Small shifts are observed for carbons C8 and C9 on changing the spacer unit. Downfield shifts occur upon complexation for carbons C6 and C2. Overall, few changes are noted in the ^{13}C NMR spectra and little information can be obtained.

Table 2.2: ^{13}C NMR chemical shifts (ppm) for methyl ether ligands and their complexes.

	C6	**C2**	**C4**	**C9**	**C8**	**OCH_3**	**CH_2**
L^{OMe}	140.9	136.1	119.2	129.8	127.6	55.8	41.4
$[Pd_2L^{OMe}{}_4][(BF_4)_4]$	141.8	138.0	124.7	130.8	128.8	57.7	41.1
$L^{O\text{-}OMe}$	140.8	136.1	119.1	119.7	128.9	55.8	-
$[Pd_2L^{O\text{-}OMe}{}_4][(BF_4)_4]$	141.3	137.8	124.3	120.7	130.4	57.8	-
$L^{NH\text{-}OMe}$	140.5	135.6	118.7	118.4	128.4	55.8	-
$[Pd_2L^{NH\text{-}OMe}{}_4][(BF_4)_4]$	141.0	137.0	122.6	119.5	129.2	57.6	-

Suitable yellow crystals for x-ray diffraction were obtained by slow diffusion of diethyl ether into an acetonitrile solution of **$[Pd_2L^{NH\text{-}OMe}{}_4][(BF_4)_4]$**. The X-ray crystal structure confirms that the tetra-stranded, dinuclear palladium(II) complex has been formed (Figure 2.34).

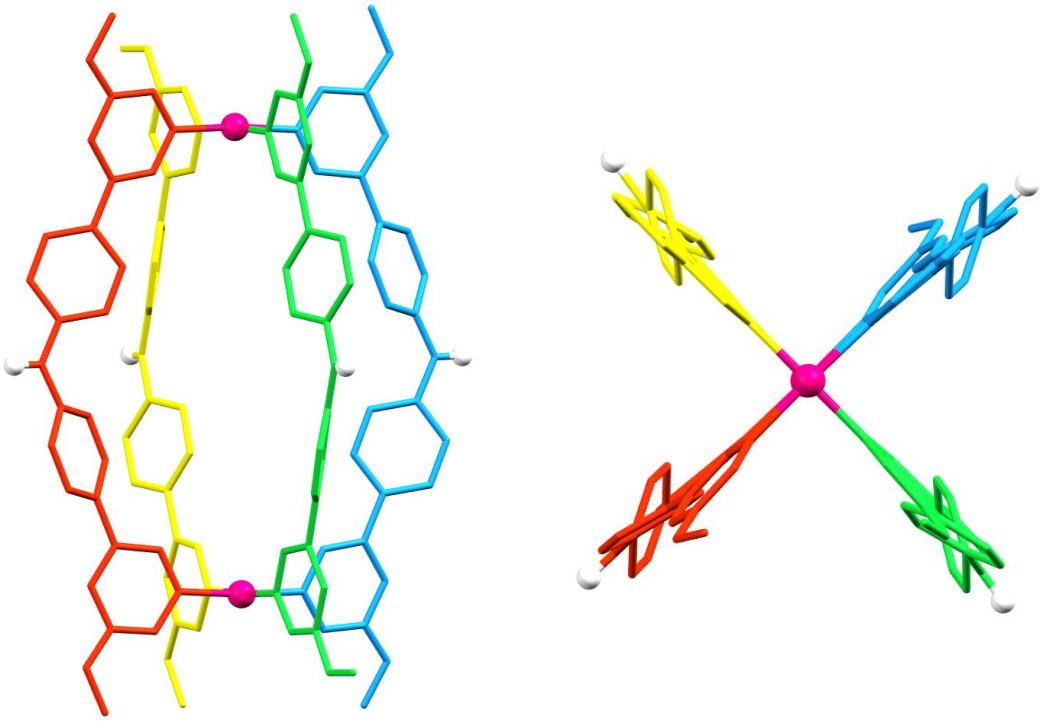

Figure 2.34: Crystal structure of **[$Pd_2L^{NH\text{-}OMe}{}_4$][$(BF_4)_4$]**, side view (left) and top view (right). Hydrogen atoms, solvent molecules and counter-ions are omitted for clarity, except the hydrogen of the NH group.

Each metal centre has a four-coordinate, square planar geometry with Pd-N bond distances of 2.021(7) - 2.042(6) Å and N-Pd-N angles of 88.3(3) - 91.8(3)º. An inversion centre at the centre of the palladium complex relates the two metal centres so that only half of the molecule is crystallographically unique with a symmetry relation of -x,-y,-z+2. There is also an approximate plane of symmetry through the four ligands which yields an achiral structure, as was also seen in **[$Pd_2L^{OMe}{}_4$][$(BF_4)_4$]**. The four ligands bridge the two palladium(II) centres resulting in a Pd···Pd separation of 13.5 Å, which is 1.1 Å greater than the intermetallic distance observed in **[$Pd_2L^{OMe}{}_4$][$(BF_4)_4$]**. This is a result of the substitution of the carbon central unit by nitrogen. Within the ligands, the phenyl rings are twisted with respect to one another by 45º and with respect to the pyridine rings by 21º

and 35º. The coordinating pyridines are nearly coplanar (5º and 12º). The disposition of the four ligands around the two palladium metal centres yields a central cavity. This cavity is home to two tetrafluoroborate counter-ions and two acetonitrile molecules that interact with each other via weak hydrogen bonds (Figure 2.35).

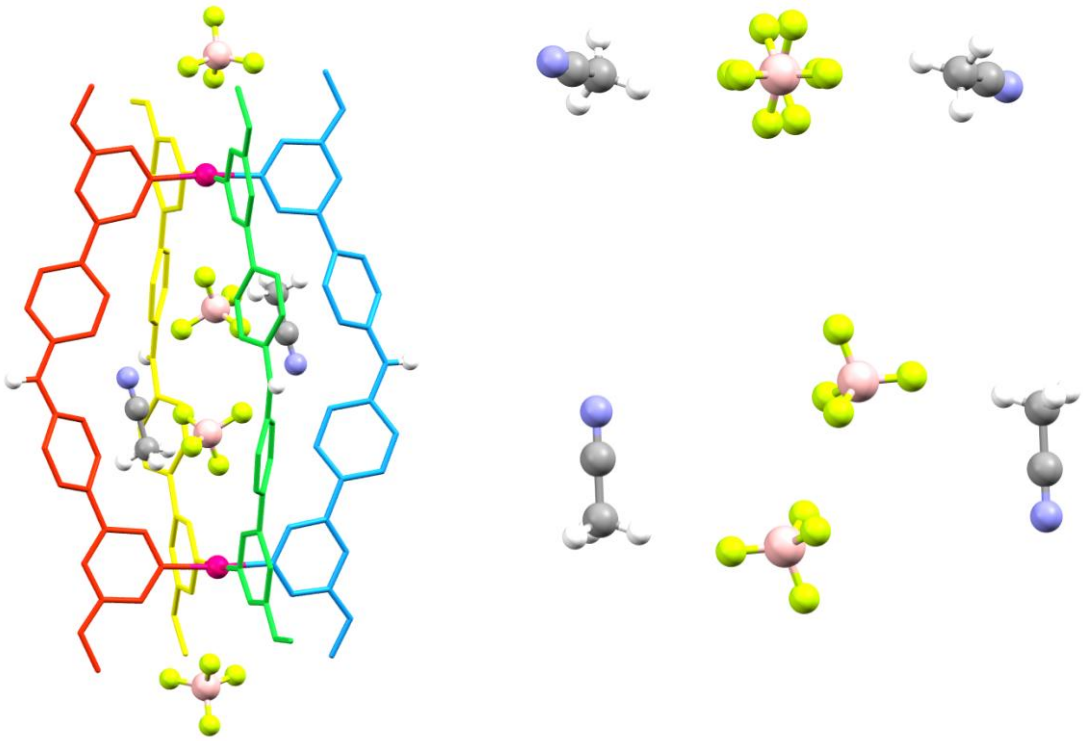

Figure 2.35: Capped sticks representation of **$[Pd_2L^{NH\text{-}OMe}{}_4][(BF_4)_4]$** (left) and interaction between encapsulated counter-ions and acetonitrile molecules (right).

The other two tetrafluoroborate counter-ions are outside the cavity along the axis of the palladium centres. They also interact with each other via weak hydrogen bonds through acetonitrile molecules as seen for **$[Pd_2L^{OMe}{}_4][(BF_4)_4]$** (Figure 2.36).

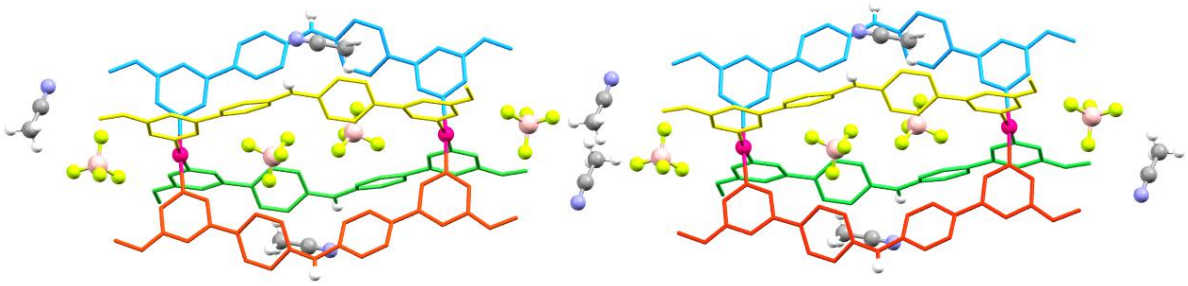

Figure 2.36: Crystal packing of two **$[Pd_2L^{NH\text{-}OMe}{}_4][(BF_4)_4]$** molecules.

Hydrogen bond contacts are also observed between a tetrafluoroborate anion and the NH groups of two palladium cylinders, with donor-acceptor distances of 2.919(13) – 3.207(16) (Figure 2.37).

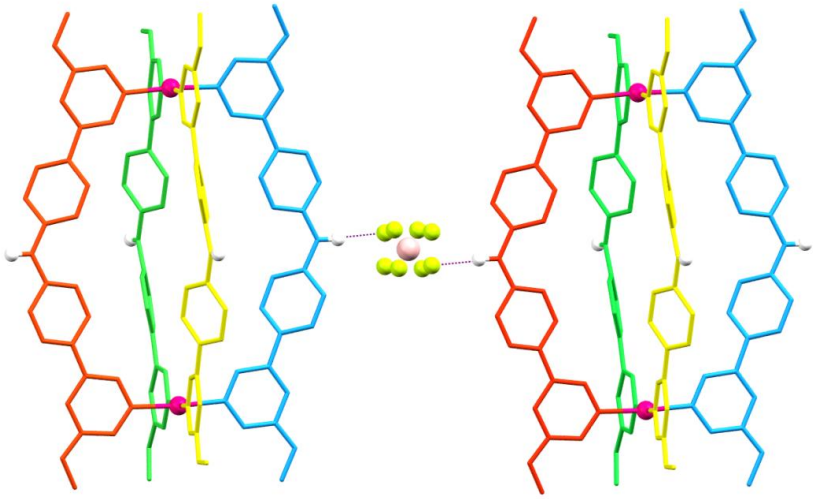

Figure 2.37: Hydrogen bond interaction between a BF_4 counter-ion and NH group of two **$[Pd_2L^{NH\text{-}OMe}{}_4][(BF_4)_4]$** molecules.

This hydrogen bond interaction combined with the weak interaction between anions along the axis of the palladium centres can be seen in the crystal packing of four cylinders as depicted in Figure 2.38.

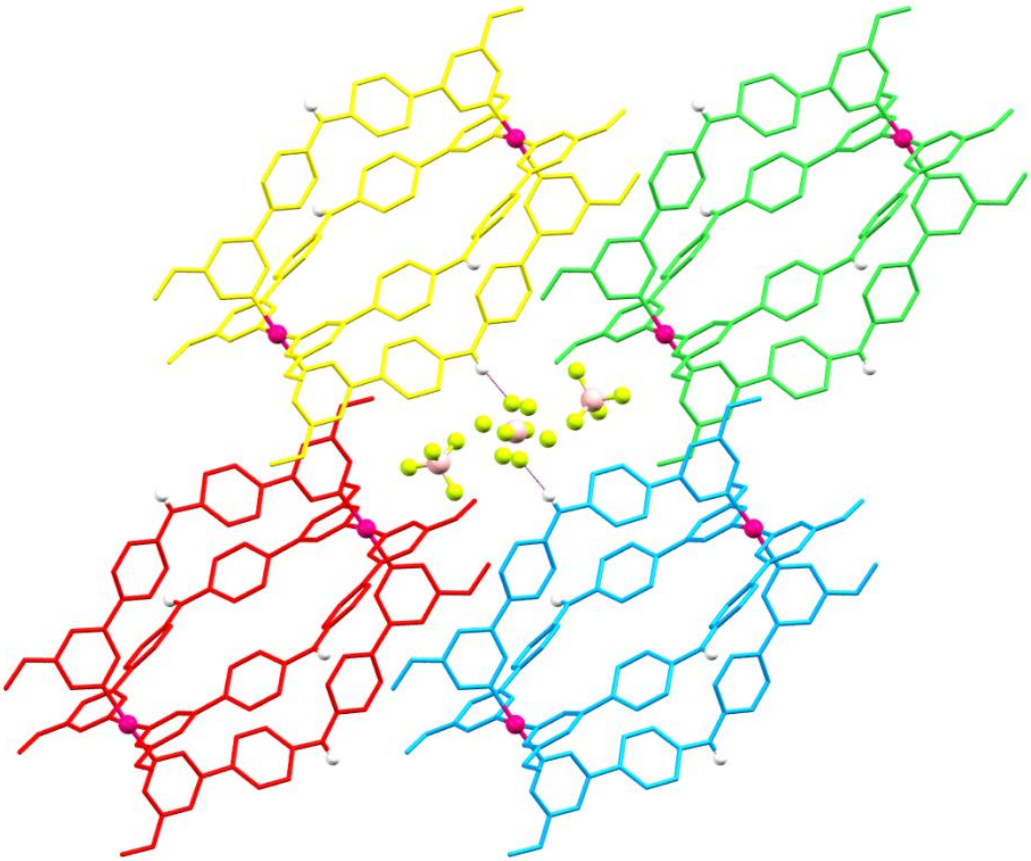

Figure 2.38: Crystal packing of 4 molecules of **[$Pd_2L^{NH\text{-}OMe}{}_4$][$(BF_4)_4$]**.

This cylinder is slightly longer than its analogous **[$Pd_2L^{OMe}{}_4$][$(BF_4)_4$]** (C···C 20.2 Å : H··H 21.5 Å), which makes it less wide, with a diameter of N···N 12.9 Å : H··H 14.6 Å measured from the central amine spacer unit of one ligand to the opposite ligand). These differences are a consequence of the different twisting angles within the ligands.

2.3.1.8. Solubility of spacer modified tetra-stranded palladium(II) complexes

The variation of the element at the spacer diphenyl unit yielded four novel compounds that are soluble in dimethyl sulfoxide and fairly soluble in acetonitrile,

with **$[Pd_2L^{O\text{-}OMe}{}_4][(BF_4)_4]$** and **$[Pd_2L^{NH\text{-}OMe}{}_4][(BF_4)_4]$** being easier to solubilise. In addition, the cylinder with the NH spacer is partially soluble in methanol. The S-modified complex is barely soluble in acetonitrile, therefore it will not be studied further.

2.3.2. Exchange of the counter-ion of the complex

The second strategy that was explored was the exchange of the counter-ions of the complex.

Nitrate salts are generally water soluble since the negative charge is distributed among the three oxygen atoms, facilitating water solvation. Chloride salts are also known to be water soluble compounds and are generally used in water soluble cationic drugs (e.g. Hannon's triple-stranded cylinder). Only silver, lead and mercury present insoluble chloride salts in a two element compound combination. It has also been demonstrated that some platinum complexes present an increase in water solubility when using triflates (trifluoromethanesulfonate) as counter-ion.[145] These three different anions were chosen to explore the solubility of the tetra-stranded palladium(II) cylinders. The tetrabutylammonium salt of the different anions (nitrate, chloride and triflate) was used to exchange the original tetrafluoroborate counter-ion. The exchange can be performed by addition of a saturated solution of the corresponding tetrabutylammonium salt into either a concentrated solution of the crude reaction mixture or into an acetonitrile solution of the pure redissolved palladium(II)

tetrafluoroborate complex. In both cases, the palladium(II) complex with the exchanged counter-ion precipitates out of the acetonitrile solution and can be isolated by filtration.

This strategy of exchange of the counter-ion was investigated for the **$[Pd_2L^{OMe}_4][(BF_4)_4]$** complex. The complex was dissolved in the minimum amount of acetonitrile and an excess of tetrabutylammonium nitrate, chloride or triflate in acetonitrile solutions was added dropwise. The complexes precipitated and were collected via filtration. They were all redissolved in deuterated acetonitrile and their ^{1}H NMR spectra compared (Figure 2.39). For BF_4^- and $CF_3SO_3^-$ the concentration was 1.5 mM. In the case of NO_3^- and Cl^- a concentration of 1.5 mM could not be reached due to the lower solubility in acetonitrile and a precipitate was observed in the NMR tube.

It is noticeable that the protons next to the nitrogen of the pyridine, H2 and H6, are displaced downfield when exchanging the counter-ion. This result might indicate the close presence of the counter-ion to the metal centre which holds the positive charge, or even a very weak bond on the sometimes observed fifth position of the palladium coordination sphere. Therefore, the proximity of different counter-ions to those H2 and H6 protons affects their chemical shift. This is in agreement with the observed location of a tetrafluoroborate counter-ion on the outer side of both palladium(II) centres in the crystal structure of the **$[Pd_2L^{OMe}_4][(BF_4)_4]$** complex.

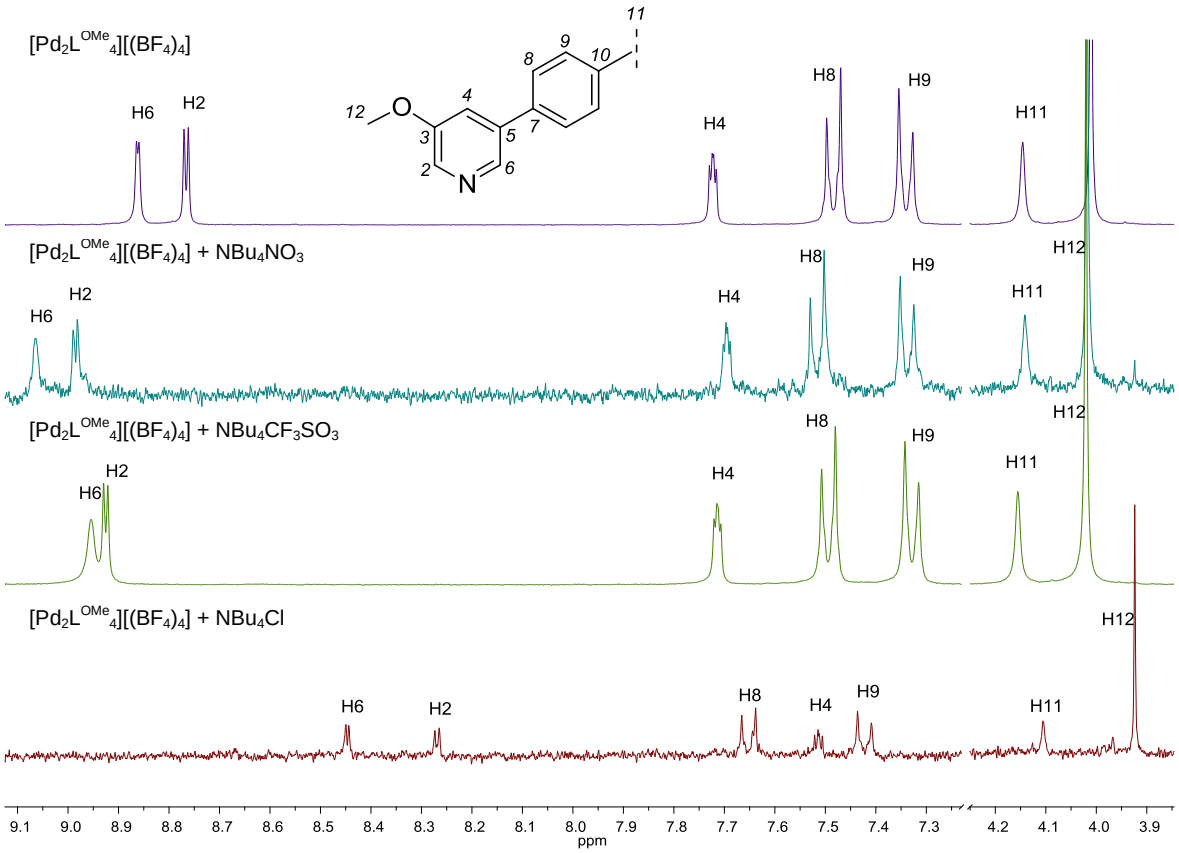

Figure 2.39: ^{1}H NMR spectra of **$[Pd_2L^{OMe}{}_4][(X)_4]$** where X = BF_4^-, NO_3^-, $CF_3SO_3^-$ and Cl^- (300 MHz, CD_3CN).

The ^{1}H NMR data also suggests the decomposition of the complex when changing the tetrafluoroborate anion to chloride, yielding the ligand. This might be due to the lability of the Pd-N bond and the formation of a stronger bond with chloride to yield $PdCl_2$ or $[PdCl_4]^{2-}$.

The newly formed **$[Pd_2L^{OMe}{}_4][(NO_3)_4]$** and **$[Pd_2L^{OMe}{}_4][(CF_3SO_3)_4]$** complexes were also analyzed by mass spectrometry and infrared spectroscopy. Different ESI+-MS methods were tested in order to obtain a spectrum, however it was impossible to ionize these complexes and make them fly through the

spectrometer. This is something commonly observed in nitrate salts. This was also observed for the triflate complex.

The infrared spectra of these complexes shows a lack of the characteristic tetrafluoroborate band at 1032 cm^{-1} and the appearance of nitrate and triflate bands at 1317 cm^{-1} and 1027 cm^{-1}, respectively.

Once the complexes were analysed, their solubility was studied. When exchanging to nitrate counter-ions, the complex becomes more soluble in organic solvents such as chloroform. The solubility of the triflate complex in acetonitrile increased considerably, however it remains insoluble in pure water. As mentioned above, the chloride complex could not be achieved. It was also reported for the first generation of compounds that when using a Dowex-Cl resin to exchange the tetrafluoroborate anions to chloride, the complex decomposed into a complicated mixture.(133)

An interesting approach to achieve an increase in solubility by exchanging the counter-ions was reported by Kuroda and co-workers.(146) They observed that their tetra-stranded palladium(II) receptor can form a 1:2 host:guest complex with *p*-toluenesulfonate (OTs^-) or 2-naphthalenesulfonate (ONs^-) via anion encapsulation. A first generation sulfonate dendrimer was able to increase the complex solubility in low polar solvents. Chiral induction was also achieved with *d*- or *l*-camphor sulfonate (Figure 2.40). These encapsulation processes occurred via π-π stacking, hydrogen bonding between host and guest and $Pd^{2+} \cdots O_3SR^-$ interactions.

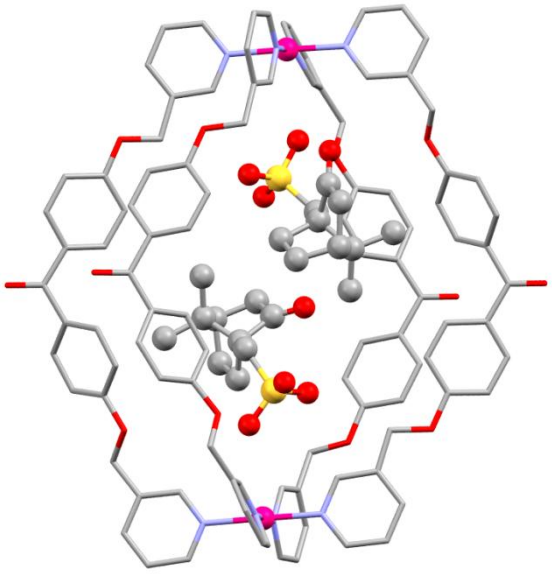

Figure 2.40: Crystal structure of Kuroda's palladium(II) tetra-stranded host with encapsulated *d*-camphor sulfonate (CCDC 827758).[146]

The crystal structures of the synthesised palladium(II) cylinders presented above showed encapsulation of two of the four counter-ions. In order to study the interaction of these complexes with different counter-ions, an anion titration NMR experiment was performed. Titration of a deuterated acetonitrile solution of tetrabutylammonium trifluoromethanesulfonate into a **$[Pd_2L^{OMe}{}_4][(BF_4)_4]$** deuterated acetonitrile solution presented the spectra shown in Figure 2.41.

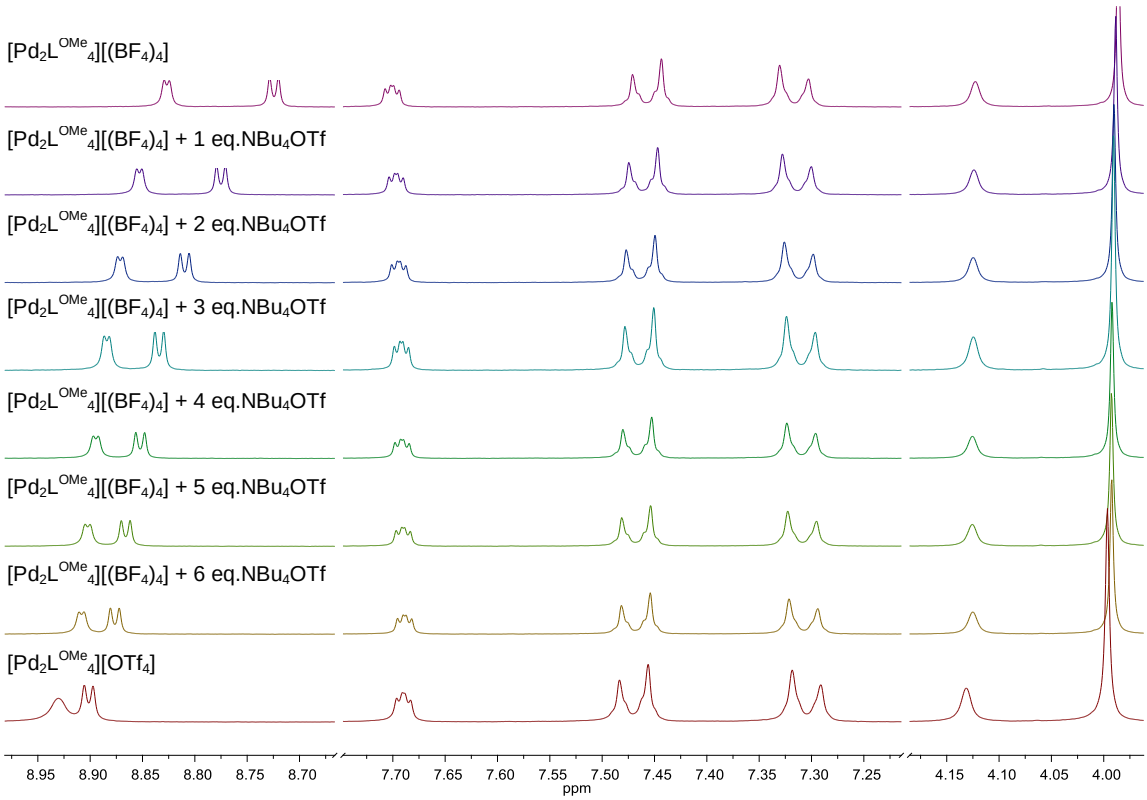

Figure 2.41: ^{1}H NMR spectra of titrations of NBu_4OTf into **$[Pd_2L^{OMe}{}_4][(BF_4)_4]$** (300 MHz, CD_3CN)

A downfield shift of the α-pyridyl protons H6 (Δδ 0.08 ppm) and H2 (Δδ 0.16 ppm) is observed. This shift suggests that the substitution of anions occurs initially on the outside of the complex as H2 presents a higher shift increment. In Kuroda's palladium(II) complex, H2 did not experience a downfield shift while H6 was moved substantially by 0.25 – 0.83 ppm.

Greater interaction with the outer triflate counter-ions was shown for the **$[Pd_2L^{NH\text{-}OMe}{}_4][(BF_4)_4$** complex. Shifts of 0.04 ppm for H6 and 0.15 ppm for H2 were observed. This might be due to the interaction of the triflate anion with the NH group of the spacer unit as seen in the crystal structure of **$[Pd_2L^{NH\text{-}OMe}{}_4][(BF_4)_4$** (*see Appendix*).

π-π stacking interactions of anion guests were assessed by titration of tetrabutylammonium *p*-toluenesulfonate (NBu_4OTs) into a **$[Pd_2L^{OMe}_4][(BF_4)_4]$** deuterated acetonitrile solution. Downfield shifts of 0.87 and 0.48 ppm were observed for H2 and H6 respectively. An upfield shift ($\Delta\delta$ 0.08 ppm) was also observed for H4 (Figure 2.42). These results indicate exchange of the counter-ions outside the cavity. π-π stacking interactions sandwiching the tosilate counter-ion between cylinders might be occurring, rather than π-π stacking between the strands and anions inside the cavity.

In contrast to Kuroda's guest, the newly synthesised palladium(II) supramolecular cylinders tend to exchange their outer counter-ions as these are readily available. Intermolecular interactions might be observed between anions and cylinders.

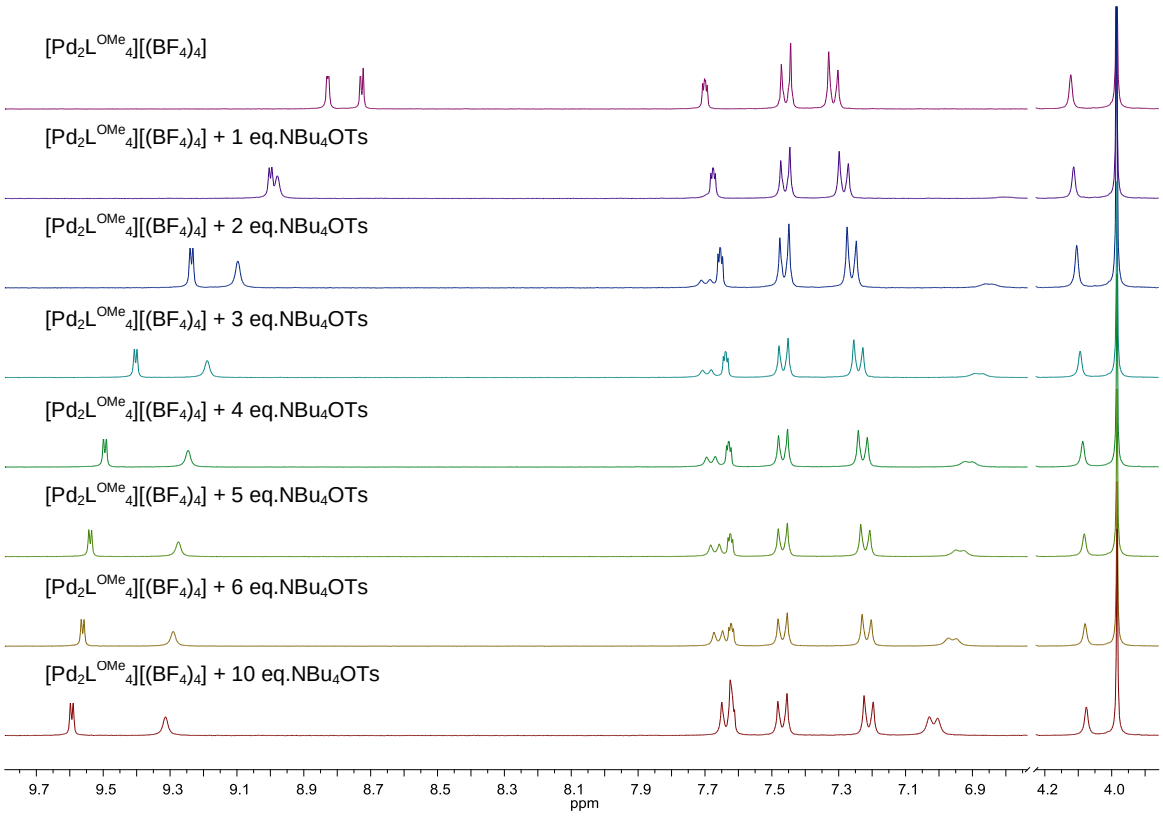

Figure 2.42: ^{1}H NMR spectra of titrations of NBu_4OTs into **$[Pd_2L^{OMe}_4][(BF_4)_4]$** (300 MHz, CD_3CN)

2.3.3. Addition of potentially solubilizing groups at the edges of the pyridine rings

As discussed above, position 3 of the pyridine ring was chosen to introduce some functionality into the molecule in order to achieve an increase in the solubility of the palladium(II) complexes. Alcohol groups, glycol chains and alkyl-chained pyrrolidines were the motifs explored and are discussed below.

2.3.3.1. Molecular design of L^{OH}

The methyl ether was introduced at position 3 of the pyridine rings on the spacer modified ligands, as well as on the methylene spacer cylinder, in order to start to introduce some functionality to the new cylinders. This methyl ether group can potentially be cleaved to further increase the solubility of the new complexes. Once the methyl ether is cleaved the ligands will have a hydroxyl functional group at each side. These hydroxyl groups might be able to hydrogen-bond to water molecules.

2.3.3.2. Synthesis of ligands L^{OH}, $L^{O\text{-}OH}$ and $L^{NH\text{-}OH}$

Ligands $\mathbf{L^{OH}}$, $\mathbf{L^{O\text{-}OH}}$ and $\mathbf{L^{NH\text{-}OH}}$ were accessed using a Lewis acid, such as boron tribromide or aluminium trichloride, for the o-demethylation. Aluminium trichloride proved to be the most successful Lewis acid for this deprotection in conjunction with ethanethiol. Initially the Lewis acid forms a complex with the ethereal oxygen atom via a dative bond. Then, the divalent sulfur acts as a soft nucleophile attacking the methyl electron deficient carbon of the oxonium species via an S_N2 mechanism. Hydrolysis leads to the deprotected alcohol (Scheme 2.9).

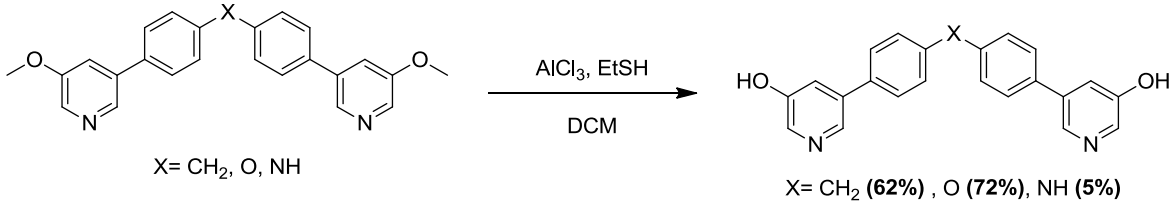

Scheme 2.9: Synthesis of ligands $\mathbf{L^{OH}}$, $\mathbf{L^{O\text{-}OH}}$ and $\mathbf{L^{NH\text{-}OH}}$.

The reaction went to completion after 2 days. More reactive species such as aluminium tribromide or chloroaluminate ionic liquids could be used in the future for a shortened reaction time, however these were not investigated.

Yields for the deprotection of $\mathbf{L^{OMe}}$ and $\mathbf{L^{O\text{-}OMe}}$ were acceptable, however very poor yields were obtained when trying to deprotect $\mathbf{L^{NH\text{-}OMe}}$. This yield was even lower when attempting a scale up of the reaction. This may be due to the fact that during the course of the reaction acidic species are produced that may protonate the NH at the spacer yielding a salt. During the work up the reaction mixture was neutralized to recover the salt into solution, however the high water solubility of ligand $\mathbf{L^{NH\text{-}OH}}$ made difficult this isolation difficult. Fortunately, yellow crystals suitable for X-ray diffraction were obtained by slow evaporation of deuterated methanol (Figure 2.43).

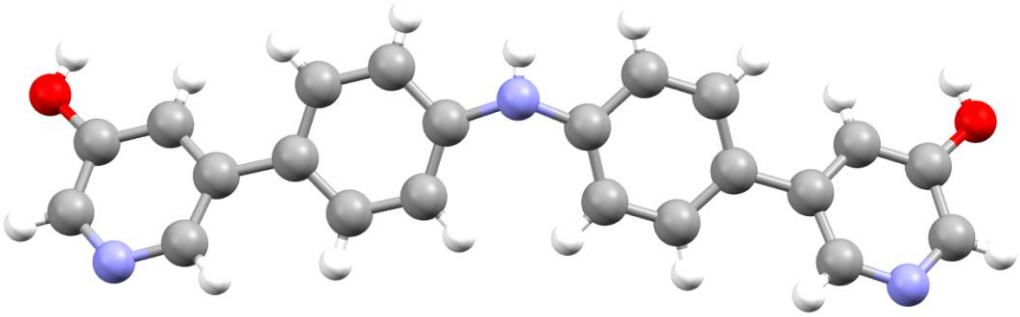

Figure 2.43: Crystal structure of $\mathbf{L^{NH\text{-}OH}}$.

Ligand $\mathbf{L^{NH\text{-}OH}}$ possesses a mirror plane located through the central NH group such that only half of the ligand is crystallographically unique with a relation given by $x,-y+{}^{1}/_{2},z$. The phenyl rings are twisted with respect to one another by 23º and with respect to the pyridine rings by 28º. Even if twisted, this bending is

smaller to that observed for the methyl ether ligands ($\mathbf{L}^{\mathbf{OMe}}$ and $\mathbf{L}^{\mathbf{O\text{-}OMe}}$). This causes an angle of 36º between the pyridine rings, while in the methyl ether ligands, these rings were nearly co-planar.

Columns of $\mathbf{L}^{\mathbf{NH\text{-}OH}}$ molecules are connected via π-π stacking interactions between the pyridine rings with a distance between the planes through the pyridine rings of 3.36 and 3.40 Å (Figure 2.44).

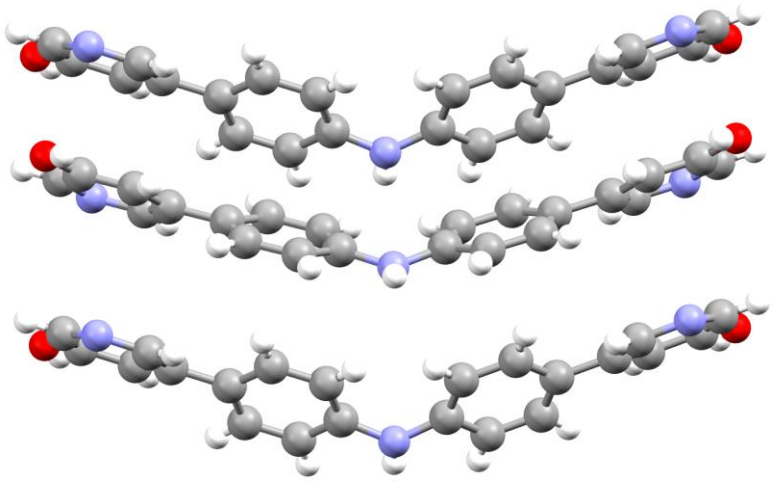

Figure 2.44: Columns of $\mathbf{L}^{\mathbf{NH\text{-}OH}}$ connected via π-π stacking between the pyridine rings.

Hydrogen bonding between ligands is also observed. Each nitrogen of each pyridine unit of one ligand interacts with the hydroxyl groups of another ligand with a distance of 2.829(4) Å between donor and acceptor (Figure 2.45).

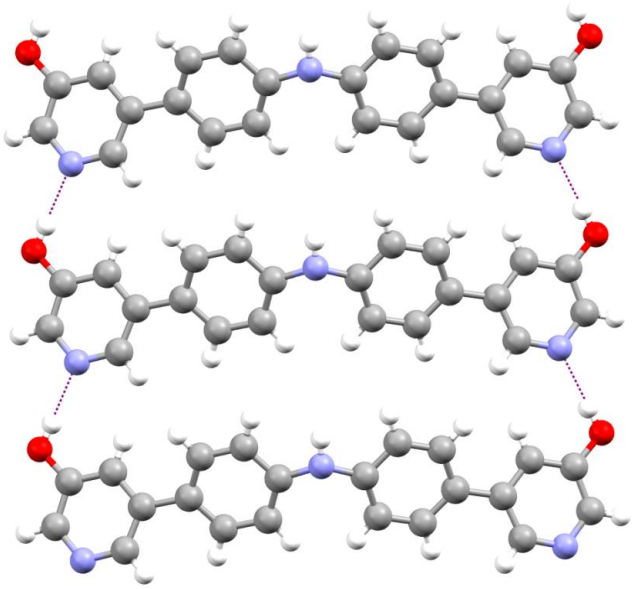

Figure 2.45: Hydrogen bonding (shown in purple) between $\mathbf{L}^{\mathbf{NH\text{-}OH}}$ ligands.

The interaction via hydrogen bonding and π-π stacking in the crystal packing of ligand $\mathbf{L}^{\mathbf{NH\text{-}OH}}$ is shown in Figure 2.46.

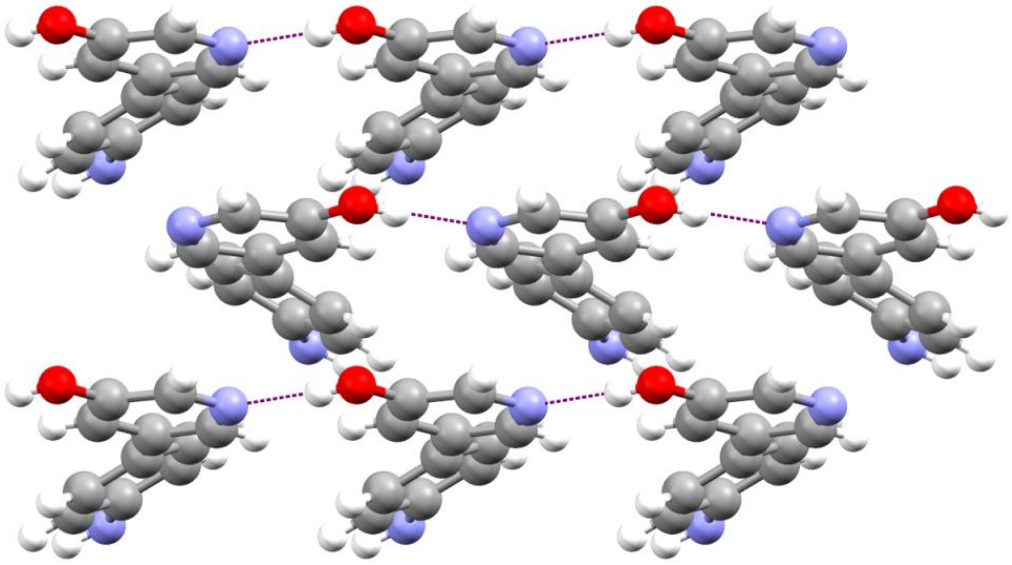

Figure 2.46: Crystal packing of ligand $\mathbf{L}^{\mathbf{NH\text{-}OH}}$.

The three ligands were characterized by NMR, ESI^+-MS and IR. The ^1H NMR is shown in Figure 2.47. As for the methyl ether ligands, all hydroxyl ligands present a very similar ^1H NMR spectrum. The main difference is the chemical shifts of the phenylene protons from the spacer unit due to the presence of the different heteroatoms. The protons from the hydroxyl groups and the proton from the amine group of ligand **L^{NH-OH}** cannot be observed as these ^1H NMR experiments were performed in deuterated methanol, therefore these protons are exchanged with the deuterium of the solvent.

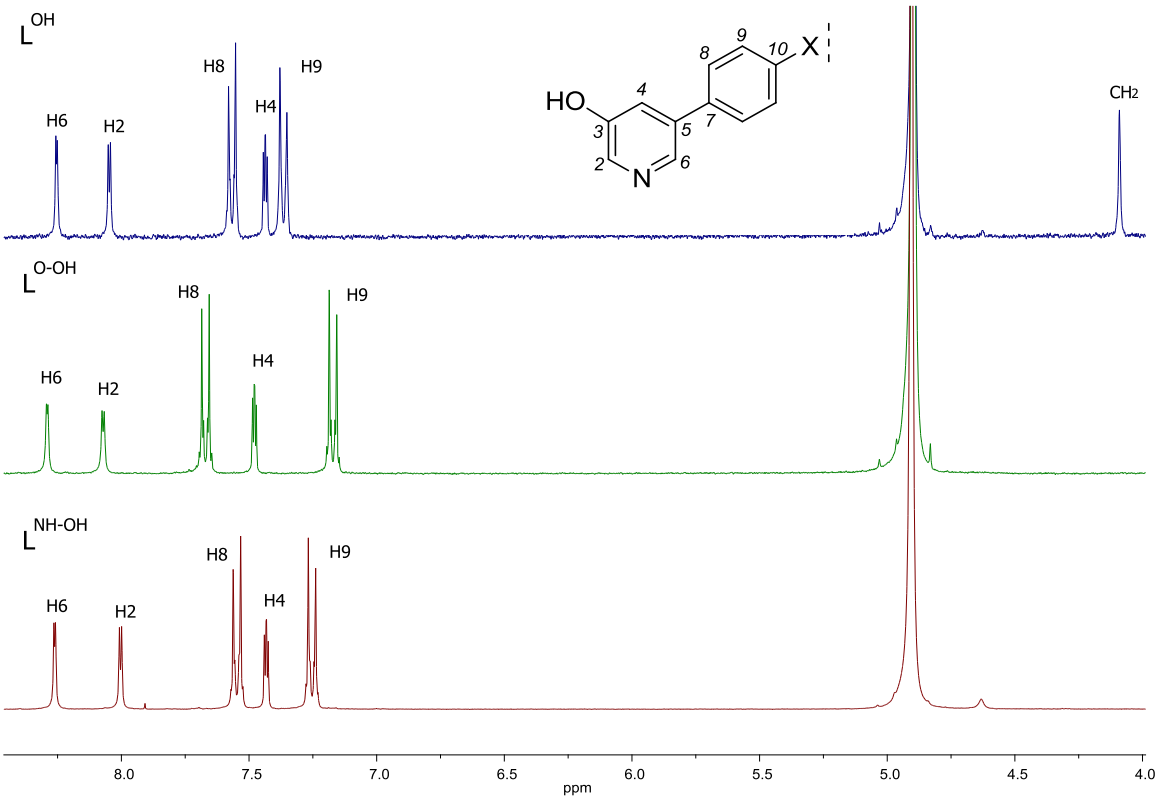

Figure 2.47: ^1H NMR spectra of ligands **L^{OH}**, **L^{O-OH}** and **L^{NH-OH}** (300 MHz, MeOD).

^{1}H NMR of **L^{NH-OH}** was recorded in deuterated dimethyl sulfoxide to confirm the presence of the hydroxyl and amine groups (Figure 2.48). These protons appear as broad singlets and integrate for two and one protons respectively.

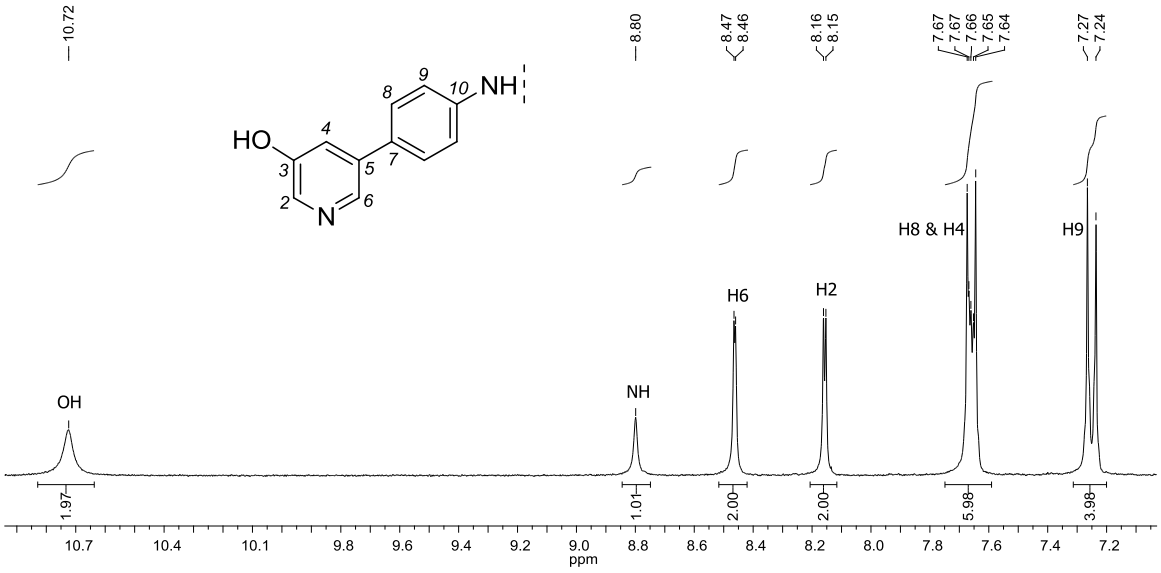

Figure 2.48: ^{1}H NMR of ligand **L^{NH-OH}** (300 MHz, DMSO-d_6).

The infrared spectra of all hydroxyl ligands show a broad band above 3000 cm^{-1} which indicates the presence of the hydroxyl groups and confirms that the deprotection of the methyl ether group has taken place.

Electrospray mass spectrometry in positive ionization mode also confirms the formation of these ligands with the presence of their molecular ion.

2.3.3.3. Synthesis of $[Pd_2L^{OH}_4][(BF_4)_4]$ and $[Pd_2L^{O\text{-}OH}_4][(BF_4)_4]$

Formation of the palladium(II) complexes of the deprotected ligands occurred as for the parent methyl ether analogues. The hydroxyl ligands were heated at 80 ºC and tetrakis(acetonitrile)palladium(II) tetrafluoroborate was added. After 6 hours the complexes were formed and isolated by precipitation with diethyl ether. Formation of **$[Pd_2L^{NH\text{-}OH}_4][(BF_4)_4]$** complex could not be achieved due to lack of sufficient material, as the yield for the formation of the ligand was very low.

It seemed that the palladium complex **$[Pd_2L^{OH}_4][(BF_4)_4]$** was soluble in acetonitrile and methanol, however when performing some NMR experiments in these deuterated solvents the spectra were noisy, hence difficult to integrate. Therefore, deuterated dimethyl sulfoxide was used to record its ^{1}H NMR. This spectrum and that of the **L^{OH}** ligand are shown in Figure 2.49. A downfield shift is observed in the palladium(II) complex spectrum indicating complexation of ligand **L^{OH}**.

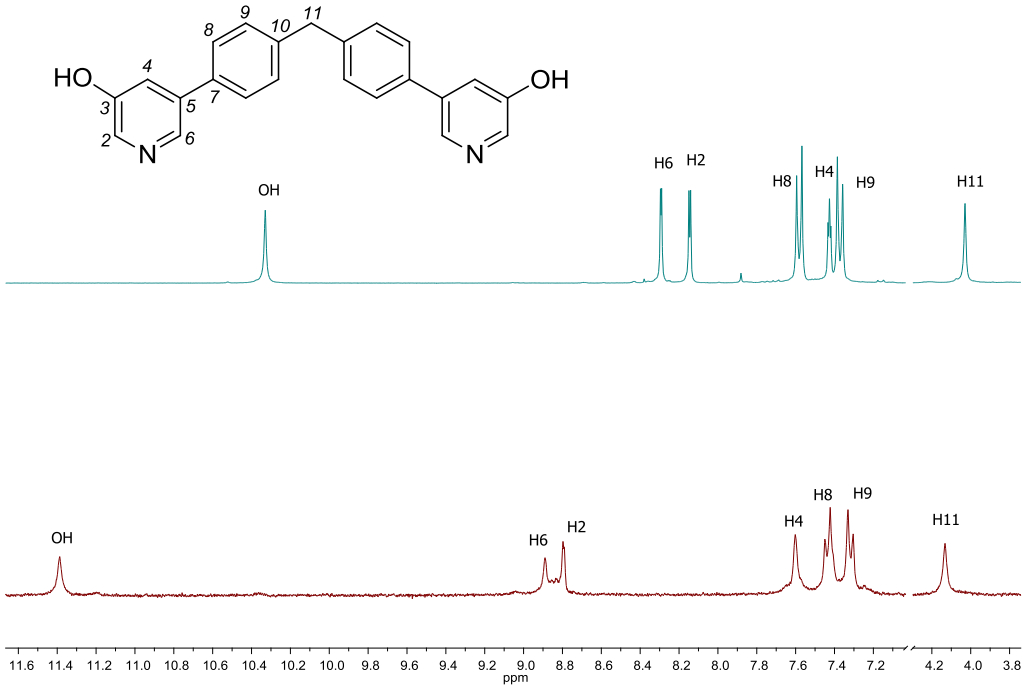

Figure 2.49: ^{1}H NMR spectra comparison between $\mathbf{L^{OH}}$ (top) and $\mathbf{[Pd_2L^{OH}{}_4][(BF_4)_4]}$ (bottom) (300 MHz, DMSO-d_6).

Colourless crystals suitable for X-ray diffraction were obtain by slow diffusion of diethyl ether into an acetonitrile solution of complex $\mathbf{[Pd_2L^{OH}{}_4][(BF_4)_4]}$ (Figure 2.50).

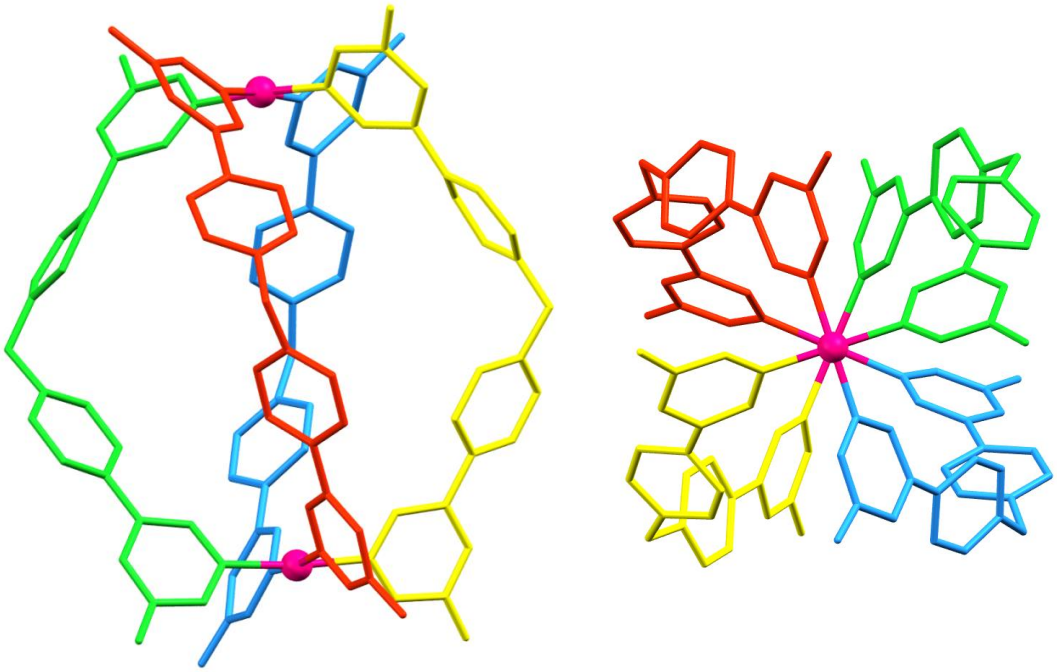

Figure 2.50: Crystal structure of **$[Pd_2L^{OH}_4][(BF_4)_4]$**; side view (left) and top view (right).

Unfortunately, the data that were collected were quite poor and therefore positions and exact distances between atoms could not be accurately determined. However, a few observations can be drawn as there is certainly evidence of the overall structure of the complex. In contrast to the structure observed for **$[Pd_2L^{OMe}_4][(BF_4)_4]$**, this crystal structure suggests the formation of a helicate. The two palladium centres are no longer equivalent as there is not an inversion centre in the centre of the molecule. However, there is a four-fold rotation axis through the centre of the molecule. This results in only one crystallographically unique ligand that is four times repeated. The palladium to ligand bonds of the two metal centres are twisted by 45º, while they were parallel to each other in the palladium complex **$[Pd_2L^{OMe}_4][(BF_4)_4]$**. In other words, the ligand strands are twisted by 45º around the metal-metal axis. Since the ligands are achiral, a racemic mixture of

minus (M) and *plus* (P) helical enantiomers should be present. This can be a consequence of the different twisting angles observed in ligands $\mathbf{L^{OMe}}$ and $\mathbf{L^{NH\text{-}OH}}$. The fact that the pyridine rings are not co-planar in the hydroxyl ligands might force the complex to adopt a helical form. This could be a result of the intermolecular forces observed in ligand $\mathbf{L^{NH\text{-}OH}}$, such as π-π stacking and hydrogen bonding interactions arising from the OH groups. Unfortunately, due to the quality of the cylinder data, this hypothesis cannot be confirmed. However, it is not uncommon to observe helical structures in tetra-stranded palladium(II) complexes as these have been reported before in the literature.(147)

In an attempt to observe this helical nature in solution, titrations of Δ-TRISPHAT (Figure 2.51) into deuterated dimethyl sulfoxide solutions of $\mathbf{[Pd_2L^{OH}{}_4][(BF_4)_4]}$ were performed. Δ-TRISPHAT is an NMR shift reagent that can be used to detect (and in some cases separate) isomers in solution by formation of diastereomeric ion pairs with cationic molecules, such as helicates.(148)

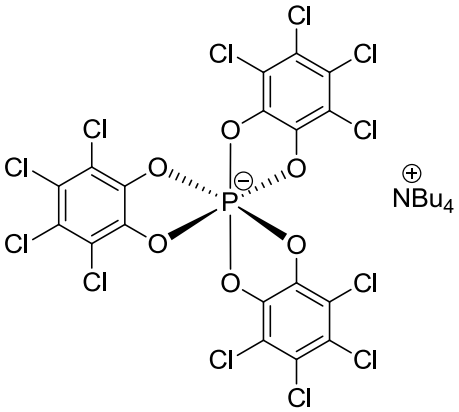

Figure 2.51: Structure of Δ-TRISPHAT.

No change was observed in the ^{1}H NMR spectra of these titrations. Therefore, verification of the helical nature of this helicate in solution was not possible. This could be due to the necessity of using dimethyl sulfoxide to dissolve the complex (less polar solvent mixtures are normally required for this experiment).[149] It may also be that the helical nature of this complex is just an artefact of the solid state.

The palladium complex **$[Pd_2L^{O\text{-}OH}{}_4][(BF_4)_4]$** was slightly soluble in acetonitrile, acetone, nitromethane and methanol, however when dissolved in dimethyl sulfoxide a gelatinous solution was formed. This made its characterization very complicated, however the ^{1}H NMR spectrum shown in Figure 2.52 in deuterated methanol could be recorded. Downfield chemical shift of pyridine protons is again observed upon complexation.

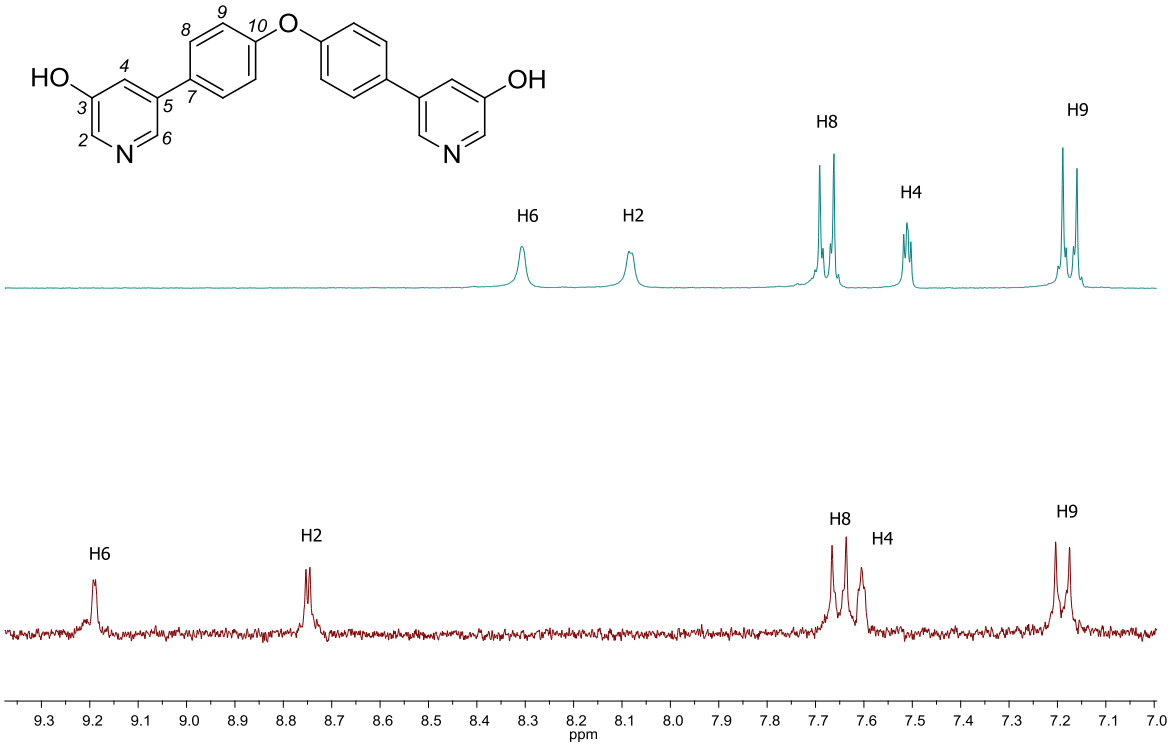

Figure 2.52: ^{1}H NMR spectra comparison between $\mathbf{L^{O\text{-}OH}}$ (top) and $\mathbf{[Pd_2L^{O\text{-}OH}{}_4][(BF_4)_4]}$ (bottom) (300 MHz, MeOD).

2.3.3.4. Molecular design of $L^{O\text{-}Glycol}$

Continuing with the strategy of the addition of potentially solubilizing groups at the edges of the pyridine ring, it was thought that a glycol chain may be appropriate. It was hoped that the oxygen atoms of the glycol chain may have a higher interaction with water molecules. This type of synthetic strategy has been extensively used in the literature.[150-154]

Diethylene glycol methyl ether was chosen as the glycol chain to add to the edges of the pyridine ring. A longer chain or polyethylene glycol could have also

been used, however a monodisperse complex was desired. The retrosynthetic analysis is shown in Scheme 2.10.

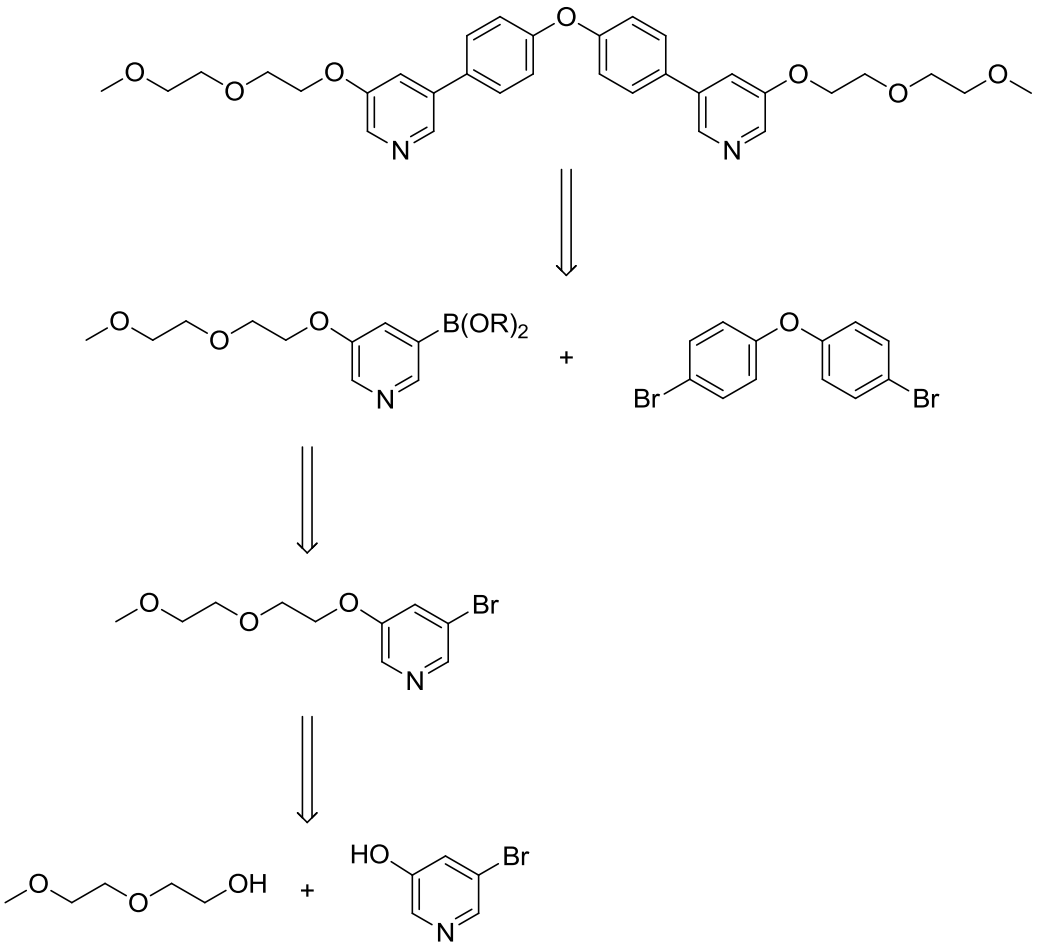

Scheme 2.10: Retrosynthetic analysis for the synthesis of ligand $\mathbf{L^{O\text{-}Glycol}}$.

The first disconnection once again leads to two Suzuki coupling substrates. Bis(4-bromophenyl) ether was chosen to act as spacer unit as it is commercially available and showed a slight increase in solubility for the methyl ether cylinder $\mathbf{[Pd_2L^{O\text{-}OMe}{}_4][(BF_4)_4]}$. A boron derivative needed to be synthesised to be able to perform the Suzuki coupling. This compound could be accessed from the bromo

derivative as seen for previous ligands. Finally, this bromo derivative can be formed via a coupling reaction to introduce the glycol chain into the pyridine ring.

2.3.3.4. Synthesis of 3-bromo-5-(2-(2-methoxyethoxy)ethoxy)pyridine (5)

In order to introduce the glycol functionality into the pyridine ring, a Mitsunobu reaction was used following a modified literature protocol.[155]

Initially, diethyl azodicarboxylate (**DEAD**) in combination with triphenylphosphine were employed as deprotonating agents of the pyridinol. It has been reported[156] that when replacing the alkoxy groups (OEt) of the diethyl azodicaboxylate molecule with strong electron donating groups, such as secondary amines, the basicity of the hydrazo anion intermediate is increased. Therefore, 1,1'-(azodicarbonyl)dipiperidine (**ADD**), depicted in Figure 2.53, was used in conjunction with tri-*n*-butylphosphine.

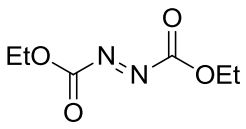

Diethyl azodicarboxylate
(**DEAD**)

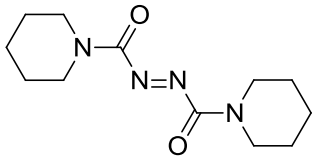

1,1'-(azodicarbonyl)dipiperidine
(**ADD**)

Figure 2.53: Mitsunobu coupling agents.

These coupling reagents led to higher yields of the Mitsunobu reaction. The crude material was purified by column chromatography on silica gel to yield 3-bromo-5-(2-(2-methoxyethoxy)ethoxy)pyridine **5** in 90% yield (Scheme 2.11).

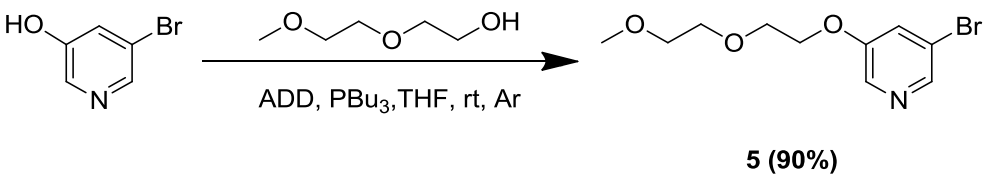

Scheme 2.11: Mitsunobu coupling to yield **5**.

The synthesis of the glycolated pyridine **5** has been recently reported by coupling diethylene glycol methyl ether to 3,5-dibromopyridine in 35% yield (Scheme 2.12).[157] Sodium hydride was used to abstract the hydrogen from the hydroxyl group so that the glycol molecule is able to react with the bromopyridine. This synthetic approach was initially attempted, however poor yield led to the search of new strategies, such as the Mitsunobu coupling discussed above.

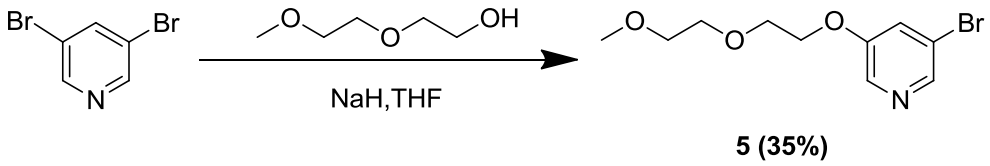

Scheme 2.12: Reported synthesis of **5**.

Glycol-modified pyridine **5** was characterized by NMR, ES^+-MS and IR to confirm its formation.

2.3.3.5. Synthesis of 3-(2-(2-methoxyethoxy)ethoxy)-5-(4,4,5,5-tetramethyl-1,3,2-dioxaborolan-2-yl)pyridine (6)

The next step towards the formation of ligand $\mathbf{L^{O\text{-}Glycol}}$ was to synthesise a suitable boron derivative for the final Suzuki coupling reaction. Several attempts to form the

boronic acid of the glycol modified pyridine **5** by using the previously reported methods always resulted in low yields. Therefore, it was decided to synthesise the boronate ester of the glycolated pyridine **5** following a modified literature protocol.[158] Bis(pinacolato)diboron was used as boron source and potassium acetate as base. In this case, [1,1'-bis(diphenylphosphino)ferrocene]-dichloropalladium(II) complex with dichloromethane was the catalyst of choice. The reaction proceeded in anhydrous dimethylformamide as the reaction is accelerated in polar solvents. Reaction materials were reacted for one hour at 160 ºC and then *tert*-butyl methyl ether was added to produce a precipitate. The filtrate was concentrated under reduced pressure and used without further purification in the next step (Scheme 2.13).

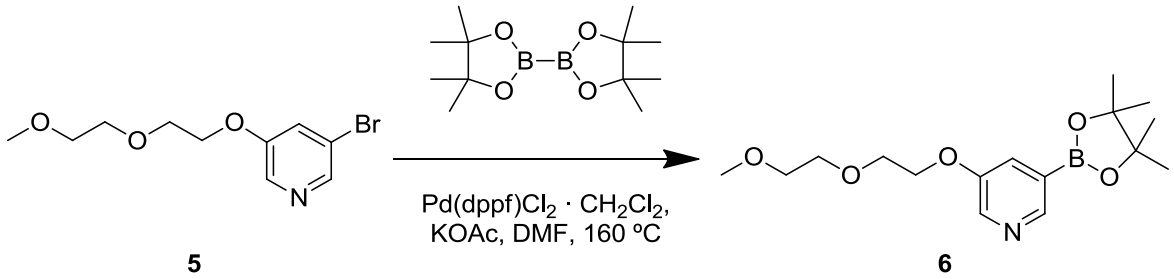

5 **6**

Scheme 2.13: Synthesis of glycolated boronate ester **6**.

2.3.3.6. Synthesis of ligand L$^{O\text{-}Glycol}$

Suzuki coupling of bis(4-bromophenyl) ether and the synthesised glycolated boronate ester **6** was performed under the same conditions of those reported for the methyl ether ligands above (Scheme 2.14). This Suzuki coupling protocol proves to be very powerful as it is valid for boronic acids and boronate esters as starting materials.

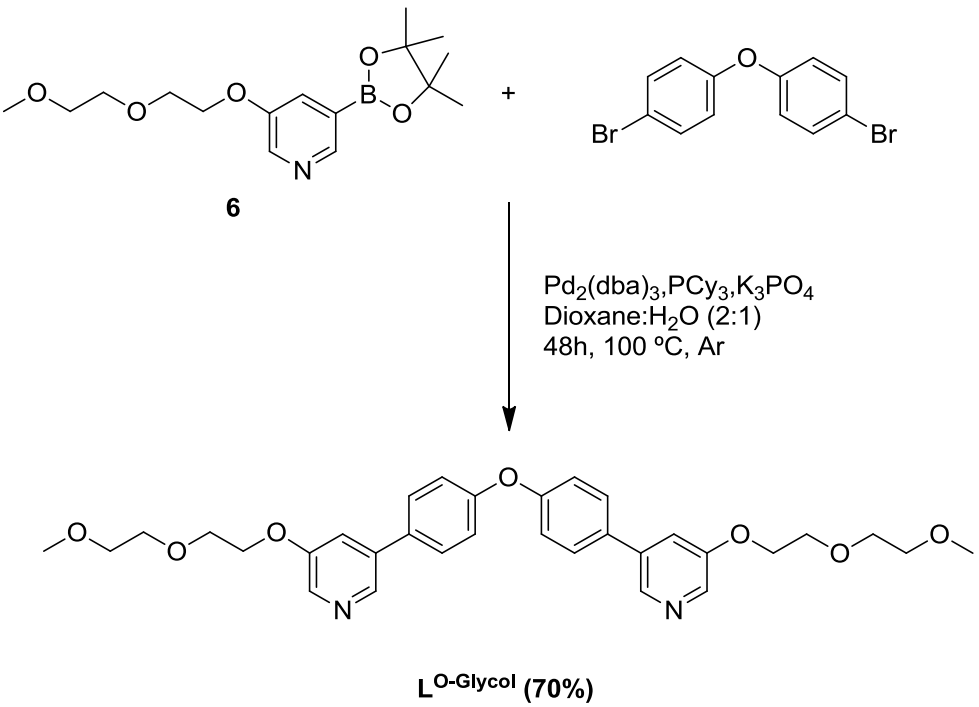

Scheme 2.14: Synthesis of ligand $\mathbf{L^{O\text{-}Glycol}}$.

Ligand $\mathbf{L^{O\text{-}Glycol}}$ was fully characterized by NMR, mass spectrometry and infrared spectroscopy.

The ^{1}H NMR spectrum confirms the symmetry of the ligand and the successful coupling of the spacer unit to the glycolated pyridine (Figure 2.54). Proton assignment was performed with the aid of a 2D-COSY and 2D-NOESY.

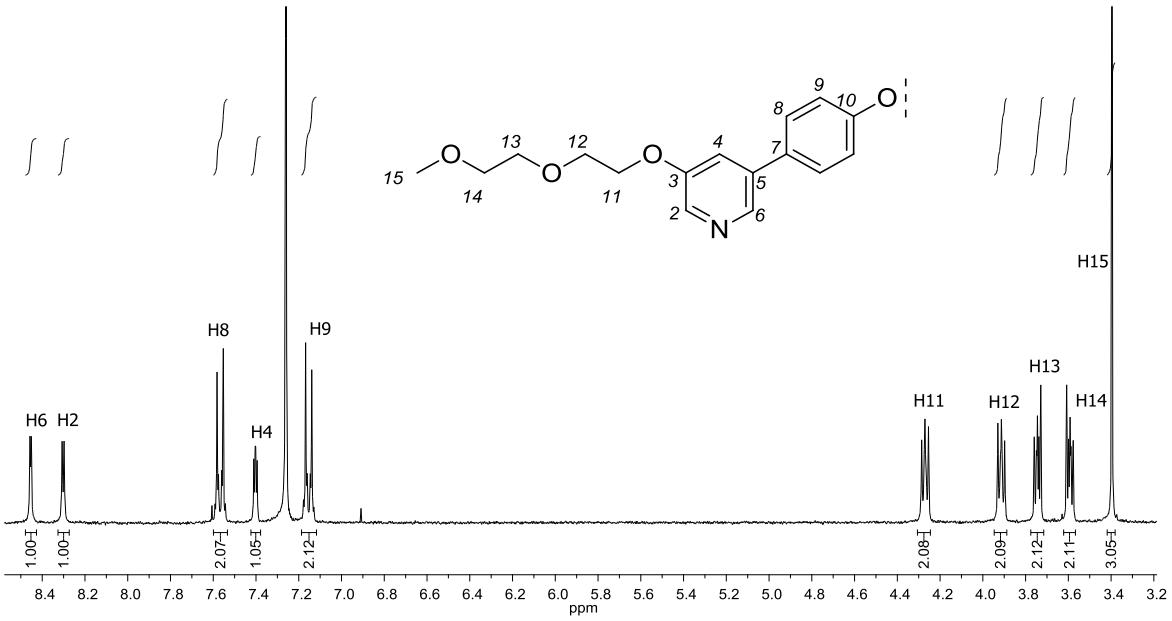

Figure 2.54: ^{1}H NMR spectra of ligand $\mathbf{L^{O\text{-}Glycol}}$ (300 MHz, $CDCl_3$).

The infrared spectrum shows two strong bands at 1130 and 1111 cm^{-1}. These bands are assigned to the presence of the ether groups on the spacer unit and on the glycol chain, respectively.

High resolution mass spectrometry confirmed the formation of ligand $\mathbf{L^{O\text{-}Glycol}}$ with the presence of an adduct formed by the molecular ion and sodium at *m/z* 583 Da.

2.3.3.7. Synthesis of $[Pd_2L^{O\text{-}Glycol}{}_4][(BF_4)_4]$

An equivalent synthetic protocol previously used for the synthesis of tetra-stranded palladium(II) complexes was employed for the synthesis of $\mathbf{[Pd_2L^{O\text{-}Glycol}{}_4][(BF_4)_4]}$. The reaction proceeded at 80 ºC and quantitative formation of the palladium(II)

cylinder was achieved after six hours. Precipitation and washing with diethyl ether afforded **[$Pd_2L^{O\text{-}Glycol}_4$][$(BF_4)_4$]** in 70% yield.

^{1}H NMR spectroscopy confirms the formation of the palladium(II) complex with a downfield chemical shift of the protons close to the metal binding site, that is H2 and H6 and H4 to a lesser extent (Figure 2.55).

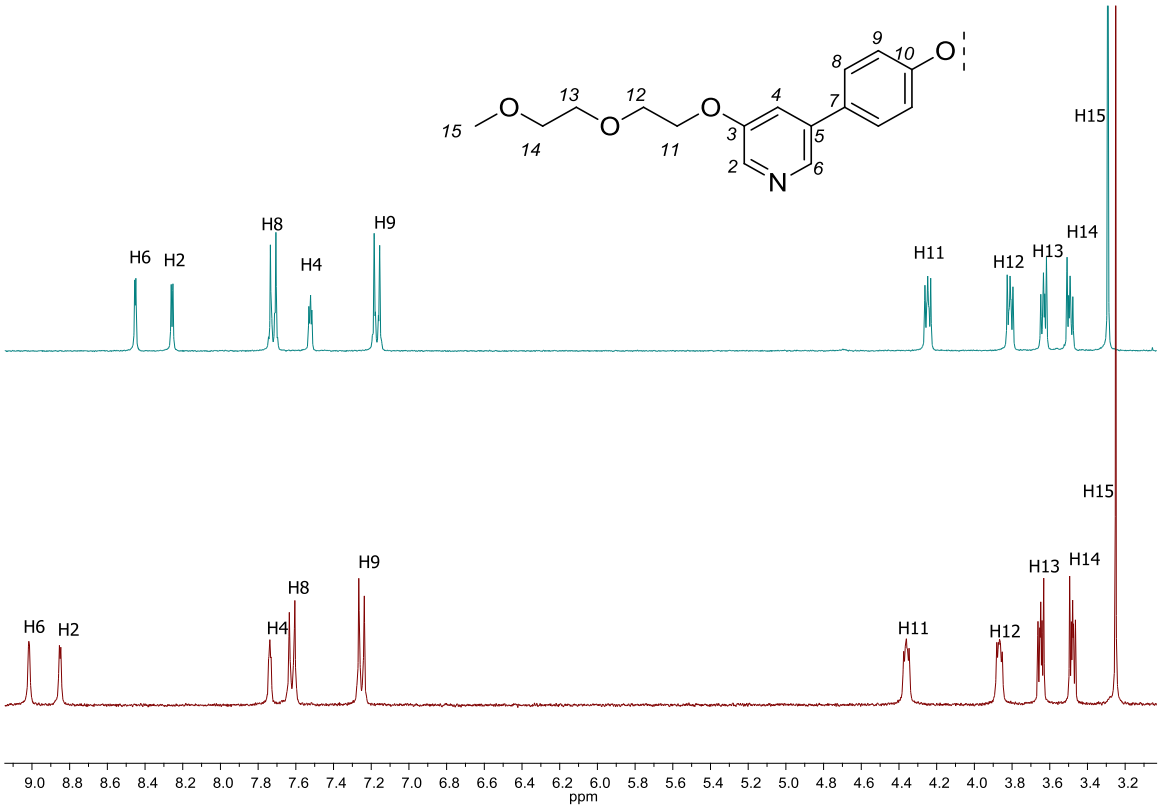

Figure 2.55: ^{1}H NMR spectra of **$L^{O\text{-}Glycol}$** (top) and **[$Pd_2L^{O\text{-}Glycol}_4$][$(BF_4)_4$]** (bottom) (300 MHz, CD_3CN).

The ^{19}F NMR spectrum presents two peaks at -150.87 and -150.92 ppm with integrals of two and eight respectively. These correspond to the different

fluorine environments created by the two different boron isotopes (^{10}B and ^{11}B) as discussed above.

2.3.3.8. Molecular design of ligand $L^{O\text{-}Pyrr}$

The last group that was added at the edges of the pyridine ring was an alkyl-chained pyrrolidine. This kind of motif, along with charged amines,[159] are used in the literature in order to improve the water solubilization of metal complexes such as G-quadruplex targeting drugs[160,161] as well as progesterone derivatives.[162] The principle lies in the fact that the cyclic tertiary amines will be protonated at physiological pH.

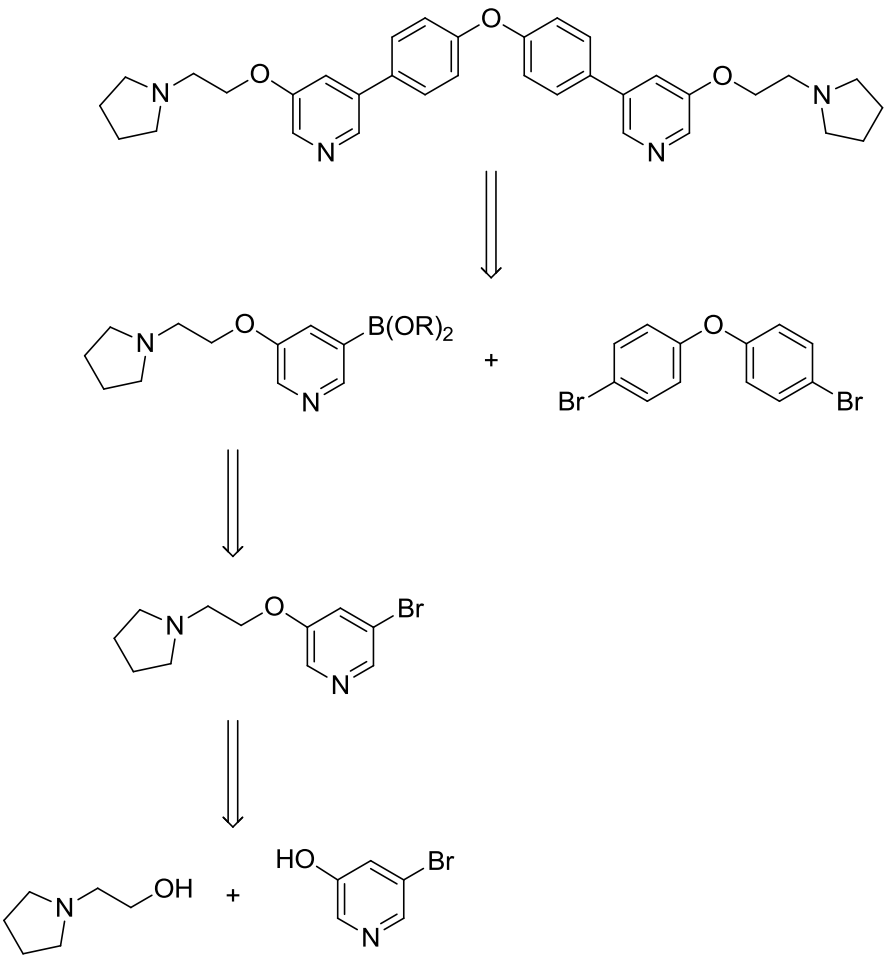

Scheme 2.15: Retrosynthetic analysis for the synthesis of ligand $\mathbf{L}^{\mathbf{O\text{-}Pyrr}}$.

The retrosynthetic analysis that was followed was analogous to that of the glycol ligand previously discussed (Scheme 2.15). First, a Mitsunobu reaction to couple the pyrrolidine motif onto the pyridine ring is required, followed by the formation of the boronate ester of the modified pyridine, and finally a Suzuki coupling reaction with bis(4-bromophenyl) ether to yield ligand $\mathbf{L}^{\mathbf{O\text{-}Pyrr}}$.

2.3.3.9. Synthesis of 3-bromo-5-(2-(pyrrolidin-1-yl)ethoxy)pyridine (7)

Formation of pyridine **7** occurred smoothly under Mitsunobu conditions using 1,1'-(azodicarbonyl)dipiperidine (ADD) in combination with tri-*n*-butylphosphine based on a modified literature protocol (Scheme 2.16).[155] Purification of this ligand was achieved via column chromatography on activated neutral aluminium oxide. Due to the high polarity of the molecule, it was not possible to use silica with any solvent. Even with aluminium oxide, highly polar solvents were necessary to elute the product.

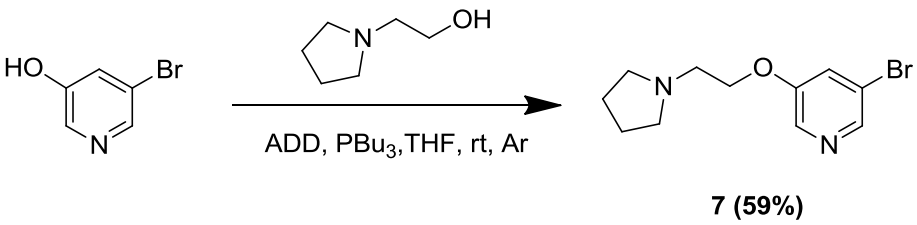

7 (59%)

Scheme 2.16: Synthesis of **7**.

Pyrrolidine-modified pyridine **7** was characterized by NMR, ES^+-MS and IR to confirm its formation.

2.3.3.10. Synthesis of 3-(2-(pyrrolidin-1-yl)ethoxy)-5-(4,4,5,5-tetramethyl-1,3,2-dioxaborolan-2-yl)pyridine (8)

The boronate ester **8** was synthesised following the same protocol applied for the formation of its glycolated analogue **6,** and it was used in the next step without further purification (Scheme 2.17).

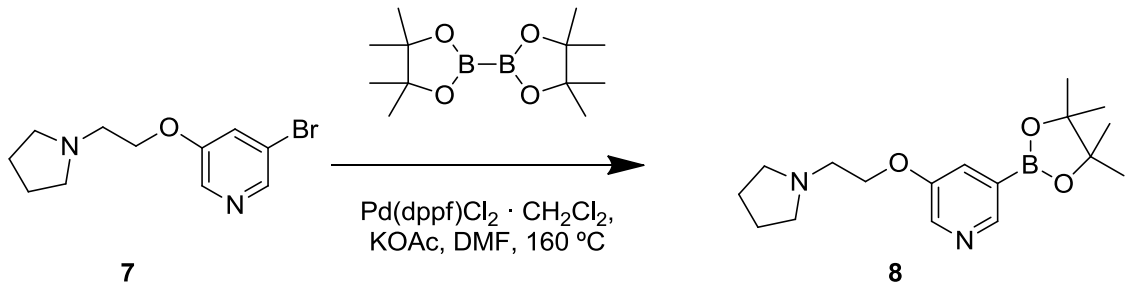

7 8

Scheme 2.17: Synthesis of **8**.

2.3.3.11. Synthesis of ligand L$^{O\text{-}Pyrr}$

The Suzuki coupling of **8** with bis(4-bromophenyl) ether was also performed under the same conditions used for all previous Suzuki coupled ligands (Scheme 2.18).

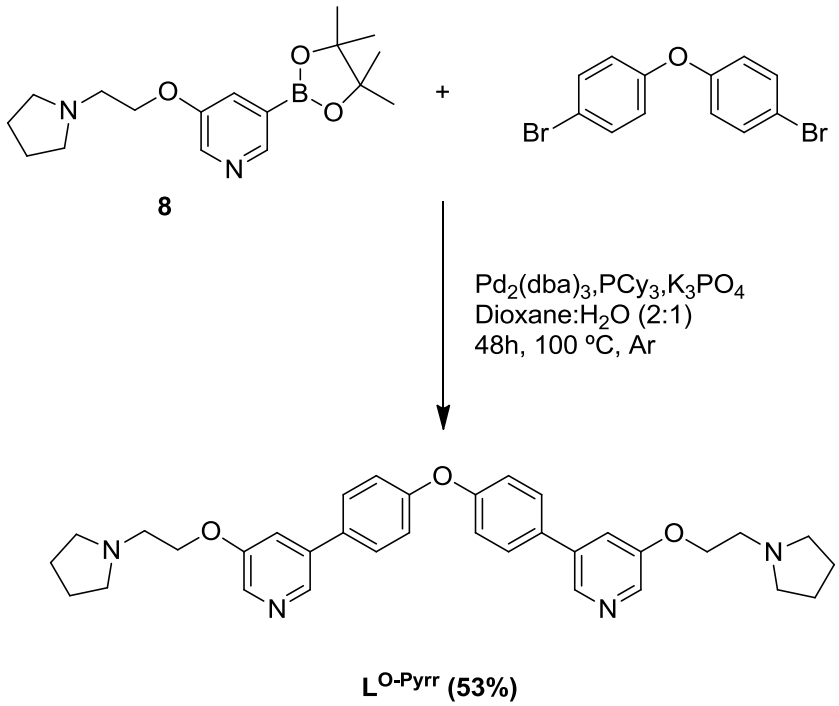

8

L$^{O\text{-}Pyrr}$ (53%)

Scheme 2.18: Synthesis of ligand **L$^{O\text{-}Pyrr}$**.

The purification of the crude mixture was even more challenging as two pyrrolidine motifs were present in the molecule. Two aluminium oxide columns were needed to obtain the final pure **L**$^{\textbf{O-Pyrr}}$ ligand. This resulted in low yields due to the high interaction between the ligand and the stationary phase.

The ^{1}H NMR spectrum confirms the formation of ligand **L**$^{\textbf{O-Pyrr}}$ with a single set of signals (Figure 2.56). Assignment of the different protons was performed with the aid of a 2D COSY and a 2D NOESY.

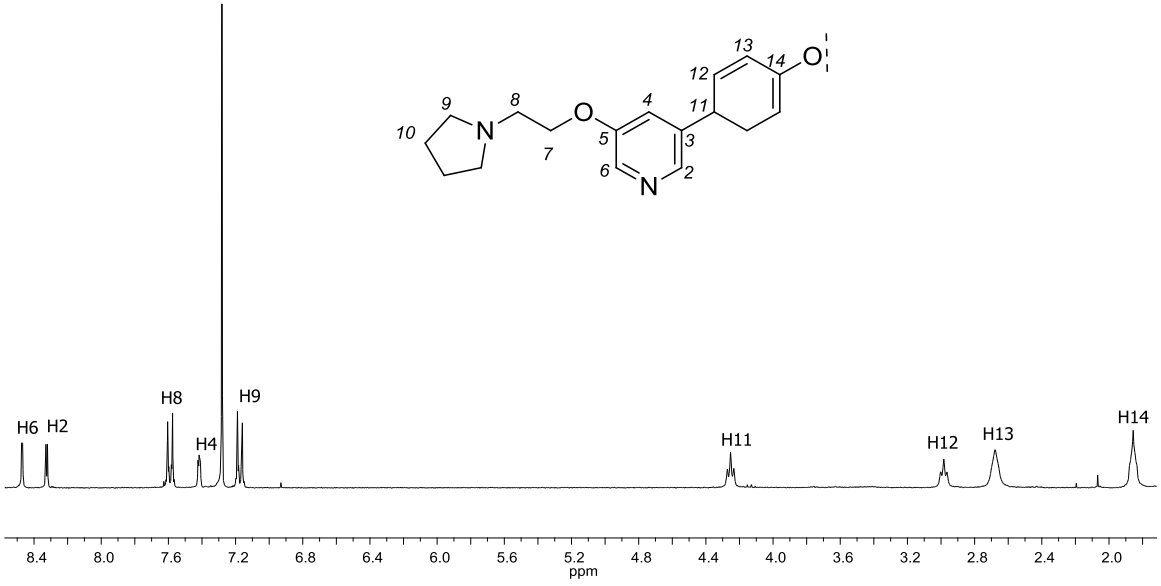

Figure 2.56: ^{1}H NMR spectrum of ligand **L**$^{\textbf{O-Pyrr}}$ (300 MHz, $CDCl_3$).

Electrospray mass spectrometry provided further evidence of the formation of ligand **L**$^{\textbf{O-Pyrr}}$ with the presence of the molecular ion at *m/z* 551.4 Da.

2.3.3.12. Synthesis of $[Pd_2L^{O\text{-}Pyrr}{}_4][(BF_4)_4]$

When reacting ligand $\mathbf{L^{O\text{-}Pyrr}}$ with $[Pd(CH_3CN)_4][(BF_4)_2]$ at 80 ºC, as performed for the formation of the complexes above, a complex mixture was obtained. The initial yellow solution became brown after one hour. This behaviour was not observed for any of the previous complex-forming reactions. Since some sort of degradation might be occurring, the reaction was then performed at room temperature overnight to evaluate whether the pyrrolidine motif is sensitive to temperature. A yellow solution was obtained and it was concentrated under reduced pressure and precipitated with diethyl ether. The obtained solid was analyzed by NMR spectroscopy.

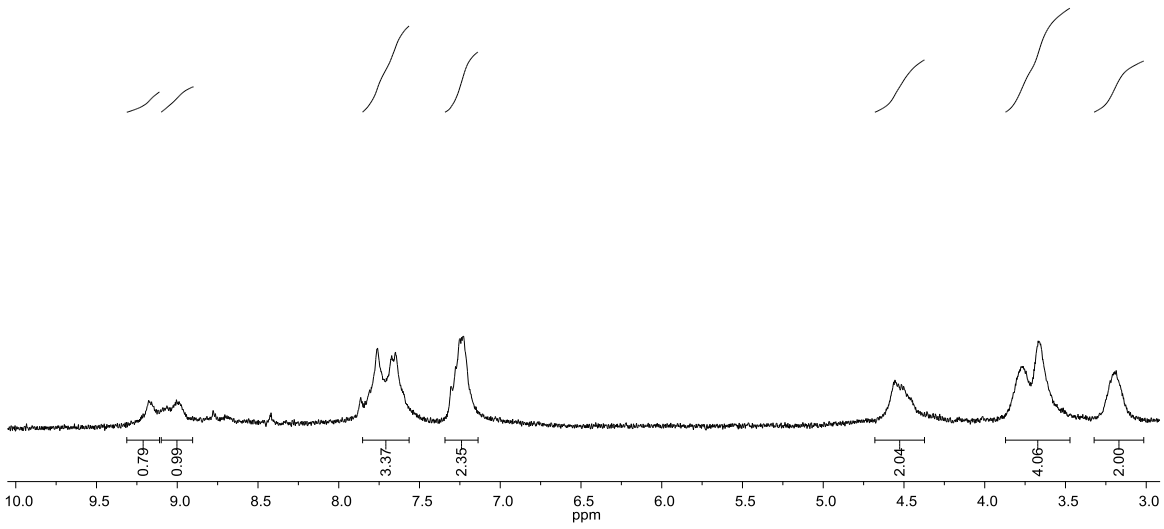

Figure 2.57: ^{1}H NMR spectrum of the crude $\mathbf{[Pd_2L^{O\text{-}Pyrr}{}_4][(BF_4)_4]}$ (300 MHz, CD_3CN).

The ^{1}H NMR spectrum shown in Figure 2.57 presents broad signals for the different proton peaks, indicating that the palladium(II) cylinder was not isolated as

its pure form. However, the relative intensities of the NMR signals indicate the correct ratio of protons expected. In addition a downfield shift, as seen for previous complexes, is also observed.

Unfortunately, any purification method attempted was unsuccessful. Therefore, **$[Pd_2L^{O\text{-}Pyrr}{}_4][(BF_4)_4]$** could not be obtained as its pure form.

2.3.3.13. Solubility of complexes with added groups at the edges

The strategy of functionalizing the complexes with the addition of different motifs at the edges of the pyridine ring proved to be the most successful. Hydroxyl complexes **$[Pd_2L^{OH}{}_4][(BF_4)_4]$** and **$[Pd_2L^{O\text{-}OH}{}_4][(BF_4)_4]$** showed a slight increase in their solubility in methanol compared to their methyl ether analogues. However, gelatinous solutions were also obtained. This might be due to the presence of eight hydroxyl groups located on the outside of the hydrophobic cylinder. The best improvement was achieved with the synthesis of **$[Pd_2L^{O\text{-}Glycol}{}_4][(BF_4)_4]$** as this new complex is highly soluble in methanol, however it remains insoluble in water. Unfortunately, synthesis of the promising **$[Pd_2L^{NH\text{-}OH}{}_4][(BF_4)_4]$** and **$[Pd_2L^{O\text{-}Pyrr}{}_4][(BF_4)_4]$** complexes could not be achieved.

2.3.4. Increase of the complex charge

The last strategy investigated to attempt to increase the water solubility of these tetra-stranded palladium(II) cylinders was to increase the overall charge of the complex. All the above complexes are 4+ charged. This charge is imparted by the

two palladium(II) centres. While maintaining the same dinuclear complex with the same metal centres, the charge could be increased by a slight modification of the ligands. This was performed by substitution of the diphenyl spacer unit by two pyridine units. Since these pyridine rings are linked to each other from the nitrogen atom by the methylene spacer, each ligand will be doubly charged (Figure 2.58). Reaction with palladium(II) may yield a tetra-stranded dinuclear species with a 12+ charge.

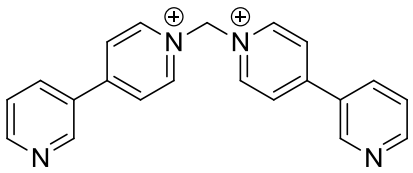

Figure 2.58: Proposed doubly charged ligand.

These type of charged ligands have been previously reported by Quintela *et al*..[163] The reaction of these charged ligands with protected palladium(II) metal centres yielded water soluble dinuclear palladium(II) complexes, which were used as macrocycles for catenane formation or as host of PAH as discussed in section 1.3.1.[114,163,164]

In order to achieve this doubly charged ligand $\mathbf{L^{N+}}$, an asymmetric bipyridine needed to be synthesised and this could be accessed via Suzuki coupling of a bromopyridine and a pyridine boronic acid, as shown in the retrosynthetic analysis in Scheme 2.19.

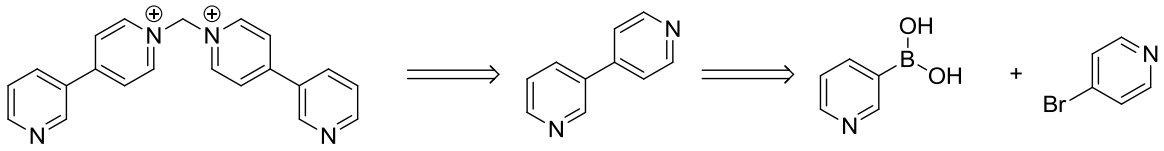

Scheme 2.19: Retrosynthetic analysis of doubly charged ligand $\mathbf{L^{N+}}$.

2.3.4.1. Synthesis of 3,4'-bipyridine (9)

The synthesis of the asymmetric bipyridine was performed via Suzuki coupling following an analogous procedure to that reported above (Scheme 2.20).

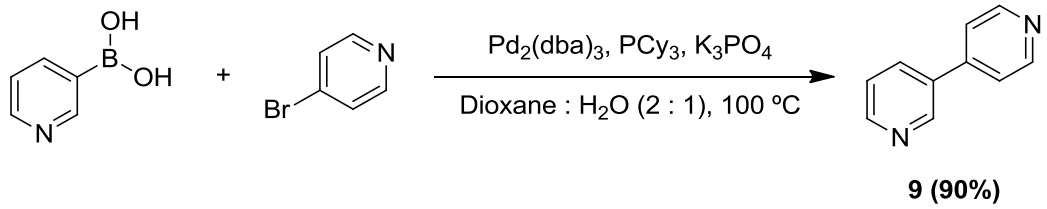

Scheme 2.20: Synthesis of asymmetric bipyridine **9**.

Characterization of bipyridine **9** was successfully performed by NMR spectroscopy, MS spectrometry and IR spectroscopy which confirmed its formation.

2.3.4.2. Synthesis of ligand L^{N+}

Once the asymmetric bipyridine was synthesised it was coupled with dibromethane yielding the 2+ ligand $\mathbf{L^{N+}}$ with two bromo counterions (Scheme 2.21).

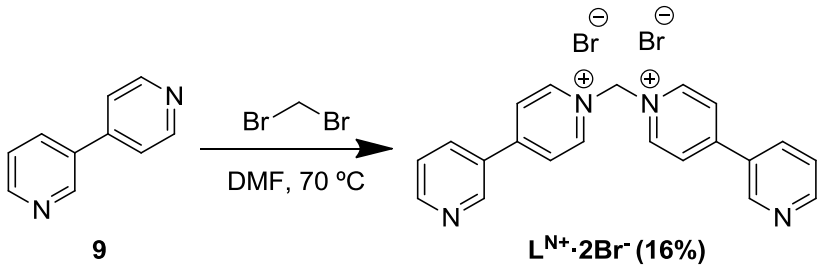

Scheme 2.21: Synthesis of charged ligand $\mathbf{L^{N+}\cdot 2Br^{-}}$.

Three different permutations (**A**, **B** and **C**) for the coupling of bipyridine **9** and dibromethane are possible (Figure 2.59).

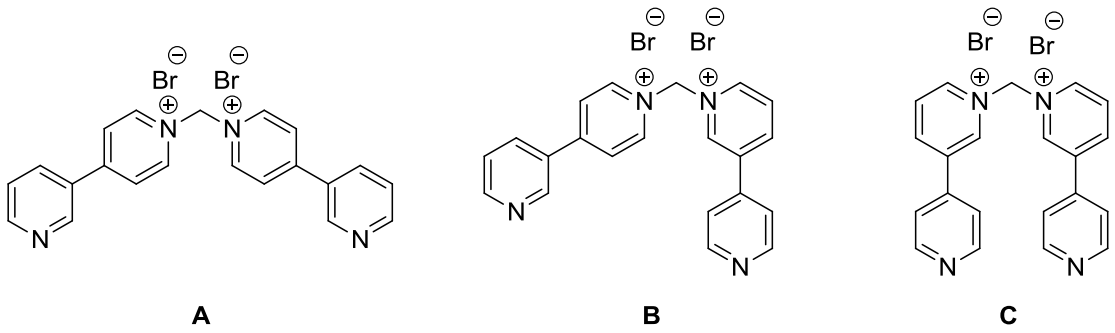

Figure 2.59: Possible coupling combinations

The analysis of the ^{1}H NMR spectrum was enough to determine whether one of the possible **A**, **B** and **C** products had formed or a mixture of two or three of them was present at the same time.

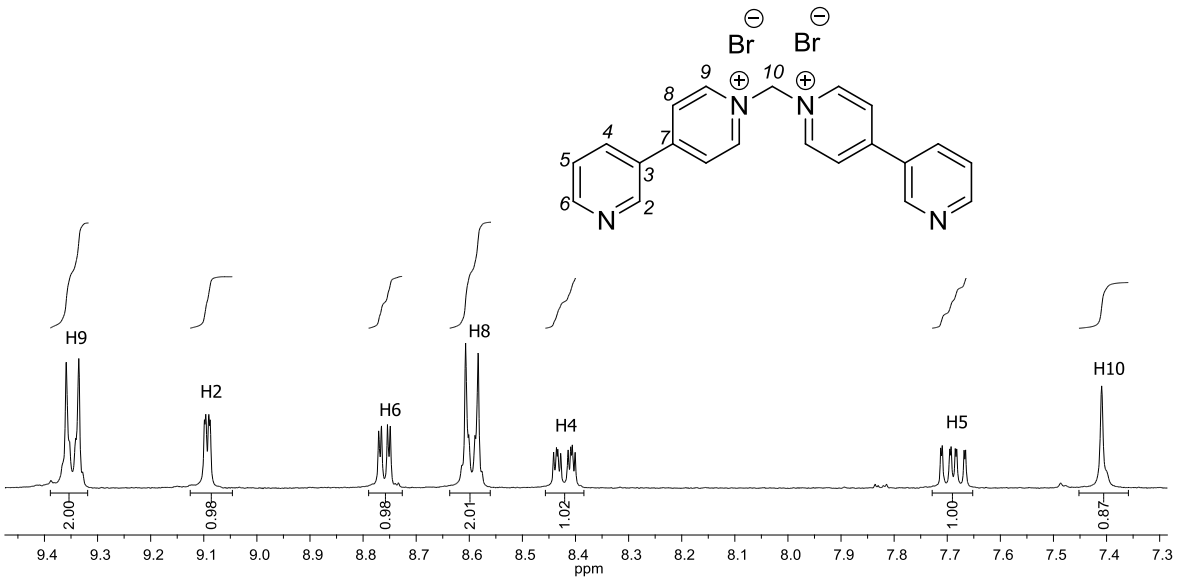

Figure 2.60: ^{1}H NMR spectrum of ligand $\mathbf{L^{N+}}$ (300MHz, D_2O).

The simple spectrum with seven different signals rules out the possibility of having formed a mixture of compounds. In addition, **B** could not have been formed as **B** is an asymmetric ligand and more signals should have been present. The highest downfield shifted protons should be those α to the positively charged nitrogen of the pyridine ring. Since this signal accounts for two protons in the NMR spectrum shown in Figure 2.60 and only two protons with the same environment can produce such a signal, **A** was confirmed as the only product.

Interestingly, after a month in the NMR tube it was observed that the central methylene proton disappeared. This could be due to its exchange with the deuterium of the NMR solvent.

2.3.4.3. Attempted synthesis of $[Pd_2L^{N+}{}_4][(BF_4)_4]$

When attempting to synthesise the palladium(II) complex of $\mathbf{L^{N+}\cdot 2Br^-}$, the cylinder was not formed. This is probably due to the formation of $PdBr_2$. Similar results were observed for the exchange of the tetrafluoroborate counter-ion of $\mathbf{[Pd_2L^{OMe}{}_4][(BF_4)_4]}$ complex by chloride. In both cases, the palladium-halogen bond seems to be stronger than the palladium-pyridine one.

To solve this problem, the bromide counter-ions of ligand $\mathbf{L^{N+}\cdot 2Br^-}$ were exchanged by hexafluorophosphates ($\mathbf{L^{N+}\cdot 2PF_6^-}$) and these by nitrates in order to obtain a water soluble ligand ($\mathbf{L^{N+}\cdot 2NO_3^-}$). Ligand $\mathbf{L^{N+}\cdot 2Br^-}$ was dissolved in water and a saturated aqueous solution of ammonium hexafluorophosphate was added to precipitate a white solid. This solid was collected by filtration and washed with water and diethyl ether. Confirmation of the exchange was readily observed by infrared spectroscopy with the presence of a strong band at 805 cm^{-1} which corresponds to the free hexafluorophosphate counter-ions. Ligand $\mathbf{L^{N+}\cdot 2PF_6^-}$ was then dissolved in acetonitrile and a saturated solution of tetrabutylammonium nitrate in acetonitrile was added to precipitate a white solid. Filtration of the solid and washing with acetonitrile and diethyl ether afforded ligand $\mathbf{L^{N+}\cdot 2NO_3^-}$. Its infrared spectrum presented a strong band at 1320 cm^{-1} confirming the successful counter-ion exchange.

Unfortunately, complex formation did not occur with the nitrate ligand $\mathbf{L^{N+}\cdot 2NO_3^-}$ either. This result might be due to the impossibility of four doubly charged ligands approaching two palladium(II) metal centres. This problem was not observed in Quintela's system as protected palladium(II) starting materials

were used. However, for a tetra-stranded complex to be formed, naked palladium(II) reagents are a requirement.

2.3.5. Exploring a new ligand system

Multi-step and time consuming reactions were required to modify and synthesise the palladium(II) tetra-stranded cylinders discussed above. Therefore, a new ligand system was explored.

In 2010, Crowley and co-workers reported the synthesis of a tetra-stranded palladium(II) saturated helicate with triazole rings coordinating to the palladium(II) metal centres. This ligand was synthesised via a CuAAC click chemistry reaction.[165]

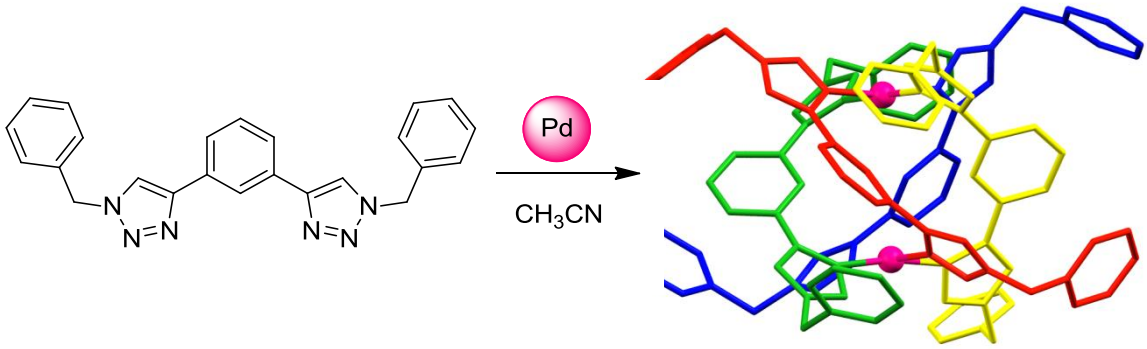

Scheme 2.22: Synthesis of Crowley's tetra-stranded helicate (CCDC 762916).[165]

This complex was used as inspiration to develop a new ligand system, in which the pyridine rings are replaced by 1,2,3-triazole rings. This could lead to a new library of compounds via an easy synthetic route.

The 1,3-dipolar cycloaddition reaction between azides and terminal alkynes was initially studied by Huisgen.[166] Its Cu(I)-catalyzed version has been recently renamed as the “click” reaction. The CuAAC or click reaction can produce, under mild reaction conditions, 1,4-substituted-1,2,3-triazoles in excellent yields.[167] 1,2,3-Triazoles can be used in coordination chemistry as they have the potential to act as N donor ligands.[165] Therefore, CuAAC reactions and triazoles represent a new powerful tool and ligand architecture for the design of metallo-supramolecular arrays. Triazole ligands formed via click reaction also present a simple synthetic route to new functionalized scaffolds, which are harder to obtain in polypyridine chemistry with multiple reaction steps as shown above.

2.3.5.1. Molecular design of ligand $L^{Click\text{-}Bn}$

Ligand $\mathbf{L^{Click\text{-}Bn}}$ was designed by incorporation of the triazole motif of Crowley’s click ligand into the diphenyl spacer-ligand used in this study and in Hannon’s helicates. The retrosynthetic analysis proposed for the synthesis of ligand $\mathbf{L^{Click\text{-}Bn}}$ is shown in Scheme 2.23.

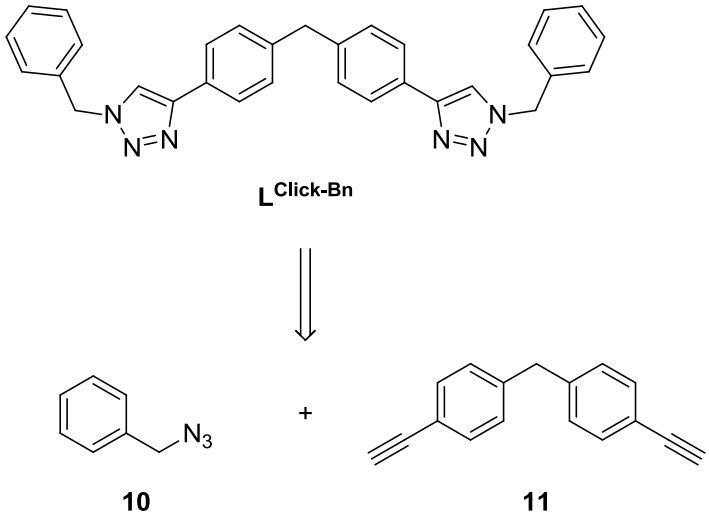

Scheme 2.23: Retrosynthetic analysis for the synthesis of ligand **L**$^{\textbf{Click-Bn}}$.

Suitable building blocks (**10** and **11**) needed to be synthesised to perform the CuAAc click reaction to form ligand **L**$^{\textbf{Click-Bn}}$.

In order to synthesise **11**, the following retrosynthetic analysis was proposed (Scheme 2.24). The triple bond functionality will be introduced by coupling a protected acetylene onto the aromatic spacer unit. Subsequent removal of the protecting group will lead to the free arylacetylene.

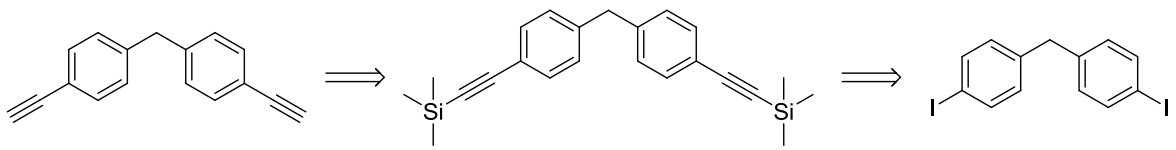

Scheme 2.24: Retrosynthetic analysis for the synthesis of **11**.

2.3.5.2. Synthesis of bis(4-iodophenyl)methane (13)

Bis(4-iodophenyl)methane **13** was synthesised as a precursor for the synthesis of the biarylacetylene **11**. 4,4'-Methylenedianiline was dissolved in concentrated sulfuric acid and was diazotized by addition of sodium nitrite. Care was taken to maintain the temperature below 5 ºC as diazonium salts in solution are unstable above that temperature with elimination of nitrogen gas (N_2). The diazonium salt was then poured into a warmed solution of potassium iodide to form compound **13** by nucleophilic aromatic substitution (Scheme 2.25). Work up and purification by column chromatography as stated in a previous reported protocol[168] yielded **13** in 47% yield.

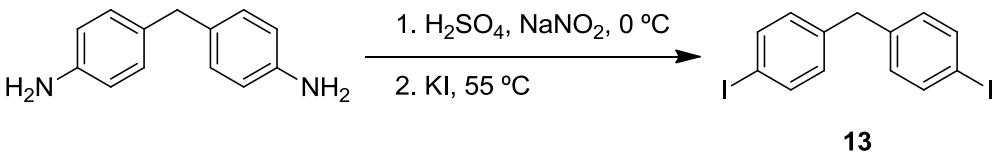

13

Scheme 2.25: Synthesis of **13**.

NMR, IR and particularly mass spectrometry aided the identification of compound **13**. The molecular ion at *m/z* 420 Da and fragments corresponding to the loss of one (*m/z* 293 Da) and both iodines (*m/z* 166 Da) were observed in electron impact mass spectrometry.

2.3.5.3. Synthesis of bis[4-[(trimethylsilyl)ethynyl]phenyl]methane (12)

Introduction of the one end protected acetylene unit into the aryl molecule **13** was performed via a palladium-copper-catalyzed cross-coupling reaction as depicted in Scheme 2.26 following a Sonogashira mechanism.[168] The palladium(0) catalyst is

generated *in situ* from palladium(II) acetate and triphenylphosphine. Copper iodide acts as an activator of the alkyne group to produce copper(I) acetylide at the free end. Triethylamine acts as a solvent and as a base forming triethylamine hydroiodide with the substracted hydrogen iodide.

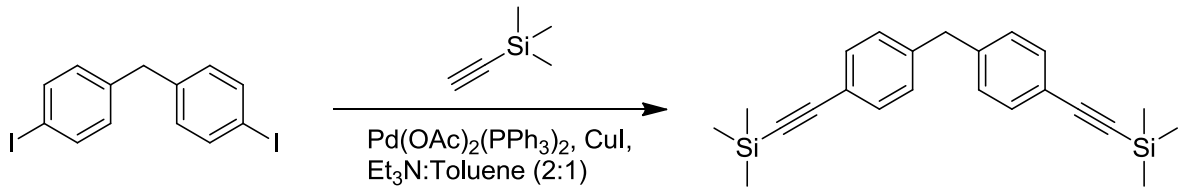

13 **12**

Scheme 2.26: Synthesis of **12**.

Compound **12** was characterized by NMR, where peaks corresponding to the methyl groups of the protecting group were observed in ^{1}H and ^{13}C NMR. The ^{1}H NMR spectrum shows a single peak integrating for 18 protons at 0.29 ppm and the^{13}C NMR a single peak at 0.2 ppm. EI+-MS shows the molecular ion at *m/z* 360 Da and a fragment at *m/z* 345 Da corresponding to the loss of one methyl group. The infrared spectra presents two characteristic bands for the vibrations of the Si-CH stretching at 2957 cm^{-1} and 1246 cm^{-1} and one very strong broad band for the Si-C bending at 836 cm^{-1}.

Characterization of compound **12** was performed after it was purified by column chromatography on silica gel. This purification step proved to be very important as a copper-free compound is mandatory for the success of the subsequent deprotecting step. Since the deprotection occurs in basic alcohol

media, the presence of copper iodide salts produced the Glaser coupling product **14**, as detected by EI+-MS with a peak at *m/z* 430 Da (Scheme 2.27).

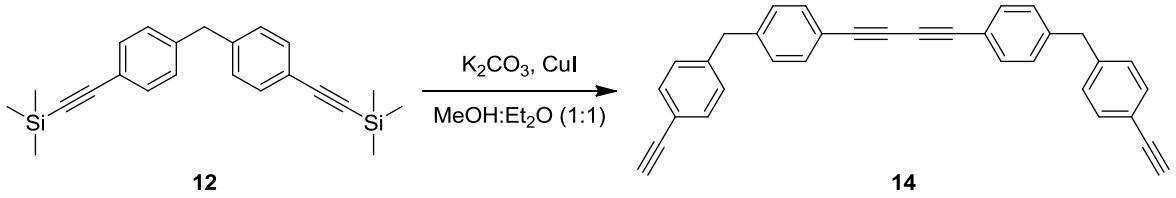

12 **14**

Scheme 2.27: Formation of Glaser coupling product **14**.

2.3.5.4. Synthesis of bis(4-ethynylphenyl)methane (11)

Removal of the trimethylsilyl protecting group was performed under inert atmosphere in a mixture of methanol and diethyl ether with anhydrous potassium carbonate (Scheme 2.28).

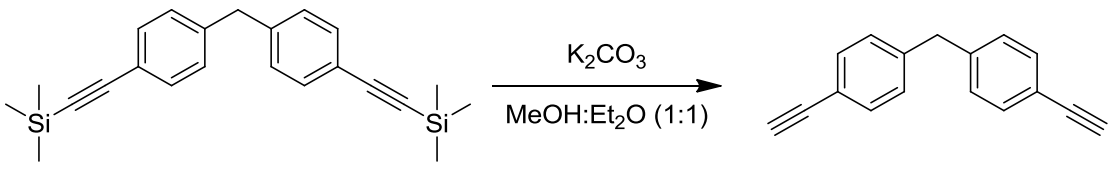

12 **11**

Scheme 2.28: Synthesis of **11**.

The free alkyne group was observed by ^{1}H NMR with a peak at 3.07 ppm accounting for two protons and corresponding to the terminal alkyne proton. Infrared spectroscopy also aided the identification of the compound with a very strong sharp band at 3274 cm^{-1} assigned to the C≡CH vibration. These data were compared to those reported in the literature.[168]

2.3.5.5. Synthesis of ligand $L^{Click\text{-}Bn}$

$L^{Click\text{-}Bn}$ ligand can be formed in a one-pot, multi-component click reaction (Scheme 2.29). Due to the explosive potential of low molecular weight azides, benzyl azide **10** was prepared *in situ* and was not isolated. The benzyl group was the substituent chosen for this ligand, for analogy to that presented by Crowley and co-workers in 2010.

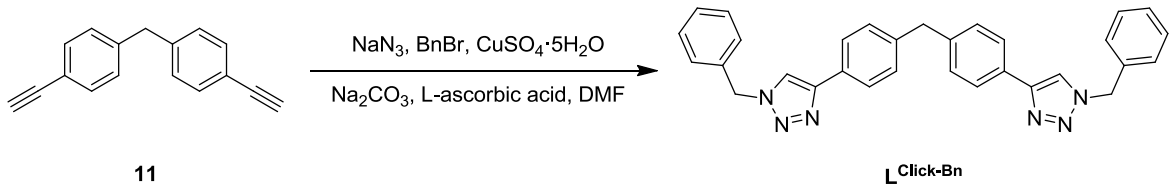

Scheme 2.29: Synthesis of ligand **$L^{Click\text{-}Bn}$**.

Benzyl bromide and sodium azide were dissolved in dimethylformamide and heated at 65 ºC for two hours. After cooling to room temperature, an aqueous solution of copper sulfate, L-ascorbic acid, sodium carbonate and alkyne **11** were added, followed by stirring for 48 hours. As copper azides and acetylides are explosive when dried, a solution of EDTA/NH_4OH (1 M) was poured into the crude reaction mixture once the reaction had concluded. Column chromatography on silica gel afforded the pure ligand **$L^{Click\text{-}Bn}$**.

Infrared spectroscopy proved very useful for the identification of ligand **$L^{Click\text{-}Bn}$** as the azide band at around 2095 cm^{-1} and the alkyne bands at 2150 and 3300 cm^{-1} were absent. The characteristic singlet of the triazole unit was also observed in the ^1H NMR spectrum (Figure 2.61).

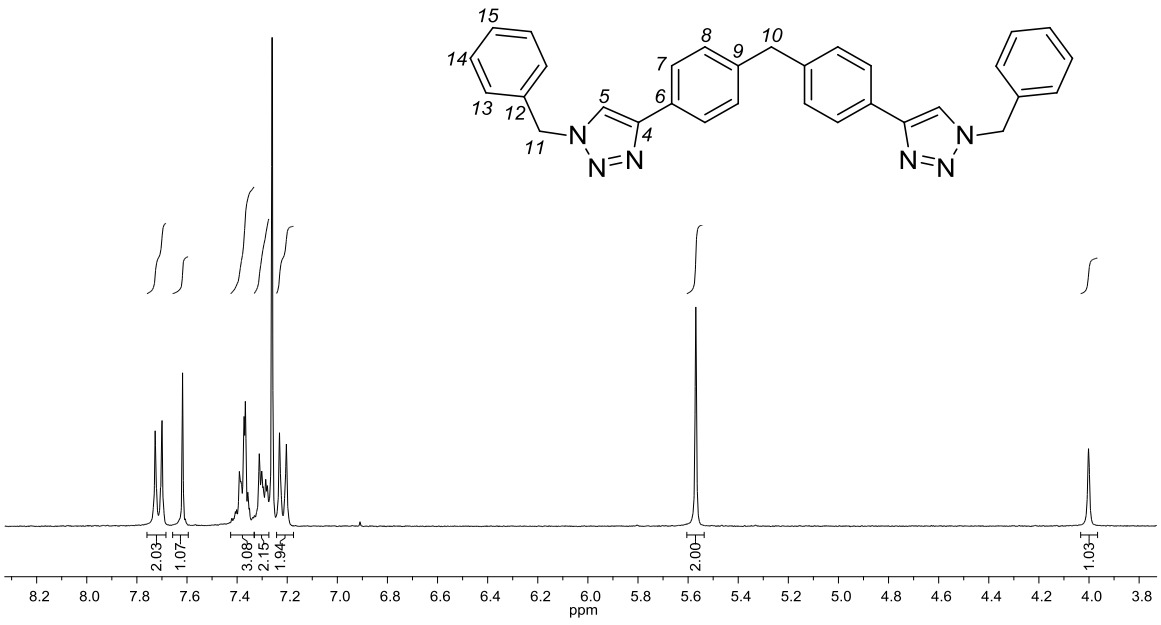

Figure 2.61: ^{1}H NMR spectrum of ligand **L**$^{\textbf{Click-Bn}}$ (300 MHz, $CDCl_3$).

Colourless crystals suitable for X-ray diffraction were successfully grown by slow evaporation of deuterated dichloromethane. The crystal structure confirms the formation of the symmetric ligand **L**$^{\textbf{Click-Bn}}$ (Figure 2.62).

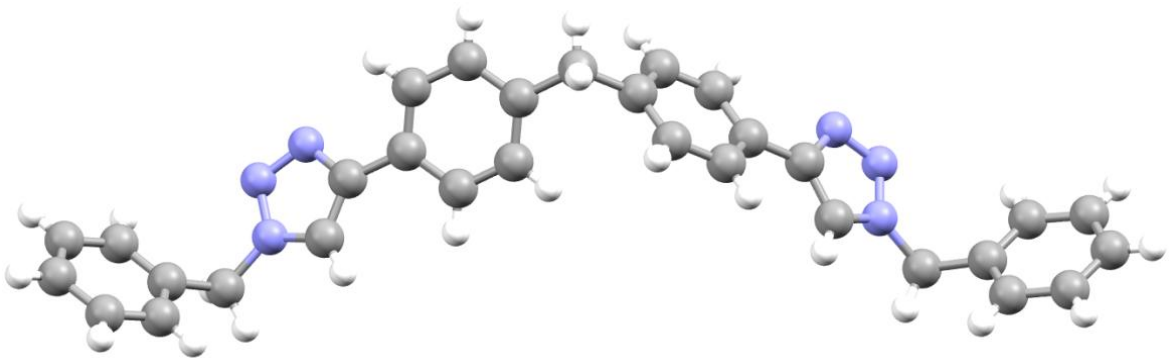

Figure 2.62: Crystal structure of ligand **L**$^{\textbf{Click-Bn}}$.

The phenyl rings are twisted about the central methylene spacer by 75º with respect to one another and by 20º and 25º with respect to the 1,2,3-triazole rings. The phenyl rings of the benzyl groups are twisted with respect to the triazole rings by 57º and 61º. The triazole rings are twisted by 67º with respect to each other. No intermolecular interactions are observed.

2.3.5.6. Attempted synthesis of $[Pd_2L^{Click\text{-}Bn}{}_4][(BF_4)_4]$

When reacting the newly synthesised **L**$^{\textbf{Click-Bn}}$ ligand with $[Pd(CH_3CN)_4][(BF_4)_2]$ at 80 ºC, a complex mixture was formed. Reaction at room temperature overnight produced the same result. The ^{1}H NMR spectrum presents broad signals that are difficult to assign or integrate. However, a downfield chemical shift of the characteristic triazole proton is observed. Unfortunately, mass spectrometry was unable to confirm the formation of the complex in its crude form. This crude mixture could not be purified by any of the common methods.

2.3.5.7. Molecular design of ligand L$^{Click\text{-}OH}$

Since the palladium(II) complex of ligand **L**$^{\textbf{Click-Bn}}$ could not be formed or isolated as its pure form, a new ligand system was investigated. A smaller group was thought to be more convenient as the benzyl groups are quite bulky groups and might interfere with the coordination process of the palladium(II) to the 1,2,3-triazole rings. An alcohol chain was the chosen motif to be added at position 4 of the triazole moieties. This alcohol group might also infer better water solubility properties into the ligand and complex. The retrosynthetic analysis for the

formation of $\mathbf{L}^{\mathbf{Click\text{-}OH}}$ is shown in Scheme 2.30. As for the previous ligand system, a CuAAC reaction between an azide and the triple bond spacer **11** should yield the desired $\mathbf{L}^{\mathbf{Click\text{-}OH}}$ ligand.

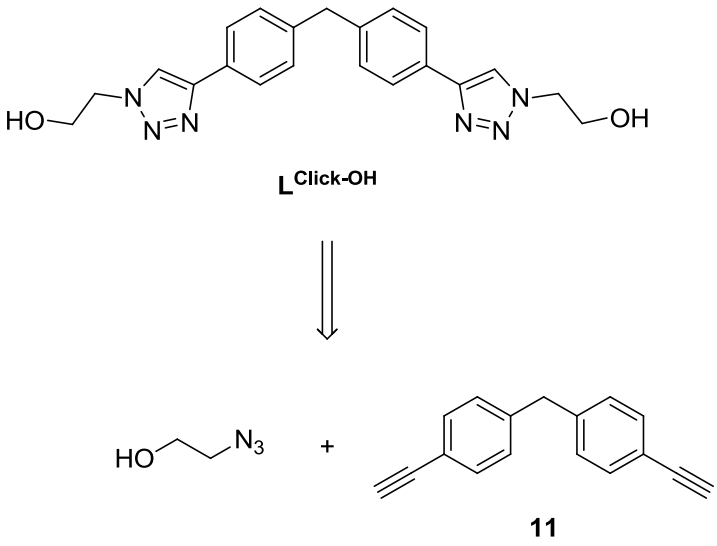

Scheme 2.30: Retrosynthetic analysis of ligand $\mathbf{L}^{\mathbf{Click\text{-}OH}}$.

2.3.5.8. Synthesis of ligand $L^{Click\text{-}OH}$

By following the same protocol reported above for ligand $\mathbf{L}^{\mathbf{Click\text{-}Bn}}$, ligand $\mathbf{L}^{\mathbf{Click\text{-}OH}}$ was formed in a one-pot click chemistry reaction between 2-bromoethanol and triple bond spacer **11** in 83% yield (Scheme 2.31).

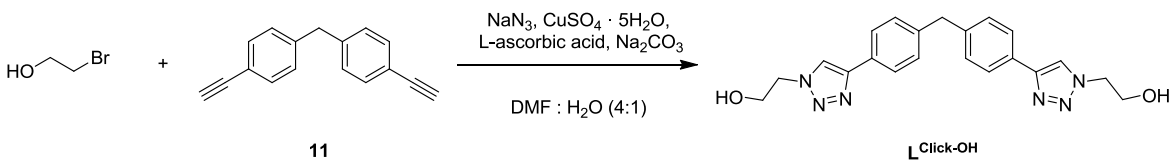

Scheme 2.31: Synthesis of ligand $\mathbf{L}^{\mathbf{Click\text{-}OH}}$.

Purification of this ligand was achieved by recrystallization of the crude mixture from hot methanol. The ^{1}H NMR spectrum confirmed the formation of the 1,4-disubstituted trizole ligand (Figure 2.63).

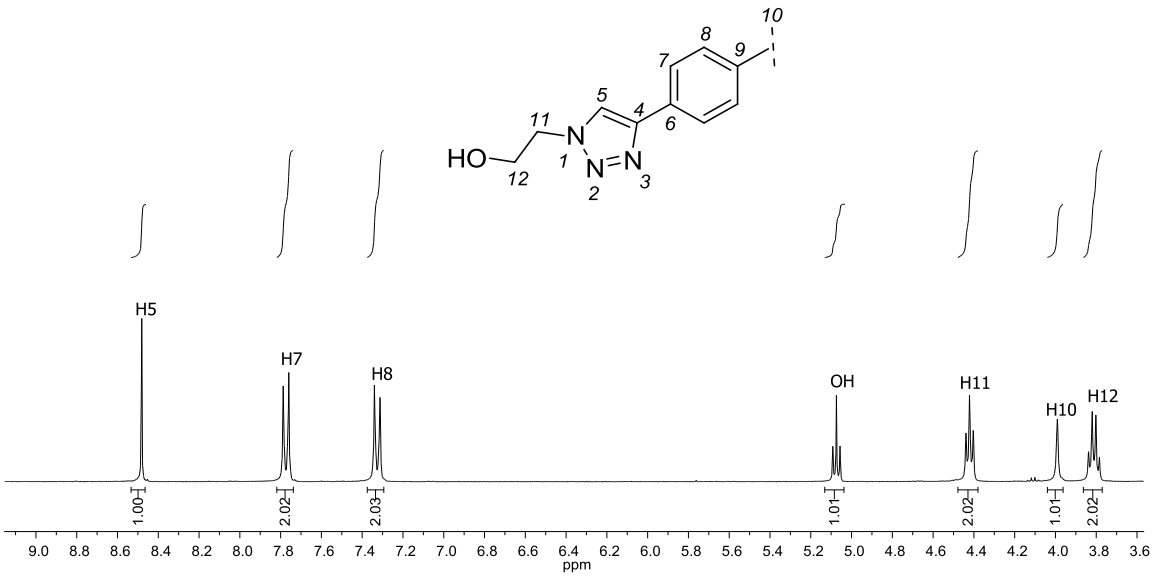

Figure 2.63: ^{1}H NMR spectrum of ligand $\mathbf{L}^{\mathbf{Click\text{-}OH}}$ (300 MHz, DMSO-d_6).

Electrospray mass spectrometry provided further evidence for the formation of ligand $\mathbf{L}^{\mathbf{Click\text{-}OH}}$ with a peak at *m/z* 413.2 Da corresponding to the sodium adduct.

2.3.5.9. Attempted synthesis of $[Pd_2L^{Click\text{-}OH}{}_4][(BF_4)_4]$

Upon reaction of ligand $\mathbf{L}^{\mathbf{Click\text{-}OH}}$ with $[Pd(CH_3CN)_4][(BF_4)_2]$ a broad ^{1}H NMR spectrum was obtained, therefore it was not possible to integrate the different peaks or unambiguously detect the triazole proton. All purification methods attempted proved unsuccessful.

2.3.5.10. Molecular design and synthesis of ligand $L^{Click\text{-}Glycol}$

Since **$[Pd_2L^{O\text{-}Glycol}{}_4][(BF_4)_4]$** proved to be the most readily soluble complex, a glycol chain was added at position 4 of the triazole ring. Ligand **$L^{Click\text{-}Glycol}$** was synthesised following an analogous protocol employed for the click reactions reported above (Scheme 2.32).

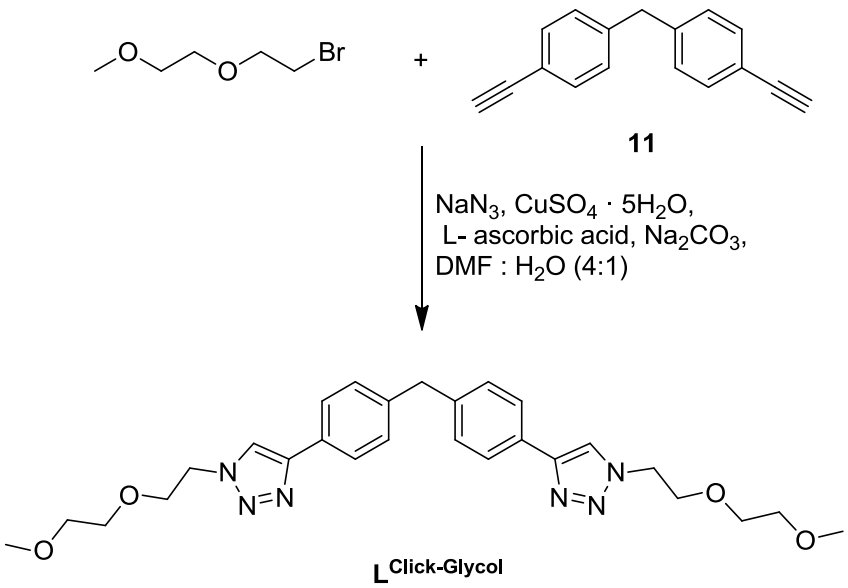

Scheme 2.32: Formation of **$L^{Click\text{-}Glycol}$** ligand.

Formation of the ligand was confirmed by NMR, MS and IR, as performed for the previously synthesised click ligands.

2.3.5.11. Attempted synthesis of $[Pd_2L^{Click\text{-}Glycol}{}_4][(BF_4)_4]$

Unfortunately, complexation of ligand **$L^{Click\text{-}Glycol}$** to a palladium(II) metal centre did not occur or could not be detected.

2.4. Closing remarks

This chapter has explored four different strategies to improve the solubility of the first generation of Hannon's tetra-stranded palladium(II) supramolecular cylinders. Modification of the spacer unit has led to four novel palladium(II) complexes that are soluble in acetonitrile, acetone and dimethyl sulfoxide. Exchanging the counter-ion of the complex only led to a solubility improvement in acetonitrile with triflate anions. Ligands were functionalised at the edges and three new cylinders were synthesised. The best results were obtained when adding a glycol chain at position 3 of the pyridine ring, resulting in a new cylinder that is highly soluble in methanol. Unfortunately, water solubility has not yet been achieved, as none of the synthesised complexes were soluble in 100% aqueous buffer. A new different ligand system was also explored. The pyridine rings were substituted by triazoles, however pure complexes could not be isolated.

Chapter 3: DNA Binding Studies of Palladium(II) Tetra-Stranded Cylinders

3.1. Introduction

The DNA binding properties of the synthesised complexes in chapter 2 were explored and will be reported in this chapter. The interaction between the tetra-stranded complexes and DNA was studied via different spectroscopic techniques, such as circular and linear dichroism and ethidium bromide displacement, as well as agarose and polyacrylamide gel electrophoresis.

Initially, the interaction between the newly synthesised cylinders and duplex DNA was investigated, in order to evaluate the binding affinity of these complexes to DNA. Then, more specific DNA four-way junction experiments were carried out.

In this chapter, preliminary cytotoxicity data of the synthesised palladium(II) cylinders against different breast and ovarian cancer cell lines will also be presented.

3.2. Circular dichroism studies

Circular dichroism (CD) is a well known electronic spectroscopic technique that can be used to study the interaction between DNA and ligands, and to observe the

DNA conformation itself. CD measures the difference in absorption of left (A_L) and right (A_R) circularly polarized light (eq. 1) and is only sensitive to chiral molecules.

$$CD\ (\lambda) = A_L\ (\lambda) - A_R\ (\lambda) \qquad \text{(eq. 1)}$$

DNA is a chiral molecule and therefore absorbs left and right circularly polarized light differently. This is measured as a wavelength function and gives rise to a CD signal under absorption bands.[169] DNA chirality arises from the right-handed chiral sugar moieties (C1' carbon atom) that form the DNA phosphate backbone. However, the specific CD spectrum of DNA depends on the orientations of the DNA bases (chromophores) as these present characteristic bands in the UV region that result from π-π* transitions. These DNA bases are not chiral, however they are held within the chiral environment created by the DNA backbone.[170] Every chiral molecule shows a particular CD spectrum. The B-DNA form of ct-DNA presents a positive band around 280 nm and a negative band around 245 nm, with the intersection point at 260 nm. Over 300 nm the CD spectrum of DNA does not present any signal or band (Figure 3.1).[171]

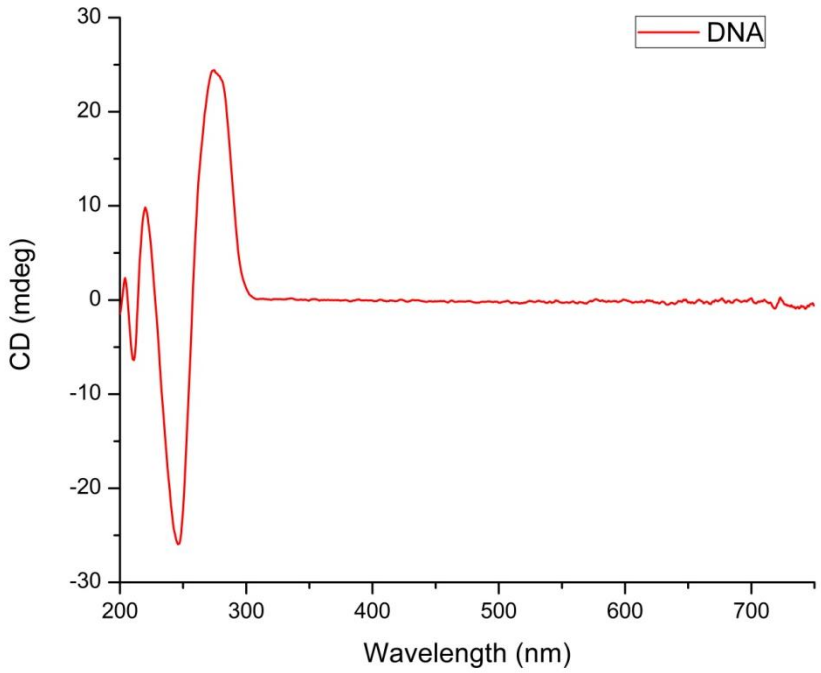

Figure 3.1: CD spectrum of B-form of DNA.
(300 μM ct-DNA in 20 mM NaCl and 1 mM $Na(CH_2)_2AsO_3 \cdot 3H_2O$ (pH 6.8)).

If a DNA-binding molecule is achiral, no CD signal is observed in the absence of DNA. However, it could acquire an induced chirality upon binding to DNA, giving rise to an induced CD (ICD) signal. Intercalators present weak and negative ICD signals if the transitions are polarized along the long axis of the intercalation pocket; and positive if perpendicular transitions occur. ICD signals for groove binders are generally positive and an order of magnitude stronger than those observed for intercalators.[172]

In this study, the interaction between the newly synthesised complexes and calf thymus DNA (ct-DNA) is assessed via CD titrations of the complexes into an aqueous buffered ct-DNA solution. The DNA concentration is kept constant during the experiment and aliquots of complexes are added, after which a CD spectrum is

measured. The overlay of the CD spectrum of each titration can be used to interpret the interactions between the complex and the DNA.

None of the synthesised palladium(II) cylinders has an intrinsic CD signal as they are not helical or, if they are, they exist as a racemic mixture of M and P enantiomers. As a result, any CD signal observed in the spectroscopic regions of the complexes is due to their interaction with DNA.

Since all the synthesised palladium(II) complexes are white or pale yellow, the major challenge for the evaluation of the DNA binding interaction was to be able to detect the ICD signal, as the spectroscopy of the complexes overlays or is very close to that of the DNA.

The CD experiment was first attempted with the **$[Pd_2L^{OMe}_4][(BF_4)_4]$** complex. As this complex is not water soluble, a concentrated dimethyl sulfoxide solution of the complex was prepared, which was then diluted with water to give a 15% dimethyl sulfoxide solution. The percentage of dimethyl sulfoxide present in the titration was 3% at most. A control experiment where DNA is titrated with increasing concentrations of a 15% dimethyl sulfoxide solution was performed. Only changes below 225 nm were observed on the CD spectra, due to the absorbance of dimethyl sulfoxide in this region, manifested by high tension spectra which produces unreliable data. Therefore, this region will not be considered during the analysis of the CD spectra of the different palladium(II) complexes.

Initially, titrations of a 500 μM stock solution of **$[Pd_2L^{OMe}_4][(BF_4)_4]$** complex over a 300 μM ct-DNA solution were performed, as these are the experimental

conditions most commonly used by Hannon and co-workers. However, it was observed that precipitation of DNA at this concentration occurred even at low complex loading, hence CD data was unreliable. Therefore, the experiment concentrations were reduced by one order of magnitude. A stock solution of 50 μM of **$[Pd_2L^{OMe}_4][(BF_4)_4]$** complex was prepared by dissolving it in DMSO and diluting with water to obtain a 1.5% DMSO solution. At the end of the titration, the DMSO percentage in the cuvette will be of 0.3%. The stability of the complex at 1.5% DMSO was assessed during the course of the CD experiment by UV-vis scans. Scans from the start and end of the experiment were superimposable. The CD spectra corresponding to the titrations of a 50 μM stock solution of **$[Pd_2L^{OMe}_4][(BF_4)_4]$** complex over a 30 μM ct-DNA solution are shown in Figure 3.2. These CD spectra present an ICD signal at around 318 nm, which increases its intensity with increasing concentrations of **$[Pd_2L^{OMe}_4][(BF_4)_4]$** complex. This indicates that the palladium(II) complex is interacting with the DNA. It is also observed that the B-conformation of DNA is retained upon cylinder binding as the DNA signature is maintained. A small decrease in intensity is observed, probably due to ligand transitions in this region.

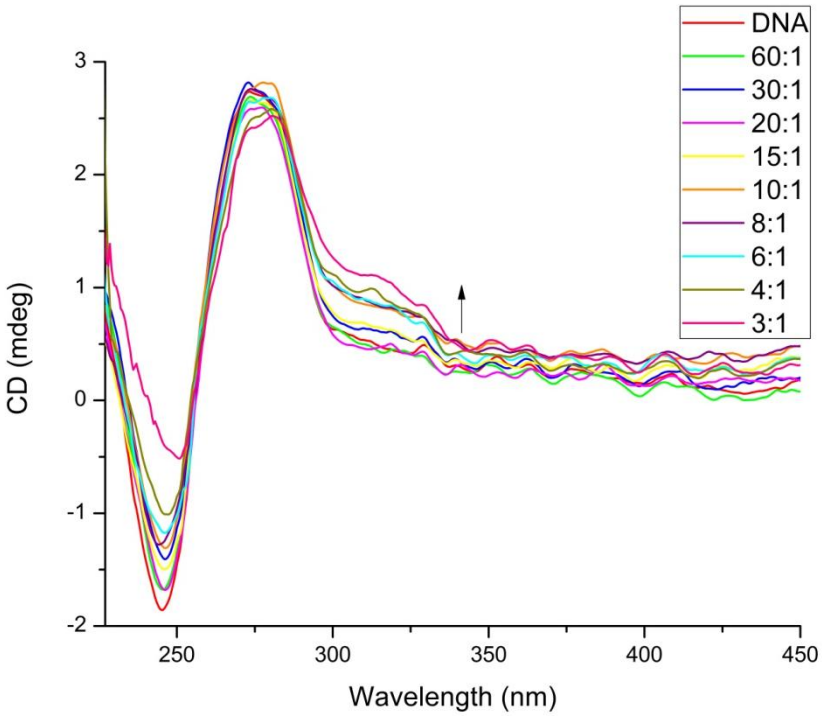

Figure 3.2: CD spectra of ct-DNA with increasing concentrations of **$[Pd_2L^{OMe}{}_4][(BF_4)_4]$** complex. Legend shows ct-DNA base:complex ratios. 0.3% max. DMSO. (30 μM ct-DNA in 20 mM NaCl and 1 mM $Na(CH_2)_2AsO_3 \cdot 3H_2O$ (pH 6.8)).

A greater interaction is observed when performing CD titrations for **$[Pd_2L^{O\text{-}OMe}{}_4][(BF_4)_4]$** in the same conditions reported above (Figure 3.3). An ICD signal is observed around 312 nm which indicates binding of the complex to the DNA. The characteristic DNA signal between 200-300 nm is lost at high loading, from a ratio of DNA base:complex of 4:1. This could mean that either the palladium(II) complex has perturbed the B-DNA upon binding at high loadings, or that an effect of the DNA and complex CD signals (from the ligands) being overlaid is being observed.

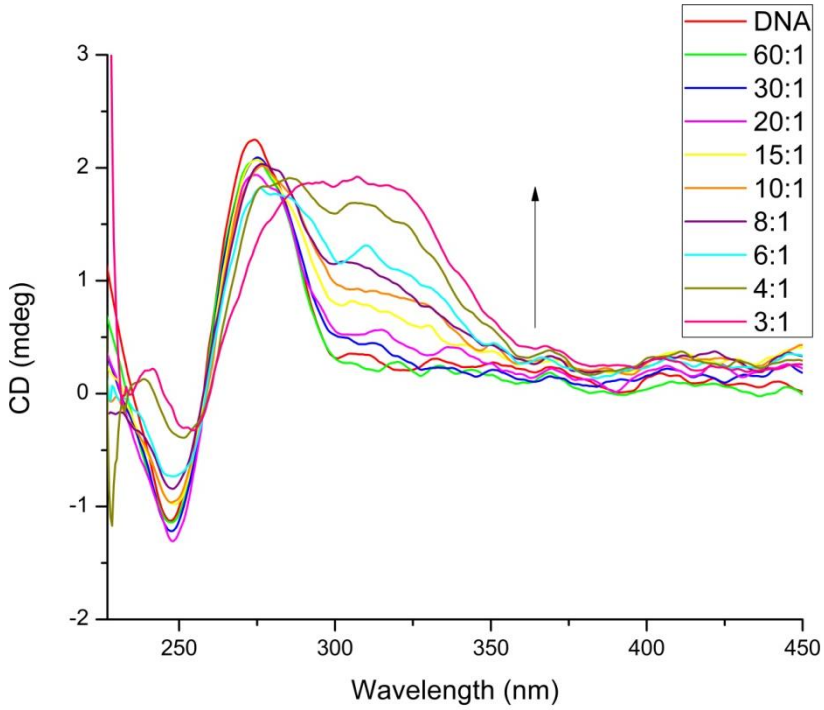

Figure 3.3: CD spectra of ct-DNA with increasing concentrations of **$[Pd_2L^{O\text{-}OMe}{}_4][(BF_4)_4]$** complex. Legend shows ct-DNA base:complex ratios. 0.3% max. DMSO. (30 μM ct-DNA in 20 mM NaCl and 1 mM $Na(CH_2)_2AsO_3 \cdot 3H_2O$ (pH 6.8)).

CD titrations with **$[Pd_2L^{NH\text{-}OMe}{}_4][(BF_4)_4]$** were also performed, however it was known that the complex degrades or forms different supramolecular structures in the presence of DMSO (as seen by ^{1}H NMR experiments). Since a small percentage of DMSO is used to solubilise the complexes, the fact that a different structure might be interacting with the DNA needs to be considered. Nevertheless, once the complex (or mixture) was in a DMSO/water solution, it seemed to be stable as observed via UV-vis scans during the CD experiment. The CD spectra presented an ICD signal around 376 nm that increases in magnitude with increasing concentrations of complex, indicating binding of the complex to the DNA (Figure 3.4). This complex is yellow in colour, consequently this band is shifted to the visible. The overall B-conformation of DNA is retained upon cylinder

binding, with small changes in the 200-300 nm region due to the ligands electronic transitions.

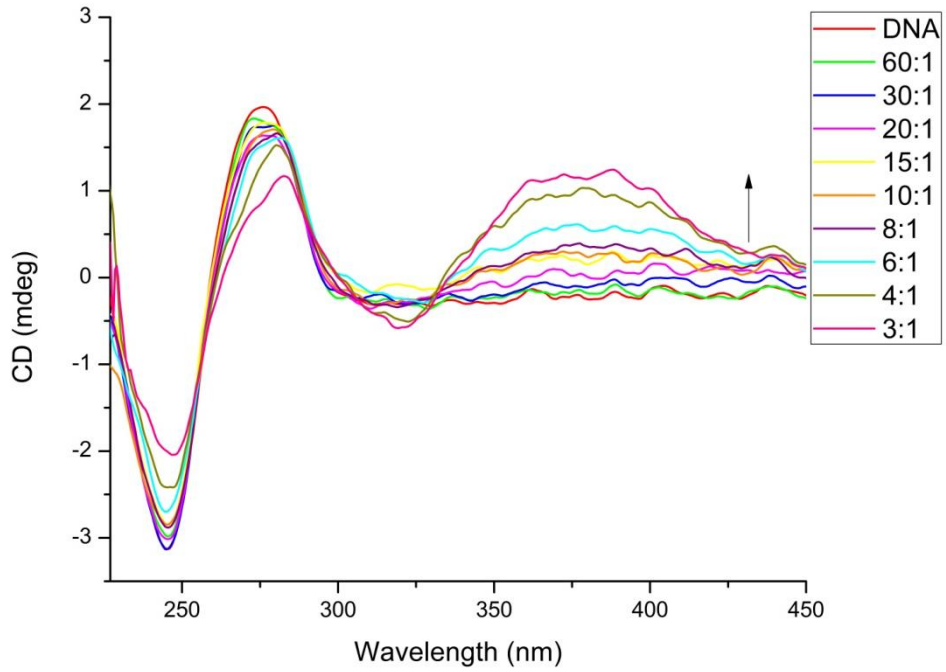

Figure 3.4: CD spectra of ct-DNA with increasing concentrations of **$[Pd_2L^{NH\text{-}OMe}{}_4][(BF_4)_4]$** complex. Legend shows ct-DNA base:complex ratios. 0.3% max. DMSO. (30 μM ct-DNA in 20 mM NaCl and 1 mM $Na(CH_2)_2AsO_3 \cdot 3H_2O$ (pH 6.8)).

An induced CD signal around 344 nm is observed for the titration of **$[Pd_2L^{S\text{-}OMe}{}_4][(BF_4)_4]$** into ct-DNA. Since the complex on its own did not have a CD signal, this ICD signal is due to the interaction of the palladium(II) complex with DNA (Figure 3.5).

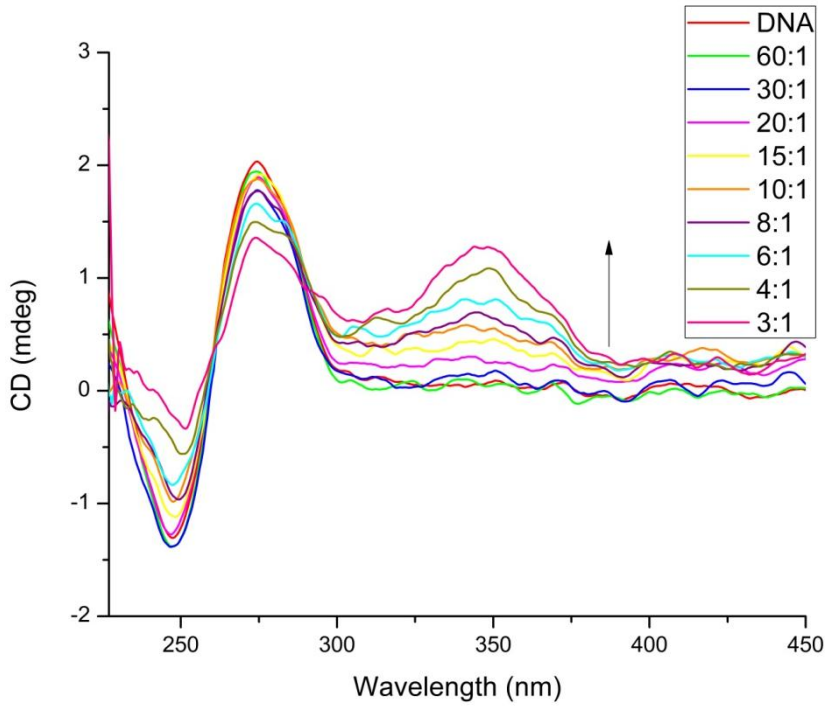

Figure 3.5: CD spectra of ct-DNA with increasing concentrations of **$[Pd_2L^{S\text{-}OMe}{}_4][(BF_4)_4]$** complex. Legend shows ct-DNA base:complex ratios. 0.6% max. DMSO. (30 μM ct-DNA in 20 mM NaCl and 1 mM $Na(CH_2)_2AsO_3 \cdot 3H_2O$ (pH 6.8)).

The parent palladium(II) complex **$[Pd_2L_4][(BF_4)_4]$** was also synthesised[‡] in order to determine its DNA binding ability, as this was not previously studied. A higher dimethyl sulfoxide percentage was required to solubilise this complex (3%), since this parent complex presents a much poorer solubility compared to the newly synthesised palladium(II) complexes. Circular dichroism titrations were performed using the same conditions applied to all palladium(II) cylinders. An ICD signal cannot be observed, suggesting a lack of interaction between the complex and DNA (Figure 3.6).

[‡] Ligand **L** was synthesised according to the Suzuki coupling protocol used for the rest of the ligands. **$[Pd_2L_4][(BF_4)_4]$** complex was synthesised by mixing ligand and $[Pd(CH_3CN)_4][(BF_4)_2]$ at high temperature, instead of at room temperature as previously reported. Characterization and full experimental procedures can be found in Chapter 5.

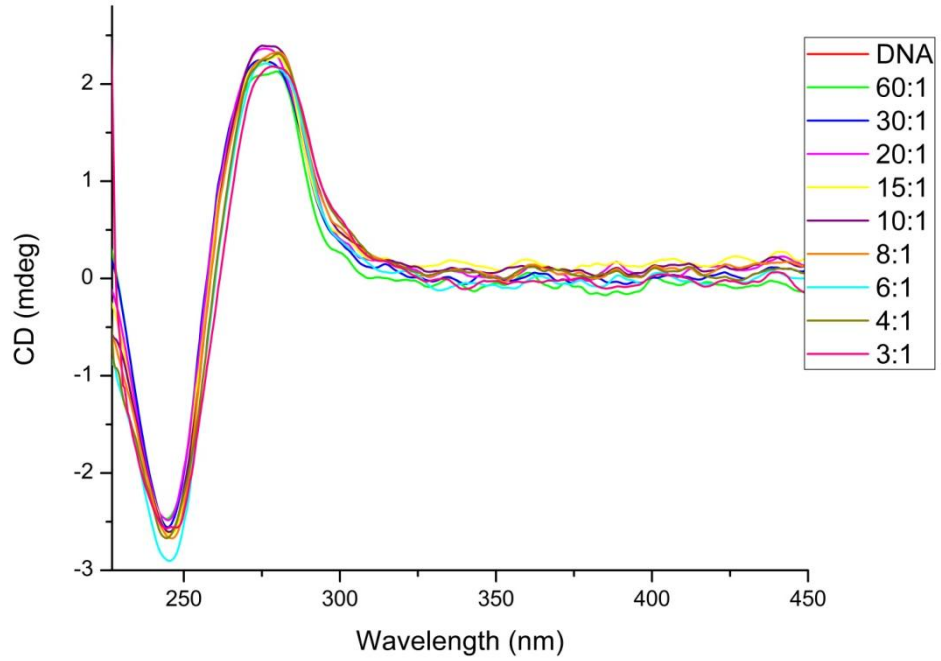

Figure 3.6: CD spectra of ct-DNA with increasing concentrations of **$[Pd_2L_4][(BF_4)_4]$** parent complex. Legend shows ct-DNA base:complex ratios. 0.3% max. DMSO. (30 μM ct-DNA in 20 mM NaCl and 1 mM $Na(CH_2)_2AsO_3 \cdot 3H_2O$ (pH 6.8)).

CD titrations of complex **$[Pd_2L^{OH}{}_4][(BF_4)_4]$** into a 30 μM solution of ct-DNA also produced no changes in the CD spectra (*see Appendix*). No ICD signal is observed in the spectroscopic region of the complex, which indicates no interaction between the cylinder and DNA.

DNA binding of complex **$[Pd_2L^{O\text{-}OH}{}_4][(BF_4)_4]$** was not investigated as it proved very difficult to solubilise as mentioned in Chapter 2.

The last complex to be studied via CD was the **$[Pd_2L^{O\text{-}Glycol}{}_4][(BF_4)_4]$** complex.

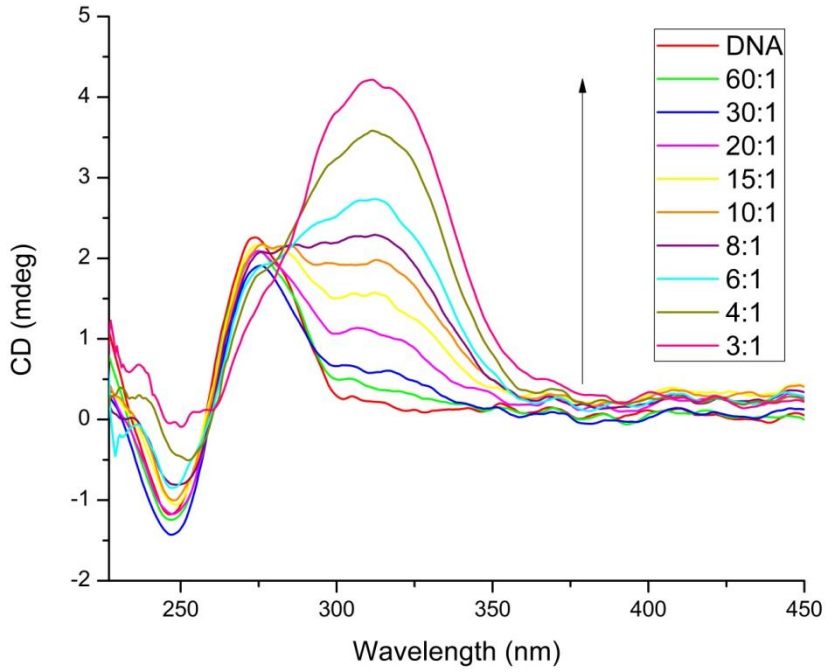

Figure 3.7: CD spectra of ct-DNA with increasing concentrations of **$[Pd_2L^{O\text{-}Glycol}{}_4][(BF_4)_4]$** complex. Legend shows ct-DNA base:complex ratios. 0.3% max. DMSO. (30 μM ct-DNA in 20 mM NaCl and 1 mM $Na(CH_2)_2AsO_3{\cdot}3H_2O$ (pH 6.8)).

Titrations were initially performed in 1.5% DMSO as for the previous complexes, in order to directly compare all of them (Figure 3.7). A very intense ICD signal around 312 nm is observed which indicates a strong interaction between the complex and DNA. As for the **$[Pd_2L^{O\text{-}OMe}{}_4][(BF_4)_4]$** complex the DNA signature between 200 and 300 nm is lost at 4:1 and 3:1 DNA base:complex concentrations, most probably due to ligand transitions in this region.

Since **$[Pd_2L^{O\text{-}Glycol}{}_4][(BF_4)_4]$** is methanol soluble, CD titrations of this complex in a 1.5% methanol solution were also performed (Figure 3.8).

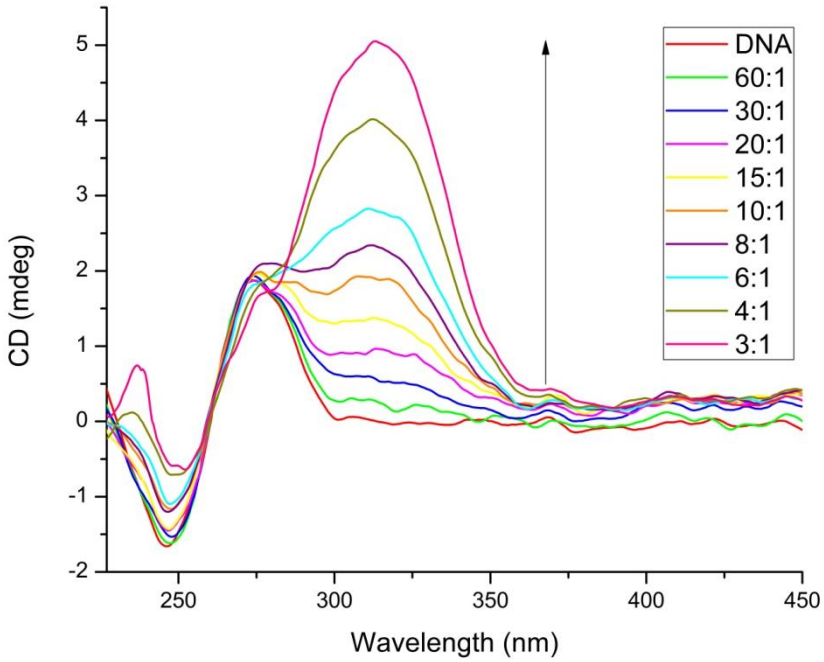

Figure 3.8: CD spectra of ct-DNA with increasing concentrations of **$[Pd_2L^{O\text{-}Glycol}{}_4][(BF_4)_4]$** complex. Legend shows ct-DNA base:complex ratios. 0.3% max. MeOH. (30 μM ct-DNA in 20 mM NaCl and 1 mM $Na(CH_2)_2AsO_3 \cdot 3H_2O$ (pH 6.8)).

The ICD signal that arises from the binding event is even greater than that observed for the 1.5% DMSO titration. Controls of the effect of methanol on DNA were also performed and no effect was observed as the CD spectra remained the same.

Comparison of the magnitude of the ICD signals produced by the DNA binding of each complex is presented in Figure 3.9.

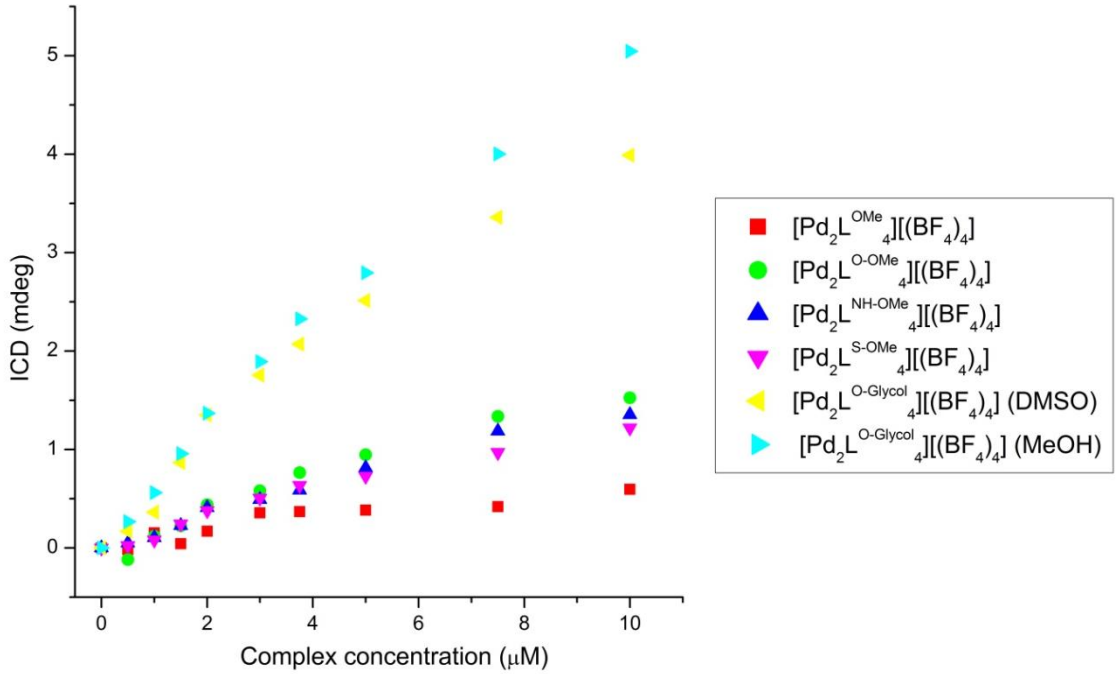

Figure 3.9: Normalized ICD signal vs complex concentration for all palladium(II) cylinder studied.

The much greater magnitude of the ICD signal with the **$[Pd_2L^{O\text{-}Glycol}{}_4][(BF_4)_4]$** cylinder is striking and it is also considerably larger if compared to previously reported iron(II), ruthenium(II) and rhodium(III) cylinders. Given that the cylinder electronic transitions should be similar between the glycol complex and the methoxy analogues, it would be tempting to ascribe this effect to a higher binding affinity. However, the CD experiment cannot be used to confirm this, and indeed a subsequent displacement assay (see section 3.4.) does not support this as a conclusion.

3.3. Linear dichroism studies

Linear dichroism (LD) is another spectroscopic technique that can be used to study DNA conformation and the effect that DNA binding drugs have on the DNA orientation upon binding. Linear dichroism is defined as the difference in absorption of light polarized parallel ($A_{||}$) and perpendicular ($A_{\perp}$) to an orientation axis (eq. 2).[169]

$$LD\ (\lambda) = A_{||}\ (\lambda) - A_{\perp}\ (\lambda) \qquad \text{(eq. 2)}$$

In flow oriented linear dichroism, shear forces can align polymeric DNA of at least 200 base pairs in length. The apparatus that generates these shear forces is a rotating cuvette cell, also called a Couette cell. The light path through the Couette cell is made of quartz (uv transparent) and can either have a rotating inner and a fixed outer cylinder or a rotating outer and a fixed inner cylinder.[173]

The LD spectrum of DNA presents a negative signal at 260 nm (Figure 3.10). This signal arises from the absorption of linearly polarized light by the DNA bases. These are situated perpendicular to the DNA axis, which is also the orientation axis in the LD experiment, hence the negative LD signal. If the Couette cell does not rotate, the LD spectrum will be zero.[174]

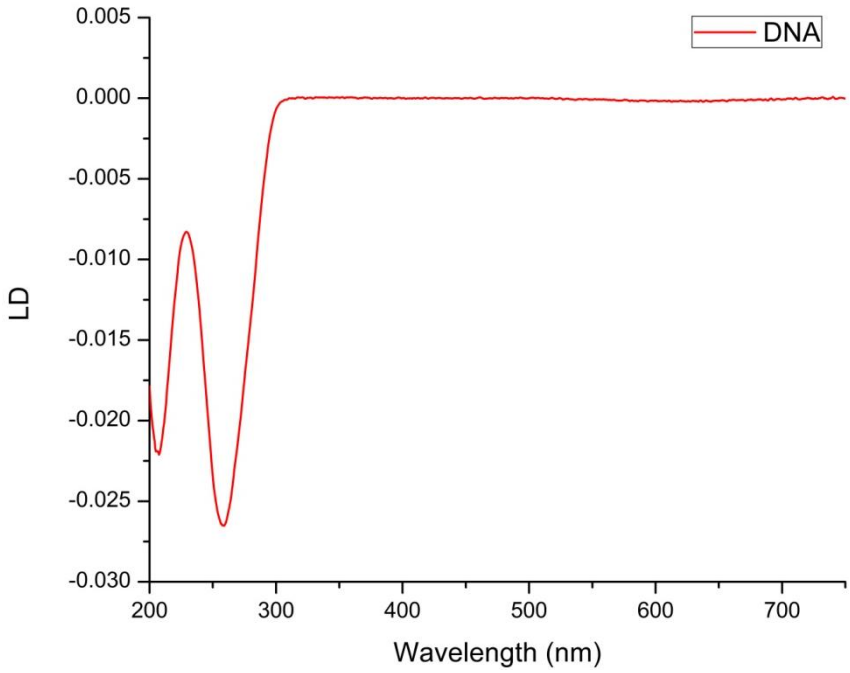

Figure 3.10: LD spectrum of B-form of DNA.
(300 μM ct-DNA in 20 mM NaCl and 1 mM $Na(CH_2)_2AsO_3 \cdot 3H_2O$ (pH 6.8)).

Since most of the DNA binding drugs are too small to be oriented themselves via viscous drag, they are unaligned and therefore do not have their own LD spectrum. However, they become oriented if bound to DNA, which gives rise to an induced LD (ILD) signal. As intercalators sandwich between DNA bases, their absorbance dipoles are also oriented perpendicularly to the DNA axis. This results in a negative ILD signal. In contrast, groove binders can present positive ILD signals, since the chromophores of the groove binder can be aligned parallel to the helical axis. Therefore, linear dichroism can give information about the DNA binding modes of drug molecules.[172]

In the work presented in this thesis, the effect on aqueous buffered ct-DNA conformation when titrating aliquots of the newly synthesised palladium(II)

cylinders is investigated. The DNA concentration is kept constant throughout the experiment and an LD spectrum is recorded after each titration. The overlay of the LD spectrum of each titration can be used to assess the interactions between complex and DNA.

Circular dichroism titrations informed on the DNA and complex concentrations that are necessary to not precipitate the DNA. This information is important as precipitation of DNA cannot readily be detected in the Couette cell but will provide inaccurate data. Therefore, titrations of a 50 μM stock solution of **$[Pd_2L^{OMe}_4][(BF_4)_4]$** complex over a 30 μM ct-DNA solution were performed. As for the CD experiments, the 50 μM stock solution of complex **$[Pd_2L^{OMe}_4][(BF_4)_4]$** was prepared by dissolving it in DMSO and diluting with water to obtain a 1.5% DMSO solution. At the end of the titration, the DMSO percentage in the Couette will be 0.3%. Control experiments to evaluate the effect of DMSO on the LD spectra of ct-DNA were carried out and no changes were observed.

As the concentration of the **$[Pd_2L^{OMe}_4][(BF_4)_4]$** complex increases, the characteristic DNA LD signal at 260 nm decreases in magnitude. This indicates that the DNA is being coiled or bent upon binding. This coiling or bending effect is observed upon addition of very small complex concentrations, indicating an immediate effect of the cylinder on the DNA. No ILD signal is apparent in this titration, which suggests either that the binding of the **$[Pd_2L^{OMe}_4][(BF_4)_4]$** complex is not oriented or that the angle of orientation is such that it is not detected (Figure 3.11).

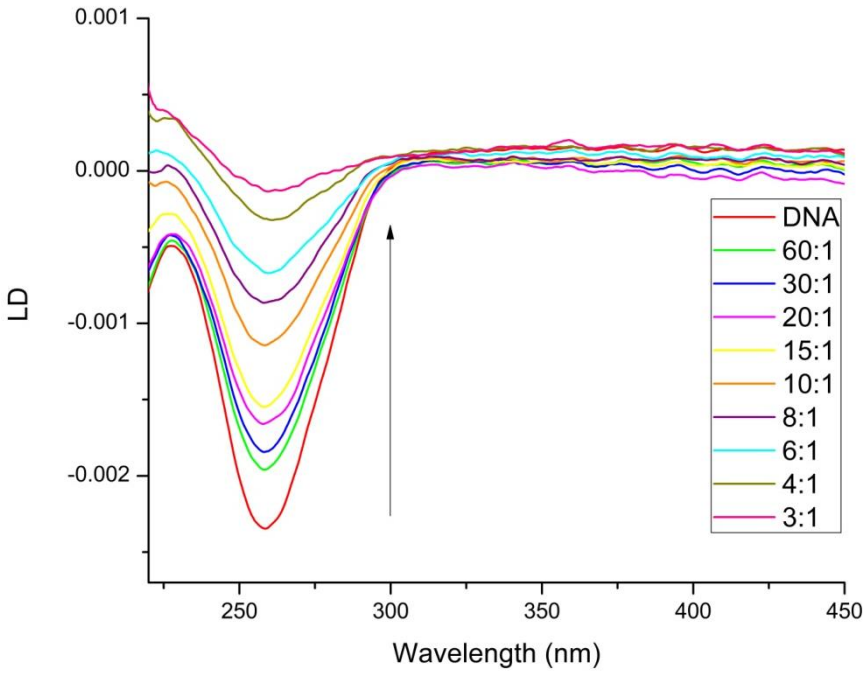

Figure 3.11: LD spectra of ct-DNA with increasing concentrations of **[$Pd_2L^{OMe}_4$][$(BF_4)_4$]** complex. Legend shows ct-DNA base:complex ratios. 0.3% max. DMSO. (30 μM ct-DNA in 20 mM NaCl and 1 mM $Na(CH_2)_2AsO_3 \cdot 3H_2O$ (pH 6.8)).

LD titrations of **[$Pd_2L^{O\text{-}OMe}_4$][$(BF_4)_4$]**, **[$Pd_2L^{NH\text{-}OMe}_4$][$(BF_4)_4$]** and **[$Pd_2L^{O\text{-}Glycol}_4$][$(BF_4)_4$]** complexes produced similar outcomes, with the **[$Pd_2L^{O\text{-}OMe}_4$][$(BF_4)_4$]** complex producing the largest amount of coiling of the DNA. The negative LD signals at 260 nm for these complexes decrease in magnitude with increasing concentrations of the complexes, indicating coiling or bending of the DNA and therefore DNA binding (*see Appendix*).

The full LD titration of **[$Pd_2L^{S\text{-}OMe}_4$][$(BF_4)_4$]** could not be recorded as precipitation of the DNA occurred from a 30:1 DNA base:complex ratio (*see Appendix*).

The LD spectra of **$[Pd_2L_4][(BF_4)_4]$** showed a smaller coiling or bending effect compared to the other studied complexes. This is observed by a smaller decrease in the magnitude of the LD signal at 260 nm (Figure 3.12).

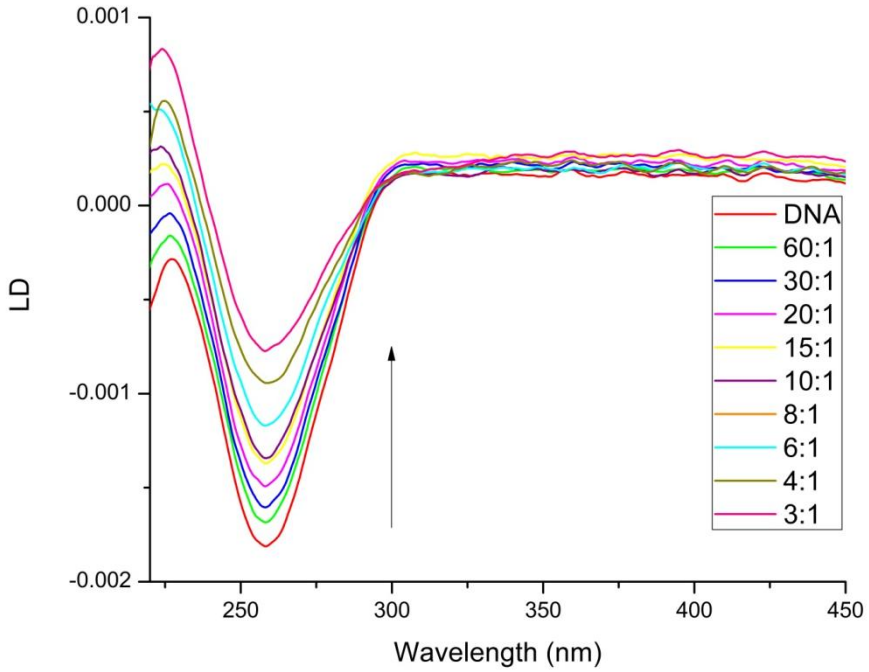

Figure 3.12: LD spectra of ct-DNA with increasing concentrations of **$[Pd_2L_4][(BF_4)_4]$** parent complex. Legend shows ct-DNA base:complex ratios. 0.3% max. DMSO. (30 μM ct-DNA in 20 mM NaCl and 1 mM $Na(CH_2)_2AsO_3 \cdot 3H_2O$ (pH 6.8)).

This is not surprising since this complex did not show a remarkable DNA interaction in the circular dichroism studies. However, the small decrease of the DNA band indicates coiling or bending, suggesting some sort of weak interaction between the complex and the DNA. Similar results were found for the **$[Pd_2L^{OH}{}_4][(BF_4)_4]$** complex (*see Appendix*).

The coiling or bending effect of all palladium(II) cylinders studied can be compared by plotting the magnitude of the LD signal at 260 nm versus the complex concentration (Figure 3.13).

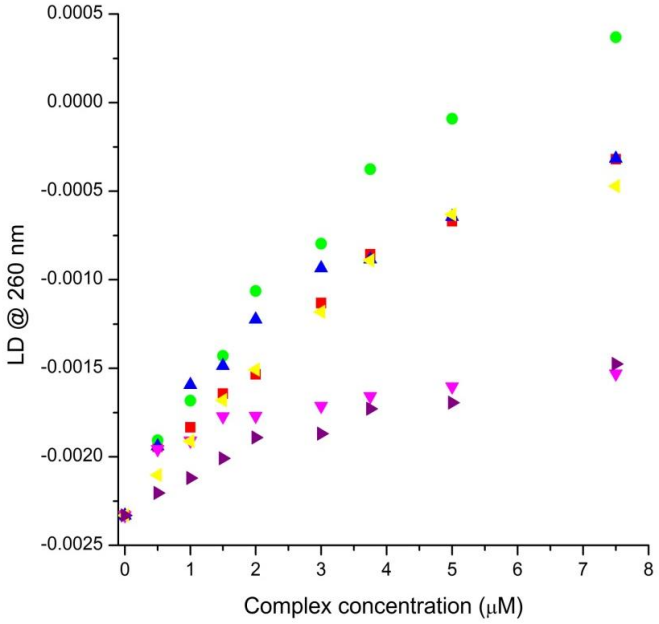

% LD loss	0.5 μM	5 μM
■ $[Pd_2L^{OMe}{}_4][(BF_4)_4]$	17%	71%
● $[Pd_2L^{O\text{-}OMe}{}_4][(BF_4)_4]$	18%	96%
▲ $[Pd_2L^{NH\text{-}OMe}{}_4][(BF_4)_4]$	17%	67%
▼ $[Pd_2L^{OH}{}_4][(BF_4)_4]$	16%	31%
◀ $[Pd_2L^{O\text{-}Glycol}{}_4][(BF_4)_4]$	10%	73%
▶ $[Pd_2L_4][(BF_4)_4]$	5%	27%

Figure 3.13: Normalized LD signal at 260 nm vs complex concentration for all palladium(II) cylinders studied (left) and percentage loss of LD signal at 260 nm for 0.5 μM (60:1 DNA base:complex) and 5 μM (6:1 DNA base: complex) concentrations.

Complexes **$[Pd_2L^{OH}{}_4][(BF_4)_4]$** and **$[Pd_2L_4][(BF_4)_4]$** produce smaller coiling effects on the DNA. The other complexes present similar orientation effects, except for that of **$[Pd_2L^{O\text{-}OMe}{}_4][(BF_4)_4]$** where the coiling effect is considerably higher from an 8:1 DNA base:complex ratio. The percentage loss of the LD signal of DNA at 260 nm gives a quantitative value of the coiling effect of all of the palladium(II) cylinders studied. At the smallest concentration of cylinder (0.5 μM or 60:1 DNA base:complex), little difference is observed between the different complexes. However, when the concentration of complex is increased by one order of magnitude (5 μM or 6:1 DNA base:complex), the coiling effect produced

by **$[Pd_2L^{O\text{-}OMe}{}_4][(BF_4)_4]$** is 96%, while the other complexes produce a 27-73% loss of the negative LD signal.

3.4. Ethidium bromide displacement experiments

Ethidium bromide is a well known fluorescent intercalating drug (*see section 1.2.3.*). However, its fluorescence can be greatly enhanced when bound to DNA, giving rise to a band at around 600 nm (Figure 3.14).

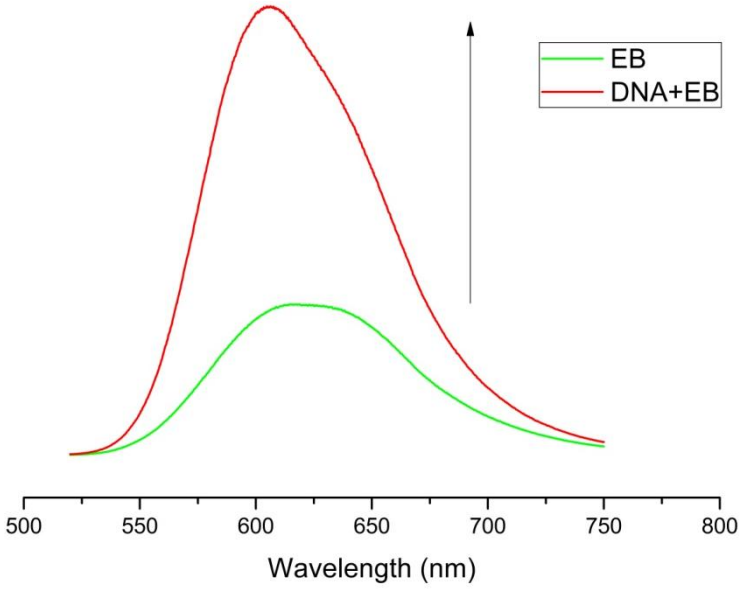

Figure 3.14: Emission spectra of ethidium bromide and its complex with DNA.

Ethidium bromide displacement is a competition binding assay where the binding affinity of ethidium bromide and another molecule is assessed. The competition will be greater if the two binders are competing for the same position,

that is if the molecule being studied is an intercalator. However, simple electrostatic interaction will ensure a DNA binding competition.[175]

In the work reported in this thesis, an ethidium bromide displacement assay is performed to evaluate the interaction between DNA and the newly synthesised palladium(II) complexes. A solution of aqueous buffered ct-DNA fully loaded with ethidium bromide molecules is excited at 500 nm and the emission spectrum produced is recorded. Aliquots of palladium(II) complexes are then titrated into this solution and the emission spectra measured. If the emission is quenched as a result of the titration, this is evidence of ethidium bromide being displaced from the DNA by the palladium(II) cylinder. However, interactions between the palladium(II) complexes and free or bound ethidium bromide can also be present and these may also decrease the emission intensity.[176]

Aliquots of a 100 μM stock solution of **$[Pd_2L^{OMe}_4][(BF_4)_4]$** complex were progressively added over a solution of 30 μM ct-DNA and 10 μM ethidium bromide. The 100 μM stock solution of the **$[Pd_2L^{OMe}_4][(BF_4)_4]$** complex was prepared by dissolving it in DMSO and diluting with water to obtain a 1.5% DMSO solution. At the end of the titration, the DMSO percentage in the cuvette will be 0.15%. The concentrations of DNA and ethidium bromide were kept constant during the experiment. The emission spectra of the titrations performed for the **$[Pd_2L^{OMe}_4][(BF_4)_4]$** complex are shown in Figure 3.15.

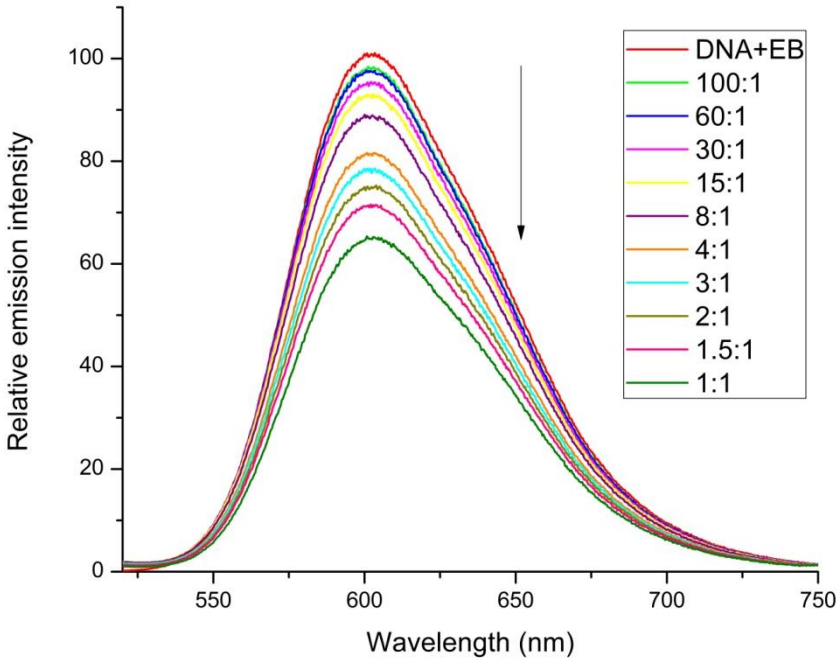

Figure 3.15: Emission spectra of displacement of ethidium bromide (10 μM) from ct-DNA with increasing concentrations of **$[Pd_2L^{OMe}{}_4][(BF_4)_4]$** complex ($\lambda_{exc}$=500 nm). Legend shows ct-DNA base:complex ratios. 0.15% max. DMSO. (30 μM ct-DNA in 50 mM NaCl and 1 mM $Na(CH_2)_2AsO_3 \cdot 3H_2O$ (pH 6.8)).

The emission of the complex formed by ethidium bromide and DNA is quenched upon addition of increasing concentrations of the complex, indicating displacement of ethidium bromide by the cylinder. All the palladium(II) complexes studied are able to displace ethidium bromide, suggesting higher binding constants for these than that of ethidium bromide. Quenching of the luminescence was not detected in free ethidium bromide solutions upon titration of complex solutions. Therefore, the decrease in luminescence of the ethidium bromide-DNA solution must be due to the interaction between the complex and DNA, and therefore displacement of the bound ethidium bromide. A comparison of all the complexes where the relative emission intensity at the emission maximum (606 nm) is plotted against complex concentration is shown in Figure 3.16.

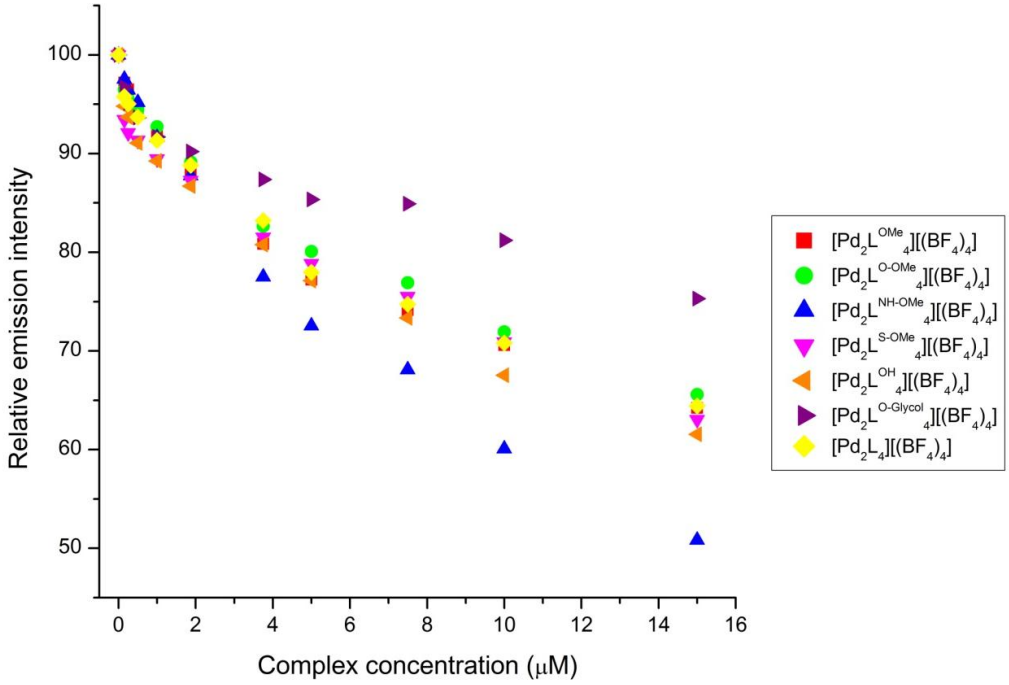

Figure 3.16: Relative emission intensity at 606 nm maximum vs complex concentration for all palladium(II) cylinder studied using an ethidium bromide displacement experiment.

Most of the complexes appear to have similar binding constants as they quench the emission of the complex between DNA and ethidium bromide by similar magnitudes. The **$[Pd_2L^{NH\text{-}OMe}{}_4][(BF_4)_4]$** complex can displace ethidium bromide from ct-DNA more efficiently than the other complexes, suggesting a higher binding constant. However, this can be due to the formation of other structures or decomposition of the complex in DMSO solutions, as seen by ^{1}H NMR. The **$[Pd_2L^{O\text{-}Glycol}{}_4][(BF_4)_4]$** complex is less efficient at displacing ethidium bromide compared with its analogues. This can be due to its bigger size and the long chains at either side of the complex, which might require a larger binding site.

3.5. Agarose gel electrophoresis unwinding experiments

Gel electrophoresis is one of the most widely used techniques by biochemists and molecular biologists. By employing this technique, macromolecules that differ in size, charge or conformation can be separated. DNA is such a molecule and will migrate to the positive pole when placed in an electric field, as the DNA phosphate backbone is negatively charged. Interactions between ligands and DNA can also be assessed by gel electrophoresis.[177]

In the work presented herein, interactions between the newly synthesised palladium(II) complexes and plasmid DNA are investigated. Plasmid DNA is a double-stranded circle that can exist in two topologically different conformations: supercoiled and open circular (Figure 3.17).

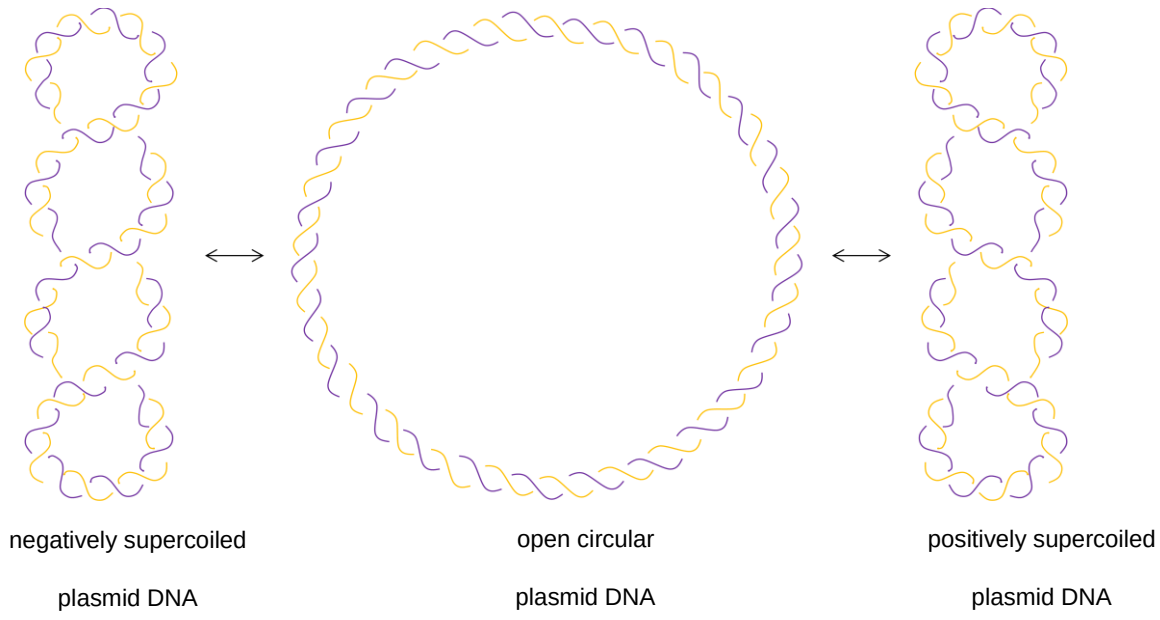

Figure 3.17: Plasmid DNA forms: negatively supercoiled (left), open circular (centre) and positively supercoiled (right).

The open circular form is relaxed duplex DNA, while the supercoiled form occurs when the duplex twists around itself. The latter is extensively found in nature in replication and transcription processes, where opening of the double helix is required. Depending on the direction of the twisting, it can be negatively supercoiled (right handed) or positively supercoiled (left handed). It is the negatively supercoiled form which causes torsional stress to the DNA favouring unwinding of the duplex, while the positively supercoiled form favours winding up of the double helicate. Conformational changes of the duplex can result from interactions with bound molecules.[178,179]

In this work, gel electrophoresis is used to study the effect caused by different concentrations of palladium(II) complexes and pBR322 plasmid DNA, which is negatively supercoiled DNA consisting of 4 361 base pairs. This form of plasmid DNA will travel faster through the gel pores, as it is smaller than the open circular DNA. 1% agarose gels were used and immersed in Tris-Acetate-EDTA (TAE) buffer, which provides ions to carry the applied current and maintains the pH at a constant value.[180] If the complexes bind to supercoiled DNA, it will unwind and therefore its size and volume will increase, resulting in a slower migration of the supercoiled bands, suggesting that the complex is binding to the DNA.[181] Once the two plasmidic forms have been separated the gel can be stained with ethidium bromide, which intercalates between the DNA base pairs and is then visible under UV light. When the supercoiled and open circular forms of the plasmid DNA co-migrate, the unwinding angle of the supercoiled form can be calculated (eq. 3).

$$\Phi = \frac{-18\sigma}{r(c)} \qquad \text{(eq. 3)}$$

The unwinding angle (Φ) is defined as the number of degrees by which the DNA is unwound about its helical axis per molecule bound. The superhelicity constant (σ) of the plasmid DNA has been determined to be -0.059 using cisplatin, since the unwinding angle of cisplatin is known (13º).[182] *r(c)* is the number of molecules bound per plasmid and is taken to be equal to the mixing ratios, as it is assumed that all the binders present in the sample are bound to the plasmidic DNA.

The unwinding experiment was performed for all synthesised palladium(II) complexes in 1% agarose gels. Sample solutions of DNA and complex at different ratios were incubated for two hours at 37 ºC. These solutions contained a 1% DMSO, required to solubilise the complexes. Controls with and without DMSO were performed to ensure that the DMSO had no effect on the DNA. Table 3.1 indicates the DNA base pairs:complex ratios used on every gel run.

Table 3.1: Relation between DNA base pairs:complex ratios and lanes in agarose gels.

Lanes	**1**	**2**	**3**	**4**	**5**	**6**	**7**	**8**	**9**	**10**	**11**
Base pairs: complex	Control (1% DMSO)	20:1	15:1	10:1	8:1	6:1	5:1	4:1	3:1	2:1	Control

The agarose gel for the **$[Pd_2L^{OMe}_4][(BF_4)_4]$** complex is shown in Figure 3.18. The band corresponding to the supercoiled DNA starts to migrate more slowly with

increasing concentrations of complex, indicating unwinding of the negatively supercoiled DNA and therefore binding to the DNA. This binding lengthens and/or stiffens the DNA structure.

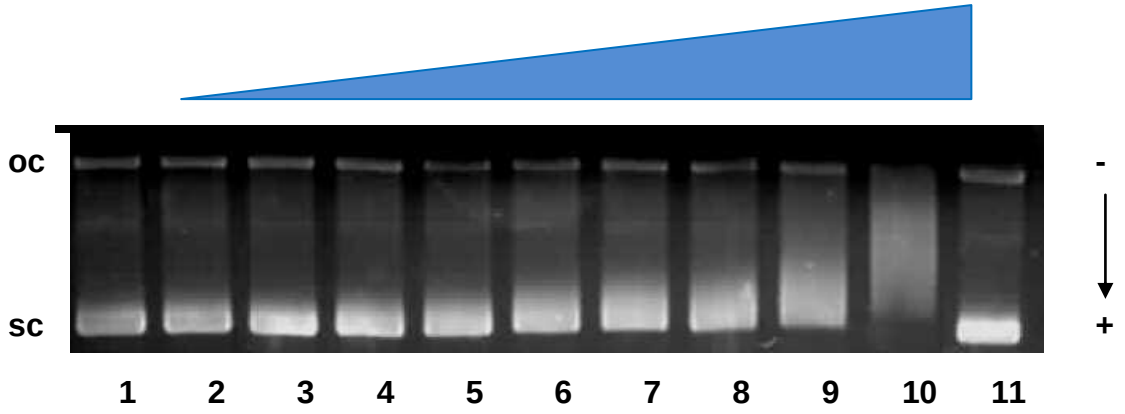

Figure 3.18: 1% Agarose gel showing changes in the electrophoretic mobility of open circular (oc) and supercoiled (sc) plasmid DNA for **$[Pd_2L^{OMe}{}_4][(BF_4)_4]$** complex.

The rest of the palladium(II) complexes studied behave in a similar manner, except for **$[Pd_2L^{NH\text{-}OMe}{}_4][(BF_4)_4]$** which does not seem to have any effect on plasmidic DNA, as the open circular (oc) and supercoiled (sc) forms of plasmid DNA migrate at the same speed at any given concentration of this complex (Figure 3.19). This can be due to the formation of other structures or decomposition of this palladium(II) cylinder in DMSO solutions, as seen by ^{1}H NMR.

Unwinding angles can only be calculated when the supercoiled and open circular forms co-migrate across the gel. For all the gels performed in this study, either both bands co-migrate at a 2:1 DNA base pairs:complex ratio or they do not co-migrate at any point, even if the complexes interact with the supercoiled form. Therefore the unwinding angle is assumed to be smaller or equal to 4º.

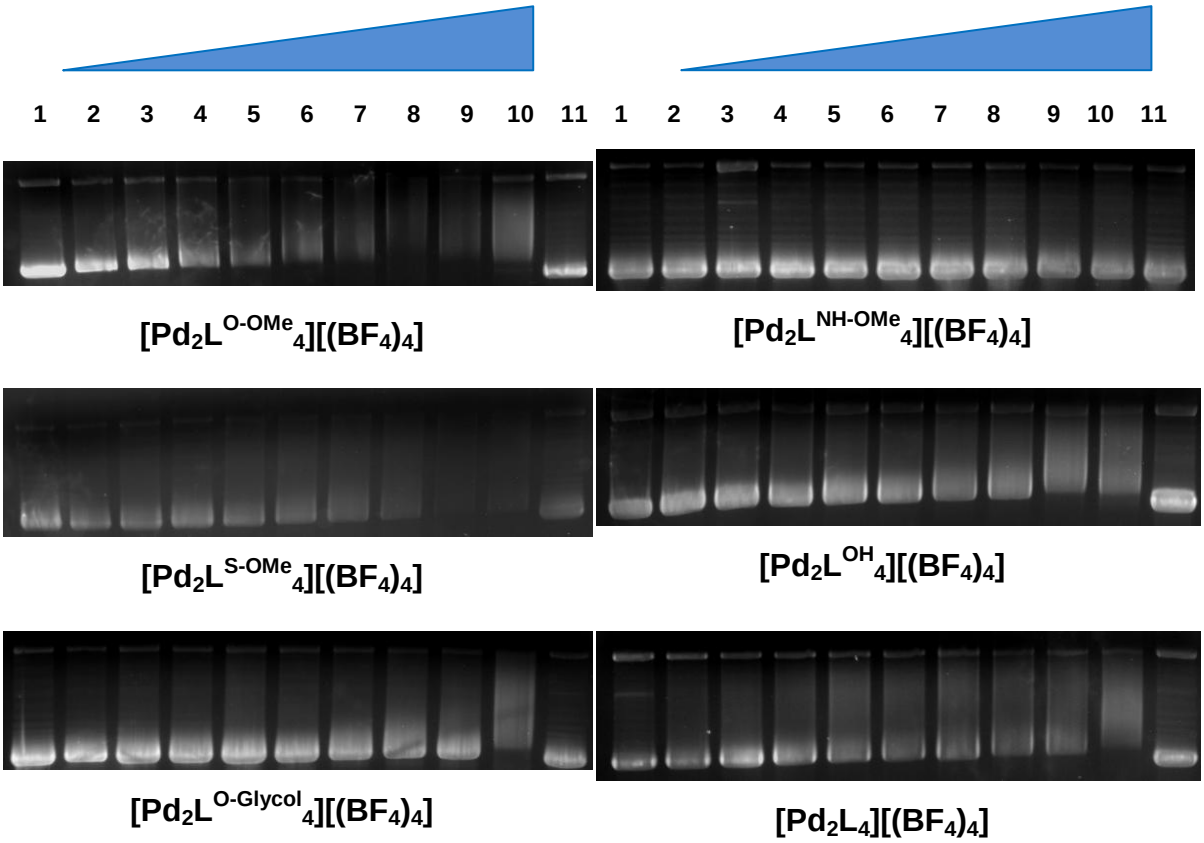

Figure 3.19: 1% Agarose gels showing changes in the electrophoretic mobility of open circular (oc) and supercoiled (sc) plasmid DNA for **$[Pd_2L^{O\text{-}OMe}{}_4][(BF_4)_4]$**, **$[Pd_2L^{NH\text{-}OMe}{}_4][(BF_4)_4]$**, **$[Pd_2L^{S\text{-}OMe}{}_4][(BF_4)_4]$**, **$[Pd_2L^{OH}{}_4][(BF_4)_4]$**, **$[Pd_2L^{O\text{-}Glycol}{}_4][(BF_4)_4]$** and **$[Pd_2L_4][(BF_4)_4]$** complexes (from left to right and top to bottom).

3.6. Polyacrylamide gel electrophoresis: DNA junction recognition experiments

Polyacrylamide is another polymer that can be used to perform gel electrophoresis experiments. Polyacrylamide gel electrophoresis (PAGE) is normally used to separate smaller DNA fragments that cannot be separated by agarose gels, since the pore size is considerably smaller. The main advantage of PAGE is that low concentrations can be used and high resolution between bands is observed.

In this work, PAGE has been used to evaluate whether the synthesised palladium(II) cylinders are able to recognize DNA junctions, such as three-way and four-way DNA junctions. In order to do this, DNA oligonucleotide strands were designed so that a non-palindromic three-way junction and a four-way junction can be formed. One of these strands was radiolabelled at the 5' terminus end with γ-^{32}P ATP, so that the gel could be visualized and quantified. This experiment is based on that reported by Hannon and co-workers for the recognition of DNA and RNA three-way junctions by iron(II) supramolecular helicates.[81,121]

Initially, a PAGE DNA three-way junction experiment was performed. In principle, the bigger size of a tetra-stranded cylinder compared to a triple-stranded cylinder will prevent binding to a DNA three-way junction and thus the stabilization of the structure, and this was the result observed. The three DNA strands were incubated with the synthesised palladium(II) tetra-stranded complexes, and also Hannon's iron(II) triple-stranded cylinder, at room temperature for one hour (Figure 3.20). Formation of DNA three-way junction was observed for the triple-stranded cylinder as expected, however none was observed for the tetra-stranded cylinders. This result emphasises the perfect fit observed between Hannon's iron(II) triple-stranded cylinder and DNA three-way junctions and that not every metal complex can fit and bind at the central cavity of a DNA three-way junction, so that size and shape are crucial for the molecular design of DNA junction binders. It also confirms that it is not purely electrostatic stabilization of the DNA three-way junction by a tetracation.

1	S3*	**7**	S3*+S2+S1+ $[Pd_2L^{S\text{-}OMe}{}_4][(BF_4)_4]$ (3:1)
2	S3*+S2	**8**	S3*+S2+S1+ $[Pd_2L^{OH}{}_4][(BF_4)_4]$ (3:1)
3	S3*+S2+S1	**9**	S3*+S2+S1+ $[Pd_2L^{O\text{-}Glycol}{}_4][(BF_4)_4]$ (3:1)
4	S3*+S2+S1+ $[Pd_2L^{OMe}{}_4][(BF_4)_4]$ (3:1)	**10**	S3*+S2+S1+ $[Pd_2L_4][(BF_4)_4]$ (3:1)
5	S3*+S2+S1+ $[Pd_2L^{O\text{-}OMe}{}_4][(BF_4)_4]$ (3:1)	**11**	S3*+S2+S1+ $[Pd_2L^{OMe}{}_4][(BF_4)_4]$ (3:1)
6	S3*+S2+S1+ $[Pd_2L^{NH\text{-}OMe}{}_4][(BF_4)_4]$ (3:1)	**12**	S3*+S2+S1+ $[Fe_2L^{im}{}_3][Cl_4]$ (3:1)

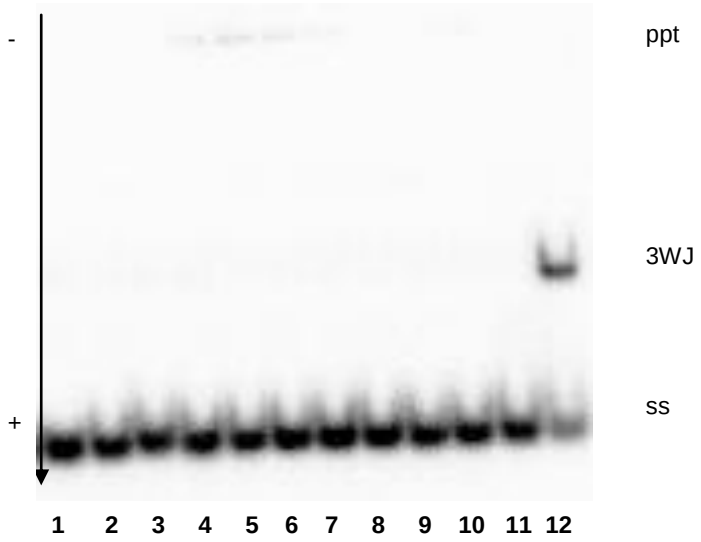

Figure 3.20: Autoradiogram of 15% polyacrylamide gel run at 25 ºC, 120 V, 4 h. S3* ^{32}P radiolabelled, incubation of samples at room temperature for 1 h. Lanes as indicated in table.

As previously mentioned, the design of DNA four-way junction binders is not as straightforward, as DNA four-way junctions can exist in two conformations.(87) DNA four-way junctions are normally the target of proteins that are involved in the homologous recombination process and little work has been focused on the binding of synthetic molecules. Initial efforts in targeting DNA four-way junctions were performed by Kallenbach and co-workers. In 1989 they reported the cleavage of a DNA four-way junction near the branch point by intercalation of methidiumpropyl-EDTA-Fe^{II} or MPE-Fe^{II} (Figure 3.21), as seen by ^{32}P radiolabelled PAGE.(183)

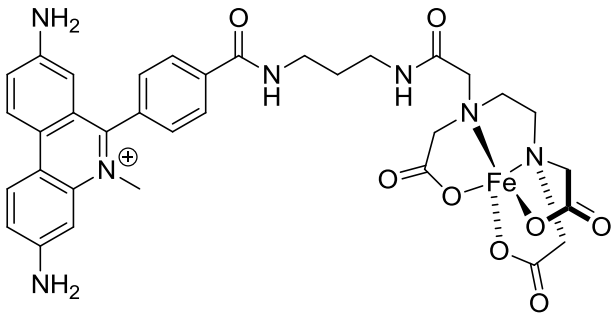

Figure 3.21: Structure of MPE-Fe^{II} four-way junction binder.

Segall *et al*. have reported a hexapeptide, WRWYCR, that is able to inhibit DNA repair intermediates by selectively interacting with the DNA four-way junction, as seen by radiolabelled gel mobility shift assays.[184] Peptide WRWYCR and its D stereoisomer, wrwycr, act as dimers via a disulfide bond and are able to inhibit bacterial cell growth, as seen by MIC assays.[185] The McAlpine group continued with this strategy and designed more rigid cyclic peptides with *C-2* symmetry that mimic the symmetry of the DNA four-way junction binding site (Figure 3.22). Hydrophobic residues are thought to stack with the nucleotides at the centre of the junction, while hydrophilic residues might form hydrogen bonds with either bound proteins or the DNA junction itself.[186]

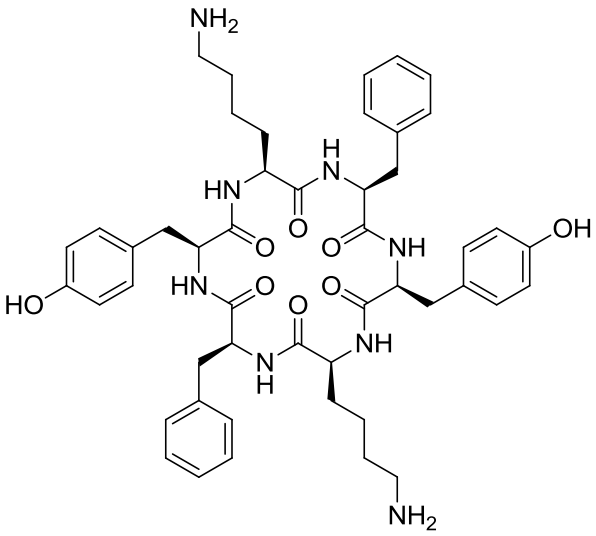

Figure 3.22: McAlpine cyclic hexapeptide with *C-2* symmetry.

More recently, Cardin and co-workers presented the crystal structure of a bis-acridine intercalator bound at the centre of the junction (*see section 1.2.6.4.*).[94]

The last example of a DNA four-way junction binder reported to date is the 9-propargylaminoacridine click ligand reported by Searcey's group (Figure 3.23). It was shown that this compound is able to recognize the DNA four-way junction, without evidence of binding to single stranded DNA, at a concentration of 50 μM when the DNA strands (one of them doubly labelled with two fluorophores) and the compound are annealed at 80 ºC. The same result was obtained after incubation at room temperature for four hours.[187] These results were also confirmed by fluorescence assays and circular dichroism spectroscopy.

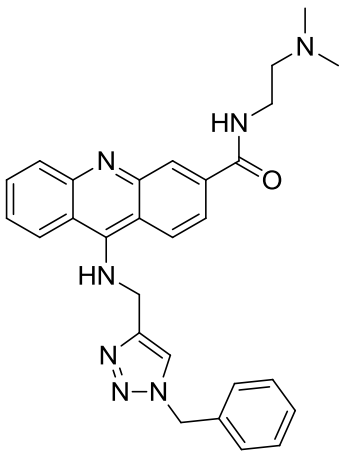

Figure 3.23: 9-propargylaminoacridine click ligand reported by Searcey's group.

In the work reported herein, radiolabelled PAGE has been performed with the synthesised palladium(II) complexes reported in Chapter 2. Initially, complexes and DNA oligonucleotides were annealed at 80 ºC for five minutes followed by slow cooling for four hours. The gel was run in the same conditions used in the Hannon group for DNA three-way junction PAGE (15% polyacrylamide gel, 120 V, 4 h). These conditions produced a gel with wide bands for the single stranded band (Figure 3.24), not seen in Searcey's gels. Formation of the four-way junction was observed with all the complexes, however it was also present in the control in the absence of magnesium cations and palladium(II) complexes (45% of Holliday junction formation in all cases). Well precipitation with the **$[Pd_2L^{OMe}{}_4][(BF_4)_4]$** complex is also observed.

1	S4*	**7**	S4*+S3+S2+S1+ 6 mM $MgCl_2$
2	S4*+S3	**8**	S4*+S3+S2+S1+ 25 μM $[Pd_2L^{OMe}{}_4][(BF_4)_4]$
3	S4*+S3+S2	**9**	S4*+S3+S2+S1+ 50 μM $[Pd_2L^{OMe}{}_4][(BF_4)_4]$
4	S4*+S3+S2+S1	**10**	S4*+S3+S2+S1+ 100 μM $[Pd_2L^{OMe}{}_4][(BF_4)_4]$
5	S4*+S3+S2+S1+ 2 mM $MgCl_2$	**11**	S4*+S3+S2+S1+ 25 μM $[Pd_2L^{O\text{-}Glycol}{}_4][(BF_4)_4]$
6	S4*+S3+S2+S1+ 4 mM $MgCl_2$	**12**	S4*+S3+S2+S1+ 50 μM $[Pd_2L^{O\text{-}Glycol}{}_4][(BF_4)_4]$

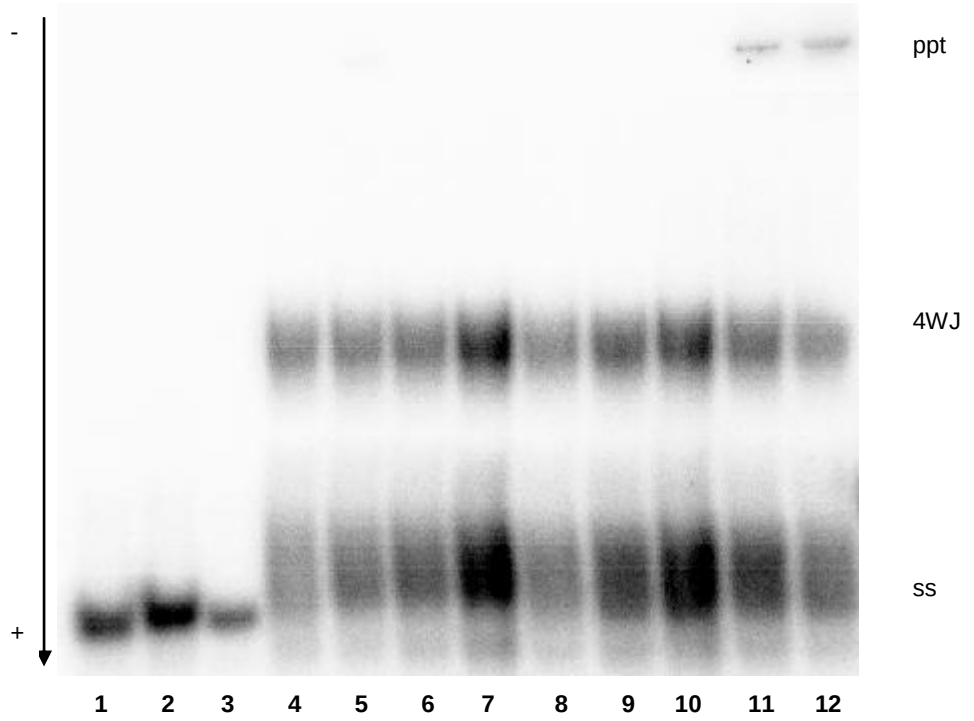

Figure 3.24: Autoradiogram of 15% polyacrylamide gel run at 25 ºC, 120 V, 4 h. S4* ^{32}P radiolabelled, incubation of samples at 80 ºC. Lanes as indicated in table.

A second gel was then performed with Searcey's conditions (12% polyacrylamide gel, 50 V, 2 h). Samples were incubated at room temperature for 24 hours. In principle, DNA four-way junction should not be formed under these conditions unless a divalent metal or a four-way junction binder is present. Searcey has reported that 60% Holliday junction is formed after 24 hours incubation of the DNA oligonucleotides in the presence of 2 mM $MgCl_2$. The gel shown in Figure 3.25 shows 80% and 78% four-way junction formation for 2 mM

and 4 mM $MgCl_2$ concentrations respectively. 74% and 72% four-way junction formation is observed for **$[Pd_2L^{OMe}{}_4][(BF_4)_4]$** and **$[Pd_2L^{O\text{-}Glycol}{}_4][(BF_4)_4]$** complexes at 25 μM concentration respectively. At higher concentrations, precipitation or condensation of the DNA is observed. This latter observation is in full agreement with the circular dichroism studies.

1	S4*	**6**	S4*+S3+S2+S1+ 50 μM $[Pd_2L^{OMe}{}_4][(BF_4)_4]$
2	S4*+S3+S2+S1+ 2 mM $MgCl_2$	**7**	S4*+S3+S2+S1+ 100 μM $[Pd_2L^{OMe}{}_4][(BF_4)_4]$
3	S4*+S3+S2+S1+ 4 mM $MgCl_2$	**8**	S4*+S3+S2+S1+ 25 μM $[Pd_2L^{O\text{-}Glycol}{}_4][(BF_4)_4]$
4	S4*+S3+S2+S1+ 6 mM $MgCl_2$	**9**	S4*+S3+S2+S1+ 50 μM $[Pd_2L^{O\text{-}Glycol}{}_4][(BF_4)_4]$
5	S4*+S3+S2+S1+ 25 μM $[Pd_2L^{OMe}{}_4][(BF_4)_4]$	**10**	S4*+S3+S2+S1+ 100 μM $[Pd_2L^{O\text{-}Glycol}{}_4][(BF_4)_4]$

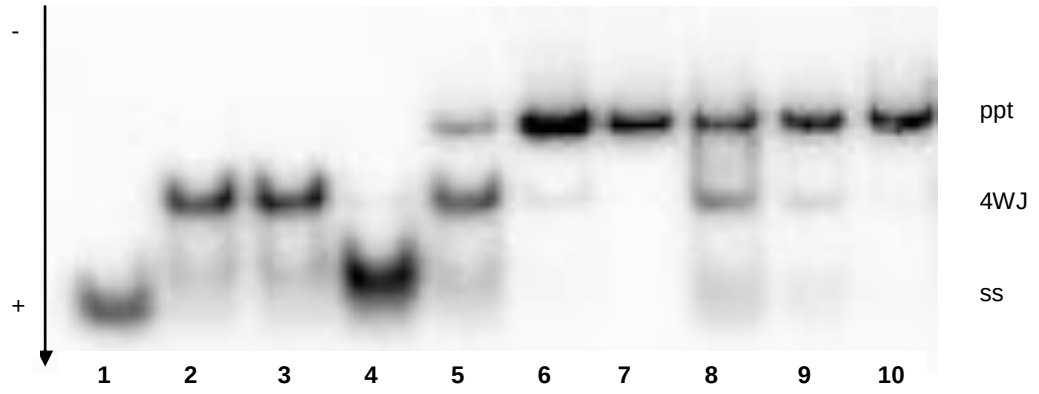

Figure 3.25: Autoradiogram of 12% polyacrylamide gel run at 25 ºC, 50 V, 2 h. S4* ^{32}P radiolabelled, incubation of samples at room temperature for 24 h. Lanes as indicated in table.

Another experiment using the same conditions was performed, however the four-way junction on its own was also loaded as a control (Figure 3.26). Lower concentrations of cylinders were also used. Four-way junction appears to be formed in the absence of any cation after incubation for 24 hours at room temperature. This result makes the detection and therefore confirmation of the formation of DNA four-way junction upon incubation of the DNA oligonucleotides with the synthesised cylinders difficult.

1 S4*
2 S4*+S3+S2+S1
3 S4*+S3+S2+S1+ 2 mM $MgCl_2$
4 S4*+S3+S2+S1+ 10 μM $[Pd_2L^{OMe}{}_4][(BF_4)_4]$
5 S4*+S3+S2+S1+ 25 μM $[Pd_2L^{OMe}{}_4][(BF_4)_4]$
6 S4*+S3+S2+S1+ 0.1 μM $[Pd_2L^{O\text{-}OMe}{}_4][(BF_4)_4]$
7 S4*+S3+S2+S1+ 1 μM $[Pd_2L^{O\text{-}OMe}{}_4][(BF_4)_4]$
8 S4*+S3+S2+S1+ 10 μM $[Pd_2L^{O\text{-}OMe}{}_4][(BF_4)_4]$
9 S4*+S3+S2+S1+ 25 μM $[Pd_2L^{O\text{-}OMe}{}_4][(BF_4)_4]$

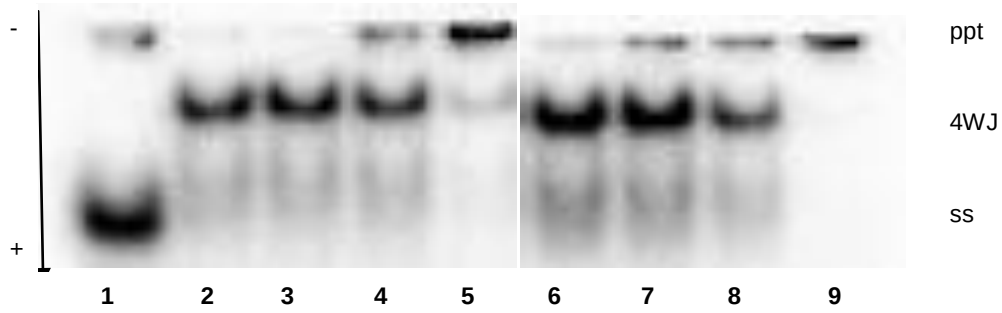

Figure 3.26: Autoradiogram of 12% polyacrylamide gel run at 25 ºC, 50 V, 2 h. S4* ^{32}P radiolabelled, incubation of samples at room temperature for 24 h. Lanes as indicated in table.

It was then explored whether incubation of the DNA oligonucleotides for only one hour at room temperature might not be sufficient for the formation of DNA four-way junction, and whether therefore the four-way junction might appear only when bound to magnesium cations or cylinders under these conditions (Figure 3.27). However, this was not successful: the DNA four-way junction was again formed in the absence of cations. Well precipitation was again observed at high complex loadings and for any given concentration of the **$[Pd_2L^{O\text{-}Glycol}{}_4][(BF_4)_4]$** cylinder.

1	S4*
2	S4*+S3+S2+S1
3	S4*+S3+S2+S1+ 0.5 mM $MgCl_2$
4	S4*+S3+S2+S1+ 2 mM $MgCl_2$
5	S4*+S3+S2+S1+ 6 mM $MgCl_2$
6	S4*+S3+S2+S1+ 10 μM $[Pd_2L^{OMe}{}_4][(BF_4)_4]$
7	S4*+S3+S2+S1+ 25 μM $[Pd_2L^{OMe}{}_4][(BF_4)_4]$
8	S4*+S3+S2+S1+ 10 μM $[Pd_2L^{O\text{-}Glycol}{}_4][(BF_4)_4]$
9	S4*+S3+S2+S1+ 25 μM $[Pd_2L^{O\text{-}Glycol}{}_4][(BF_4)_4]$
10	S4*+S3+S2+S1+ 10 μM $[Pd_2L^{O\text{-}OMe}{}_4][(BF_4)_4]$
11	S4*+S3+S2+S1+ 25 μM $[Pd_2L^{O\text{-}OMe}{}_4][(BF_4)_4]$

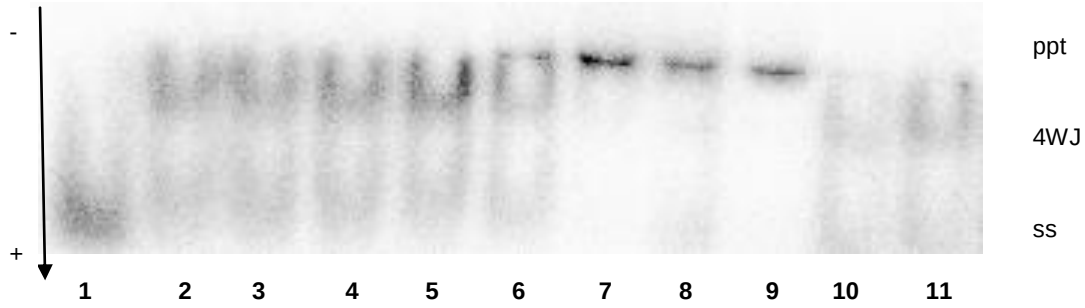

Figure 3.27: : Autoradiogram of 12% polyacrylamide gel run at 25 ºC, 50 V, 2 h. S4* ^{32}P radiolabelled, incubation of samples at room temperature for 1 h. Lanes as indicated in top table.

It can be concluded from the gel experiments performed that there is not a dramatic shift from single strand to four-way junction when incubating the DNA oligonucleotides with the different cylinders. However, most of the DNA present seems to have already formed four-way junction, and perhaps the single stranded DNA observed is either excess or for some reason cannot form a four-way junction. These results are also inconclusive as magnesium does not seem to affect this ratio either. It is unclear why despite apparently using the same conditions as Searcey, different four-way junction stability is observed

3.7. Cytotoxicity Tests

In order to explore the anti-cancer activity of the synthesised palladium(II) cylinders, preliminary cytotoxicity tests were performed by Hannah Pritchard from

the Hannon group. The cytotoxicity was determined using the 3-[4,5-dimethylthiazol-2-yl]-2,5-diphenyl tetrazolium bromide (MTT) assay.[188] The A2780 ovarian and the T47D breast cancer cell lines were grown in 96 well plates in the presence of the palladium(II) complexes at different concentrations. After 72 hours of incubation at 37 ºC and 5% CO_2, the amount of living cells present was determined by the addition of MTT. The mitochondrial enzyme succinate dehydrogenase is able to convert the yellow water soluble MTT into blue formazan crystals in viable cells (Scheme 3.1).

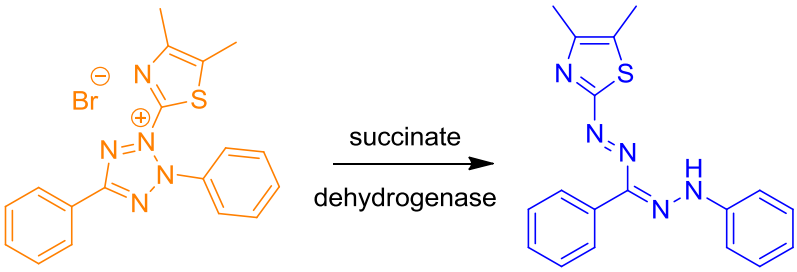

Scheme 3.1: Reduction of yellow MTT to blue formazan by succinate dehydrogenase.

These blue crystals are then dissolved in DMSO to give a purple solution and the absorbance is measured at 590 nm. An IC_{50} value can be determined from a dose response curve. The IC_{50} is the concentration of complex required to inhibit 50% of cell growth.[189]

Three cylinders were initially tested against A2780 and T47D cells. Each assay was performed in duplicate. Table 3.2 summarizes the obtained IC_{50} values.

Table 3.2: Preliminary IC_{50} values (μM) for some of the synthesised palladium(II) cylinders and cisplatin

	A2780		T47D	
$[Pd_2L^{OMe}{}_4][(BF_4)_4]$	87	53	21	34
$[Pd_2L^{O\text{-}OMe}{}_4][(BF_4)_4]$	11	5	9	26
$[Pd_2L^{NH\text{-}OMe}{}_4][(BF_4)_4]$	10	8	>100	>100
Cisplatin	2	1	15	29

The $[Pd_2L^{OMe}{}_4][(BF_4)_4]$ complex does not seem to be very toxic against the A2780 ovarian cancer cell line, however it shows good cytotoxicity against the T47D breast cancer cell line. The $[Pd_2L^{O\text{-}OMe}{}_4][(BF_4)_4]$ complex is the most toxic of all the compounds tested, presenting good cytotoxicity in both ovarian and breast cancer cell lines. The $[Pd_2L^{NH\text{-}OMe}{}_4][(BF_4)_4]$ complex is not active against T47D cells, although it is quite toxic against the ovarian A2780 cancer cell line.

These results are only preliminary and need to be repeated to obtain more accurate data with the corresponding standard deviation. The other synthesised palladium(II) complexes need to also be tested. Nevertheless, it can be concluded that in general the modifications performed on the cylinders in order to acquire better solubility have not quenched their cytotoxic activity, however it may have conferred some selectivity. The reason for this possible selectivity has not yet been explored.

3.8. Closing remarks

In this chapter DNA binding studies of the newly synthesised palladium(II) cylinders have been presented. Circular dichroism gave information on the DNA binding properties of the methoxy cylinders, as well as the **$[Pd_2L^{O\text{-}Glycol}{}_4][(BF_4)_4]$** complex. A binding event was indicated by the presence of an ICD signal in the spectroscopic region of the complexes. An ethidium bromide displacement assay also confirmed the binding of these complexes to duplex DNA. Quenching of the luminescence of the DNA-ethidium bromide complex upon addition of increasing concentrations of cylinder indicates the displacement of the ethidium bromide intercalator by the complex. Linear dichroism showed the coiling or bending effect caused by the synthesised palladium(II) cylinders, confirming the DNA interaction of all complexes. Agarose gel electrophoresis was also performed and this technique showed that all the synthesised complexes, except **$[Pd_2L^{NH\text{-}OMe}{}_4][(BF_4)_4]$**, are able to unwind supercoiled DNA and retard its migration in a 1% agarose gel. The interaction of these complexes with a DNA four-way junction was also investigated in a radiolabelled PAGE experiment. Unfortunately, the results are inconclusive and this subject needs further investigation.

Chapter 4. Conclusions and Future Work

The work described in this thesis has been focused on the design and synthesis of novel palladium(II) tetra-stranded supramolecular cylinders that might be capable of recognizing a DNA four-way junction. Tetra-stranded cylinders were previously synthesised by Hannon, Ryabova and Kaur, however their poor water solubility prevented detailed DNA binding studies.[133,134] These palladium(II) complexes are highly toxic against different ovarian and breast cancer cell lines, suggesting a possible use of these cylinders as anti-cancer drugs. In this work, four different strategies to increase the water solubility of these complexes have been explored. This was to allow DNA binding studies to be carried out to give a better understanding of the mode of action of these supramolecular cylinders.

Modification of the central spacer unit provided an increase in the solubility of the first generation of complexes; when exchanging the carbon spacer by oxygen, the palladium(II) complex became more soluble in organic solvent/water mixtures.[133,134] Therefore, this was the first strategy that was explored in this work. The carbon spacer unit was substituted by oxygen, nitrogen and sulfur. These changes were performed in a newly synthesised ligand with methyl ether groups at the 3 position of the pyridine rings ($\mathbf{L^{OMe}}$). This functional group was chosen as 3-bromo-5methoxypyridine is commercially available, it could be cleaved in a later stage and would provide an easy synthetic route while protected.

All spacer-modified ligands ($\mathbf{L^{O\text{-}OMe}}$, $\mathbf{L^{NH\text{-}OMe}}$ and $\mathbf{L^{S\text{-}OMe}}$), as well as the carbon analogue ($\mathbf{L^{OMe}}$), were formed via Suzuki coupling of smaller molecules. Formation of the palladium(II) complex of ligand $\mathbf{L^{OMe}}$ was initially performed at room temperature overnight. This yielded two supramolecular species of different size, as seen by DOSY NMR spectroscopy. These two products were identified as the desired tetra-stranded dinuclear palladium(II) cylinder and a double walled triangle. The complexation reaction at 80 ºC yielded the desired tetra-stranded cylinders as the only products. These four new complexes were soluble in dimethyl sulfoxide, acetone, acetonitrile and organic solvent/water mixtures, with a smaller percentage of organic solvent required compared with the first generation of complexes.

Deprotection of the methyl ether groups of the synthesised ligands yielded three new ligands ($\mathbf{L^{OH}}$, $\mathbf{L^{O\text{-}OH}}$ and $\mathbf{L^{NH\text{-}OH}}$), which were more soluble in protic solvents. The tetra-stranded palladium(II) complexes of ligands $\mathbf{L^{OH}}$ and $\mathbf{L^{O\text{-}OH}}$ were successfully formed, however they tend to form gelatinous solutions and this made the characterization complicated. Nevertheless, the $\mathbf{[Pd_2L^{OH}{}_4][(BF_4)_4]}$ complex could be solubilised in dimethyl sulfoxide/water mixtures. Ligand $\mathbf{L^{NH\text{-}OH}}$ presented water solubility properties, however the formation of its palladium(II) complex could not be achieved since the yield for the formation of this ligand was low.

A short glycol chain was introduced at the edges of the pyridine rings, which gave the $\mathbf{[Pd_2L^{O\text{-}Glycol}{}_4][(BF_4)_4]}$ complex methanol solubility. Other motifs, such as alkyl-chained pyrrolidines were also added at position 3 of the pyridine rings,

however formation of the palladium(II) complex of ligand $\mathbf{L^{Pyr}}$ could not be achieved in its pure form.

Exchange of the tetrafluoroborate counter-ion of the $\mathbf{[Pd_2L^{OMe}{}_4][(BF_4)_4]}$ complex was also explored. Triflate anions considerably increased the solubility of this complex in acetonitrile, while nitrate counter-ions yielded a complex more soluble in organic solvents. When treating $\mathbf{[Pd_2L^{OMe}{}_4][(BF_4)_4]}$ complex with a saturated solution of chloride anions, ligand $\mathbf{L^{OMe}}$ was obtained as the complex fell apart. Two of the four tetrafluoroborate counter-ions were observed to be located in the central cavity of $\mathbf{[Pd_2L^{OMe}{}_4][(BF_4)_4]}$ and $\mathbf{[Pd_2L^{NH\text{-}OMe}{}_4][(BF_4)_4]}$ complexes via X-ray diffraction. Therefore, triflate and tosilate anion titrations monitored by ^{1}H NMR were performed. These experiments revealed that the outer anions are exchanged first as these are more readily available.

An increase in the overall charge of the cylinder was also investigated. This led to the formation of the doubly charged $\mathbf{L^{N+}}$ ligand, in which the central phenylene spacer units were replaced by pyridine rings. Unfortunately, formation of the tetra-stranded complex could not be achieved. A single charged ligand might be more suitable as the overall charge of the complex will be 8+ instead of 12+. This might allow a better interaction between the charged ligands and the metal ions.

In summary, four different modifications of the basic structure of the parent palladium(II) cylinder have been explored. An increase in solubility in organic solvent/water mixtures has been observed and has allowed detailed DNA binding

studies to be performed. A highly methanol-soluble complex has also been synthesised, however solubility in aqueous buffer could not be obtained. Four different changes at four different positions were investigated and no aqueous solubility was achieved.

Changing the metal ion was not explored in this study as this did not improve the water solubility of the first generation of compounds and yielded other structures, such as polymeric structures for silver ions and complex mixtures for platinum complexes, that needed to be purified with two consecutive HPLC runs. However, if a water soluble palladium(II) cylinder could be synthesised, the synthesis of its platinum(II) analogue would be interesting due to its higher stability and the numerous existing platinum anti-cancer drugs, so that cytotoxic activities between platinum complexes could be compared.

Ishikawa has reported that by disrupting the molecular planarity and symmetry of drug molecules, an improvement in water solubility is achieved.[190] The high symmetry and the square planar conformation of the palladium(II) complexes could be the reason for their poor water solubility. Therefore, disruption of the symmetry could be investigated in future studies (e.g. singly charged ligands). However, this could lead to mixtures that might be challenging to purify.

Even though the synthesised complexes were not water soluble, their DNA binding properties were studied via circular and linear dichroism, ethidium bromide displacement and agarose and polyacrylamide gel electrophoresis. Sample

solutions were prepared by dissolving the complexes in a small percentage of DMSO.

The methoxy cylinders and the **$[Pd_2L^{O\text{-}Glycol}{}_4][(BF_4)_4]$** complex showed affinity for duplex DNA as seen by circular dichroism, while **$[Pd_2L^{OH}{}_4][(BF_4)_4]$** and the parent **$[Pd_2L_4][(BF_4)_4]$** complexes did not seem to bind DNA. However, an ethidium bromide displacement assay confirmed the DNA binding properties of all of the synthesised complexes.

Oriented binding to ct-DNA was not observed for any of the studied complexes, however coiling or bending effects were observed via linear dichroism spectroscopy. The **$[Pd_2L^{O\text{-}OMe}{}_4][(BF_4)_4]$** complex produced the greatest loss of DNA LD signal, with the rest showing similar coiling effects.

Unwinding angles of 4º or lower were determined by agarose gel electrophoresis of plasmid DNA. All the complexes, except the **$[Pd_2L^{NH\text{-}OMe}{}_4][(BF_4)_4]$** complex, were shown to interact with the supercoiled form of plasmidic DNA, indicating DNA binding.

From these experiments, it can be concluded that the newly synthesised palladium(II) complexes are able to recognize and bind to duplex DNA. In terms of DNA junction recognition, the results reported herein are inconclusive, as the DNA four-way junction is quantitatively formed in the absence of divalent cations or cylinder. Therefore, detection of stabilization or binding of the cylinder to a DNA four-way junction is difficult to confirm. Further investigations might involve either the detection of palladium via ICP-MS on four-way junction bands, or cylinder

detection via MALDI spectroscopy. This issue needs to be addressed as the palladium(II) cylinders may only be duplex binders or coiling agents.

Preliminary cytotoxicity tests showed that in general the synthesised cylinders remain toxic against breast and ovarian cancer cell lines, and some selectivity can be observed. However, these are only initial results and need to be further investigated. Future work may also involve the study of cellular uptake mechanisms, as well as detection of the localization of the complexes in cells. Distribution of the complexes in the cell (cytoplasm or nuclei) could be detected by ICP-MS.

A new ligand system was also explored in this study, however formation of a dinuclear, tetra-stranded palladium(II) complex has not yet been achieved. This new ligand system replaced the coordinating pyridines by 1,2,3-triazoles moieties that are shown to coordinate metal ions. These triazole ligands can be easily synthesised via the click chemistry reaction, in one step with high yields and with a wide variety of functionalization groups. This could allow the synthesis of large libraries of compounds and metallo-supramolecular structures. Initial studies towards the application of this new ligand system in Hannon's iron(II) triple stranded cylinder have been explored. The coordinating pyridine group was also replaced by a 1,2,3-triazole unit (Scheme 4.1). However, ligand $\mathbf{L}^{\mathbf{im\text{-}click}}$ could not be obtained. ^{1}H NMR indicated a mixture of species with the aldehyde present, and mass spectrometry confirmed the presence of the aldehyde and half ligand. A one pot synthesis was performed with the immediate formation of an orange solution, however this coloration faded with time. NMR and mass spectrometry

studies were inconclusive in determining whether the complex had been formed. The synthesis of mononuclear iron(II) complexes might give a better understanding of this new ligand system.

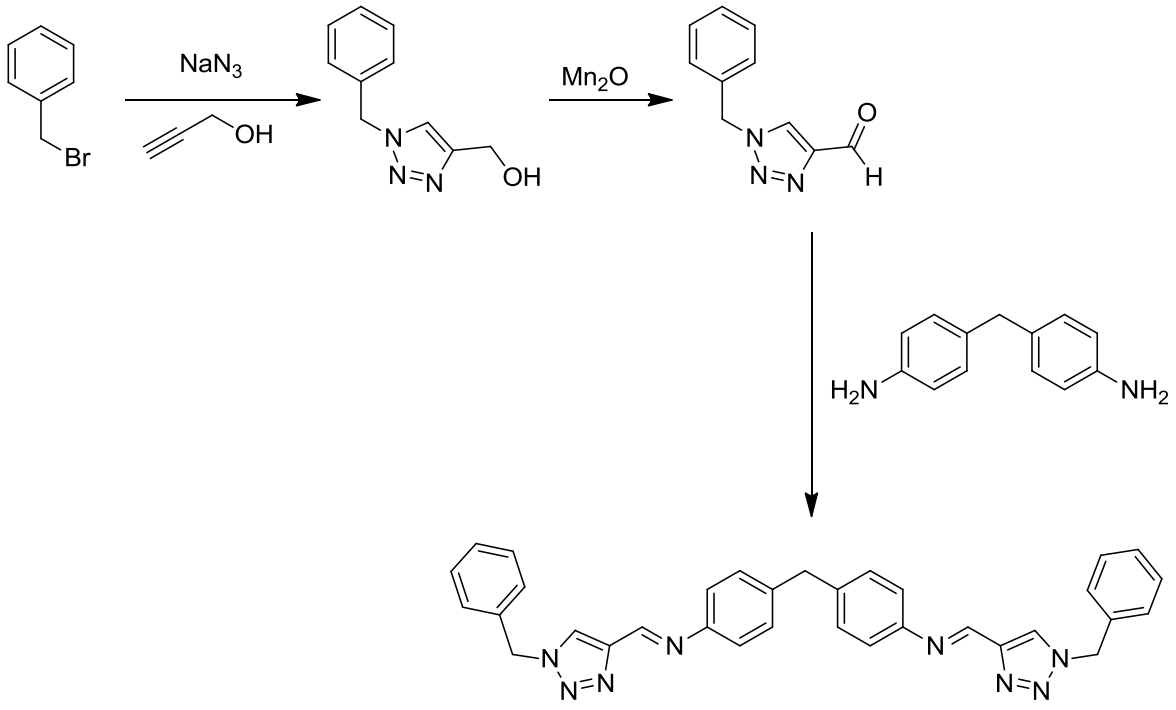

Scheme 4.1: Synthesis of ligand $\mathbf{L}^{\text{im-click}}$.

Although much has been learnt from the design and synthesis of the novel palladium(II) cylinders, some questions remain unanswered. Several modifications of the parent palladium(II) cylinder have been performed and water solubility could not be obtained. A new ligand system was also explored, however it was not possible to obtain the dinuclear palladium(II) complexes. Future work might involve a completely new molecular design in order to acquire water solubility.

Even though the synthesised complexes were not soluble in 100% aqueous buffer, DNA binding studies could be performed with small percentages of organic solvents. In this regard, this is a success as these DNA binding studies could not be performed for the first generation of complexes. Binding of the complexes to duplex DNA has been observed and it is likely they do so by binding in the major groove, due to their large size. However, further confirmation is needed and this could be investigated by NMR, computer modelling or by crystallization of the complex with duplex DNA. AFM studies could also be performed in order to confirm the coiling observed by linear dichroism

Four-way junction studies were unfortunately inconclusive and this needs further investigation. Detection of palladium in four-way junction bands in gels or study of the stabilization of the four-way junction via circular dichroism spectroscopy upon addition of aliquots of complex could be explored.

Chapter 5. Experimental

5.1. General materials and methods for synthetic protocols

All solvents and reagents were purchased from Sigma Aldrich, Fisher Scientific, Alfa Aesar and Fluorochem and were used without further purification. Anhydrous tetrahydrofuran, dichloromethane, toluene, methanol, diethyl ether and acetonitrile were collected from a Pure Solv-MD Solvent Purification System. Reaction temperatures refer to the temperature measured in an external oil bath. NMR spectra were recorded on AV300, AVIII300, AV400, AVIII400 and DRX500 Bruker spectrometers in the deuterated solvents indicated, which were purchased from Goss Scientific. NMR spectra were processed using MestReNova 6.0.2 software with calibration on residual solvent peaks given by reported values.[191] Chemical shifts (δ) are quoted in ppm and coupling constants (J) are quoted in Hz. Progress of reactions was monitored by thin layer chromatography using Merck Silica Gel 60 F254 aluminium plates which were visualized with UV light or potassium permanganate. Flash column chromatography was carried out using 60 Å Silica Gel or activated neutral aluminium oxide in the solvent systems indicated. Infrared spectra were recorded on a Perking Elmer Spectrum 100 FTIR spectrometer as neat films, wavelengths (ν) are quoted in cm^{-1}. Electrospray Ionisation (ESI+) spectra were recorded on a Micromass LCT Time of Flight mass spectrometer in positive ionization mode. Electron impact (EI) spectra were recorded on a Waters

Micromass Zabspec/Magnetic sector mass spectrometer. Matrix-Assisted Laser Desorption Ionization (MALDI) spectra were recorded on a Bruker Bi-flex MALDI Time of Flight mass spectrometer. X-ray diffraction data was collected either at the National Crystallography Service at the University of Southampton in a Rigaku FR-E Ultra High Flux diffractometer or at the University of Birmingham in a Bruker Smart 6000 CCD diffractometer. COLLECT was used for data collection and DENZO for data refinement. Experimental absorption correction was performed with SADABS. Crystal structures were solved by direct methods using SIR92, and refinement was performed by a full-matrix least-squares procedure on F^2 in SHELXL-97. All non-hydrogen atoms were refined with anisotropic displacement parameters. All hydrogen atoms (except NH on $\mathbf{L^{NH\text{-}OH}}$) were fixed as riding models. Mercury 3.0[192] and Chimera 1.6rc[193] were used to process .cif and .pdb files of crystal structures solved by Dr. Louise Male or downloaded from the Cambridge Crystallographic Data Centre (CCDC)[194] or from the Protein Data Bank (PDB)[195]. High Performance Liquid Chromatography (HPLC) analyses were performed using a Dionex HPLC system with Chromeleon software. UV-Vis spectra were recorded using a Varian Cary 5000 UV-Vis spectrometer in 1 cm quartz cuvettes.

5.1.1. Synthesis of (5-methoxypyridin-3-yl)boronic acid (1)

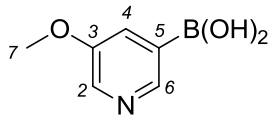

$C_6H_8BNO_3$

FW: 153.06

1

Dry toluene (12 mL) was placed in a dry flask under argon atmosphere at -78 ºC. *n*-Butyllithium (7.30 mL, 11.70 mmol, 1.6 M in hexanes) followed by 3-bromo-5-methoxypyridine (2.00 g, 10.64 mmol) in dry toluene (6 mL) were added and the reaction mixture was left to stir for 30 minutes. A brown precipitate was formed and dry THF (6 mL) was added slowly, keeping the temperature below -78 ºC. After stirring for an additional 15 minutes, triisopropylborate (3.00 mL, 12.76 mmol) was added and the dark brown solution was allowed to warm to -15 ºC. 2 M HCl (15 mL) was then added and the reaction mixture left to warm to room temperature forming a biphasic light brown solution that was partitioned. The acidic water phase was neutralized with saturated $NaHCO_3$ solution and extracted with ethyl acetate (3 X 30 mL). Sodium chloride was added to the water phase and it was extracted again with ethyl acetate (3 X 30 mL). The combined organic phases were evaporated to give a brown oil that was dissolved in a mixture of THF:methanol (1:1) and filtered to remove the inorganic salts. The filtrate was then evaporated giving a brown solid (1.26 g, 76% yield). ^{1}H NMR (300 MHz, MeOD): δ 8.20 (s br, 1H, H2), 8.19 (s br, 1H, H6), 7.99 (s br, 1H, H4), 3.96 (s, 3H, H7). LRMS (EI+): *m/z* (%) 165 (20) $[M\text{-}2H+CH_3(^{10}B)]^+$, 167 (80) $[M\text{-}2H+CH_3(^{11}B)]^+$. IR (Neat): ν_{max} 2942 (m), 1578 (m), 1412 (s), 1313 (s), 1254 (s), 1018 (s), 1049 (s), 904 (m), 830 (m), 721 (s).

Alternative "*in situ*" protocol:

3-Bromo-5-methoxypyridine (0.50 g, 2.66 mmol) dissolved in THF (20 mL) was placed in a dry flask under argon atmosphere at -78 ºC. Triisopropylborate (0.63 mL, 2.71 mmol) was added followed by dropwise addition of *n*-butyllithium (1.83 mL, 2.92 mmol, 1.6 M in hexanes).The reaction mixture was left stirring at -78 ºC for 1 hour, after which it was allowed to warm to room temperature overnight. 2 M HCl (7 mL) was added and the mixture stirred for 20 minutes. The crude mixture was evaporated to dryness, redissolved in water and extracted with ethyl acetate (3 X 30 mL). The combined aqueous phases were evaporated under reduced pressure to yield a yellow solid (0.20 g, 48% yield). ^{1}H NMR (300 MHz, D_2O): δ 8.47 (s br, 1H, H2), 8.41 (d, J = 2.6 Hz, 1H, H6), 8.34 – 8.31 (m, 1H, H4), 3.99 (s, 3H, H7). LRMS (EI+): *m/z* (%) 189 (20) $[M+HCl(^{11}B)]^+$. IR (Neat): ν_{max} 3194 (m, br), 1612 (m), 1566 (s), 1451 (s), 1433 (s), 1395 (m), 1339 (s), 1321 (m), 1275 (s), 1261 (s), 1117 (m), 1022 (s), 1006 (s), 865 (m), 773 (m), 693 (s).

5.1.2. Synthesis of bis(4-bromophenyl)methanol (3)[140]

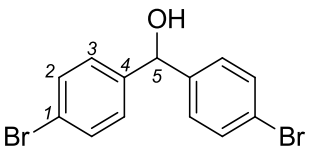

3

$C_{13}H_{10}Br_2O$

FW: 342.03

1,4-Dibromobenzene (0.83 g, 3.52 mmol) dissolved in dry THF (8 mL) was placed in an argon purged dry flask at -78 ºC. *n*-Butyllithium (2.00 mL, 3.20 mmol, 1.6 M in hexanes) was added dropwise to the solution, keeping the rate of addition

constant to maintain the temperature at -78 ºC. The cream slurry was stirred under an argon atmosphere for 1 hour before adding it to a solution of 4-bromobenzylaldehyde (0.53 g, 2.87 mmol) in THF (8 mL) which had also been cooled to -78 ºC. The resulting solution was kept at that temperature for 1 hour after which it was allowed to warm to room temperature. It was then stirred overnight before being poured into ice (50 g). The suspension was extracted with ethyl acetate (3 X 30 mL), washed with water (2 X 20 mL) and brine (1 X 20 mL) and dried over magnesium sulfate. The solvent was removed in vacuo and the yellow oil material precipitated and washed with hexane to yield the required product as a white solid (0.61 g, 82% yield). ^{1}H NMR (300 MHz, $CDCl_3$): δ 7.49 – 7.44 (m, 4H, H2), 7.25 – 7.21 (m, 4H, H3), 5.76 (d, J = 3.4 Hz, 1H, H5), 2.21 (d, J = 3.4 Hz, 1H, OH). ^{13}C NMR (100 MHz, $CDCl_3$): δ 142.4 C_q, 131.9 C2, 128.3 C3, 121.9 C_q, 75.2 C5. LRMS (EI+): *m/z* (%) 342 (26) $[M]^+$, 261 (14) $[M\text{-}Br]^+$, 185 (100) $[M\text{-}2Br]^+$. HRMS (EI+) calculated for $C_{13}H_{10}Br_2O$ $[M]^+$ 339.9098, found 339.9087. FTIR (film): ν_{max} 3327 (s, br), 2890 (w), 1645 (w), 1589 (m), 1482 (s), 1404 (m), 1328 (w), 1188 (m), 1115 (m), 1069 (s), 1038 (s), 1008 (s), 790 (s), 693 (m).

5.1.3. Synthesis of bis(4-bromophenyl)methane (2)[140]

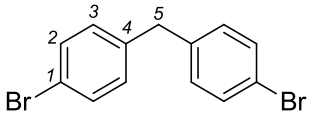

$C_{13}H_{10}Br_2$

FW: 326.03

2

To a solution of bis(4-bromophenyl)methanol (1.60 g, 4.70 mmol) in TFA (40 mL), sodium borohydride (1.79 g, 47.00 mmol) was slowly added. The white slurry was

stirred for 2 hours and then poured into ice (50 g). 2 N Sodium hydroxide was then carefully added to make the suspension alkaline. The mixture was extracted with diethyl ether (3 X 30 mL) and the combined fractions washed with water (2 X 30 mL) and brine (1 X 30 mL) and dried over magnesium sulfate. Diethyl ether was removed under reduced pressure. The residue was then purified by column chromatography on silica gel with hexane as eluent to yield a white solid (1.42 g, 93% yield). ^{1}H NMR (300 MHz, $CDCl_3$): δ 7.43 – 7.38 (m, 4H, H2), 7.05 – 7.00 (m, 4H, H3), 3.88 (s, 2H, H5). ^{13}C NMR (100 MHz, $CDCl_3$): δ 139.6 C_q, 131.8 C2, 130.7 C3, 120.4 C_q, 40.8 C5. LRMS (EI+): *m/z* (%) 326 (100) $[M]^+$, 245 (77) $[M\text{-}Br]^+$, 165 (84) $[M\text{-}2Br]^+$. HRMS (EI+) calculated for $C_{13}H_{10}Br_2$ $[M]^+$ 323.9149, found 323.9150. FTIR (film): ν_{max} 2920 (w), 2852 (w), 1484 (s), 1437 (m), 1400 (m), 1201 (w), 1111 (w), 1067 (s), 1010 (s), 858 (s), 806 (s), 776 (s).

5.1.4. General Suzuki Coupling Procedure

Pyridineboronic acid or ester (3.92 mmol), bis(4-bromophenyl) (1.78 mmol), tricyclohexylphosphine (0.086 mmol) and tris(dibenzylideneacetone)dipalladium(0) (0.036 mmol) were placed in a Schlenk flask. The Schlenk flask was evacuated and refilled with argon five times. Dioxane (10 mL) followed by an aqueous solution (5 mL) of potassium phosphate tribasic (6.06 mmol) were added via syringe followed by three evacuation/refill cycles. The sealed flask was heated in an oil bath at 100 ºC for 48 hours. The mixture was then filtered and washed with

ethyl acetate (100 mL), dried over sodium sulfate and evaporated under reduced pressure. The residue was then purified by column chromatography.

5.1.5. Synthesis of ligand L^{OMe}

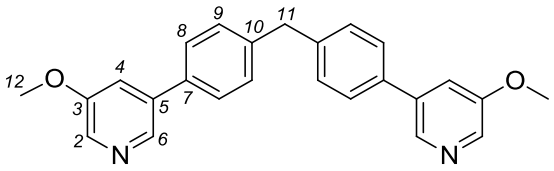

L^{OMe}

$C_{25}H_{22}N_2O_2$

FW: 382.45

The title compound was prepared according to the *General Suzuki Coupling Procedure* with (5-methoxypyridin-3-yl)boronic acid (0.60 g, 3.92 mmol) and bis(4-bromophenyl)methane (0.58 g, 1.78 mmol). Purification by column chromatography on silica gel with ethyl acetate as eluent yielded a white solid (0.45 g, 66% yield).^{1}H NMR (300 MHz, $CDCl_3$): δ 8.45 (d, J = 1.8 Hz, 2H, H6), 8.28 (d, J = 2.8 Hz, 2H, H2), 7.56 – 7.50 (m, 4H, H8), 7.37 – 7.31 (m, 6H, H9 and H4), 4.09 (s, 2H, H11), 3.92 (s, 6H, H12). ^{13}C NMR (100 MHz, $CDCl_3$): δ 155.9 C_q, 141.1 C_q, 140.9 C6, 137.2 C_q, 136.1 C2, 135.9 C_q, 129.8 C9, 127.6 C8, 119.2 C4, 55.8 C12, 41.4 C11. LRMS (ES+): *m/z* (%) 383.2 (23) $[M+H]^+$, 405.2 (100) $[M+Na]^+$, 406.2 (11) $[M+Na+H]^+$. HRMS (ES+) calculated for $C_{25}H_{22}N_2O_2Na$ $[M+Na]^+$ 405.1579, found 405.1581. FTIR (film): ν_{max} 3041 (w), 2971 (w), 1579 (s), 1515 (m), 1431 (s), 1398 (s), 1313 (s), 1218 (s), 1189 (m), 1157 (m), 1064 (m), 1015 (s), 910 (m), 875 (m), 807 (s), 708 (s).

5.1.6. General Tetrafluoroborate Tetra-Stranded Palladium(II) Cylinder Procedure

Tetrakis(acetonitrile)palladium(II) tetrafluoroborate (0.038 mmol) was added to a suspension of ligand $\mathbf{L^X}$ (0.076 mmol) in acetonitrile (5 mL) at 80 ºC. The resulting mixture was stirred at 80 ºC for 6 hours after which it was filtered to remove a suspended solid. Diethyl ether (50 mL) was added to precipitate a solid which was further washed with diethyl ether (50 mL) and dried in vacuo.

5.1.7. Synthesis of $[Pd_2L^{OMe}{}_4][BF_4]_4$

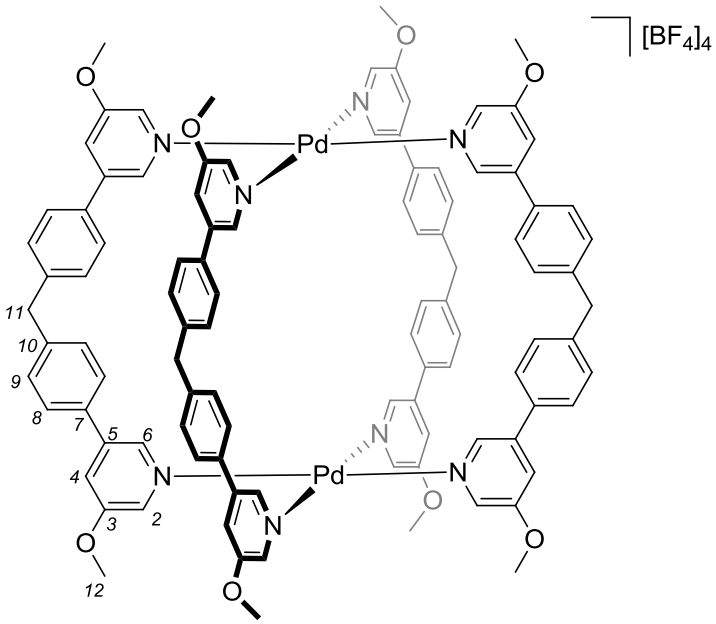

$[Pd_2(C_{25}H_{22}N_2O_2)_4][BF_4]_4$

FW: 2088.49

The title compound was prepared according to the *General Tetrafluoroborate Tetra-Stranded Palladium(II) Cylinder Procedure* with ligand $\mathbf{L^{OMe}}$ (28.9 mg, 0.076 mmol) to yield a white solid (31.0 mg, 78% yield). ^{1}H NMR (300 MHz, CD_3CN): δ 8.83 (d, J = 1.5 Hz, 8H, H6), 8.72 (d, J = 2.4 Hz, 8H, H2), 7.70 (dd, J =

2.4, 1.5 Hz, 8H, H4), 7.47 – 7.44 (m, 16H, H8), 7.33 – 7.30 (m, 16H, H9), 4.12 (s, 8H, H11), 3.99 (s, 24H, H12). ^{13}C NMR (100 MHz, CD_3CN): δ 158.8 C_q, 143.3 C_q, 142.1 C_q, 141.8 C6, 138.0 C2, 134.1 C_q, 130.8 C9, 128.8 C8, 124.7 C4, 57.7 C12, 41.1 C11. ^{19}F NMR (282 MHz, CD_3CN): δ -150.35 (s, 2F), -150.40 (s, 8F). LRMS (ES+): *m/z* (%) 383.4 (1) $[L^{OMe}+H]^+$, 435.9 (2) $[Pd_2L^{OMe}_4]^{4+}$, 610.1 (43) $[Pd_2L^{OMe}_4(BF_4)]^{3+}$, 958.2 (100) $[Pd_2L^{OMe}_4(BF_4)_2]^{2+}$, 2003.5 (3) $[Pd_2L^{OMe}_4(BF_4)_3]^+$. FTIR (film): ν_{max} 3086 (w), 1589 (s), 1516 (w), 1464 (m), 1439 (m), 1403 (m), 1332 (m), 1263 (w), 1226 (s), 1185 (w), 1055 (s), 1032 (s), 1002 (s), 878 (m), 799 (s), 764 (w), 700 (s), 627 (m), 576 (m). UV-Vis (CH_3CN): λ_{max} (ε_{max}/dm^{3}mol^{-1}cm^{-1}) 294 (61 000), 256 (81 900) nm.

5.1.8. Synthesis of ligand $L^{O\text{-}OMe}$

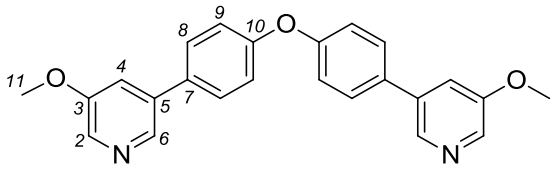

$L^{O\text{-}OMe}$

$C_{24}H_{20}N_2O_3$

FW: 384.43

The title compound was prepared according to the *General Suzuki Coupling Procedure* with (5-methoxypyridin-3-yl)boronic acid (0.60 g, 3.92 mmol) and bis(4-bromophenyl) ether (0.58 g, 1.78 mmol). Purification by column chromatography on silica gel with ethyl acetate as eluent yielded a white solid (0.49 g, 71% yield).^{1}H NMR (300 MHz, $CDCl_3$): δ 8.46 (d, J = 1.8 Hz, 2H, H6), 8.30 (d, J = 2.7 Hz, 2H, H2), 7.62 – 7.54 (m, 4H, H8), 7.36 (dd, J = 2.7, 1.8 Hz, 2H, H4), 7.20 – 7.13 (m, 4H, H9), 3.93 (s, 6H, H11). ^{13}C NMR (100 MHz, $CDCl_3$): δ 157.4

C_q, 140.8 C6, 136.8 C_q, 136.1 C2, 133.7 C_q, 133.2 C_q, 128.9 C8, 119.7 C9, 119.1 C4, 55.8 C11. LRMS (ES+): *m/z* (%) 385.3 (100) $[M+H]^+$, 407.3 (46) $[M+Na]^+$, 406.2 (10) $[M+Na+H]^+$. HRMS (ES+) calculated for $C_{24}H_{21}N_2O_3$ $[M+H]^+$ 385.1552, found 385.1546. FTIR (film): ν_{max} 3041 (w), 2973 (w), 2955 (w), 2850 (w), 1912 (w), 1599 (w), 1584 (m), 1507 (m), 1470 (w), 1450 (w), 1430 (m), 1396 (m), 1335 (w), 1312 (m), 1259 (m), 1219 (s), 1175 (m), 1163 (m), 1112 (m), 1062 (m), 1015 (m), 913 (w), 882 (m), 834 (s), 709 (m), 687 (m), 642 (w), 578 (m).

5.1.9. Synthesis of $[Pd_2L^{O\text{-}OMe}{}_4][BF_4]_4$

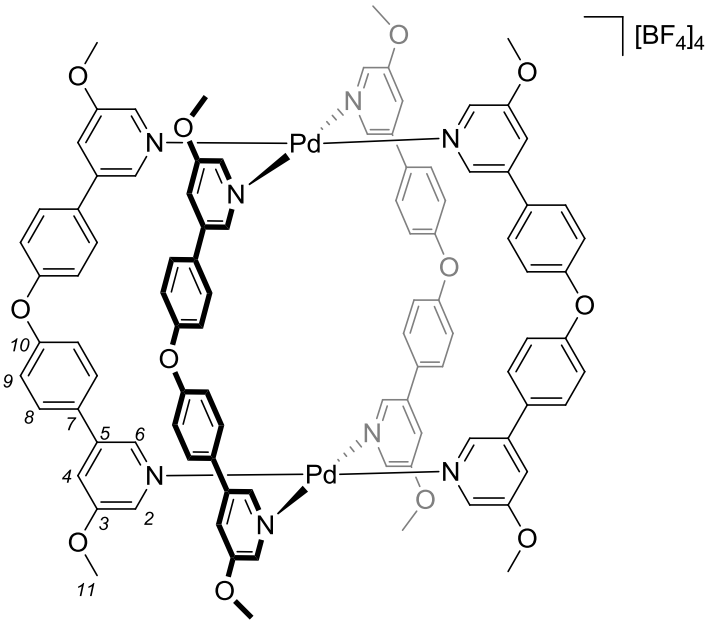

$[Pd_2(C_{24}H_{20}N_2O_3)_4][BF_4]_4$

FW: 2096.41

The title compound was prepared according to the *General Tetrafluoroborate Tetra-Stranded Palladium(II) Cylinder Procedure* with ligand $\mathbf{L^{O\text{-}OMe}}$ (29.1 mg, 0.076 mmol). A white solid was yielded after washing with chloroform (50 mL) that was dried in vacuo (18 mg, 46% yield). ^{1}H NMR (300 MHz, CD_3CN): δ 9.02 (d, J =

1.5 Hz, 8H, H6), 8.88 (d, J = 2.4 Hz, 8H, H2), 7.70 (dd, J = 2.4, 1.5 Hz, 8H, H4), 7.65 – 7.60 (m, 16H, H8), 7.28 – 7.23 (m, 16H, H9), 4.03 (s, 24H, H11). ^{13}C NMR (100 MHz, CD_3CN): δ 159.1 C_q, 159.0 C_q, 141.7 C_q, 141.3 C6, 137.8 C2, 131.5 C_q, 130.4 C8, 124.3 C4, 120.7 C9, 57.8 C11. ^{19}F NMR (282 MHz, CD_3CN): δ -150.35 (s, 2F), -150.41 (s, 8F). LRMS (ES+): *m/z* (%) 611.2 (91) $[Pd_2L^{O\text{-}OMe}{}_4(BF_4)]^{3+}$, 959.8 (100) $[Pd_2L^{O\text{-}OMe}{}_4(BF_4)_2]^{2+}$. FTIR (film): ν_{max} 3088 (w), 1593 (s), 1507 (s), 1454 (m), 1439 (m), 1401 (w), 1321 (m), 1224 (s), 1178 (m), 1154 (m), 1055 (s), 1032 (s), 1004 (s), 871 (m), 832 (s), 698 (m), 600 (w), 578 (w). UV-Vis (CH_3CN): λ_{max} (ε_{max}/dm^{3}mol^{-1}cm^{-1}) 292 (66 000), 274 (53 600) nm.

5.1.10. Synthesis of ligand $L^{NH\text{-}OMe}$

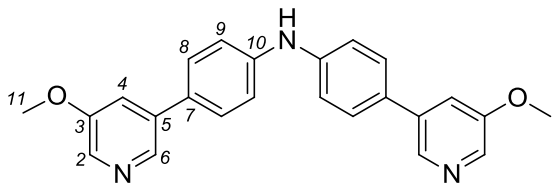

$L^{NH\text{-}OMe}$

$C_{24}H_{21}N_3O_2$

FW: 383.44

The title compound was prepared according to the *General Suzuki Coupling Procedure* with (5-methoxypyridin-3-yl)boronic acid (0.60 g, 3.92 mmol) and bis(4-bromophenyl)amine (0.58 g, 1.78 mmol). Purification by column chromatography on silica gel with ethyl acetate as eluent yielded a white solid (0.58 g, 85% yield). ^{1}H NMR (300 MHz, $CDCl_3$): δ 8.46 (s br, 2H, H6), 8.26 (d, J = 1.9 Hz, 2H, H2), 7.58 – 7.47 (m, 4H, H8), 7.35 (dd, J = 2.7, 1.9 Hz, 2H, H4), 7.25 – 7.17 (m, 4H, H9), 6.12 (s br, 1H, NH), 3.92 (s, 6H, H11). ^{13}C NMR (100 MHz,

$CDCl_3$): δ 156.0 C_q, 143.0 C_q, 140.5 C6, 137.1 C_q, 135.6 C2, 130.6 C_q, 128.4 C8, 118.7 C4, 118.4 C9, 55.8 C11. LRMS (ES+): *m/z* (%) 384.2 (100) $[M+H]^+$, 385.3 (11) 406.2 (20) $[M+Na]^+$, 438.2 (9) $[M+Na+MeOH]^+$. HRMS (ES+) calculated for $C_{24}H_{22}N_3O_2Na$ $[M+H+Na]^+$ 384.1712, found 384.1711. FTIR (film): ν_{max} 3427 (w), 2974 (w), 1605 (m), 1581 (m), 1521 (m), 1472 (w), 1422 (m), 1404 (w), 1387 (w), 1310 (m), 1250 (w), 1216 (s), 1185 (m), 1160 (w), 1064 (w), 1025 (m), 908 (w), 873 (m), 828 (s), 819 (m), 708 (m), 694 (w), 645 (w), 581 (m).

5.1.11. Synthesis of $[Pd_2L^{NH\text{-}OMe}_4][BF_4]_4$

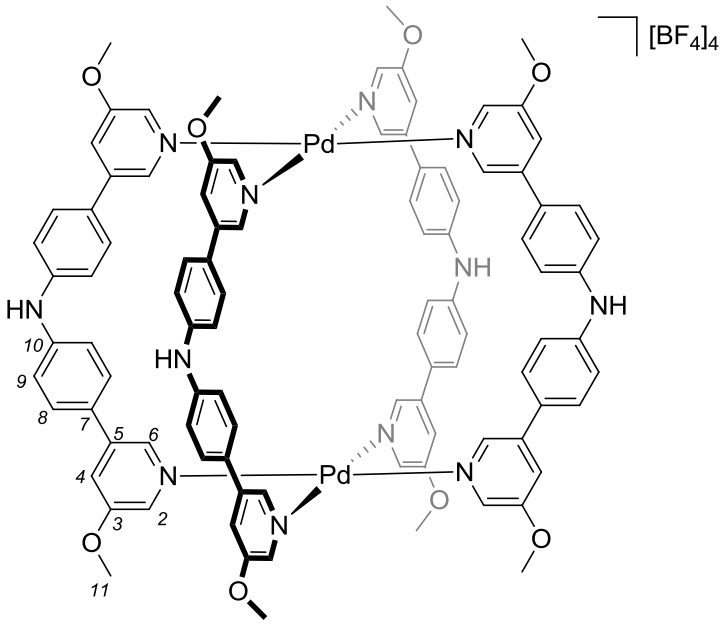

$[Pd_2(C_{24}H_{21}N_3O_2)_4][BF_4]_4$

FW: 2092.47

The title compound was prepared according to the *General Tetrafluoroborate Tetra-Stranded Palladium(II) Cylinder Procedure* with ligand $\mathbf{L^{NH\text{-}OMe}}$ (29.0 mg, 0.076 mmol) to yield a yellow solid (20.2 mg, 51% yield). ^{1}H NMR (300 MHz, CD_3CN): δ 9.28 (d, J = 1.4 Hz, 8H, H6), 8.81 (d, J = 2.4 Hz, 8H, H2), 7.74 – 7.71

(m, 16H, H8), 7.70 – 7.68 (m, 8H, H4), 7.33 – 7.30 (m, 16H, H9), 7.27 (s br, 4H, NH), 4.00 (s, 24H, H11). ^{13}C NMR (100 MHz, CD_3CN): δ 159.0 C_q, 151.8 C_q, 145.4 C_q, 141.0 C6, 137.0 C2, 129.2 C8, 127.4 C_q, 122.6 C4, 119.5 C9, 57.6 C11. ^{19}F NMR (282 MHz, CD_3CN): δ -150.46 (s, br, 10F). LRMS (ES+): *m/z* (%) 611.1 (69) $[Pd_2L^{NH\text{-}OMe}{}_4(BF_4)]^{3+}$, 960.2 (100) $[Pd_2L^{NH\text{-}OMe}{}_4(BF_4)_2]^{2+}$. FTIR (film): ν_{max} 3380 (w, br), 3088 (w), 1585 (s), 1524 (s), 1455 (m), 1409 (w), 1317 (m), 1270 (w), 1222 (s), 1188 (m), 1156 (m), 1057 (s), 1032 (s), 1003 (s), 874 (m), 820 (s), 762 (w), 698 (m), 602 (w), 576 (w). UV-Vis (CH_3CN): λ_{max} (ε_{max}/dm^{3}mol^{-1}cm^{-1}) 351 (107 900), 278 (78 500) nm.

5.1.12. Synthesis of bis(4-bromophenyl)sulfide (4)

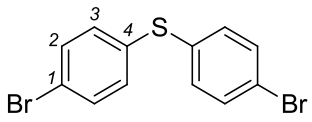

$C_{12}H_8Br_2S$

FW: 344.06

4

To a solution of diphenyl sulfide (1.00 mL, 5.98 mmol) in dichloromethane (25 mL), bromine (1.20 mL, 23.9 mmol) was added followed by water (25 mL). The red solution was stirred for 6 hours. Saturated sodium thiosulfate aqueous solution was added to quench the excess bromine. The two phases were extracted. The organic phase was washed with water (50 mL) and brine (50 mL), dried over magnesium sulfate and evaporated to dryness. The residue was then purified by column chromatography on silica gel with hexane as eluent to yield a white solid (1.65 g, 80% yield). ^{1}H NMR (300 MHz, $CDCl_3$): δ 7.46 – 7.40 (m, 4H, H2), 7.21 – 7.16 (m, 4H, H3). ^{13}C NMR (100-MHz, $CDCl_3$): δ 134.7 C_q, 132.7 C2, 132.6 C3,

121.7 C_q. LRMS (EI+): *m/z* (%) 344 (100) $[M]^+$, 265 (44) $[M-Br+2H]^+$, 184 (62) $[M-2Br]^+$. HRMS (EI+) calculated for $C_{12}H_8Br_2S$ $[M]^+$ 341.8713, found 341.8716. FTIR (film): ν_{max} 3066 (m), 2934 (w), 1893 (m), 1779 (w), 1646 (w), 1553 (w), 1467 (s), 1391 (m), 1348 (w), 1235 (w), 1104 (w), 1079 (m), 1066 (s), 1005 (s), 955 (m), 805 (s), 724 (s), 692 (m), 625 (m).

5.1.13. Synthesis of ligand $L^{S\text{-}OMe}$

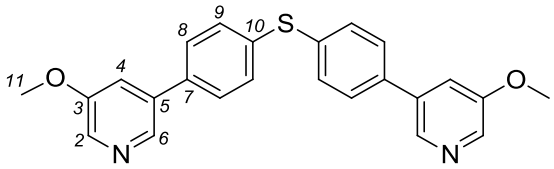

$L^{S\text{-}OMe}$

$C_{24}H_{20}N_2O_2S$

FW: 400.49

The title compound was prepared according to the *General Suzuki Coupling Procedure* with (5-methoxypyridin-3-yl)boronic acid (0.60 g, 3.92 mmol) and bis(4-bromophenyl)sulfide (0.61 g, 1.78 mmol). Purification by column chromatography on silica gel with ethyl acetate as eluent yielded a white solid (0.33 g, 46%). ^{1}H NMR (300 MHz, $CDCl_3$): δ 8.45 (d, J = 1.8 Hz, 2H, H6), 8.31 (d, J = 2.8 Hz, 2H, H2), 7.59 – 7.52 (m, 4H, H8), 7.52 – 7.45 (m, 4H, H9), 7.35 (dd, J = 2.8, 1.8 Hz, 2H, H4), 3.93 (s, 6H, H11). ^{13}C NMR (100 MHz, $CDCl_3$): δ 156.0 C_q, 140.7 C6, 136.8 C_q, 136.6 C_q, 136.5 C2, 136.0 C_q, 131.8 C9, 128.2 C8, 119.1 C4, 55.8 C11. LRMS (ES+): *m/z* (%) 401.3 (38) $[M+H]^+$, 423.3 (100) $[M+Na]^+$. HRMS (ES+) calculated for $C_{24}H_{20}N_2O_2SNa$ $[M+Na]^+$ 423.1143, found 423.1153. FTIR (film): ν_{max} 3038 (w), 2968 (w), 2845 (w), 1789 (w), 1578 (s), 1547 (w), 1495 (m),

1426 (s), 1391 (m), 1314 (s), 1218 (s), 1188 (m), 1157 (m), 1090 (m), 1063 (m), 1017 (m), 967 (w), 910 (w), 881 (m), 874 (m), 834 (m), 817 (s), 757 (w), 707 (s), 653 (m), 582 (s).

5.1.14. Synthesis of $[Pd_2L^{S\text{-}OMe}{}_4][BF_4]_4$

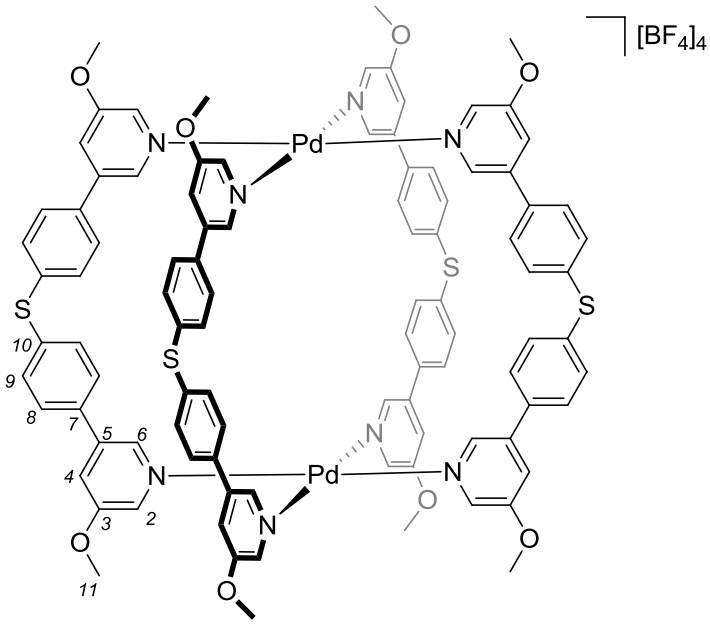

$[Pd_2(C_{24}H_{20}N_2O_2S)_4][BF_4]_4$

FW: 2160.32

The title compound was prepared according to the *General Tetrafluoroborate Tetra-Stranded Palladium(II) Cylinder Procedure* with ligand $\mathbf{L^{S\text{-}OMe}}$ (28.9 mg, 0.076 mmol) to yield a white solid (20.0 mg, 49% yield). ^{1}H NMR (300 MHz, CD_3CN): δ 8.96 (d, J = 1.6 Hz, 8H, H6), 8.82 (d, J = 2.4 Hz, 8H, H2), 7.71 (dd, J = 2.4, 1.6 Hz, 8H, H4), 7.64 – 7.59 (m, 16H, H8), 7.55 – 7.51 (m, 16H, H9), 4.01 (s, 24H, H11). ^{19}F NMR (282 MHz, CD_3CN): δ -150.67 (s, br, 10F). LRMS (ES+): *m/z* (%) 612.1 (27) $[Pd_2L^{S\text{-}OMe}{}_4(BF_4)]^{3+}$, 725.0 (43) $[Pd_2L^{OMe}{}_3F_2]^{2+}$. FTIR (film): ν_{max} 3094 (w), 1591 (s), 1499 (w), 1452 (m), 1440 (m), 1394 (w), 1321 (m), 1269 (w),

1226 (s), 1188 (w), 1153 (m), 1056 (s), 1032 (s), 1005 (s), 878 (m), 820 (s), 778 (w), 698 (s), 607 (m), 577 (m). UV-Vis (DMSO): λ_{max} (ε_{max}/dm^{3}mol^{-1}cm^{-1}) 303 (109 500) nm.

5.1.15. Synthesis of $[Pd_2L^{OMe}_4][NO_3]_4$

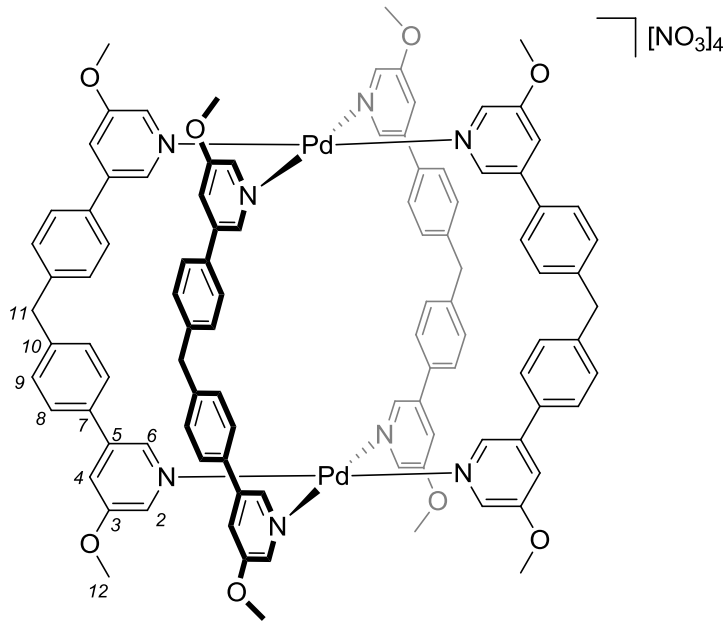

$[Pd_2(C_{25}H_{22}N_2O_2)_4][NO_3]_4$

FW: 1988.43

The title compound was prepared according to the *General Tetrafluoroborate Tetra-Stranded Palladium(II) Cylinder Procedure* with precipitation occurring with a saturated solution of tetrabutylammonium nitrate. The white solid was washed with acetonitrile (10 mL) and diethyl ether (50 mL) and dried in vacuo (29.0 mg, 76% yield). Alternatively, excess tetrabutylammonium nitrate was added to a solution of pure **$[Pd_2L^{OMe}_4][BF_4]_4$** in acetonitrile to precipitate the nitrate salt of the complex. The solid was washed with acetonitrile (2 mL) and diethyl ether (10 mL) and dried in vacuo. ^{1}H NMR (300 MHz, DMSO-d_6): δ 9.32 (s br, 2H, H6), 8.99 (d, J = 2.4 Hz,

2H, H2), 7.90 (s br, 2H, H4), 7.64 – 7.62 (m, 4H, H8), 7.37 – 7.34 (m, 4H, H9), 4.16 (s, 2H, H11), 4.00 (s, 6H, H12). FTIR (film): ν_{max} 3072 (w), 1588 (s), 1517 (w), 1456 (m), 1438 (m), 1391 (m), 1317 (s), 1265 (w), 1225 (s), 1187 (w), 1153 (m), 1070 (w), 1033 (s), 1005 (s), 886 (m), 811 (s), 798 (s), 700 (s), 626 (m), 578 (m). UV-Vis (DMSO): λ_{max} (ε_{max}/dm^{3}mol^{-1}cm^{-1}) 291 (63 600), 264 (70 800) nm.

5.1.16. Synthesis of $[Pd_2L^{OMe}{}_4][CF_3SO_3]_4$

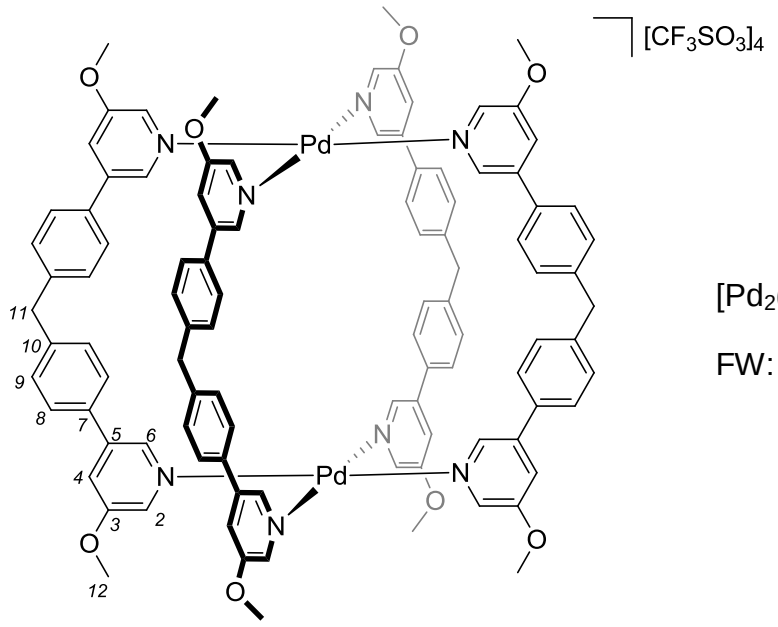

$[Pd_2(C_{25}H_{22}N_2O_2)_4][CF_3SO_3]_4$

FW: 2336.29

The title compound was prepared according to the *General Tetrafluoroborate Tetra-Stranded Palladium(II) Cylinder Procedure* with precipitation occurring with a saturated solution of tetrabutylammonium trifluoromethanesulfonate. The white solid was washed with acetonitrile (10 mL) and diethyl ether (50 mL) and dried in vacuo (21.7 mg, 67% yield). Alternatively, excess tetrabutylammonium trifluoromethanesulfonate was added to a solution of pure **$[Pd_2L^{OMe}{}_4][BF_4]_4$** in

acetonitrile to precipitate the nitrate salt of the complex. The solid was washed with acetonitrile (2 mL) and diethyl ether (10 mL) and dried in vacuo. ^{1}H NMR (300 MHz, CD_3CN): δ 8.93 (s br, 2H, H6), 8.90 (d, J = 2.4 Hz, 2H, H2), 7.69 (dd, J = 2.4, 1.7 Hz, 2H, H4), 7.48 – 7.46 (m, 4H), 7.32 – 7.29 (m, 4H), 4.13 (s, 2H), 4.00 (s, 6H). LRMS (ES+): *m/z* (%) 630.3 (100) $[Pd_2L^{OMe}{}_4(CF_3SO_3)]^{3+}$, 1019.9 (87) $[Pd_2L^{OMe}{}_4(CF_3SO_3)_2]^{2+}$. FTIR (film): ν_{max} 3086 (w), 1590 (m), 1518 (w), 1464 (m), 1441 (m), 1404 (m), 1333 (m), 1320 (m), 1269 (m), 1244 (s), 1224 (s), 1155 (s), 1027 (s), 1006 (s), 880 (w), 850 (w), 814 (m), 799 (m), 760 (w), 699 (m), 636 (s). UV-Vis (CH_3CN): λ_{max} (ε_{max}/$dm^3mol^{-1}cm^{-1}$) 293 (63 300), 231 (172 200) nm.

5.1.17. General Deprotection Procedure

Ethanethiol (74.27 mmol) was added to aluminium chloride (8.63 mmol) in dry dichloromethane (10 mL) in a cooling ice-salt bath. Ligand $\mathbf{L^{X\text{-}OMe}}$ (0.52 mmol) dissolved in dry dichloromethane (10 mL) was then added dropwise to the slurry mixture to form a red solution. The reaction mixture remained in the cooling bath for one hour and was then left to warm to room temperature for two days. The reaction was quenched with water and neutralized with sodium hydroxide. The crude mixture was evaporated under reduce pressure. The residue was then purified by column chromatography on silica gel.

5.1.18. Synthesis of L^{OH}

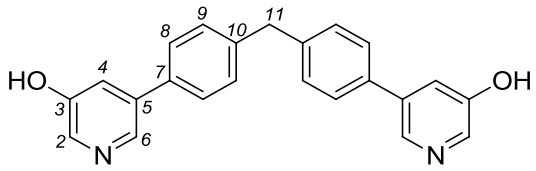

L^{OH}

$C_{23}H_{18}N_2O_2$

FW: 354.40

The title compound was prepared according to the *General Deprotection Procedure* with ligand L^{OMe} (0.20 g, 0.52 mmol). Purification by column chromatography on silica gel with ethyl acetate:methanol (9:1) as eluent yielded a yellow solid (0.12 g, 62% yield). ^{1}H NMR (300 MHz, MeOD): δ 8.25 (d, J = 1.9 Hz, 2H, H6), 8.05 (d, J = 2.6 Hz, 2H, H2), 7.60 – 7.53 (m, 4H, H8), 7.44 (dd, J = 2.6, 1.9 Hz, 2H, H4), 7.39 – 7.33 (m, 4H, H9), 4.09 (s, 2H, H11). ^{1}H NMR (300 MHz, DMSO-d_6): δ 10.33 (s br, 2H, OH), 8.29 (d, J = 1.8 Hz, 2H, H6), 8.14 (d, J = 2.6 Hz, 2H, H2), 7.59 – 7.57 (m, 4H, H8), 7.44 – 7.41 (m, 2H, H4), 7.39 – 7.36 (m, 4H, H9), 4.03 (s, 2H, H11). ^{13}C NMR (100 MHz, DMSO-d_6): δ 154.0 C_q, 141.1 C_q, 138.2 C6, 136.8 C2, 136.1 C_q, 135.0 C_q, 129.4 C9, 127.0 C8, 119.8 C4, 42.3 C11. LRMS (ES+): *m/z* (%) 355.3 (100) $[M+H]^+$, 356.3 (11) $[M+2H]^+$, 377.3 (11) $[M+Na]^+$. HRMS (ES+) calculated for $C_{23}H_{19}N_2O_2$ $[M+H]^+$ 355.1447, found 355.1440. FTIR (film): ν_{max} 3029 (w), 2918 (w), 1734 (w), 1584 (s), 1515 (m), 1440 (s), 1401 (s), 1322 (m), 1302 (s), 1145 (s), 1018 (m), 908 (m), 854 (m), 811 (s), 792 (s), 747 (w), 705 (w).

5.1.19. Synthesis of $[Pd_2L^{OH}_4][BF_4]_4$

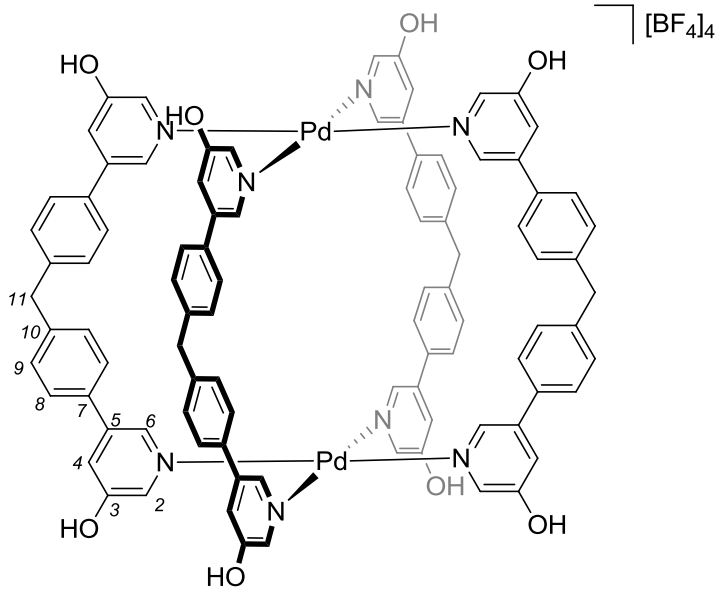

$[Pd_2(C_{23}H_{18}N_2O_2)_4][BF_4]_4$

FW: 1976.37

The title compound was prepared according to the *General Tetrafluoroborate Tetra-Stranded Palladium(II) Cylinder Procedure* with ligand **L^{OH}** (28.9 mg, 0.076 mmol) to yield a white solid (26.0 mg, 70% yield). ^{1}H NMR (300 MHz, DMSO-d_6): δ 11.39 (s br, 8H, OH), 8.89 (s br, 8H, H6), 8.80 – 8.79 (m, 8H, H2), 7.60 (s br, 8H, H4), 7.45 – 7.41 (m, 16H, H8), 7.33 – 7.30 (m, 16H, H9), 4.13 (s, 8H, H11). LRMS (ES+): *m/z* (%) 659.9 (30) $[Pd_2L^{OH}_3+F_2]^{2+}$, 870.9 (5) $[Pd_2L^{OH}_4+BF_4+F]^{2+}$. FTIR (film): ν_{max} 3088 (w), 1590 (s), 1517 (w), 1482 (m), 1444 (s), 1403 (m), 1337 (m), 1300 (w), 1225 (w), 1152 (m), 1052 (s), 1029 (s), 999 (s), 921 (m), 875 (w), 856 (w), 799 (s), 763 (w), 699 (s), 623 (m). UV-Vis (DMSO): λ_{max} (ε_{max}/dm^{3}mol^{-1}cm^{-1}) 306 (48 900) nm.

5.1.20. Synthesis of $L^{O\text{-}OH}$

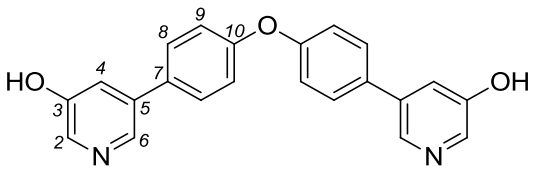

$L^{O\text{-}OH}$

$C_{22}H_{16}N_2O_3$

FW: 356.37

The title compound was prepared according to the *General Deprotection Procedure* with ligand $L^{O\text{-}OMe}$ (0.20 g, 0.52 mmol). Purification by column chromatography on silica gel with ethyl acetate:methanol (9:1) as eluent yielded a yellow solid (0.13 g, 72% yield). ^{1}H NMR (300 MHz, MeOD): δ 8.31 (s br, 2H, H6), 8.08 (d, J = 1.8 Hz, 2H, H2), 7.72 – 7.64 (m, 4H, H8), 7.51 (dd, J = 2.5, 1.8 Hz, 2H, H4), 7.21 – 7.14 (m, 4H, H9). ^{13}C NMR (75 MHz, MeOD): δ 158.9 C_q, 156.2 C_q, 139.1 C_q, 138.7 C6, 136.4 C2, 133.8 C_q, 129.8 C8, 122.8 C4, 120.6 C9. LRMS (ES+): *m/z* (%) 357.3 (100) $[M+H]^+$, 358.3 (6) $[M+2H]^+$, 379.3 (2) $[M+Na]^+$. HRMS (ES+) calculated for $C_{22}H_{17}N_2O_3$ $[M+H]^+$ 357.1239, found 357.1232. FTIR (film): ν_{max} 3063 (w), 2924 (w), 1582 (s), 1506 (s), 1492 (s), 1443 (s), 1397 (m), 1310 (s), 1261 (s), 1216 (s), 1170 (m), 1149 (m), 1104 (m), 1059 (w), 1029 (m), 1013 (m), 909 (m), 850 (s), 827 (s), 784 (m), 716 (s), 698 (s), 624 (m), 595 (m).

5.1.21. Synthesis of $[Pd_2L^{O\text{-}OH}{}_4][BF_4]_4$

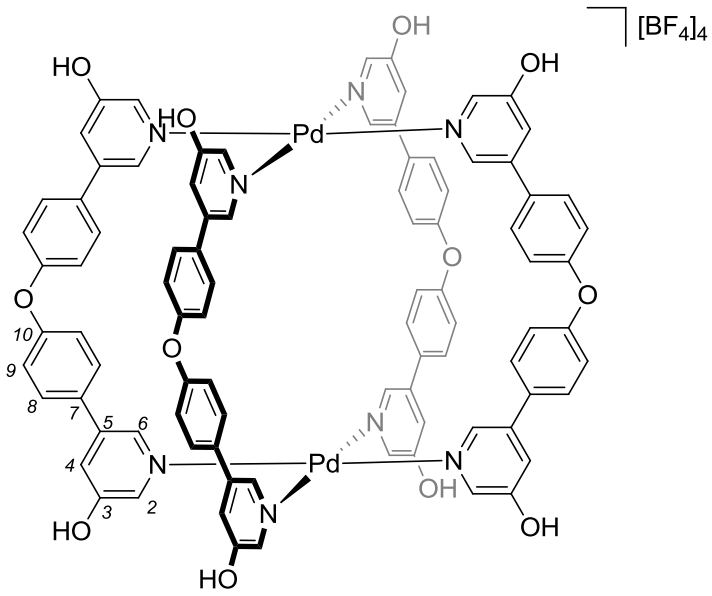

$[Pd_2(C_{22}H_{16}N_2O_3)_4][BF_4]_4$

FW: 1984.28

The title compound was prepared according to the *General Tetrafluoroborate Tetra-Stranded Palladium(II) Cylinder Procedure* with ligand **$L^{O\text{-}OH}$** (28.9 mg, 0.076 mmol) to yield a white solid (27.0 mg, 72% yield). ^{1}H NMR (300 MHz, MeOD): δ 9.19 (d, J = 1.4 Hz, 8H, H6), 8.75 (d, J = 2.3 Hz, 8H, H2), 7.67 – 7.64 (m, 16H, H8), 7.60 (dd, J = 2.3, 1.4 Hz, 8H, H4), 7.23 – 7.16 (m, 16H, H9). LRMS (ES+): *m/z* (%) 409.7 (21) $[Pd_2L^{O\text{-}OH}{}_4\text{-H}]^{4+}$, 662.9 (100) $[Pd_2L^{O\text{-}OH}{}_3\text{+F}_2]^{2+}$, 840.9 (26) $[Pd_2L^{O\text{-}OH}{}_4\text{+F}_2]^{2+}$. FTIR (film): ν_{max} 3072 (w), 1593 (s), 1504 (s), 1447 (s), 1401 (m), 1338 (m), 1282 (w), 1227 (s), 1177 (s), 1153 (s), 1051 (s), 1025 (s), 1011 (s), 923 (m), 872 (m), 850 (w), 829 (s), 697 (m), 600 (m).

5.1.22. Synthesis of L^{NH-OH}

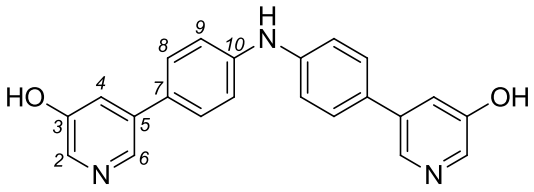

L^{NH-OH}

$C_{22}H_{17}N_3O_2$

FW: 355.39

The title compound was prepared according to the *General Deprotection Procedure* with ligand L^{NH-OMe} (0.20 g, 0.52 mmol). Purification by column chromatography on silica gel with ethyl acetate:methanol (9:1) as eluent yielded a yellow solid (0.01 g, 5% yield). ^{1}H NMR (300 MHz, MeOD): δ 8.26 (d, J = 2.0 Hz, 2H, H6), 8.00 (d, J = 2.6 Hz, 2H, H2), 7.58 – 7.53 (m, 4H, H8), 7.44 (dd, J = 2.6, 2.0 Hz, 2H, H4), 7.29 – 7.24 (m, 4H, H9). ^{1}H NMR (300 MHz, DMSO-d_6): δ 10.72 (s br, 2H, OH), 8.80 (s br, 1H, NH), 8.46 (d, J = 1.6 Hz, 2H, H6), 8.16 (d, J = 2.5 Hz, 2H, H2), 7.74 – 7.58 (m, 6H, H8 & H4), 7.27 – 7.24 (m, 4H, H9). ^{13}C NMR (100 MHz, DMSO-d_6): δ 156.4 C_q, 144.1 C_q, 139.4 C_q, 130.6 C6, 128.3 C8, 127.9 C_q, 126.6 C2, 125.3 C4, 117.4 C9. LRMS (ES+): *m/z* (%) 356.3 (100) $[M+H]^+$, 378.4 (6) $[M+Na]^+$. HRMS (ES+) calculated for $C_{22}H_{18}N_3O_2$ $[M+H]^+$ 356.1399, found 356.1393. FTIR (film): ν_{max} 3285 (w), 2943 (w), 1592 (s), 1564 (m), 1478 (s), 1369 (s), 1348 (s), 1224 (s), 1193 (s), 1003 (m), 907 (m), 809 (s), 705 (m), 656 (s), 593 (s).

5.1.23. General Mitsunobu Coupling Procedure

To a solution of 3-bromo-5-hydroxypyridine (5.75 mmol) in dry THF (70 mL) cooled in an ice bath, 1,1'-(azodicarbonyl)-dipiperidine (8.62 mmol) in THF (30 mL), tri-*n*-butylphosphine (8.62 mmol) and primary alcohol (6.90 mmol) were added under an argon atmosphere. After one hour of stirring, the ice bath was removed and the reaction was stirred at room temperature overnight. The resulting mixture was added to a saturated aqueous solution of sodium bicarbonate and ethyl acetate. The two layers were extracted and the organic layer was washed with water (50 mL) and brine (50 mL), dried over sodium sulfate and evaporated under reduce pressure. The crude residue was then purified by column chromatography.

5.1.24. Synthesis of 3-bromo-5-(2-(2-methoxyethoxy)ethoxy)pyridine (5)

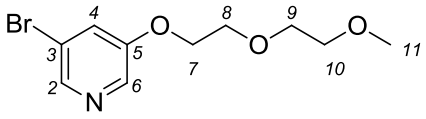

$C_{10}H_{14}BrNO_3$

FW: 276.13

5

The title compound was prepared according to the *General Mitsunobu Coupling Procedure* with 2-(2-methoxyethoxy)ethanol (0.81 mL, 6.90 mmol). Purification by column chromatography on silica gel with ethyl acetate:hexane (9:1) as eluent yielded a yellow oil (1.42 g, 90% yield). ^{1}H NMR (300 MHz, $CDCl_3$): δ 8.28 (d, J = 1.9 Hz, 1H, H2), 8.25 (d, J = 2.5 Hz, 1H, H6), 7.40 (dd, J = 2.5, 1.9 Hz, 1H, H4), 4.18 (dd, J = 5.4, 4.0 Hz, 2H, H7), 3.87 (dd, J = 5.4, 4.0 Hz, 2H, H8), 3.75 – 3.68 (m, 2H, H9), 3.61 – 3.55 (m, 2H, H10), 3.39 (s, 3H, H11). ^{13}C NMR (100 MHz,

$CDCl_3$): δ 155.5 C_q, 143.3 C2, 136.8 C6, 124.4 C4, 120.4 C_q, 72.1 C10, 71.0 C9, 69.7 C8, 68.4 C7, 59.3 C11. LRMS (ES+): *m/z* (%) 276.1 (5) $[M]^+$, 278.1 (5) $[M+2H]^+$, 298.1 (100) $[M+Na]^+$, 300.1 (98) $[M+Na+2H]^+$. HRMS (ES+) calculated for $C_{10}H_{14}NO_3BrNa$ $[M+Na]^+$ 298.0055, found 298.0048. FTIR (film): ν_{max} 2933 (w), 2876 (w, br), 2828 (w), 1574 (s), 1555 (m), 1445 (m), 1430 (s), 1356 (w), 1310 (m), 1262 (s), 1221 (m), 1107 (s), 1053 (m), 1008 (s), 937 (m), 858 (s), 695 (s), 611 (m).

5.1.25. General Pyridine Boronate Ester Procedure

3-bromo pyridine (2.09 mmol), bis(pinacolato)diboron (2.51 mmol), [1,1'-bis(diphenylphosphino)ferrocene]dichloropalladium(II) complex with dichloromethane (0.063 mmol) and potassium acetate (6.28 mmol) in dry DMF (2 mL) were heated to 160 ºC under an argon atmosphere for 1 hour. The reaction mixture was concentrated and tert-butyl methyl ether was added to produce a brown precipitate which was filtered. The filtrate was concentrated to yield a red-brown oil, which was used in the next reaction step without further purification.

5.1.26. Synthesis of 3-(2-(2-methoxyethoxy)ethoxy)-5-(4,4,5,5-tetramethyl-1,3,2-dioxaborolan-2-yl)pyridine (6)

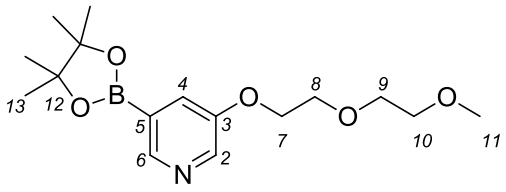

$C_{16}H_{26}BNO_5$

FW: 323.19

6

The title compound was prepared according to the *General Pyridine Boronate Ester Procedure* with 3-bromo-5-(2-(2-methoxyethoxy)ethoxy)pyridine **5** (0.58 g, 2.09 mmol). ^{1}H NMR (300 MHz, $CDCl_3$): δ 8.54 (d, J = 1.2 Hz, 1H, H6), 8.39 (d, J = 3.1 Hz, 1H, H2), 7.56 (dd, J = 3.1, 1.2 Hz, 1H, H4), 4.20 (dd, J = 5.4, 4.2 Hz, 2H, H7), 3.87 (dd, J = 5.4, 4.2 Hz, 2H, H8), 3.76 – 3.68 (m, 2H, H9), 3.64 – 3.53 (m, 2H, H10), 3.39 (s, 3H, H11), 1.34 (s, 12H, H13). ^{13}C NMR (100 MHz, $CDCl_3$): δ 154.6 C_q, 148.1 C_q, 146.5 C6, 141.5 C2, 126.1 C4, 84.4 C_q, 72.1 C7, 71.0 C8, 69.8 C9, 67.9 C10, 59.25 C11, 25.0 C13. LRMS (ES+): *m/z* (%) 324.2 (40) $[M+H]^+$, 346.2 (100) $[M+Na]^+$. HRMS (ES+) calculated for $C_{16}H_{26}NO_5Na^{11}B$ $[M+Na]^+$ 346.1802, found 346.1813. FTIR (film): ν_{max} 2977 (m), 2930 (w), 2878 (w), 1578 (w), 1518 (w), 1453 (m), 1420 (m), 1360 (m), 1301 (m), 1254 (m), 1141 (s), 1108 (s), 1053 (m), 1025 (m), 971 (m), 883 (w), 849 (m), 803 (w), 743 (w), 713 (m), 675 (m), 578 (w).

5.1.27. Synthesis of $L^{O\text{-}Glycol}$

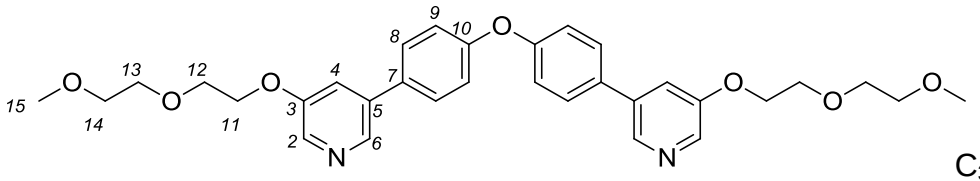

$L^{O\text{-}Glycol}$

$C_{32}H_{36}N_2O_7$

FW: 560.64

The title compounds was prepared according to the *General Suzuki Coupling Procedure* with 3-(2-(2-methoxyethoxy)ethoxy)-5-(4,4,5,5-tetramethyl-1,3,2-dioxaborolan-2-yl)pyridine **6** (1.27 g, 3.92 mmol) and bis(4-bromophenyl) ether (0.58 g, 1.78 mmol). Purification by column chromatography on silica gel with ethyl acetate:methanol (9:1) as eluent yielded a white solid (0.62 g, 70% yield). ^{1}H NMR (300 MHz, $CDCl_3$): δ 8.45 (d, J = 1.8 Hz, 2H, H6), 8.30 (d, J = 2.7 Hz, 2H, H2), 7.63 – 7.52 (m, 4H, H8), 7.40 (dd, J = 2.7, 1.8 Hz, 2H, H4), 7.20 – 7.10 (m, 4H, H9), 4.27 (dd, J = 5.4, 4.1 Hz, 4H, H11), 3.91 (dd, J = 5.4, 4.1 Hz, 4H, H12), 3.80 – 3.71 (m, 4H, H13), 3.65 – 3.55 (m, 4H, H14), 3.40 (s, 6H, H15). ^{13}C NMR (100 MHz, $CDCl_3$): δ 157.4 C_q, 155.3 C_q, 140.8 C6, 136.7 C_q, 136.5 C2, 133.1 C_q, 128.8 C8, 120.0 C4, 119.6 C9, 72.1 C14, 71.0 C13, 69.8 C12, 68.1 C11, 59.2 C15. LRMS (ES+): *m/z* (%) 583.3 (100) $[M+Na]^+$. HRMS (ES+) calculated for $C_{32}H_{36}N_2O_7Na$ $[M+Na]^+$ 583.2420, found 583.2432. FTIR (film): ν_{max} 2877 (m), 2816 (w),, 1910 (w), 1582 (m), 1509 (m), 1455 (w), 1434 (m), 1397 (m), 1314 (m), 1276 (m), 1261 (m), 1243 (m), 1221 (m), 1201 (m), 1130 (s), 1111 (s), 1054 (m), 1015 (w), 966 (w), 940 (m), 914 (w), 876 (m), 834 (s), 829 (s), 709 (m), 693 (m), 604 (m), 589 (m).

5.1.28. Synthesis of $[Pd_2L^{O\text{-}Glycol}{}_4][(BF_4)_4]$

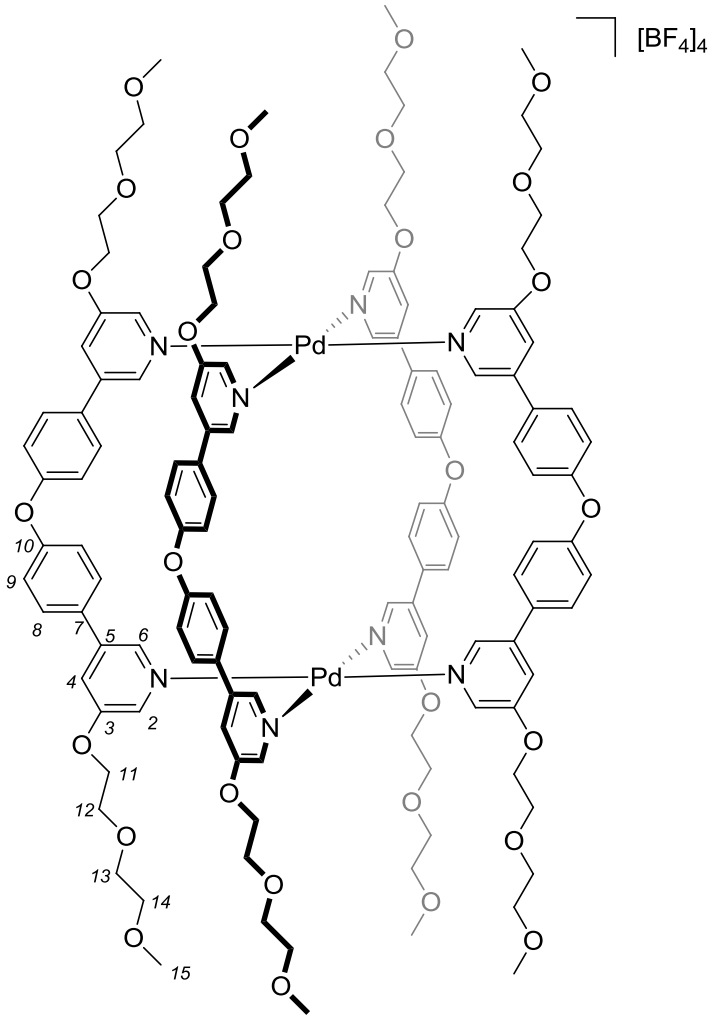

$[Pd_2(C_{32}H_{36}N_2O_7)_4][BF_4]_4$

FW: 2800.83

The title compound was prepared according to the *General Tetrafluoroborate Tetra-Stranded Palladium(II) Cylinder Procedure* with ligand $\mathbf{L^{O\text{-}Glycol}}$ (42.4 mg, 0.076 mmol) to yield a white solid (37 mg, 70% yield). ^{1}H NMR (300 MHz, CD_3CN): δ 9.02 (s br, 8H, H6), 8.85 (d, *J* = 2.3 Hz, 8H, H2), 7.79 – 7.71 (m, 8H, H4), 7.69 – 7.57 (m, 16H, H8), 7.34 – 7.20 (m, 16H, H9), 4.37 – 4.35 (m, 16H, H11), 3.91 – 3.80 (m, 16H, H12), 3.70 – 3.58 (m, 16H, H13), 3.54 – 3.42 (m, 16H, H14), 3.25 (s, 24H, H15). ^{19}F NMR (282 MHz, CD_3CN): δ -150.87 (s, 2F), -150.92

(s, 8F). LRMS (ES+): *m/z* (%) 561.4 (19) $[L^{O\text{-}Glycol}]^+$, 583.4 (34) $[L^{O\text{-}Glycol}+Na]^+$, 847.1 (52) $[Pd_2L^{O\text{-}Glycol}{}_4(BF_4)]^{3+}$, 1314.6 (100) $[Pd_2L^{O\text{-}Glycol}{}_4(BF_4)_2]^{2+}$. FTIR (film): ν_{max} 3088 (w), 2878 (w), 1591 (s), 1508 (s), 1446 (s), 1403 (m), 1323 (m), 1283 (w), 1245 (s), 1223 (s), 1180 (w), 1158 (w), 1057 (s), 1035 (s), 1012 (s), 956 (w), 875 (w), 833 (s), 799 (w), 699 (s), 599 (w). UV-Vis (MeOH): λ_{max} (ε_{max}/$dm^3mol^{-1}cm^{-1}$) 293 (75 500), 245 (98 400) nm.

5.1.29. Synthesis of 3-bromo-5-(2-(pyrrolidin-1-yl)ethoxy)pyridine (7)

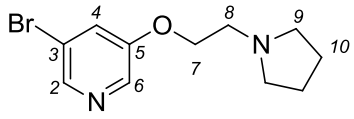

$C_{11}H_{15}BrN_2O$

FW: 271.15

7

The title compound was prepared according to the *General Mitsunobu Coupling Procedure* with 1-(2-hydroxyethyl)pyrrolidine (0.81 mmol, 6.90 mmol). Purification by column chromatography on neutral aluminium oxide with ethyl acetate as eluent yielded a yellow oil (0.92 g, 59% yield). ^{1}H NMR (300 MHz, $CDCl_3$): δ 8.27 (d, J = 1.9 Hz, 1H, H2), 8.26 (d, J = 2.5 Hz, 1H, H6), 7.38 (dd, J = 2.5, 1.9 Hz, 1H, H4), 4.13 (t, J = 5.8 Hz, 2H, H7), 2.91 (t, J = 5.8 Hz, 2H, H8), 2.71 – 2.55 (m, 4H, H9), 1.88 – 1.77 (m, 4H, H10). ^{13}C NMR (100 MHz, $CDCl_3$): δ 155.5 C_q, 143.2 C2, 136.7 C6, 124.2 C4, 120.5 C_q, 68.1 C7, 54.9 C9, 54.9 C8, 23.7 C10. LRMS (ES+): *m/z* (%) 271.2 (100) $[M]^+$, 273.2 (93) $[M+2H]^+$. HRMS (ES+) calculated for $C_{11}H_{16}N_2OBr$ $[M+H]^+$ 271.0446, found 271.0440. FTIR (film): ν_{max} 2962 (w), 1668 (m), 1575 (s), 1557 (s), 1429 (s), 1311 (s), 1264 (s), 1222 (m), 1166 (m), 1140 (w), 1010 (m), 863 (m), 697 (s).

5.1.30. Synthesis of 3-(2-(pyrrolidin-1-yl)ethoxy)-5-(4,4,5,5-tetramethyl-1,3,2-dioxaborolan-2-yl)pyridine (8)

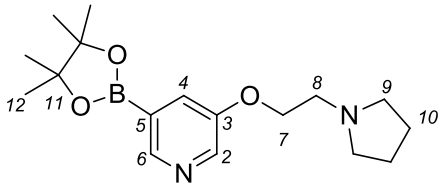

$C_{17}H_{27}BN_2O_3$

FW: 318.22

8

The title compound was prepared according to the *General Pyridine Boronate Ester Procedure* with 3-bromo-5-(2-(pyrrolidin-1-yl)ethoxy)pyridine **7** (0.57 g, 2.09 mmol). ^{1}H NMR (300 MHz, $CDCl_3$): δ 8.54 (d, J = 1.2 Hz, 1H, H6), 8.39 (d, J = 3.1 Hz, 1H, H2), 7.55 (dd, J = 3.1, 1.2 Hz, 1H, H4), 4.17 (t, J = 5.8 Hz, 2H, H7), 2.93 (t, J = 5.8 Hz, 2H, H8), 2.76 – 2.57 (m, 4H, H9), 1.92 – 1.77 (m, 4H, H10), 1.35 (s, 12H, H12). ^{13}C NMR (100 MHz, $CDCl_3$): δ 154.6 C_q, 147.9 C6, 141.2 C2, 126.2 C4, 84.4 C_q, 83.1 C_q, 67.3 C7, 54.9 C8, 54.7 C9, 25.0 C12, 23.6 C10. LRMS (ES+): *m/z* (%) 319.3 (76) $[M+H]^+$, 341.2 (100) $[M+Na]^+$. HRMS (ES+) calculated for $C_{17}H_{27}N_2O_3Na^{11}B$ $[M+Na]^+$ 341.2012, found 341.2020. FTIR (film): ν_{max} 2975 (m), 1577 (w), 1518 (w), 1474 (m), 1454 (s), 1362 (s), 1273 (m), 1145 (s), 1097 (w), 1035 (m), 981 (m), 882 (w), 850 (m), 805 (w), 714 (m), 675 (s), 578 (w).

5.1.31. Synthesis of $L^{O\text{-}Pyrr}$:

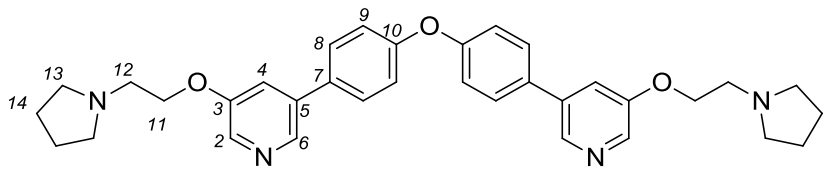

$C_{34}H_{38}N_4O_3$

FW: 550.69

$L^{O\text{-}Pyrr}$

The title compounds was prepared according to the *General Suzuki Coupling Procedure* with 3-(2-(pyrrolidin-1-yl)ethoxy)-5-(4,4,5,5-tetramethyl-1,3,2-dioxaborolan-2-yl)pyridine **8** (1.25 g, 3.92 mmol) and bis(4-bromophenyl) ether (0.58 g, 1.78 mmol). Purification by column chromatography on activated neutral aluminium oxide with ethyl acetate:acetone:methanol (8:1.5:0.5) as eluent yielded a white solid (0.52 g, 53% yield). ^{1}H NMR (300 MHz, $CDCl_3$): δ 8.45 (d, *J* = 1.8 Hz, 2H, H6), 8.30 (d, *J* = 2.7 Hz, 2H, H2), 7.60 – 7.54 (m, 4H, H8), 7.40 (dd, *J* = 2.7, 1.8 Hz, 2H, H4), 7.19 – 7.11 (m, 4H, H9), 4.23 (t, *J* = 5.8 Hz, 4H, H11), 2.96 (t, *J* = 5.8 Hz, 4H, H12), 2.70 – 2.61 (m, 8H, H13), 1.85 – 1.81 (m, 8H, H14). ^{13}C NMR (100 MHz, $CDCl_3$): δ 157.4 C_q, 155.2 C_q, 140.7 C6, 136.8 C_q, 136.4 C2, 133.1 C_q, 128.8 C8, 119.9 C4, 119.6 C9, 67.6 C11, 55.1 C12, 54.9 C13, 23.6 C14. LRMS (ES+): *m/z* (%) 551.4 (100) $[M+H]^+$. HRMS (ES+) calculated for $C_{34}H_{39}N_4O_3$ $[M+H]^+$ 551.3022, found 551.3024. FTIR (film): ν_{max} 3039 (w), 2953 (w), 2791 (w), 1598 (m), 1582 (s), 1507 (s), 1455 (m), 1433 (s), 1396 (m), 1313 (m), 1273 (m), 1258 (s), 1241 (s), 1214 (s), 1159 (s), 1111 (m), 1014 (m), 972 (w), 924 (w), 873 (s), 833 (s), 710 (s), 617 (m), 589 (m).

5.1.32. Synthesis of 3,4'-bipyridine (9)[141]

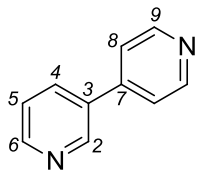

$C_{10}H_8N_2$

FW: 156.18

9

The title compounds was prepared according to the *General Suzuki Coupling Procedure* with 3-pyridinylboronic acid (0.24 g, 1.96 mmol) and 4-bromopyridine (0.35 g, 1,78 mmol). Purification by column chromatography on silica gel with ethyl acetate:methanol (9:1) as eluent yielded a yellow oil (0.27 g, 97% yield). ^{1}H NMR (300 MHz, $CDCl_3$): δ 8.88 (d, *J* = 1.7 Hz, 1H, H2), 8.76 – 8.61 (m, 3H, H9 & H6), 7.91 (ddd, *J* = 7.9, 2.3, 1.7 Hz, 1H, H4), 7.50 (dd, *J* = 4.6, 1.7 Hz, 2H, H8), 7.41 (ddd, *J* = 7.9, 4.6, 0.8 Hz, 1H, H5). ^{13}C NMR (100 MHz, $CDCl_3$): δ 150.7 C9, 150.3 C6, 148.3 C2, 145.3 C_q, 134.4 C4, 133.9 C_q, 123.9 C5, 121.7 C8. LRMS (ES+): *m/z* (%) 157.1 (100) $[M+H]^+$. HRMS (ES+) calculated for $C_{10}H_9N_2$ $[M+H]^+$ 157.0766, found 157.0763. FTIR (film): ν_{max} 2919 (w), 1596 (s), 1578 (m), 1544 (w), 1474 (m), 1425 (m), 1401 (s), 1322 (w), 1221 (w), 1191 (w), 1071 (w), 1027 (m), 1015 (m), 994 (m), 838 (m), 795 (s), 764 (m), 636 (s), 611 (m), 656 (s).

5.1.33. Synthesis of ligand $L^{N+}\cdot 2Br^-$

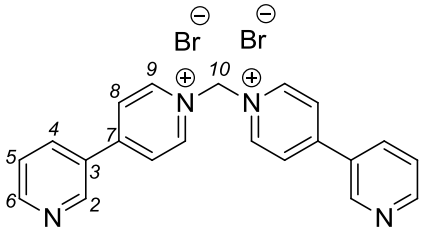

$C_{21}H_{18}N_4Br_2$

FW: 486.20

$L^{N+}\cdot 2Br^-$

3,4'-bipyridine (0.60 g, 3.86 mmol) and a 0.4 M DMF solution of dibromomethane (2.42 mL, 1.15 mmol) were stirred at 70 ºC overnight. A precipitate was formed and it was collected via filtration and washed with DMF (1 mL) and diethyl ether (20 mL) to yield an off-white solid (0.08 g, 16% yield). ^{1}H NMR (300 MHz, D_2O): δ 9.36 – 9.34 (m, 4H, H9), 9.09 (dd, *J* = 2.4, 0.8 Hz, 2H, H2), 8.76 (dd, *J* = 5.0, 1.6 Hz, 2H, H6), 8.63 – 8.55 (m, 4H, H8), 8.42 (ddd, *J* = 8.2, 2.4, 1.6 Hz, 2H, H4), 7.69 (ddd, *J* = 8.2, 5.0, 0.8 Hz, 2H, H5), 7.41 (s, 2H, H10). ^{13}C NMR (100 MHz, D_2O): δ 157.6 C_q, 152.3 C6, 148.2 C2, 145.1 C9, 137.3 C4, 129.8 C_q, 126.5 C8, 125.0 C5, 77.1 C10. LRMS (ES+): *m/z* (%) 163.1 (100) $[L^{N+}]^{2+}$, 408.1 (3) $[L^{N+}\cdot Br]^+$, 509.1 (3) $[L^{N+}\cdot Br_2+Na]^+$. HRMS (ES+) calculated for $C_{21}H_{18}N_4Na^{79}Br^{81}Br$ $[L^{N+}\cdot Br_2+Na]^+$ 508.9775, found 508.9777. FTIR (film): ν_{max} 3423 (m), 3387 (m), 3032 (m), 1636 (s), 1591 (s), 1581 (m), 1562 (m), 1473 (s), 1425 (s), 1353 (s), 1306 (m), 1184 (s), 1132 (m), 1011 (s), 848 (s), 809 (s), 765 (m), 700 (s), 628 (w), 592 (m), 554 (s).

5.1.34. Synthesis of ligand $L^{N+}\cdot 2PF_6^-$

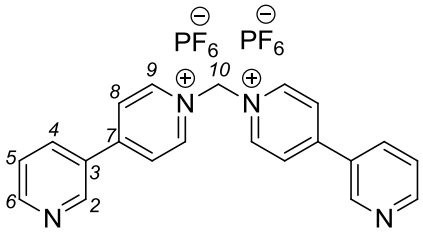

$C_{21}H_{18}N_4P_2F_{12}$

FW: 616.32

$L^{N+}\cdot 2PF_6^-$

Ligand **$L^{N+}\cdot 2Br^-$** was dissolved in the minimum amount of water and an aqueous saturated solution of ammonium hexafluorophosphate was added to precipitate a white solid. LRMS (ES+): *m/z* (%) 163.0 (100) $[L^{N+}]^{2+}$, 471.0 (53) $[L^{N+}\cdot PF_6]^+$. FTIR (film): ν_{max} 3628 (w), 3141 (w), 3078 (w), 1636 (s), 1590 (m), 1472 (m), 1419 (m), 1345 (w), 1306 (w), 1179 (s), 1129 (w), 1015 (w), 822 (s), 805 (s), 742 (s), 707 (s), 645 (w), 621 (w), 554 (s).

5.1.35. Synthesis of ligand $L^{N+}\cdot 2NO_3^-$

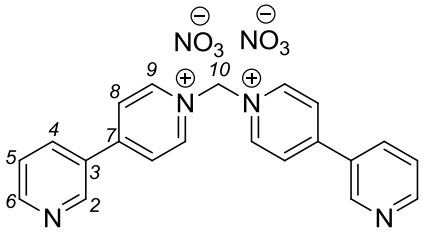

$C_{21}H_{18}N_6O_6$

FW: 450.41

$L^{N+}\cdot 2NO_3^-$

Ligand **$L^{N+}\cdot 2PF_6^-$** was dissolved in the minimum amount of acetonitrile and a saturated solution of tetrabutylammonium nitrate in acetonitrile was added to precipitate a white solid. FTIR (film): ν_{max} 3130 (w), 3050 (m), 3032 (m), 1637 (s),

1592 (m), 1580 (m), 1558 (w), 1525 (w), 1475 (m), 1421 (w), 1370 (s), 1320 (s), 1241 (w), 1193 (s), 1132 (m), 1098 (m), 1010 (m), 827 (m), 810 (s), 760 (w), 726 (w), 702 (s), 644 (w), 626 (w), 553 (s).

5.1.36. Synthesis of bis(4-iodophenyl)methane (13)[168]

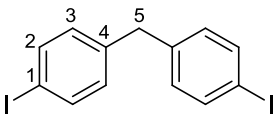

$C_{13}H_{10}I_2$

FW: 420.03

13

4,4'-Methylenedianiline (4.25 g, 21.43 mmol) was dissolved in sulfuric acid (75 mL). The brown solution was cooled to 0 - 5 ºC and sodium nitrite (4.25 g, 61.59 mmol) dissolved in water (7.5 mL) was added dropwise, maintaining the temperature below 5 ºC. When the addition was concluded, the solution was kept below 5 ºC for 30 minutes and was then slowly poured into an aqueous solution (500 mL) of potassium iodide (25.00 g, 150.60 mmol) that was preheated to 55 ºC. The resulting mixture was stirred for 1 hour at 55 ºC. After cooling, dichloromethane (250 mL) was added to the mixture. 2 M sodium hydroxide aqueous solution was then added to neutralize the mixture and a saturated aqueous sodium bisulfate solution to decolorize it. The organic phase was extracted and washed successively with 2 M HCl aqueous solution (150 mL), water (150 mL), saturated aqueous sodium bicarbonate solution (150 mL) and water (150 mL). The organic phase was then dried over magnesium sulfate and the solvent removed in vacuo. The brown oil was purified by silica column

chromatography with hexane as eluent to obtain a white solid (4.20 g, 47%). ^{1}H NMR (300 MHz, $CDCl_3$): δ 7.64 – 7.57 (m, 4H, H2), 6.94 – 6.87 (m, 4H, H3), 3.85 (s, 2H, H5). ^{13}C NMR (100 MHz, $CDCl_3$): δ 140.0 C_q, 137.7 C2, 131.0 C3, 91.7 C_q, 40.9 C5. LRMS (EI+): *m/z* (%) 166 (6) $[M-2I]^+$, 293 (13) $[M-I]^+$, 420 (100) $[M]^+$. HRMS (EI+) calculated for $C_{13}H_{10}I_2$ $[M]^+$ 419.8872, found 419.8840. FTIR (film): ν_{max} 3018 (w), 2914 (w), 2846 (w), 1903 (w), 1581 (w), 1479 (s), 1434 (m), 1395 (s), 1202 (w), 1181 (w), 1108 (w), 1057 (s), 1006 (s), 961 (w), 857 (m), 804 (s), 774 (s), 719 (w).

5.1.37. Synthesis of bis(4-((trimethylsilyl)ethynyl)phenyl)methane (12)[168]

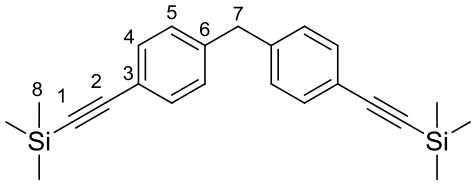

$C_{23}H_{28}Si_2$

FW: 360.64

12

Bis(4-iodophenyl)methane (4.00 g, 9.50 mmol), ethynyltrimethylsilane (3.43 mL, 24.30 mmol), palladium(II) acetate (21.3 mg, 0.10 mmol), triphenylphosphine (0.07 g, 0.29 mmol) and copper(I) iodide (18.1 mg, 0.01 mmol) were placed in a Schlenk flask and deaerated with argon. Triethylamine (50 mL) and toluene (25 mL) were added and the flask was deaerated again. The yellow solution was heated at 86 ºC for 16 hours. After the mixture was cooled to room temperature the grey precipitate that had formed was filtered off and washed with diethyl ether (100 mL). The filtrate was evaporated to yield a thick yellow oil which was

redissolved in diethyl ether (100 mL) and washed with 10 % HCl (100 mL), water (100 mL), a saturated aqueous solution of sodium bicarbonate (100 mL) and water (100 mL). The ethereal phase was dried over magnesium sulfate and concentrated to an oil that crystallized on standing. Silica column chromatography was used to purify the crude, with hexane:ethyl acetate (50:1) as eluent, to obtain a pale yellow solid (3.30 g, 97%). ^{1}H NMR (300 MHz, $CDCl_3$): δ 7.43 – 7.41 (m, 4H, H4), 7.11 – 7.08 (m, 4H, H5), 3.95 (s, 2H, H7), 0.29 (s, 18H, H8). ^{13}C NMR (100 MHz, $CDCl_3$): δ 141.2 C_q, 132.3 C4, 129.0 C5, 121.2 C_q, 105.2 C_q, 94.0 C_q, 41.8 C7, 0.2 C8. LRMS (EI+): *m/z* (%) 345 (100) $[M\text{-}CH_3]^+$, 360 (35) $[M]^+$. HRMS (EI+) calculated for $C_{23}H_{28}Si_2$ $[M]^+$ 360.1730, found 360.1749. FTIR (film): ν_{max} 3027 (w), 2957 (w), 2900 (w), 2157 (m), 1915 (w), 1605 (w), 1505 (m), 1410 (w), 1246 (m), 1221 (w), 1106 (w), 1019 (w), 9194 (w), 836 (s), 810 (s), 755 (s), 697 (m), 633 (m), 596 (m), 560 (m).

5.1.38. Synthesis of bis(4-ethynylphenyl)methane (11)[168]

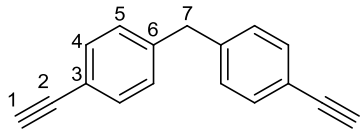

11

$C_{17}H_{12}$

FW: 216.28

A deaerated suspension of bis(4-((trimethylsilyl)ethynyl)phenyl)methane (2.80 g, 7.76 mmol) and potassium carbonate (0.86 g, 6.21 mmol) in anhydrous methanol (30 mL) and anhydrous diethyl ether (30 mL) was stirred at room temperature under argon for 16 hours. The solvent was removed in vacuo and the crude solid

was purified by silica column chromatography with hexane:ethyl acetate (15:1) as eluent to give a yellow solid (1.38 g, 82%). ^{1}H NMR (300 MHz, $CDCl_3$): δ 7.49 – 7.41 (m, 4H, H4), 7.18 – 7.09 (m, 4H, H5), 3.98 (s, 2H, H7), 3.07 (s, 2H, H1). ^{13}C NMR (100 MHz, $CDCl_3$): δ 141.5 C_q, 132.5 C4, 129.1 C5, 120.2 C_q, 83.7 C_q, 77.2 C1, 41.8 C7. LRMS (EI+): *m/z* (%) 215.1 (100) $[M-H]^+$, 216.1 (88) $[M]^+$, 217.1 (8) $[M+H]^+$. HRMS (EI+) calculated for $C_{17}H_{12}$ $[M]^+$ 216.0939, found 216.0943. FTIR (film): ν_{max} 3274 (s), 3028 (w), 2927 (w), 2106 (w), 1917 (w), 1604 (m), 1502 (s), 1444 (w), 1410 (m), 1240 (m), 1109 (m), 1019 (m), 867 (s), 819 (s), 797 (s), 758 (s).

5.1.39. General Click Reaction Procedure

A bromo derivative (5.54 mmol) and sodium azide (11.1 mmol) were stirred for 2 hours at 65 ºC in DMF (4 mL). After cooling the mixture to room temperature, copper(II) sulfate pentahydrate (1.84 mmol) dissolved in water (2 mL) was added, followed by L-ascorbic acid (1.84 mmol), sodium carbonate anhydrous (5.54 mmol), bis(4-ethynylphenyl)methane (1.84 mmol) and DMF (4 mL) were added. The resulting suspension was stirred at room temperature for 16 hours. The reaction mixture was then poured into a 0.1 M EDTA/NH_4OH solution (100 mL) and stirred vigorously for 30 minutes. The resulting white precipitate was isolated via filtration and purified as indicated.

5.1.40. Synthesis of ligand $L^{Click\text{-}Bn}$

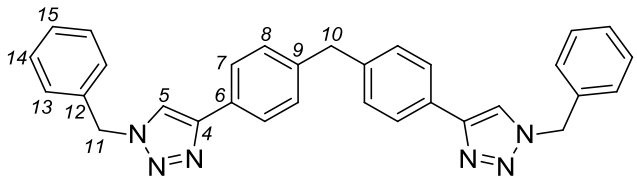

$C_{31}H_{26}N_6$

FW: 482.58

$L^{Click\text{-}Bn}$

The title compound was prepared according to the *General Click Reaction Procedure* with benzyl bromide (0.66 mL, 5.54 mmol). Purification by column chromatography on silica gel with ethyl acetate as eluent yielded a white solid (0.72 g, 81% yield). ^{1}H NMR (300 MHz, $CDCl_3$): δ 7.73 – 7.70 (m, 4H, H7), 7.62 (s, 2H, H5), 7.43 – 7.34 (m, 6H, H14 & H15), 7.32 – 7.27 (m, 4H, H13), 7.23 – 7.20 (m, 4H, H8), 5.57 (s, 4H, H11), 4.00 (s, 2H, H10). ^{13}C NMR (100 MHz, $CDCl_3$): δ 148.0 C_q, 140.9 C_q, 134.7 C_q, 129.4 C8, 129.2 C14, 128.8 C15, 128.6 C_q, 128.0 C13, 125.9 C7, 119.3 C5, 54.2 C11, 41.4 C10. LRMS (ES+): *m/z* (%) 505.3 (100) $[M+Na]^+$. HRMS (EI+) calculated for $C_{31}H_{26}N_6Na$ $[M+Na]^+$ 505.2117, found 505.2115. FTIR (film): ν_{max} 3134 (w), 3036 (w), 2910 (w), 1560 (w), 1494 (s), 1452 (s), 1436 (s), 1416 (m), 1343 (m), 1222 (s), 1208 (m), 1184 (m), 1110 (m), 1070 (s), 1049 (s), 976 (s), 915 (m), 865 (s), 815 (s), 792 (s), 704 (s), 692 (s), 665 (s), 646 (s), 634 (s), 585 (s).

5.1.41. Synthesis of ligand $L^{Click\text{-}OH}$

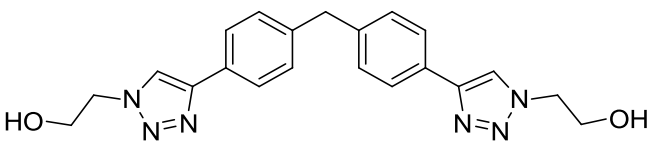

$L^{Click\text{-}OH}$

$C_{21}H_{22}N_6O_2$

FW: 390.44

The title compound was prepared according to the *General Click Reaction Procedure* with 2-bromoethanol (0.40 mL, 5.54 mmol). Purification via recrystallization in hot methanol yielded a white solid (0.55 g, 76% yield). ^{1}H NMR (300 MHz, DMSO-d_6): δ 8.48 (s, 2H, H5), 7.79 – 7.76 (m, 4H, H7), 7.34 – 7.31 (m, 4H, H8), 5.07 (t, *J* = 5.4 Hz, 2H, OH), 4.42 (t, *J* = 5.4 Hz, 4H, H11), 3.99 (s, 2H, H10), 3.81 (q, *J* = 5.4 Hz, 4H, H12). ^{13}C NMR (100 MHz, DMSO-d_6): δ 146.0 C8, 140.7 C7, 129.2 C_q, 128.8 C5, 125.3 C_q, 121.6 C_q, 59.8 C12, 52.4 C11, 39.7 C10. LRMS (ES+): *m/z* (%) 413.2 (100) $[M+Na]^+$. HRMS (ES+) calculated for $C_{21}H_{22}N_6O_2Na$ $[M+Na]^+$ 413.1702, found 413.1703. FTIR (film): ν_{max} 3292 (w, br), 3140 (w), 2926 (w), 1458 (m), 1428 (m), 1416 (m), 1357 (w), 1319 (w), 1220 (m), 1156 (m), 1077 (s), 1062 (s), 1038 (s), 977 (m), 912 (w), 866 (m), 815 (s), 791 (s), 727 (w), 666 (m), 630 (m).

5.1.42. Synthesis of ligand $L^{Click\text{-}Glycol}$

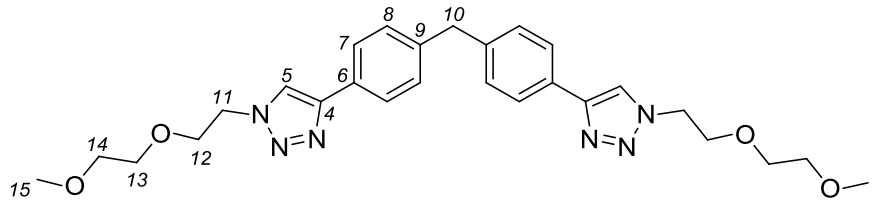

$C_{27}H_{34}N_6O_4$

FW: 506.60

$L^{Click\text{-}Glycol}$

The title compound was prepared according to the *General Click Reaction Procedure* with 1-bromo-2-(2-methoxyethoxy)ethane (0.75 mL, 5.54 mmol). Purification by column chromatography on silica gel with ethyl acetate:methanol (9:1) as eluent yielded a white solid (0.73 g, 78% yield). ^{1}H NMR (300 MHz, $CDCl_3$): δ 7.97 (s, 2H, H5), 7.78 – 7.76 (m, 4H, H7), 7.28 – 7.26 (m, 4H, H8), 4.63 – 4.57 (m, 4H, H11), 4.04 (s, 2H, H10), 3.93 – 3.87 (m, 4H, H12), 3.65 – 3.59 (m, 4H, H13), 3.56 – 3.48 (m, 4H, H14), 3.37 (s, 6H, H15). ^{13}C NMR (100 MHz, $CDCl_3$): δ 168.6 C_q, 165.0 C_q, 140.8 C_q, 129.4 C8, 125.9 C7, 120.8 C5, 71.8 C14, 70.6 C13, 69.6 C12, 59.1 C15, 50.3 C11, 41.5 C10. LRMS (ES+): *m/z* (%) 529.3 (100) $[M+Na]^+$. HRMS (ES+) calculated for $C_{27}H_{34}N_6O_4Na$ $[M+Na]^+$ 529.2539, found 529.2536. FTIR (film): ν_{max} 3141 (w), 2888 (m), 2867 (m), 2811 (w), 1499 (m), 1457 (s), 1429 (m), 1417 (m), 1348 (s), 1221 (m), 1200 (m), 1171 (m), 1102 (s), 1071 (s), 1048 (s), 1023 (s), 978 (m), 930 (m), 912 (w), 864 (m), 850 (s), 814 (m), 791 (s), 696 (m), 666 (m), 630 (s).

5.1.43. Synthesis of ligand L

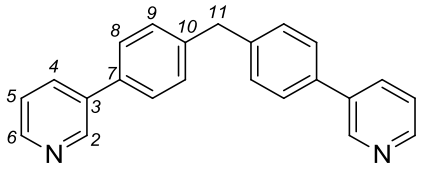

$C_{23}H_{18}N_2$

FW: 322.40

L

The title compound was prepared according to the *General Suzuki Coupling Procedure* with 3-pyridinylboronic acid (0.60 g, 3.92 mmol) and bis(4-bromophenyl)methane (0.72 g, 2.22 mmol). Purification by column chromatography on silica gel with ethyl acetate as eluent yielded a white solid (0.66 g, 92% yield). ^{1}H NMR (300 MHz, $CDCl_3$): δ 8.84 (dd, *J* = 2.3, 0.6 Hz, 2H, H2), 8.58 (dd, *J* = 4.8, 1.7 Hz, 2H, H6), 7.86 (ddd, *J* = 7.9, 2.3, 1.7 Hz, 2H, H4), 7.57 – 7.51 (m, 4H, H8), 7.40 – 7.31 (m, 6H, H5 & H9), 4.10 (s, 2H, H11). ^{13}C NMR (100 MHz, $CDCl_3$): δ 148.5 C6, 148.4 C2, 141.0 C_q, 136.5 C_q, 136.0 C_q, 134.3 C4, 129.8 C9, 127.5 C8, 123.7 C5, 41.4 C11. LRMS (ES+): *m/z* (%) 323.2 (100) $[M+H]^+$. HRMS (ES+) calculated for $C_{23}H_{19}N_2$ $[M+H]^+$ 323.1548, found 323.1546. FTIR (film): ν_{max} 3028 (w), 2916 (w), 2852 (w), 1900 (w), 1606 (w), 1576 (m), 1515 (m), 1473 (s), 1440 (w), 1395 (m), 1283 (s), 1187 (w), 1134 (w), 1115 (w), 1060 (m), 1023 (m), 1001 (s), 945 (s), 865 (m), 830 (s), 798 (s), 786 (s), 758 (s), 710 (s), 630 (m), 611 (s).

5.1.44. Synthesis of $[Pd_2L_4][BF_4]_4$

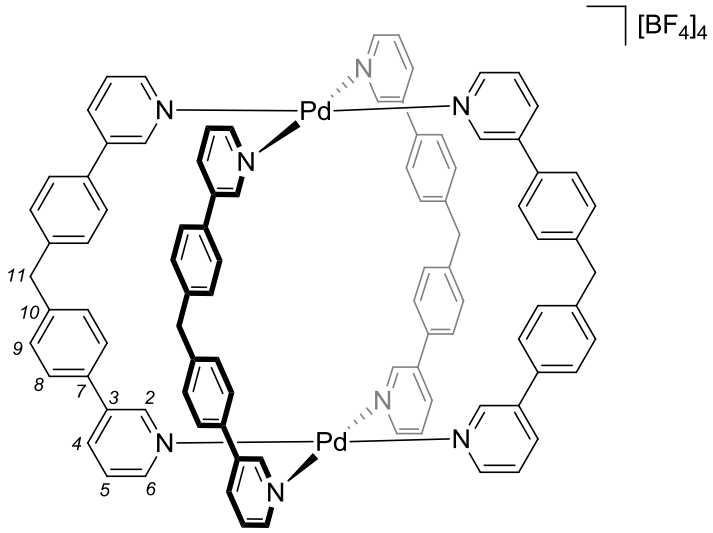

$[Pd_2(C_{23}H_{18}N_2)_4][BF_4]_4$

FW: 1848.41

The title compound was prepared according to the *General Tetrafluoroborate Tetra-Stranded Palladium(II) Cylinder Procedure* with ligand **L** (29.1 mg, 0.076 mmol) to yield a white solid after further washing with chloroform (50 mL) and dried in vacuo (18 mg, 46% yield). ^{1}H NMR (300 MHz, CD_3CN): δ 9.20 (d, *J* = 1.4 Hz, 2H, H2), 8.96 (dd, *J* = 5.7, 0.9 Hz, 2H, H6), 8.23 – 8.14 (m, 2H, H4), 7.65 (dd, *J* = 8.0, 5.7 Hz, 2H, H5), 7.48 – 7.40 (m, 4H, H8), 7.34 – 7.31 (m, 4H, H9), 4.11 (s, 2H, H11). ^{13}C NMR (100 MHz, CD_3CN): δ 150.4 C6, 150.1 C2, 143.3 C_q, 141.4 C_q, 140.1 C4, 134.2 C_q, 130.8 C9, 128.8 C8, 128.3 C5, 41.2 C11. ^{19}F NMR (282 MHz, CD_3CN): δ -150.52 (s, 2F), -150.57 (s, 8F). LRMS (ES+): *m/z* (%) 323.2 (100) [L+H], 529.9 (81) $[Pd_2L_4(BF_4)]^{3+}$, 817.4 (28) $[Pd_2L_4(BF_4)_2]^{2+}$, 1763.7 (3) $[Pd_2L_4(BF_4)_3]^{+}$ FTIR (film): ν_{max} 3094 (w), 1606 (m), 1581 (w), 1518 (w), 1481 (s), 1439 (s), 1403 (s), 1339 (w), 1287 (w), 1247 (w), 1194 (m), 1055 (s), 1037 (s), 1015 (s), 919 (m), 857 (m), 798 (s), 763 (m), 703 (s), 666 (m), 621 (m). UV-Vis (CH_3CN): λ_{max} (ε_{max}/$dm^3mol^{-1}cm^{-1}$) 259 (84 400), 235 (86 100) nm.

5.2. General materials and methods for spectroscopic DNA binding studies

Solutions were prepared with ultrapure water (18.2 MΩ) purchased from Fisher Scientific. Highly polymerized calf thymus DNA (ct-DNA) was purchased from Sigma Aldrich and was used without further purification. 3000 μM stock solutions of ct-DNA were prepared and kept frozen until the day of the experiment, when they were diluted to the required concentration. The DNA concentration was determined by UV-Vis measurements using the known molar extinction coefficient of ε_{258} = 6 600 $mol^{-1}dm^3cm^{-1}$ per DNA base. Stock solutions of sodium chloride (1 M) and sodium cacodylate ($Na(CH_2)_2AsO_2 \cdot 3H_2O$) buffer (100 mM) were prepared and kept refrigerated until the day of the experiment, when both were diluted to the required concentration.

5.2.1. Circular and linear dichroism experiments

Circular dichroism (CD) measurements were recorded in a Jasco J-810 spectropolarimeter operated with the following parameters: sensitivity, 100 mdeg; start wavelength, 450 nm; end wavelength, 200 nm; data pitch, 0.5 nm; scanning mode, continuous; scanning speed, 200 nm/min; response, 1 second; bandwidth, 2; accumulation, 3. A 1 cm quartz cuvette was used to perform the CD measurements.

Linear dichroism (LD) measurements were recorded in a Jasco J-810 spectropolarimeter modified for *LD* spectroscopic measurement. The

spectropolarimeter was operated in *LD* mode with the following parameters: sensitivity, 0.1 dOD; start wavelength, 450 nm; end wavelength, 200; data pitch, 0.5 nm; scanning mode, continuous; scanning speed, 500 nm/min; response, 0.25 seconds; bandwidth, 2.0; accumulation, 3. A flow Couette cell (Krometek) with a 0.1 cm pathlength was used to perform the LD measurements. CD and LD titrations were carried out using three solutions; solution A (a 30 μM ct-DNA solution, containing 20 mM NaCl and 1 mM sodium cacodylate); solution B (a 50 μM palladium(II) cylinder solution) and solution C (a 60 μM ct-DNA solution, containing 40 mM NaCl and 2 mM sodium cacodylate). Initially, solution A was recorded and then equal aliquots of solutions B and C were added to ensure a constant concentration of DNA throughout the titration. DNA base:complex ratios of 60:1, 30:1, 20:1, 15:1, 10:1, 8:1, 6:1, 4:1 and 3:1 were used. Data was processed with Origin (OriginLab, Northampton, Massachusetts).

5.2.2. Ethidium bromide displacement experiments

The fluorescence spectra for ethidium bromide displacement experiments were recorded using a Shimadzu RF-5301 PC Fluorescence Spectrophotometer with the following parameters: λ_{exc} = 500 nm; range emission = 520-750 nm; resolution = 0.4nm; speed = medium; excitation split = 5; emmision split = 5; sensitivity = high. Titrations were carried out using three solutions; solution A (a 30 μM ct-DNA solution, containing 50 mM NaCl, 1 mM sodium cacodylate and 10 mM ethidium bromide); solution B (a 100 μM palladium(II) cylinder solution) and solution C (a 60 μM ct-DNA solution, containing 100 mM NaCl, 2 mM sodium cacodylate and

20 mM ethidium bromide). Initially, solution A was recorded and then equal aliquots of solutions B and C were added to ensure a constant concentration of DNA throughout the titration. DNA base:complex ratios of 100:1, 60:1, 30:1, 15:1, 8:1, 4:1, 3:1, 2:1, 1.5:1 and 1:1 were used. Data was processed with Origin (OriginLab, Northampton, Massachusetts).

5.3. General materials and methods for agarose gel electrophoresis

Solutions were prepared with ultrapure water (18.2 MΩ) purchased from Fisher Scientific. pBR322 plasmid DNA was purchased from New England Biolabs and used without further purification. Agarose was purchased from USB Corporation and Tris-Acetate-EDTA (TAE) buffer was purchased from Sigma Aldrich.

5.3.1. Agarose gel electrophoresis experiment

1% Agarose gels were prepared by warming 2 g of agarose in 1x TAE buffer until a clear solution was obtained. This solution was poured into a gel tray (210 x 150 mm) fitted with a 15 toothed comb. The gel was left to set at room temperature for 30 minutes. Sample solutions of 16 µl were prepared from a 1540 µM pBR322 plasmid DNA stock solution and a 60 µM complex stock solution to obtain plasmid:complex ratios ranging from 20:1 to 2:1. These sample solutions were incubated for 2 hours at 37 ºC, after which 4 µl of loading buffer (30%

glycerol, 0.25% bromophenol blue) was added. The samples were mixed and 16 µl of the samples were loaded into the gel wells. The gel was run for 2.5 hours in an Amersham Biosciences HE99X Maxi submarine kit with an electrophoresis Power Supply-EPS 301 system, at a constant voltage of 120 V and 400 mA, in 1x TAE running buffer. The gel was then stained with an ethidium bromide solution (0.5 mg.ml-1) in 200 ml of water for 20 minutes and visualised using a UVtec-uvipro platinum 2.0 system (UVidoc, Cambridge, UK) at 312 nm.

5.4. General materials and methods for polyacrylamide gel electrophoresis

Solutions were prepared with ultrapure water (18.2 MΩ) purchased from Fisher Scientific. Gel electrophoresis purified DNA oligonucleotides were purchased from Eurofins MWG Operon and used without further purification.

DNA oligonucleotide sequences used for three-way junction recognition experiments:

3WJ-S1: 5’ - CGG AAC GGC ACT CG - 3’

3WJ-S2: 5’ - CGA GTG CAG CGT GG - 3’

3WJ-S3: 5’ - CCA CGC TCG TTC CG - 3’

DNA oligonucleotide sequences used for four-way junction recognition experiments:

4WJ-S1: 5’ - GCC TAG CAT GAT ACT GCT ACC G - 3’

4WJ-S2: 5’ - CGG TAG CAG TAC CGT TGG TGG C - 3’

4WJ-S3: 5’ - GCC ACC AAC GGC GTC AAC TGC C - 3’

4WJ-S4: 5’ - GGC AGT TGA CGT CAT GCT AGG C - 3’

γ-^{32}P labelled ATP (3 000 Ci/mmol) was purchased from PerkinElmer. Bacteriophage T4 polynucleotide kinase was purchased from New England Biolabs. A QIAquick nucleotide removal kit was purchased from QIAGEN. 40% Acrylamide (29:1) was purchased from Geneflow.

5.4.1. Radioactive labelling of DNA

3WJ-S3 and 4WJ-S4 DNA oligonucleotide strands were radio-labelled with γ-^{32}P at the 5’ terminus by mixing 9.6 μL of ultrapure water, 2 μL of 10x bacteriophage T4 polynucleotide kinase buffer, 2.4 μL of 100 μM oligonucleotide (3WJ-S3 or 4WJ-S4), 2 μL of bacteriophage T4 polynucleotide kinase and 4 μL of γ-^{32}P ATP (3 000 Ci/mmol). This solution was incubated at 37 ºC for 40 minutes, followed by 3 minutes at 80 ºC in order to deactivate the polynucleotide kinase. A QIAquick nucleotide removal kit was used to purify the radioactive-labelled DNA oligonucleotide from any unreacted ATP fragments. 200 μL of PN buffer was added to the reaction mixture. This solution was transferred to a QIAquick spin column with a 2 mL collection tube and the mixture was centrifuge at 6 000 rpm for 1 minute. The flow-through was discarded after centrifugation and the QIAquick

spin column was placed in a new collection tube. 500 μL of PE buffer was added to wash the radiolabelled-DNA oligonucleotide and the mixture was centrifuged at 6 000 rpm for one minute. The flow-through was discarded and the washing process repeated one again. The spin column was then centrifuged at 13 000 rpm for 1 minute to remove any remaining buffer. 30 μL of ultrapure water was added onto the column to elute the radioactive-labelled DNA oligonucleotide. The solution was allowed to stand for 5 minutes and then was centrifuged at 13 000 rpm for 2 minutes to obtain an 8 μM stock solution of radiolabelled DNA oligonucleotide.

5.4.2. Polyacrylamide gel preparation

A 15% native polyacrylamide solution was prepared by mixing 100 mL of 10x Tris-Borate (TB) buffer, 375 mL of 40 % acrylamide (29:1) and 525 mL of HPLC grade water and was kept in the fridge until the day of the experiment. 10x TB buffer was prepared by mixing 108 g of Tris-base and 55 g of boric acid in 1 L of HPLC grade water. On the day of the experiment, 50 mL of 15% native polyacrylamide solution was mixed with 150 μL of 10 % (w/v) ammonium persulfate and 25 μL of tetramethylenediamine (TEMED). This solution was poured onto a set of glass plates and a 19 toothed comb was placed between them. The gel was left to polymerise for 30 – 40 minutes, after which it was placed in the fridge for 10 minutes. Wells were washed with water and TB running buffer and the gel was pre-run at 300 V for 10 minutes.

5.4.3. PAGE electrophoresis experiment

Sample solutions of 10 μL were prepared by mixing 2 μM stock solutions of each oligonucleotide strand and 1 μL of a (10x TB buffer + 1 M sodium chloride) solution, and 2 μM complex stock solution to give final concentrations of 0.2 μM for each DNA strand and 0.2 μM of complex. The sample solutions were incubated for 1 hour at room temperature and then placed on ice for 15 - 20 minutes. 5 μL of 30% glycerol solution was added to each sample and 13 μL of the sample was loaded onto the gel. The gel was run for 4 hours at 120 V using Gel System equipment and then exposed on a phosphor imaging plate for 1 - 16 hours, depending on how fresh the radioactive ATP used was. A radiogel image was obtained using a Bio-Rad Molecular Imager FX and PDQuest software. Quantification was carried out using Quantity One software.

5.5. General materials and methods for cell culture

RPMI medium and FBS were purchased from Invitrogen. Antibiotic antimycotic solution, L-glutamine, trypsin-EDTA, HEPES buffer, sodium pyruvate, MTT and DMSO were purchased from Sigma-Aldrich. Tissue culture flasks and 96 well microtiter plates were purchased from Appleton Woods, UK. A2780 and T47D cancer cell lines were purchased from the Health Protection Agency, European collection of cell cultures (ECACC). All reagents and materials were autoclaved before use. Manipulations with cells were carried out in sterile conditions in a class 1 tissue culture hood (Aura B4, Bio Air).

5.5.1. MTT assay

Sample solutions of 200 μM were prepared in a 1% DMSO solution in DMEM medium. After 24 hours incubation, cells were treated with 100 μL of six different concentrations of the complex. Cells were incubated for 72 hours, after which 50 μL of MTT solution (5 mg/mL in PBS) was added and further incubated for 2 hours. MTT was removed and the formazan crystals were dissolved by the addition of 200 μL of DMSO. The absorbance was measured using a microplate reader (Bio Rad) set at 590 nm.

Appendix

A.1. Crystallographic data for **[$Pd_2L^{OMe}_4$][$(BF_4)_4$]** complex.

Empirical formula	$C_{100}H_{88}N_8O_8Pd_2$ 4(BF_4) 2(C_2H_3N) 4(H_2O)	
Formula weight	2244.00	
Temperature (K)	100(2)	
Wavelength (Å)	0.71075	
Crystal system	Triclinic	
Space group	P -1	
Unit cell dimensions	a = 12.499(19) Å	α= 98.05(3)°
	b = 13.844(19) Å	β= 106.056(16)°
	c = 16.16(2) Å	γ = 97.392(19)°
Volume ($Å^3$)	2619(7)	
Z	1	
Calculated density (mg/m^3)	1.423	
Absorption coefficient (mm^{-1})	0.436	
Crystal size (mm^3)	0.07 x 0.05 x 0.01	
Reflections collected	23097	
Independent reflections	9233 [R(int) = 0.0955]	
Refinement method	Full-matrix least-squares on F^2	
Data / restraints / parameters	9233 / 6 / 680	
Goodness-of-fit on F^2	1.107	
Final R indices [I>2σ(I)]	R_1 = 0.1121, wR_2 = 0.2801	
R indices (all data)	R_1 = 0.1475, wR_2 = 0.3148	

A.2. Crystallographic data for ligand $\mathbf{L^{O\text{-}OMe}}$.

Empirical formula	$C_{24}H_{20}N_2O_3$	
Formula weight	384.42	
Temperature (K)	120(2)	
Wavelength (Å)	1.54184	
Crystal system	Monoclinic	
Space group	C 2/c	
Unit cell dimensions	a = 38.7788(7) Å	α= 90°
	b = 6.6075(1) Å	β= 100.784(1)°
	c = 7.3762(1) Å	γ = 90°
Volume (Å^3)	1856.63(5)	
Z	4	
Calculated density (mg/m^3)	1.375	
Absorption coefficient (mm^{-1})	0.739	
Crystal size (mm^3)	0.32 x 0.20 x 0.08	
Reflections collected	8642	
Independent reflections	1758 [R(int) = 0.0201]	
Absorption correction	Semi-empirical from equivalents	
Refinement method	Full-matrix least-squares on F^2	
Data / restraints / parameters	1758 / 0 / 134	
Goodness-of-fit on F^2	1.042	
Final R indices [I>2σ(I)]	R_1 = 0.0332, wR_2 = 0.0894	
R indices (all data)	R_1 = 0.0338, wR_2 = 0.0901	
Extinction coefficient	0.00135(17)	

A.3. Crystallographic data for **$[Pd_2L^{NH\text{-}OMe}{}_4][(BF_4)_4]$** complex.

Empirical formula	$C_{96}H_{84}N_{12}O_8Pd_2$ 4(BF_4) $C_4H_{10}O$ 5.5(C_2H_3N)	
Formula weight	2393.71	
Temperature (K)	100(2)	
Wavelength (Å)	0.71075	
Crystal system	Triclinic	
Space group	P -1	
Unit cell dimensions	a = 11.362(16) Å	α= 109.64(2)°
	b = 16.33(2) Å	β= 104.52(2)°
	c = 18.17(3) Å	γ = 92.287(16)°
Volume ($Å^3$)	3045(8)	
Z	1	
Calculated density (mg/m^3)	1.305	
Absorption coefficient (mm^{-1})	0.379	
Crystal size (mm^3)	0.20 x 0.14 x 0.07	
Reflections collected	18645	
Independent reflections	9949 [R(int) = 0.1040]	
Absorption correction	Semi-empirical from equivalents	
Refinement method	Full-matrix least-squares on F^2	
Data / restraints / parameters	9949 / 79 / 809	
Goodness-of-fit on F^2	1.513	
Final R indices [$I>2\sigma(I)$]	R_1 = 0.1260, wR_2 = 0.3512	
R indices (all data)	R_1 = 0.1373, wR_2 = 0.3691	

A.4. Crystallographic data for ligand $\mathbf{L^{NH\text{-}OH}}$.

Empirical formula	$C_{22}H_{17}N_3O_2$	
Formula weight	355.39	
Temperature (K)	100(2)	
Wavelength (Å)	0.71070	
Crystal system	Orthorhombic	
Space group	P nma	
Unit cell dimensions	a = 7.094(8) Å	α= 90°
	b = 38.24(4) Å	β= 90°
	c = 5.921(7) Å	γ = 90°
Volume (Å^3)	1606(3)	
Z	4	
Calculated density (mg/m^3)	1.470	
Absorption coefficient (mm^{-1})	0.096	
Crystal size (mm^3)	0.34 x 0.24 x 0.03	
Reflections collected	5642	
Independent reflections	1529 [R(int) = 0.0542]	
Absorption correction	None	
Refinement method	Full-matrix least-squares on F^2	
Data / restraints / parameters	1529 / 0 / 127	
Goodness-of-fit on F^2	1.055	
Final R indices [I>2σ(I)]	R_1 = 0.0543, wR_2 = 0.1295	
R indices (all data)	R_1 = 0.0576, wR_2 = 0.1327	

A.5. Crystallographic data for ligand $\mathbf{L}^{\mathbf{Click\text{-}Bn}}$.

Empirical formula	$C_{31}H_{26}N_6$	
Formula weight	482.58	
Temperature (K)	120(2)	
Wavelength (Å)	1.54184	
Crystal system	Orthorhombic	
Space group	P $na2_1$	
Unit cell dimensions	a = 8.2284(5) Å	α= 90°
	b = 5.6886(3) Å	β= 90°
	c = 50.573(3) Å	γ = 90°
Volume (Å^3)	2367.2(2)	
Z	4	
Calculated density (mg/m^3)	1.354	
Absorption coefficient (mm^{-1})	0.649	
Crystal size (mm^3)	0.22 x 0.18 x 0.04	
Reflections collected	9849	
Independent reflections	2208 [R(int) = 0.0259]	
Absorption correction	Semi-empirical from equivalents	
Max. and min. transmission	0.9745 and 0.8704	
Refinement method	Full-matrix least-squares on F^2	
Data / restraints / parameters	2208 / 1 / 334	
Goodness-of-fit on F^2	1.102	
Final R indices [I>2σ(I)]	R_1 = 0.0292, wR_2 = 0.0747	
R indices (all data)	R_1 = 0.0302, wR_2 = 0.0756	

A.6. ^{13}C NMR of **$[Pd_2L^{OMe}{}_4][(BF_4)_4]$** (100 MHz, CD_3CN).

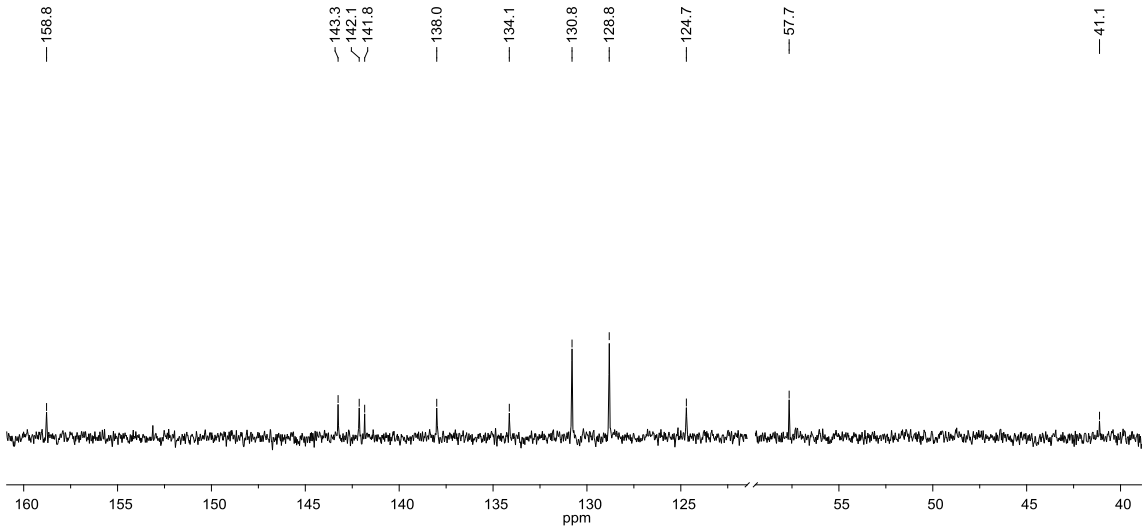

A.7. ^{13}C-^{1}H HSQC NMR of **$[Pd_2L^{OMe}{}_4][(BF_4)_4]$** (100 MHz-400 MHz, CD_3CN).

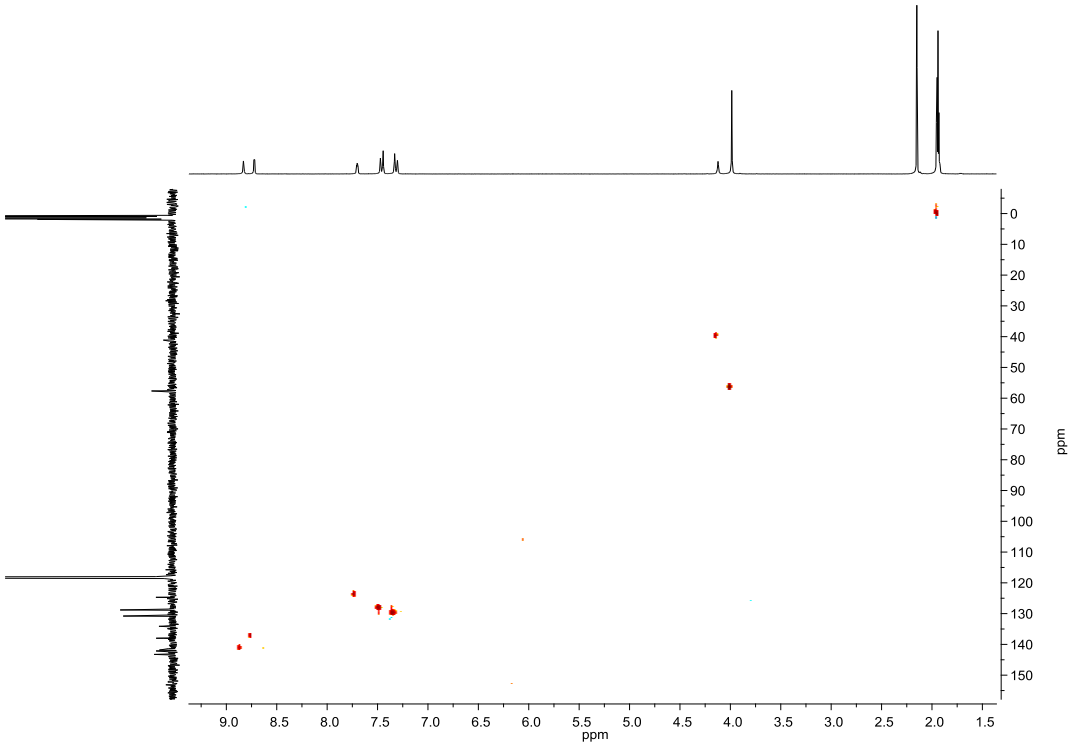

A.8. ^{1}H-^{1}H COSY NMR of **[Pd$_2$L$^{OMe}_4$][(BF$_4$)$_4$]** (400 MHz, CD$_3$CN).

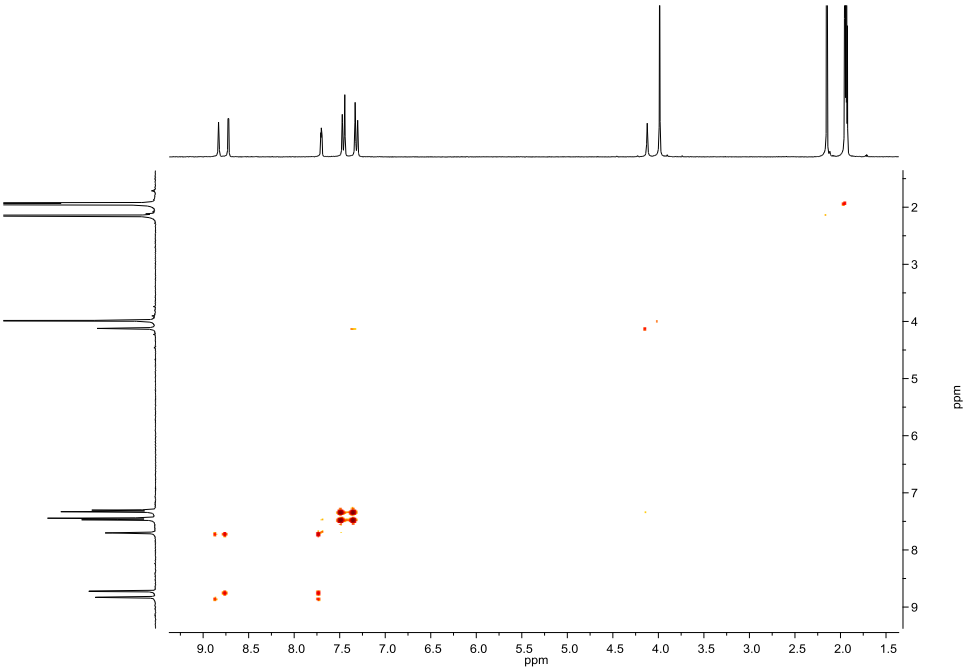

A.9. ^{1}H-^{1}H NOESY NMR of **[Pd$_2$L$^{OMe}_4$][(BF$_4$)$_4$]** (400 MHz, CD$_3$CN).

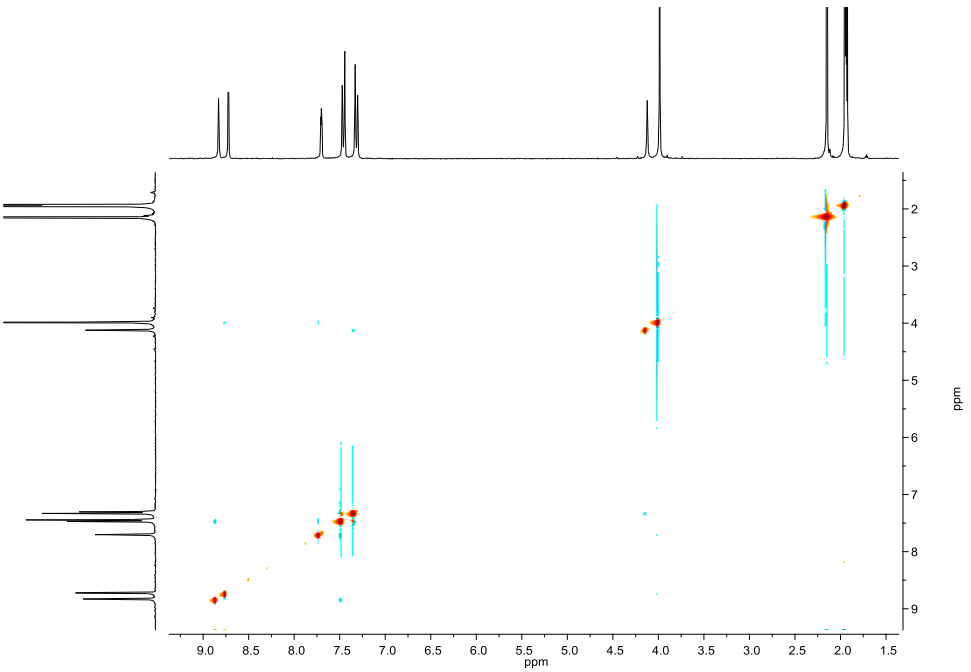

A.10. ^{1}H NMR spectra of titrations of NBu_4OTf into **$[Pd_2L^{NH\text{-}OMe}{}_4][(BF_4)_4]$** (300 MHz, CD_3CN).

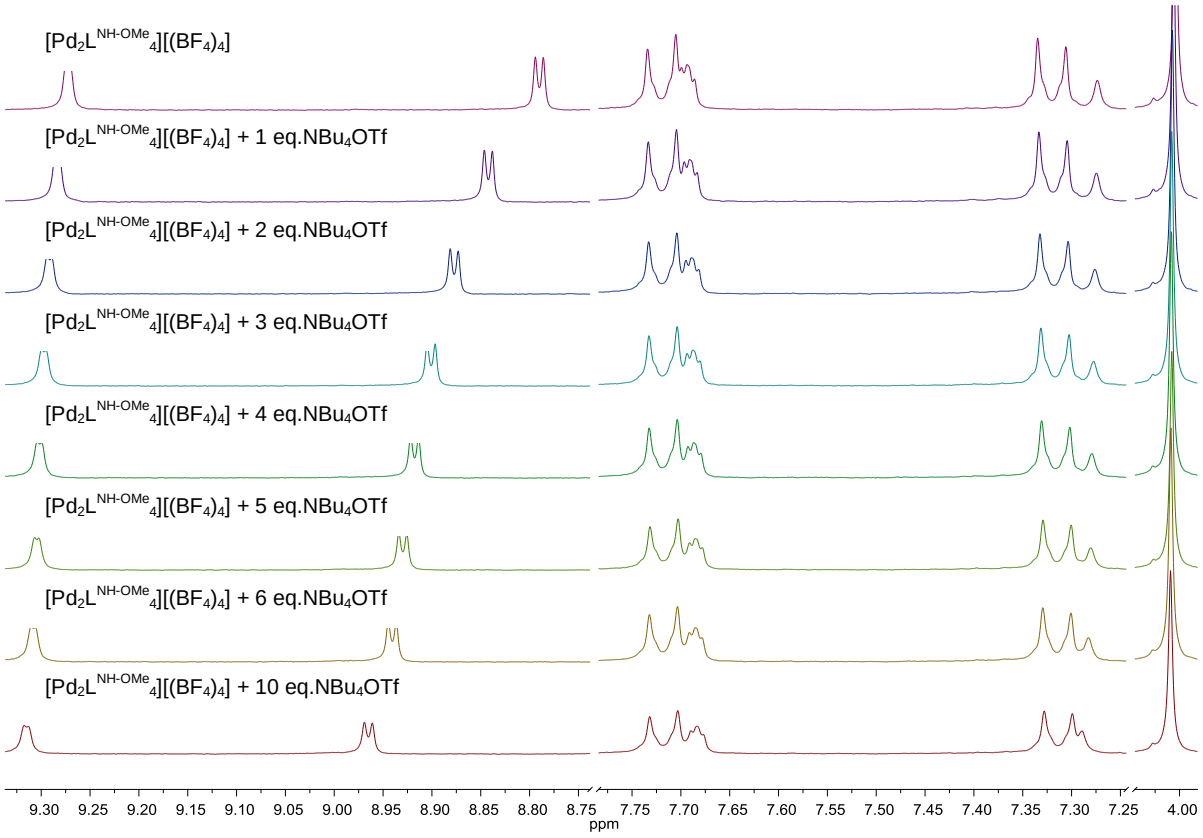

A.11. CD spectra of ct-DNA with increasing concentrations of **$[Pd_2L^{OH}{}_4][(BF_4)_4]$** complex. Legend shows ct-DNA base:complex ratios. 0.3% max. DMSO. (30 μM ct-DNA in 20 mM NaCl and 1 mM $Na(CH_2)_2AsO_3 \cdot 3H_2O$ (pH 6.8)).

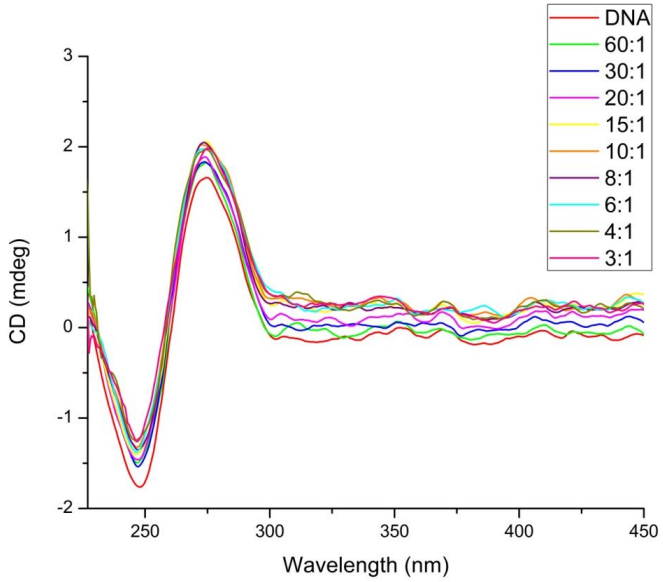

A.12. LD spectra of ct-DNA with increasing concentrations of **$[Pd_2L^{O\text{-}OMe}{}_4][(BF_4)_4]$** complex. Legend shows ct-DNA base:complex ratios. 0.3% max. DMSO. (30 μM ct-DNA in 20 mM NaCl and 1 mM $Na(CH_2)_2AsO_3 \cdot 3H_2O$ (pH 6.8)).

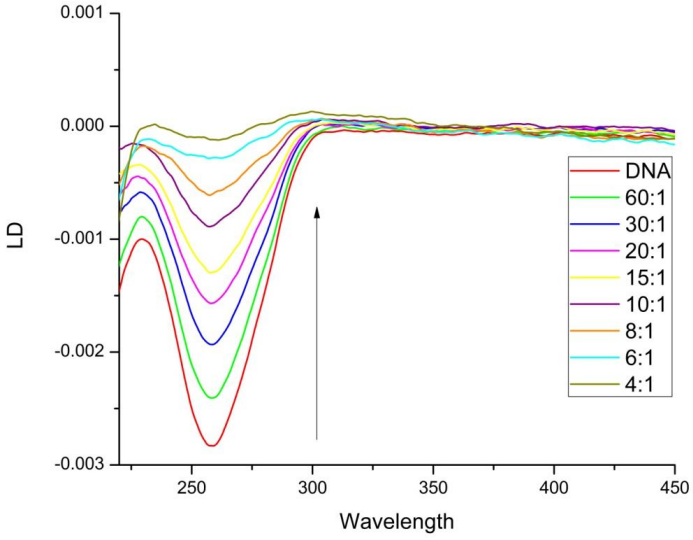

A.13. LD spectra of ct-DNA with increasing concentrations of **[$Pd_2L^{NH\text{-}OMe}_4$][$(BF_4)_4$]** complex. Legend shows ct-DNA base:complex ratios. 0.3% max. DMSO. (30 μM ct-DNA in 20 mM NaCl and 1 mM $Na(CH_2)_2AsO_3 \cdot 3H_2O$ (pH 6.8)).

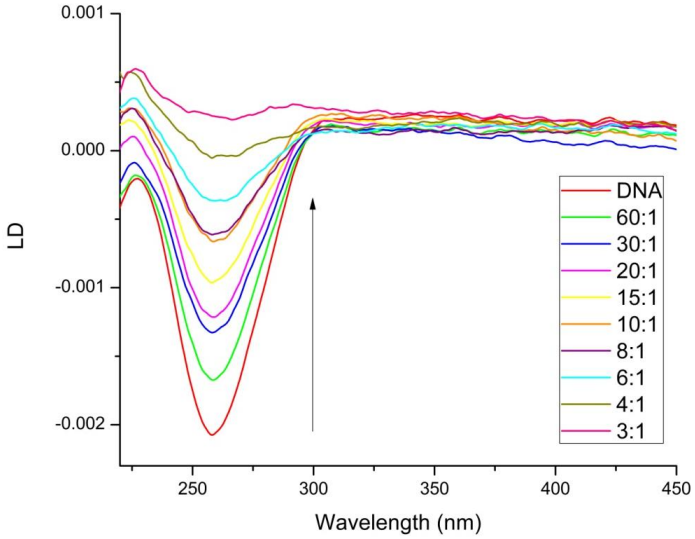

A.14. LD spectra of ct-DNA with increasing concentrations of **[$Pd_2L^{S\text{-}OMe}_4$][$(BF_4)_4$]** complex. Legend shows ct-DNA base:complex ratios. 0.3% max. DMSO. (30 μM ct-DNA in 20 mM NaCl and 1 mM $Na(CH_2)_2AsO_3 \cdot 3H_2O$ (pH 6.8)).

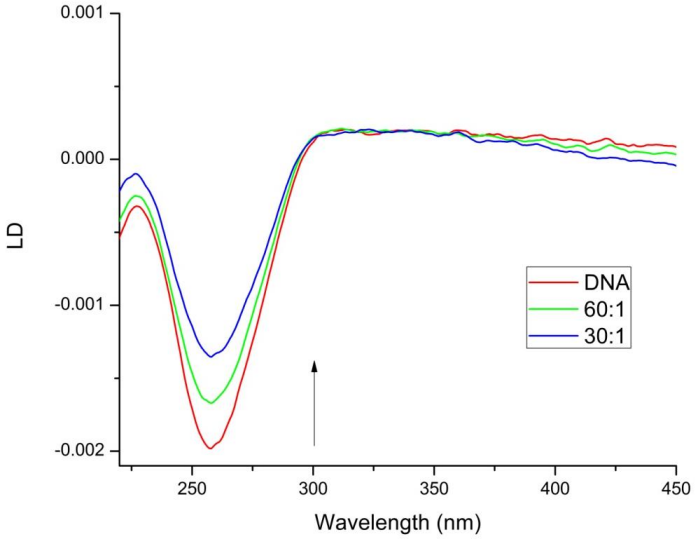

A.15. LD spectra of ct-DNA with increasing concentrations of **[$Pd_2L^{OH}_4$][$(BF_4)_4$]** complex. Legend shows ct-DNA base:complex ratios. 0.3% max. DMSO. (30 μM ct-DNA in 20 mM NaCl and 1 mM $Na(CH_2)_2AsO_3 \cdot 3H_2O$ (pH 6.8)).

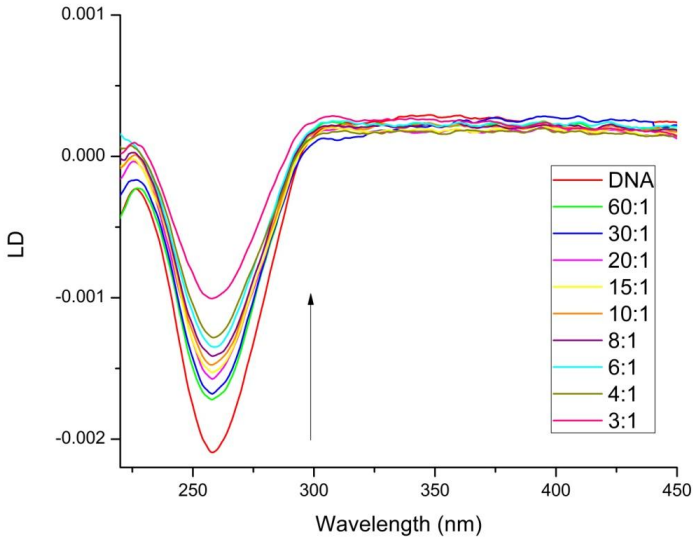

A.16. LD spectra of ct-DNA with increasing concentrations of **[$Pd_2L^{O\text{-}Glycol}_4$][$(BF_4)_4$]** complex. Legend shows ct-DNA base:complex ratios. 0.3% max. MeOH. (30 μM ct-DNA in 20 mM NaCl and 1 mM $Na(CH_2)_2AsO_3 \cdot 3H_2O$ (pH 6.8)).

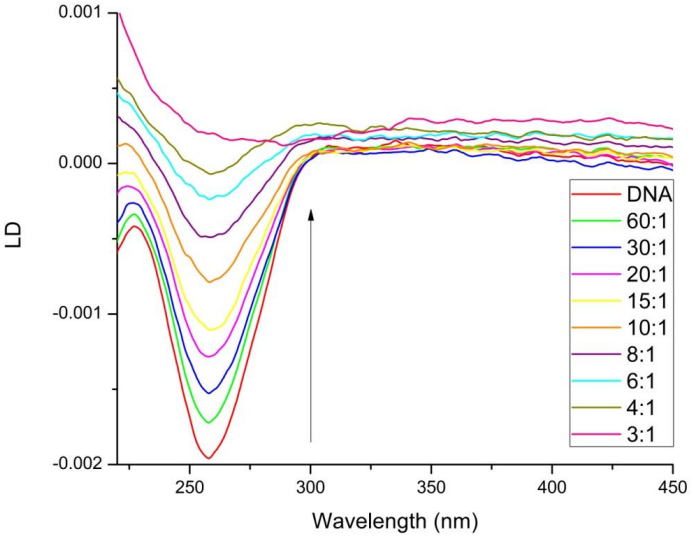

References

(1) Mathews, C.; Van Holde, K.; Ahern, K. *Biochemistry*; 3rd ed.; Addison-Wesley: San Francisco, California, 2000.
(2) Watson, J.; Crick, F. *Nature* **1953**, *171*, 737.
(3) Garrett, R.; Grisham, C. *Biochemistry*; 4th ed.; Saunders College Publishing, 1995.
(4) Lehninger, N.; Nelson, D.; Cox, M. *Principles of Biochemistry*; 5th ed.; WH Freeman & Co.: New York, 2008.
(5) Gao, Y. G.; Robinson, H.; Wang, A. H. J. *Eur. J. Biochem.* **1999**, *261*, 413.
(6) Drew, H. R.; Wing, R. M.; Takano, T.; Broka, C.; Tanaka, S.; Itakura, K.; Dickerson, R. E. *Proc. Natl. Acad. Sci. USA* **1981**, *78*, 2179.
(7) Wang, A.; Quigley, G. J.; Kolpak, F. J.; Crawford, J. L.; Van Boom, J. H.; van der Marel, G.; Rich, A. *Nature* **1979**, *282*, 680.
(8) Alberts, B. *Molecular Biology of the Cell*; 5th ed.; Garland Science, 2008.
(9) Hannon, M. J. *Chem. Soc. Rev.* **2006**, *36*, 280.
(10) Hamilton, P. L.; Arya, D. P. *Nat. Prod. Rep.* **2012**, *29*, 134.
(11) Paul, A.; Bhattacharya, S. *Curr. Sci.* **2012**, *102*, 212.
(12) Nadassy, K.; Wodak, S. J.; Janin, J. *Biochemistry* **1999**, *38*, 1999.
(13) Pabo, C. O.; Nekludova, L. *J. Mol. Biol.* **2000**, *301*, 597.
(14) Xiong, Y.; Sundaralingam, M. In *eLS*; John Wiley & Sons, Ltd: 2001.
(15) Schuetz, A.; Nana, D.; Rose, C.; Zocher, G.; Milanovic, M.; Koenigsmann, J.; Blasig, R.; Heinemann, U.; Carstanjen, D. *Cell.Mol.Life Sci.* **2011**, *68*, 3121.
(16) Semenyuk, A.; Darian, E.; Liu, J.; Majumdar, A.; Cuenoud, B.; Miller, P.; MacKerell Jr, A.; Seidman, M. *Biochemistry* **2010**, *49*, 7867.
(17) Singhal, G.; Akhter, M.; Stern, D.; Gupta, S.; Ahuja, A.; Sharma, U.; Jagannathan, N.; Rajeswari, M. *Cancer Gene Ther.* **2011**, *18*, 520.
(18) Nakamoto, K.; Tsuboi, M.; Strahan, G. D. *Drug-DNA interactions: structures and spectra*; 1st ed.; Wiley, 2008; Vol. 51.
(19) Nielsen, P. E.; Egholm, M.; Berg, R. H.; Buchardt, O. *Science* **1991**, *254*, 1497.
(20) Betts, L.; Josey, J. A.; Veal, J. M.; Jordan, S. R. *Science* **1995**, *270*, 1838.
(21) Khutia, A.; Sanz Miguel, P. J.; Lippert, B. *Chem. Eur. J.* **2011**, *17*, 4195.
(22) Navarro, J. A. R.; Barea, E.; Galindo, M. A.; Salas, J. M.; Romero, M. A.; Quirós, M.; Masciocchi, N.; Galli, S.; Sironi, A.; Lippert, B. *J. Solid State Chem.* **2005**, *178*, 2436.
(23) Kim, H. J.; Lee, M. H.; Mutihac, L.; Vicens, J.; Kim, J. S. *Chem. Soc. Rev.* **2012**, *41*, 1173.
(24) Galindo, M. A.; Olea, D.; Romero, M. A.; Gómez, J.; del Castillo, P.; Hannon, M. J.; Rodger, A.; Zamora, F.; Navarro, J. A. R. *Chem. Eur. J.* **2007**, *13*, 5075.
(25) Navarro, J. A. R.; Freisinger, E.; Lippert, B. *Inorg. Chem.* **2000**, *39*, 2301.
(26) Zadmard, R.; Schrader, T. *Angew. Chem. Int. Ed.* **2006**, *45*, 2703.

(27) Hu, W.; Blecking, C.; Kralj, M.; Šuman, L.; Piantanida, I.; Schrader, T. *Chem. Eur. J.* **2012**, *18*, 3589.
(28) Bishop, E. P.; Rohs, R.; Parker, S. C. J.; West, S. M.; Liu, P.; Mann, R. S.; Honig, B.; Tullius, T. D. *ACS Chem. Biol.* **2011**, *6*, 1314.
(29) Pazos, E.; Mosquera, J.; Vázquez, M. E.; Mascareñas, J. L. *ChemBioChem* **2011**, *12*, 1958.
(30) Uytterhoeven, K.; Sponer, J.; Van Meervelt, L. *Eur. J. Biochem.* **2002**, *269*, 2868.
(31) Pelton, J. G.; Wemmer, D. E. *Proc. Natl. Acad. Sci. USA* **1989**, *86*, 5723.
(32) Deng, J.; Pan, B.; Sundaralingam, M. *Acta Crystallogr. Sect. D: Biol. Crystallogr.* **2003**, *59*, 2342.
(33) Wang, S.; Munde, M.; Wilson, W. D. *Biochemistry* **2011**, *50*, 7674.
(34) Sánchez, M. I.; Vázquez, O.; Vázquez, M. E.; Mascareñas, J. L. *Chem. Commun.* **2011**, *47*, 11107.
(35) Miao, Y.; Lee, M. P. H.; Gary, N.; Batista-Parra, A.; Ismail, M. A.; Neidle, S.; Boykin, D. W.; Wilson, W. D. *Biochemistry* **2005**, *44*, 14701.
(36) Liu, Y.; Kumar, A.; Depauw, S.; Nhili, R.; David-Cordonnier, M. H.; Lee, M. P.; Ismail, M. A.; Farahat, A. A.; Say, M.; Chackal-Catoen, S. *J. Am. Chem. Soc.* **2011**, *133*, 10171.
(37) Dervan, P. B. *Bioorg. Med. Chem.* **2001**, *9*, 2215.
(38) Kielkopf, C. L.; White, S.; Szewczyk, J. W.; Turner, J. M.; Baird, E. E.; Dervan, P. B.; Rees, D. C. *Science* **1998**, *282*, 111.
(39) Chenoweth, D. M.; Dervan, P. B. *Proc. Natl. Acad. Sci. USA* **2009**, *106*, 13175.
(40) Watkins, D.; Harris, L. A.; Koudelka, G. B.; Williams, L. D. *Frontiers in Nucleic Acids*; ACS Symposium Series: Washington, 2011.
(41) Juo, Z. S.; Chiu, T. K.; Leiberman, P. M.; Baikalov, I.; Berk, A. J.; Dickerson, R. E. *J. Mol. Biol.* **1996**, *261*, 239.
(42) Neidle, S. *Nucleic Acid Structure and Recognition*; 1st ed.; Oxford University Press, 2002.
(43) Liu, H. K.; Sadler, P. J. *Acc. Chem. Res.* **2011**, *44*, 349.
(44) Wu, H.; Sun, T.; Li, K.; Liu, B.; Kou, F.; Jia, F.; Yuan, J.; Bai, Y. *Bioinorg. Chem. Appl.* **2011**, *2012*.
(45) Reymer, A.; Nordén, B. *Chem. Commun.* **2012**, *48*, 4941.
(46) Davis, K. J.; Carrall, J. A.; Lai, B.; Aldrich-Wright, J. R.; Ralph, S. F.; Dillon, C. T. *Dalton Trans.* **2012**, *41*, 9417.
(47) Jennette, K.; Lippard, S.; Vassiliades, G.; Bauer, W. *Proc. Natl. Acad. Sci. USA* **1974**, *71*, 3839.
(48) Neidle, S. *Nature Chem.* **2012**, *4*, 594.
(49) Song, H.; Kaiser, J. T.; Barton, J. K. *Nature Chem.* **2012**, *4*, 615.
(50) Niyazi, H.; Hall, J. P.; O'Sullivan, K.; Winter, G.; Sorensen, T.; Kelly, J. M.; Cardin, C. J. *Nature Chem.* **2012**, *4*, 621.
(51) Nazif, M. A.; Rubbiani, R.; Alborzinia, H.; Kitanovic, I.; Wölfl, S.; Ott, I.; Sheldrick, W. S. *Dalton Trans.* **2012**, *41*, 5587.
(52) Komeda, S.; Moulaei, T.; Woods, K. K.; Chikuma, M.; Farrell, N. P.; Williams, L. D. *J. Am. Chem. Soc.* **2006**, *128*, 16092.

(53) Mangrum, J. B.; Farrell, N. P. *Chem. Commun.* **2010**, *46*, 6640.
(54) Komeda, S.; Moulaei, T.; Chikuma, M.; Odani, A.; Kipping, R.; Farrell, N. P.; Williams, L. D. *Nucleic Acids Res.* **2011**, *39*, 325.
(55) Pizarro, A. M.; Sadler, P. J. *Biochimie* **2009**, *91*, 1198.
(56) Klein, A. V.; Hambley, T. W. *Chem. Rev.* **2009**, *109*, 4911.
(57) Takahara, P. M.; Rosenzweig, A. C.; Frederick, C. A.; Lippard, S. J. *Nature* **1995**, *377*, 649.
(58) Wang, D.; Lippard, S. J. *Nat. Rev. Drug Discov.* **2005**, *4*, 307.
(59) Wheate, N. J.; Walker, S.; Craig, G. E.; Oun, R. *Dalton Trans.* **2010**, *39*, 8113.
(60) Alberto, M. E.; Butera, V.; Russo, N. *Inorg. Chem.* **2011**, *50*, 6965.
(61) Di Pasqua, A. J.; Goodisman, J.; Dabrowiak, J. C. *Inorg. Chim. Acta* **2012**, *389*, 29.
(62) Edayathumangalam, R. S.; Weyermann, P.; Gottesfeld, J. M.; Dervan, P. B.; Luger, K. *Proc. Natl. Acad. Sci. USA* **2004**, *101*, 6864.
(63) Stryer, L.; Berg, J. M.; Tymoczko, J. L. *Biochemistry*; 5th ed.; WH Freeman and Co, 2002.
(64) Cardew, A. S.; Brown, T.; Fox, K. R. *Nucleic Acids Res.* **2012**, *40*, 3753.
(65) Cassidy, S. A.; Strekowski, L.; Fox, K. R. *Nucleic Acids Res.* **1996**, *24*, 4133.
(66) Holt, P. A.; Ragazzon, P.; Strekowski, L.; Chaires, J. B.; Trent, J. O. *Nucleic Acids Res.* **2009**, *37*, 1280.
(67) Jacobsen, M. F.; Ravnsbæk, J. B.; Gothelf, K. V. *Org. Biomol. Chem.* **2010**, *8*, 50.
(68) Blackburn, E. H. *Angew. Chem. Int. Ed.* **2010**, *49*, 7405.
(69) Greider, C. W. *Angew. Chem. Int. Ed.* **2010**, *49*, 7422.
(70) Szostak, J. W. *Angew. Chem. Int. Ed.* **2010**, *49*, 7386.
(71) Xu, Y. *Chem. Soc. Rev.* **2011**, *40*, 2719.
(72) Karsisiotis, A. I.; Hessari, N. M.; Novellino, E.; Spada, G. P.; Randazzo, A.; Webba da Silva, M. *Angew. Chem. Int. Ed.* **2011**, *50*, 10645.
(73) Zahler, A. M.; Williamson, J. R.; Cech, T. R.; Prescott, D. M. *Nature* **1991**, *350*, 718.
(74) Lee, M. P. H.; Haider, S.; Parkinson, G. N.; Neidle, S. *to be published*.
(75) Collie, G. W.; Promontorio, R.; Hampel, S. M.; Micco, M.; Neidle, S.; Parkinson, G. N. *J. Am. Chem. Soc.* **2012**, *134*, 2723.
(76) Campbell, N. H.; Karim, N. H. A.; Parkinson, G. N.; Gunaratnam, M.; Petrucci, V.; Todd, A. K.; Vilar, R.; Neidle, S. *J. Med. Chem.* **2011**, *55*, 209.
(77) Mao, Z. W.; Zheng, X. H.; Chen, H. Y.; Tong, M. L.; Ji, L. N. *Chem. Commun.* **2012**, *48*, 7607.
(78) Fujita, M.; Ibukuro, F.; Yamaguchi, K.; Ogura, K. *J. Am. Chem. Soc.* **1995**, *117*, 4175.
(79) Kieltyka, R.; Englebienne, P.; Fakhoury, J.; Autexier, C.; Moitessier, N.; Sleiman, H. F. *J. Am. Chem. Soc.* **2008**, *130*, 10040.
(80) Muhuri, S.; Mimura, K.; Miyoshi, D.; Sugimoto, N. *J. Am. Chem. Soc.* **2009**, *131*, 9268.

(81) Oleksi, A.; Blanco, A. G.; Boer, R.; Usón, I.; Aymamí, J.; Rodger, A.; Hannon, M. J.; Coll, M. *Angew. Chem. Int. Ed.* **2006**, *45*, 1227.
(82) Tanada, M.; Tsujita, S.; Sasaki, S. *J. Org. Chem.* **2006**, *71*, 125.
(83) Thiviyanathan, V.; Luxon, B. A.; Leontis, N. B.; Illangasekare, N.; Donne, D. G.; Gorenstein, D. G. *J. Biomol. NMR* **1999**, *14*, 209.
(84) Kerckhoffs, J. M. C. A.; Peberdy, J. C.; Meistermann, I.; Childs, L. J.; Isaac, C. J.; Pearmund, C. R.; Reudegger, V.; Khalid, S.; Alcock, N. W.; Hannon, M. J. *Dalton Trans.* **2007**, 734.
(85) Machwe, A.; Karale, R.; Xu, X.; Liu, Y.; Orren, D. K. *Biochemistry* **2011**, *50*, 6774.
(86) Ishino, Y.; Nishino, T.; Morikawa, K. *Chem. Rev.* **2006**, *106*, 324.
(87) Lilley, D. M. J. *Q. Rev. Biophys.* **2000**, *33*, 109.
(88) Rass, U.; Compton, S. A.; Matos, J.; Singleton, M. R.; Ip, S. C. Y.; Blanco, M. G.; Griffith, J. D.; West, S. C. *Genes Dev.* **2010**, *24*, 1559.
(89) Khuu, P. A.; Voth, A. R.; Hays, F. A.; Ho, P. S. *J. Mol. Recognit.* **2006**, *19*, 234.
(90) Biswas, T.; Aihara, H.; Radman-Livaja, M.; Filman, D.; Landy, A.; Ellenberger, T. *Nature* **2005**, *435*, 1059.
(91) Mandal, P.; Venkadesh, S.; Gautham, N. *Acta Crystallogr. Sect. F: Struct. Biol. Cryst. Commun.* **2011**, *67*, 1506.
(92) Zlatanova, J.; Van Holde, K. *FASEB J.* **1998**, *12*, 421.
(93) Vitoc, C. I.; Mukerji, I. *Biochemistry* **2011**, *50*, 1432.
(94) Brogden, A. L.; Hopcroft, N. H.; Searcey, M.; Cardin, C. J. *Angew. Chem. Int. Ed.* **2007**, *46*, 3850.
(95) Lehn, J. M. *Angew. Chem. Int. Ed. Engl.* **1990**, *29*, 1304.
(96) Atkinson, I. M.; Lindoy, L. F. *Self assembly in supramolecular systems*; Royal Society of Chemistry, 2000; Vol. 7.
(97) Uhlenheuer, D. A.; Petkau, K.; Brunsveld, L. *Chem. Soc. Rev.* **2010**, *39*, 2817.
(98) Nielsen, K. A. *Tetrahedron Lett.* **2012**, *53*, 5616.
(99) Caballero, A.; Zapata, F.; White, N. G.; Costa, P. J.; Félix, V.; Beer, P. D. *Angew. Chem. Int. Ed.* **2012**, *51*, 1876.
(100) Jurow, M.; Schuckman, A. E.; Batteas, J. D.; Drain, C. M. *Coord. Chem. Rev.* **2010**, *254*, 2297.
(101) Bassani, D. M. *Nature* **2011**, *480*, 326.
(102) Campaña, A. G.; Carlone, A.; Chen, K.; Dryden, D. T. F.; Leigh, D. A.; Lewandowska, U.; Mullen, K. M. *Angew. Chem. Int. Ed.* **2012**, *51*, 5480.
(103) Albelda, M. T.; Frías, J. C.; García-España, E.; Schneider, H. J. *Chem. Soc. Rev.* **2012**, *41*, 3859.
(104) Keene, F. R. *Dalton Trans.* **2011**, *40*, 2405.
(105) Carboni, S.; Gennari, C.; Pignataro, L.; Piarulli, U. *Dalton Trans.* **2011**, *40*, 4355.
(106) Leininger, S.; Olenyuk, B.; Stang, P. J. *Chem. Rev.* **2000**, *100*, 853.
(107) Cecchini, M.; Samorì, P. *Chem. Soc. Rev.* **2012**, *41*, 3713.
(108) Chakrabarty, R.; Mukherjee, P. S.; Stang, P. J. *Chem. Rev.* **2011**, *111*, 6810.

(109) Alexeev, Y. E.; Kharisov, B.; García, T.; Garnovskii, A. *Coord. Chem. Rev.* **2010**, *254*, 794.
(110) Debata, N. B.; Tripathy, D.; Chand, D. K. *Coord. Chem. Rev.* **2012**, *256*, 1831.
(111) Stephenson, A.; Ward, M. D. *Dalton Trans.* **2011**, *40*, 10360.
(112) Thomas, J. A. *Dalton Trans.* **2011**, *40*, 12005.
(113) Brusilowskij, B.; Dzyuba, E. V.; Troff, R. W.; Schalley, C. A. *Dalton Trans.* **2011**, *40*, 12089.
(114) Blanco, V.; García, M. D.; Terenzi, A.; Pía, E.; Fernández-Mato, A.; Peinador, C.; Quintela, J. M. *Chem. Eur. J.* **2010**, *16*, 12373.
(115) Terenzi, A.; Ducani, C.; Blanco, V.; Zerzankova, L.; Westendorf, A. F.; Peinador, C.; Quintela, J. M.; Bednarski, P. J.; Barone, G.; Hannon, M. J. *Chem. Eur. J.* **2012**, *18*, 10983.
(116) Glasson, C. R. K.; Lindoy, L. F.; Meehan, G. V. *Coord. Chem. Rev.* **2008**, *252*, 940.
(117) Stephenson, A.; Ward, M. D. *Chem. Commun.* **2012**, *48*, 3605.
(118) Hannon, M. J.; Painting, C. L.; Jackson, A.; Hamblin, J.; Errington, W. *Chem. Commun.* **1997**, 1807.
(119) Hannon, M. J.; Meistermann, I.; Isaac, C. J.; Blomme, C.; Aldrich-Wright, J. R.; Rodger, A. *Chem. Commun.* **2001**, 1078.
(120) Hannon, M. J.; Moreno, V.; Prieto, M. J.; Moldrheim, E.; Sletten, E.; Meistermann, I.; Isaac, C. J.; Sanders, K. J.; Rodger, A. *Angew. Chem. Int. Ed.* **2001**, *40*, 879.
(121) Phongtongpasuk, S. PhD dissertation, University of Birmingham, 2011.
(122) Yu, H.; Wang, X.; Fu, M.; Ren, J.; Qu, X. *Nucleic Acids Res.* **2008**, *36*, 5695.
(123) Yu, H.; Li, M.; Liu, G.; Wang, J.; Ren, J.; Zhao, C.; Qu, X. *Chem. Sci.* **2012**, *3*, 3145.
(124) Hotze, A. C. G.; Hodges, N. J.; Hayden, R. E.; Sanchez-Cano, C.; Paines, C.; Male, N.; Tse, M. K.; Bunce, C. M.; Chipman, J. K.; Hannon, M. J. *Chem. Biol.* **2008**, *15*, 1258.
(125) Ducani, C.; Leczkowska, A.; Hodges, N. J.; Hannon, M. J. *Angew. Chem. Int. Ed.* **2010**, *49*, 8942.
(126) McMorran, D. A.; Steel, P. J. *Angew. Chem. Int. Ed.* **1998**, *37*, 3295.
(127) Freye, S.; Hey, J.; Torras-Galán, A.; Stalke, D.; Herbst-Irmer, R.; John, M.; Clever, G. H. *Angew. Chem. Int. Ed.* **2012**, *51*, 2191.
(128) Sekiya, R.; Fukuda, M.; Kuroda, R. *J. Am. Chem. Soc.* **2012**, *134*, 10987.
(129) Lippert, B.; Miguel, P. J. S. *Chem. Soc. Rev.* **2011**, *40*, 4475.
(130) Clodt, J. I.; Fröhlich, R.; Eul, M.; Würthwein, E. U. *Eur. J. Inorg. Chem.* **2012**, *2012*, 1210.
(131) Fujita, M.; Sasaki, O.; Mitsuhashi, T.; Fujita, T.; Yazaki, J.; Yamaguchi, K.; Ogura, K. *Chem. Commun.* **1996**, 1535.
(132) Chand, D. K.; Biradha, K.; Kawano, M.; Sakamoto, S.; Yamaguchi, K.; Fujita, M. *Chem. Asian J.* **2006**, *1*, 82.
(133) Kaur-Banwait, S. PhD dissertation, University of Birmingham, 2010.
(134) Hannon, M. J.; WO 2009/068885: 2009.

(135) Hutchinson, D. J.; Cameron, S. A.; Hanton, L. R.; Moratti, S. C. *Inorg. Chem.* **2012**, *51*, 5070.
(136) Cai, D.; Larsen, R. D.; Reider, P. J. *Tetrahedron Lett.* **2002**, *43*, 4285.
(137) Islam, T. M. B.; Yoshino, K.; Nomura, H.; Mizuno, T.; Sasane, A. *Anal. Sci.* **2002**, *18*, 363.
(138) Wakabayashi, S.; Imamura, S.; Sugihara, Y.; Shimizu, M.; Kitagawa, T.; Ohki, Y.; Tatsumi, K. *J. Org. Chem.* **2008**, *73*, 81.
(139) Bruce, I.; WO Patent WO/2009/010,530: 2009.
(140) Tour, J. M.; Rawlett, A. M.; Kozaki, M.; Yao, Y.; Jagessar, R. C.; Dirk, S. M.; Price, D. W.; Reed, M. A.; Zhou, C. W.; Chen, J. *Chem. Eur. J.* **2001**, *7*, 5118.
(141) Kudo, N.; Perseghini, M.; Fu, G. C. *Angew. Chem. Int. Ed.* **2006**, *45*, 1282.
(142) Childs, L. J.; Alcock, N. W.; Hannon, M. J. *Angew. Chem. Int. Ed.* **2002**, *41*, 4244.
(143) Childs, L. J.; Pascu, M.; Clarke, A. J.; Alcock, N. W.; Hannon, M. J. *Chem. Eur. J.* **2004**, *10*, 4291.
(144) Falcone, R. D.; Baruah, B.; Gaidamauskas, E.; Rithner, C. D.; Correa, N. M.; Silber, J. J.; Crans, D. C.; Levinger, N. E. *Chem. Eur. J.* **2011**, *17*, 6837.
(145) Wang, P.; Leung, C. H.; Ma, D. L.; Sun, R. W. Y.; Yan, S. C.; Chen, Q. S.; Che, C. M. *Angew. Chem. Int. Ed.* **2011**, *50*, 2554.
(146) Sekiya, R.; Kuroda, R. *Chem. Commun.* **2011**, *47*, 12346.
(147) Tripathy, D.; Pal, A. K.; Hanan, G. S.; Chand, D. K. *Dalton Trans.* **2012**, *41*, 11273.
(148) Jodry, J. J.; Lacour, J. *Chem. Eur. J.* **2000**, *6*, 4297.
(149) Lacour, J.; Goujon-Ginglinger, C.; Torche-Haldimann, S.; Jodry, J. J. *Angew. Chem. Int. Ed.* **2000**, *39*, 3695.
(150) Uslu, A.; Güvenaltın, Ş. *Dalton Trans.* **2010**, *39*, 10685.
(151) Hirano, T.; Akiyama, J.; Mori, S.; Kagechika, H. *Org. Biomol. Chem.* **2010**, *8*, 5568.
(152) Gao, B.; Li, H.; Liu, H.; Zhang, L.; Bai, Q.; Ba, X. *Chem. Commun.* **2011**, *47*, 3894.
(153) Tuncel, S.; Dumoulin, F.; Gailer, J.; Sooriyaarachchi, M.; Atilla, D.; Durmuş, M.; Bouchu, D.; Savoie, H.; Boyle, R. W.; Ahsen, V. *Dalton Trans.* **2011**, *40*, 4067.
(154) Zhu, S.; Zhang, J.; Vegesna, G.; Luo, F. T.; Green, S.; Liu, H. *Org. Lett.* **2011**, *13*, 438.
(155) Tumey, L. N.; Boschelli, D. H.; Bhagirath, N.; Chen, J. J.; Floyd, M. B.; Li, Z.; Niu, C.; Shim, J.; Wang, Y.; Wang, Y. D.; Wu, B.; Eid, C. N.; WO Patent WO/2009/076,602: 2009.
(156) Humphries, P. S.; Do, Q. Q. T.; Wilhite, D. M. *Beilstein J. Org. Chem.* **2006**, *2*, 21.
(157) Nanashima, Y.; Yokoyama, A.; Yokozawa, T. *J. Polym. Sci., Part A: Polym. Chem.* **2012**, *50*, 1054.
(158) Heng, R.; Koch, G.; Schlapbach, A.; Seiler, M. P.; US Patent US/2010/010,5664: 2010.
(159) Larsen, A. F.; Nielsen, M. C.; Ulven, T. *Chem. Eur. J.* **2012**, *18*, 10892.
(160) Arola-Arnal, A.; Benet-Buchholz, J.; Neidle, S.; Vilar, R. *Inorg. Chem.* **2008**, *47*, 11910.

(161) Suntharalingam, K.; White, A. J. P.; Vilar, R. *Inorg. Chem.* **2009**, *48*, 9427.
(162) Guthrie, D. B.; Stein, D. G.; Liotta, D. C.; Lockwood, M. A.; Sayeed, I.; Atif, F.; Arrendale, R. F.; Reddy, G. P.; Evers, T. J.; Marengo, J. R. *ACS Med. Chem. Lett.* **2012**, *3*, 362.
(163) Chas, M.; Abella, D.; Blanco, V.; Pía, E.; Blanco, G.; Fernández, A.; Platas-Iglesias, C.; Peinador, C.; Quintela, J. M. *Chem. Eur. J.* **2007**, *13*, 8572.
(164) Blanco, V.; Chas, M.; Abella, D.; Peinador, C.; Quintela, J. M. *J. Am. Chem. Soc.* **2007**, *129*, 13978.
(165) Crowley, J. D.; Gavey, E. L. *Dalton Trans.* **2010**, *39*, 4035.
(166) Huisgen, R. *Angew. Chem.* **2006**, *75*, 604.
(167) Schweinfurth, D.; Pattacini, R.; Strobel, S.; Sarkar, B. *Dalton Trans.* **2009**, 9291.
(168) Austin, W. B.; Bilow, N.; Kelleghan, W. J.; Lau, K. S. Y. *J. Org. Chem.* **1981**, *46*, 2280.
(169) Rodger, A.; Norden, B. *Circular Dichroism and Linear Dichroism*; Oxford University Press, USA, 1997; Vol. 1.
(170) Vorlickova, M.; Kypr, J.; Sklenar, V. *Encyclopedia of Analytical Science* **2005**, *6*, 391.
(171) Vorlíčková, M.; Kejnovská, I.; Bednářová, K.; Renčiuk, D.; Kypr, J. *Chirality* **2012**, *24*, 691.
(172) Nordén, B.; Kurucsev, T. *J. Mol. Recognit.* **2004**, *7*, 141.
(173) Rodger, A.; Marrington, R.; Geeves, M. A.; Hicks, M.; de Alwis, L.; Halsall, D. J.; Dafforn, T. R. *PCCP* **2006**, *8*, 3161.
(174) Norden, B.; Kubista, M.; Kurucsev, T. *Q. Rev. Biophys.* **1992**, *25*, 51.
(175) Dragan, A.; Bishop, E.; Strouse, R.; Casas-Finet, J.; Schenerman, M.; Geddes, C. *Chem. Phys. Lett.* **2009**, *480*, 296.
(176) Peberdy, J. C.; Malina, J.; Khalid, S.; Hannon, M. J.; Rodger, A. *J. Inorg. Biochem.* **2007**, *101*, 1937.
(177) Keyser, U. F.; van Dorp, S.; Lemay, S. G. *Chem. Soc. Rev.* **2010**, *39*, 939.
(178) Kanaar, R.; Cozzarelli, N. R. *Curr. Opin. Struct. Biol.* **1992**, *2*, 369.
(179) Schvartzman, J. B.; Stasiak, A. *EMBO reports* **2004**, *5*, 256.
(180) Brody, J. R.; Kern, S. E. *Anal. Biochem.* **2004**, *333*, 1.
(181) Malina, J.; Hannon, M. J.; Brabec, V. *Nucleic Acids Res.* **2008**, *36*, 3630.
(182) Keck, M. V.; Lippard, S. J. *J. Am. Chem. Soc.* **1992**, *114*, 3386.
(183) Guo, Q.; Seeman, N. C.; Kallenbach, N. R. *Biochemistry* **1989**, *28*, 2355.
(184) Kepple, K. V.; Boldt, J. L.; Segall, A. M. *Proc. Natl. Acad. Sci. USA* **2005**, *102*, 6867.
(185) Su, L. Y.; Willner, D. L.; Segall, A. M. *Antimicrob. Agents Chemother.* **2010**, *54*, 1888.
(186) Pan, P. S.; Curtis, F. A.; Carroll, C. L.; Medina, I.; Liotta, L. A.; Sharples, G. J.; McAlpine, S. R. *Bioorg. Med. Chem.* **2006**, *14*, 4731.
(187) Howell, L. A.; Waller, Z. Ű. A. E.; Bowater, R.; O'Connell, M.; Searcey, M. *Chem. Commun.* **2011**, *47*, 8262.
(188) Mosmann, T. *J Immunol methods* **1983**, *65*, 55.
(189) Teicher, B. A.; Andrews, P. A. *Anticancer drug development guide: preclinical screening, clinical trials, and approval*; Humana Pr Inc, 2004; Vol. 1.

(190) Ishikawa, M.; Hashimoto, Y. *J. Med. Chem.* **2011**, *54*, 1539.
(191) Gottlieb, H. E.; Kotlyar, V.; Nudelman, A. *J. Org. Chem.* **1997**, *62*, 7512.
(192) Macrae, C. F.; Bruno, I. J.; Chisholm, J. A.; Edgington, P. R.; Mccabe, P.; Pidcock, E.; Rodriguez-Monge, L.; Taylor, R.; Streek, J.; Wood, P. A. *J. Appl. Crystallogr.* **2008**, *41*, 466.
(193) Pettersen, E. F.; Goddard, T. D.; Huang, C. C.; Couch, G. S.; Greenblatt, D. M.; Meng, E. C.; Ferrin, T. E. *J. Comput. Chem.* **2004**, *25*, 1605.
(194) Allen, F. H. *Acta Crystallogr. Sect. B: Struct. Sci.* **2002**, *58*, 380.
(195) Berman, H. M.; Westbrook, J.; Feng, Z.; Gilliland, G.; Bhat, T.; Weissig, H.; Shindyalov, I. N.; Bourne, P. E. *Nucleic Acids Res.* **2000**, *28*, 235.